PHENIX

PX No. 257 **BNL-72162-2004**
FORMAL REPORT

PHENIX Experiment at RHIC: Decadal Plan 2004 – 2013

William A. Zajc
PHENIX Collaboration
Brookhaven National Laboratory
Upton, New York 11973, USA

Prepared for:
BNL Lab Management
Mr. Tom Kirk's Office

Physics Department

Brookhaven National Laboratory
Operated by
Brookhaven Science Associates
Upton, NY 11973

Under Contract with the United States Department of Energy
Contract Number DE-AC02-98CH10886

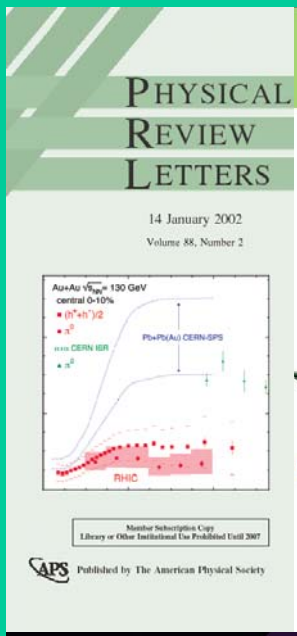
PHYSICAL REVIEW LETTERS
14 January 2002
Volume 88, Number 2
Au+Au √sNN = 130 GeV
central 0-10%
Pb+Pb(Au) CERN-SPS
CERN ISR
RHIC
Member Subscription Copy
Library or Other Institutional Use Prohibited Until 2007
Published by The American Physical Society

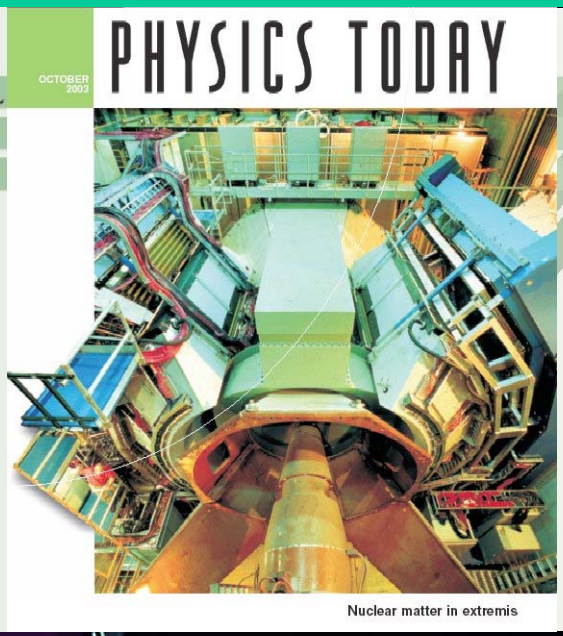
OCTOBER 2003
PHYSICS TODAY
Nuclear matter in extremis

PHYSICAL REVIEW LETTERS
Articles published week ending
15 AUGUST 2003
Volume 91, Number 7
PHENIX
PHOBOS
BRAHMS
STAR
Member Subscription Copy
Library or Other Institutional Use Prohibited Until 2008
Published by The American Physical Society

PHENIX
Decadal Plan 2004-2013

PHENIX Experiment at RHIC: Decadal Plan 2004-2013

Brookhaven National Laboratory

Relativistic Heavy Ion Collidier

November, 2003

Spokesperson:	William A. Zajc, *Columbia University*
Deputy Spokesperson:	Glenn R. Young, *Oak Ridge National Laboratory*
Operations Manager:	Edward O'Brien, *Brookhaven National Laboratory*
Upgrades Manager:	Axel Drees, *Stony Brook University*

Executive Summary

The PHENIX Collaboration has developed a plan for the detailed investigation of quantum chromodynamics in the next decade. The demonstrated capabilities of the PHENIX experiment to measure rare processes in hadronic, leptonic and photonic channels, in combination with RHIC's unparalleled flexibility as a hadronic collider, provides a physics program of extraordinary breadth and depth. A superlative set of measurements to elucidate the states of both hot and cold nuclear matter, and to measure the spin structure of the proton has been identified. The components of this plan include

- Definitive measurements that will establish the nature of the matter created in nucleus+nucleus collisions, that will determine if the description of such matter as a quark-gluon plasma is appropriate, and that will quantify both the equilibrium and non-equilibrium features of the produced medium.
- Precision measurements of the gluon structure of the proton, and of the spin structure of the gluon and sea-quark distributions of the proton via polarized proton+proton collisions.
- Determination of the gluon distribution in cold nuclear matter using proton+nucleus collisions.

Each of these fundamental fields of investigation will be addressed through a program of correlated measurements in some or all of the following channels:

- Particle production at high transverse momentum, studied via single particle inclusive measurements of identified charged and neutral hadrons, multi-particle correlations and jet production.
- Direct photon, photon+jet and virtual photon production.
- Light and heavy vector mesons.
- Heavy flavor production.

These measurements, together with the established PHENIX abilities to identify hadrons at low transverse momentum, to perform detailed centrality selections, and to monitor polarization and luminosity with high precision create a superb opportunity for performing world-class science with PHENIX for the next decade.

A portion of this program is achievable using the present capabilities of PHENIX experimental apparatus, but the physics reach is considerably extended and the program made even more compelling by a proposed set of upgrades which include

- An aerogel and time-of-flight system to provide complete π/K/p separation for momenta up to 10 GeV/c.
- A vertex detector to detect displaced vertices from the decay of mesons containing charm or bottom quarks.
- A hadron-blind detector to detect and track electrons near the vertex.
- A micro-TPC to extend the range of PHENIX tracking in azimuth and pseudo-rapidity.
- A forward detector upgrade for an improved muon trigger to preserve sensitivity at the highest projected RHIC luminosities.
- A forward calorimeter to provide photon+jet studies over a wide kinematic range.

The success of the proposed program is contingent upon several factors external to PHENIX. Implementation of the upgrades is predicated on the availability of R&D funds to develop the required detector technologies on a timely, and in some cases urgent, basis. The necessity for such funding, and the physics merit of the proposed PHENIX program, has been endorsed in the first meeting of BNL's Detector Advisory Committee in December, 2002. Progress towards the physics goals depends in an essential way on the development of the design values for RHIC luminosity, polarization and availability. An analysis based on the guidance from the Collider Accelerator Department indicates that moderate increases in the yearly running time lead to very considerable increases in progress toward the enunciated goals. Efficient access to the rarest probes in the proposed program is achieved via the order-of-magnitude increase in luminosity provided by RHIC-II.

Introduction

In February of 2003, Dr. T. Kirk acting in his capacity as Associate Laboratory Director for High Energy and Nuclear Physics at Brookhaven National Laboratory, charged the PHENIX Collaboration with the task of producing a Decadal Plan. A primary goal in this effort is the identification of those future physics opportunities at RHIC that are achievable within the decadal time-frame, specified as 2004 to 2013. Information on the required upgrades to pursue those goals, together with the R&D necessary to develop those items was also solicited. The plan was specifically requested to address "the strategic physics goals of the collaboration as it evolves into the high luminosity phase of the RHIC program, a period that will be reached operationally not before about 2009 and will likely be complete only after 2010.

This document, prepared in response to the decadal charge, provides a detailed description of the anticipated physics from, and the planned evolution of, the PHENIX experiment. The PHENIX Decadal Plan draws on many existing resources, ranging from the previous decade's Conceptual Design Report to the recently completed Beam Use Proposal for Runs 4 to 8 at RHIC. Given that the next decade at RHIC will see increasing attention to the measurement of rare processes, the published PHENIX results on high transverse momenta phenomena, open charm and charmonium production have been of particular utility in developing quantitative, well-calibrated measures for the planned program of investigation in heavy ion, spin and proton-nucleus physics.

This document is organized as follows:

Chapter 1 provides a brief review of the evolution of the PHENIX experiment from RHIC Run-1 to the present, together with a summary of the data acquired in each run.

Chapter 2 presents the physics of PHENIX, beginning with a description of the long-standing physics goals of PHENIX, then an analysis of progress towards those goals. The following sections provide a comprehensive treatment of the prospects for future measurements in nucleus-nucleus collisions, in polarized proton physics, and in proton-nucleus physics. The last section develops the proposed implementation of this program in the PHENIX run plan for the next 5-7 years.

Chapter 3 discusses planned PHENIX Upgrades, including a description of the overall strategy for augmenting the considerable strengths of the existing apparatus, specific information on each proposed subsystem, and discussions of the upgrade implications for data acquisition and computing.

Appendix A gives the complete text of the charge for this document.

Lists of Figures, Tables, and References are given at the end of the document.

Contents

1 Overview of the PHENIX Experiment at RHIC **1–1**
1.1 Conceptual Design of the PHENIX Experiment 1–1
1.2 Detector Evolution 1–2
1.3 Collaboration Status 1–5

2 PHENIX Physics Program for the next Decade **2–1**
2.1 Introduction 2–1
2.2 Heavy-Ion Collision Physics 2–2
2.2.1 Hard processes 2–6
2.2.1.1 Introduction 2–6
2.2.1.2 PHENIX Insights into Soft Processes 2–7
2.2.1.3 Transition From Soft to Hard Processes 2–8
2.2.1.4 Medium Modification of Jets 2–9
2.2.1.5 Baryon Puzzle and the Jet Fragmentation Functions 2–12
2.2.2 Direct Photons 2–17
2.2.2.1 The gluon structure function in p-p and p+A collisions . . . 2–17
2.2.2.2 Polarized proton collisions 2–20
2.2.2.3 A+A collisions 2–20
2.2.2.4 Direct Photon Appendix—Effect of End Cap EMCalorimeter Upgrade 2–20
2.2.3 Thermal Radiation 2–22
2.2.3.1 Thermal Di-Leptons: Predictions and Previous Experimental Results 2–22
2.2.3.2 Photons: Previous Experimental Results and Predictions . . 2–25
2.2.3.3 Di-leptons: PHENIX rates and expectations. 2–26
2.2.3.4 Photons: PHENIX rates and expectations. 2–28
2.2.4 Light Vector Mesons 2–30
2.2.4.1 Introduction 2–30
2.2.4.2 Predictions 2–31
2.2.4.3 Previous experimental results 2–32
2.2.4.4 PHENIX rates and expectations. 2–33
2.2.5 Heavy Quarks 2–36
2.2.5.1 Introduction 2–36

2.2.5.2 Systematic Studies . . . 2–37
2.2.5.3 Energy Loss of Heavy Quarks . . . 2–38
2.2.5.4 Charm Flow? . . . 2–42
2.2.5.5 Open Charm and Beauty Cross Sections . . . 2–43
2.2.5.6 Charmonium Yields . . . 2–44
2.2.5.7 Bottomonium Yields . . . 2–47
2.2.5.8 Correlated Charm . . . 2–48
2.2.5.9 Heavy quark physics timeline . . . 2–50
2.3 Spin Physics . . . 2–51
2.3.1 Introduction . . . 2–51
2.3.2 Gluon Polarization . . . 2–54
2.3.3 π^0 and $\pi^\pm$ Production in polarized pp collisions at PHENIX . . . 2–54
2.3.4 Open Charm and Bottom Production . . . 2–55
2.3.5 Prompt Photon Production . . . 2–56
2.3.6 Flavor Decomposition of Quark and Anti-Quark Polarization . . . 2–57
2.3.7 Transversity . . . 2–58
2.3.8 New Physics Searches . . . 2–61
2.4 Proton-Nucleus Collision Physics . . . 2–62
2.4.1 Effects on jets of cold nuclear medium . . . 2–63
2.4.2 Nuclear Shadowing . . . 2–65
2.4.3 J/Ψ Production . . . 2–66
2.4.4 Open-charm Production . . . 2–70
2.4.5 Centrality Tagging . . . 2–72
2.4.6 Other physics opportunities at high luminosity . . . 2–73
2.5 The PHENIX Run Plan . . . 2–76

3 Upgrades Program **3–2**
3.1 Introduction . . . 3–2
3.1.1 Physics Goals and Upgrades Strategy . . . 3–3
3.1.2 Study of QCD at high temperatures . . . 3–3
3.1.3 Extended exploration of the spin structure of the nucleon . . . 3–5
3.1.4 Exploration of the nucleon structure in nuclei . . . 3–6
3.1.5 Upgrade Strategy . . . 3–6
3.2 Specific Detectors for Planned Upgrades . . . 3–7
3.2.1 Aerogel . . . 3–9
3.2.1.1 Introduction . . . 3–9
3.2.1.2 Physics with High p_T Particle ID . . . 3–9
3.2.1.3 The Aerogel Counter . . . 3–10
3.2.1.4 Future Expansion . . . 3–13
3.2.2 Silicon Vertex Detector . . . 3–14
3.2.3 Hadron Blind Detector . . . 3–19
3.2.3.1 The HBD concept . . . 3–19
3.2.3.2 HBD R&D Results . . . 3–21

3.2.4 A Fast, Compact Time Projection Chamber 3–24
3.2.5 Forward Detector Upgrade 3–27
3.2.5.1 Performance of the Present Muon Trigger 3–27
3.2.5.2 Trigger Upgrade Options 3–28
3.2.5.3 The Nosecone Calorimeter 3–29
3.2.5.4 Schedule and Funding 3–29
3.3 Data Acquisition 3–30
3.3.1 Summary of Current PHENIX Online System 3–30
3.3.2 PHENIX Upgrade Program: DAQ Implications 3–31
3.3.3 PHENIX Upgrade Program: The Next Step for DAQ 3–31
3.4 Computing 3–33

Appendix A: Charge Letter **A–1**

List of Figures **F–1**

List of Tables **T–1**

References **R–1**

PHENIX Participants November, 2003

Abilene Christian University, *Abilene, TX 79699, USA*
C.R. Baldwin, J.L. Drachenberg, M.N. Hagiwara, D. Isenhower, L. Isenhower, M.C. McCain, O.O. Omiwade, W.C. Smith, R.S. Towell*

Institute of Physics, Academia Sinica, *Taipei 11529, Taiwan*
W.C. Chang*

Department of Physics, Banaras Hindu University, *Varanasi 221005, India*
C.P. Singh*, V. Singh, S.K. Tuli

Bhabha Atomic Research Centre, *Bombay 400 085, India*
P. Chand, R.K. Choudhury*, D. Dutta, A.K. Mohanty, P. Shukla

Brookhaven National Laboratory, *Upton, NY 11973-5000, USA*
S.H. Aronson, B. Azmoun, A. Bazilevsky, S. Belikov, S. Boose, H. Buesching, G. Bunce, G. David, E.J. Desmond, A. Franz, P. Giannotti, J.S. Haggerty, M. Harvey, B.M. Johnson, H.-J. Kehayias, E. Kistenev, P.J. Kroon, Y.I. Makdisi, S. Mioduszewski, J.T. Mitchell, D.P. Morrison, E. O'Brien, C. Pinkenburg, R.P. Pisani, M.L. Purschke, S. Sato, S.N. White, T.K. Shea, I.V. Sourikova, S.P. Stoll, M.J. Tannenbaum*, C.L. Woody

University of California - Riverside, *Riverside, CA 92521, USA*
K.N. Barish*, S. Bathe, F. Bauer, S.-Y. Fung, D. Kotchetkov, X.H. Li, M. Muniruzzaman, R. Seto, W. Xie

China Institute of Atomic Energy (CIAE), *Beijing, People's Republic of China*
C. Li, X. Li, S. Lu, Y. Yang, J. Zhou, S. Zhou*

Center for Nuclear Study, Graduate School of Science, University of Tokyo, *7-3-1 Hongo, Bunkyo, Tokyo 113-0033, Japan*
T. Gunji, H. Hamagaki*, R. Hayano, M. Inuzuka, T. Isobe, F. Kajihara, S. Kametani, T. Kawabata, N. Kurihara, Susumu S., K. Ozawa, T. Sakaguchi

University of Colorado, *Boulder, CO 80309*
S. Kelly, E. Kinney, J.L. Nagle*

Columbia University, *New York, NY 10027* and **Nevis Laboratories,** *Irvington, NY 10533, USA*
C. Aidala, S. Batsouli, M.T. Bjorndal, C.Y. Chi*, M. Chiu, B.A. Cole, D. d'Enterria, J.E. Frantz, J. Jin, F.W. Sippach, D. Winter, W.A. Zajc, C. Zhang, L. Zhang

Dapnia, CEA Saclay, *F-91191, Gif-sur-Yvette, France*
A. Baldisseri*, H. Borel, Y. Cobigo, J. Gosset, H. Pereira, F. Staley

Debrecen University, *H-4010 Debrecen, Egyetem tér 1, Hungary*
J. Imrek, P. Tarjan*, R. Vertesi

ELTE, Eötvös Loránd University, *H - 1117 Budapest, Pázmány P. s. 1/A, Hungary*
M. Csanad, A. Hegedus, A. Kiss*

Florida State University, *Tallahassee, FL 32306, USA*
K. Das, A.D. Frawley*, J.R. Hutchins

Georgia State University, *Atlanta, GA 30303, USA*
C.R. Cleven, X. He*, G.C. Mishra, H. Qu

Hiroshima University, *Kagamiyama, Higashi-Hiroshima 739-8526, Japan*
A. Enokizono, T. Hachiya, H. Harada, K. Haruna, K. Homma, K. Kitamura, R. Kohara, T. Nakamura, K. Shigaki, N. Sugita, T. Sugitate*, Y. Tsuchimoto

Institute for High Energy Physics (IHEP), *Protvino, Russia*
V. Babintsev, V. Bumazhnov, S. Chernichenko, A. Denisov, A. Durum, V. Kochetkov, V. Semenov, I. Shein, A. Soldatov, N. Tyurin*, A. Yanovich

University of Illinois at Urbana-Champaign, *Urbana, IL 61801*
M. Chiu, D. Gabbert, M. Grosse Perdekamp, H. Hiejima, J.-C. Peng*

Iowa State University, *Ames, IA 50011, USA*
P. Constantin, N. Grau, J.C. Hill*, J.G. Lajoie, A. Lebedev, R. McKay, C.A. Ogilvie, H. Pei, J. Rak, M. Rosati, H.D. Skank, S. Skutnik, G.A. Sleege, X. Zong

Joint Institute for Nuclear Research, *141980 Dubna, Moscow Region, Russia*
S. Afanasiev, A. Isupov, V. Kolesnikov, A. Litvinenko*, A. Malakhov, V. Penev, V. Peresedov, P. Rukoyatkin, L. Zolin

KAERI, Cyclotron Application Laboratory, *Seoul, South Korea*
J.-S. Chai*

Kangnung National University, *Kangnung 210-702, South Korea*
D.W. Kim*, S. Lee, G. Kim

KEK, High Energy Accelerator Research Organization, *Tsukuba-shi, Ibaraki-ken 305-0801, Japan*
J. Chiba, S. Nagamiya, S. Sawada*, K.H. Tanaka

KFKI Research Institute for Particle and Nuclear Physics (RMKI), *H-1525 Budapest 114, POBox 49, Hungary*
T. Csorgo*, A. Ster, J. Sziklai, J. Zimanyi

Korea University, *Seoul, 136-701, Korea*
B. Hong, M.J. Kweon, W.J. Park, K.S. Sim*

Russian Research Center "Kurchatov Institute", *Moscow, Russia*
S.T. Belyaev, S.L. Fokin, M.S. Ippolitov, K.V. Karadjev, A.V. Kazantsev, V.A. Lebedev, V.I. Manko*, N.I. Mishustin, T.V. Moukhanova, S.A. Nikolaev, A.S. Nyanin, D.Yu. Peressounko, Iou.G. Sibiryak, A.A. Tsvetkov, A.A. Vasiliev, A.A. Vinogradov, I.E. Yushnanov

Kyoto University, *Kyoto 606, Japan*
K. Aoki, Y. Fukao, H. Funahashi, K. Imai*, T. Murakami, R. Muto, M. Nakamura, H. Okada, N. Saito, F. Sakuma, H.D. Sato, M. Togawa, H. Torii, M. Yosoi

Laboratoire Leprince-Ringuet, Ecole Polytechnique, CNRS-IN2P3, *Route de Saclay, F-91128, Palaiseau, France*
S. Borenstein, A. Debraine, O. Drapier, F. Fleuret, F. Gastaldi, M. Gonin*, R. Granier de Cassagnac, L. Kluberg, P. Petiau, A. Romana, V-N. Tram

Lawrence Livermore National Laboratory, *Livermore, CA 94550, USA*
E.P. Hartouni, M. Heffner, S.C. Johnson, J. Newby, R.A. Soltz*

Los Alamos National Laboratory, *Los Alamos, NM 87545, USA*
P.D. Barnes*, J.G. Boissevain, M.L. Brooks, J.M. Burward-Hoy, H.W. van Hecke, G.J. Kunde, D.M. Lee, M.J. Leitch, M.X. Liu, P.L. McGaughey, J.M. Moss, B. Norman, A.P.T. Palounek, W.E. Sondheim, J.P. Sullivan

LPC, Université Blaise Pascal, CNRS-IN2P3, *Clermont-Fd, 63177 Aubiere Cedex, France*
B. Forestier, S. Gadrat, G. Roche*, P. Rosnet

Department of Physics, Lund University, *Box 118, SE-221 00 Lund, Sweden*
H.-A. Gustafsson, J. Nystrand, A. Oskarsson*, L. Osterman, I. Otterlund, S. Rosendahl, E. Stenlund, H. Tydesjo

Institut für Kernphysik, University of Muenster, *D-48149 Muenster, Germany*
D. Bucher, N. Heine, C. Klein-Boesing, K. Reygers, W. Verhoeven, J. Wessels*, O. Zaudkte

Myongji University, *Yongin, Kyonggido 449-728, Korea*
K.S. Joo*

Nagasaki Institute of Applied Science, *Nagasaki-shi, Nagasaki 851-0193, Japan*
K. Kiyoyama, T. Matsumoto, Y. Tanaka*

University of New Mexico, *Albuquerque, NM 87131, USA*
B. Bassalleck, D.E. Fields*, R. Hobbs, Malik M.D., T.L. Thomas

New Mexico State University, *Las Cruces, NM 88003, USA*
A. Al-Jamel, G.S. Kyle, V. Papavassiliou, S.F. Pate*, R. Armendariz, M. Stepanov, X.R. Wang

Oak Ridge National Laboratory, *Oak Ridge, TN 37831, USA*
G. Alley, T.C. Awes*, M. Bobrek, C.L. Britton Jr., W.L. Bryan, V. Cianciolo, Y.V. Efremenko, M.S. Emery, M.N. Ericson, S.S. Frank, T.F. Gee, U. Jagadish, J.P. Jones Jr., J.A. Moore, K.F. Read, D. Silvermyr, D.E. Smith, M.C. Smith, P.W. Stankus, B.R. Whitus, A.L. Wintenberg, G.R. Young

IPN-Orsay, Universite Paris Sud, CNRS-IN2P3, *BP1, F-91406, Orsay, France*
M.P. Comets, B. Espagnon, D. Jouan*, Y. LeBornec, C. Suire, N. Willis

Peking University, *Beijing, People's Republic of China*
R. Han, Y. Mao*, Z. You

PNPI, Petersburg Nuclear Physics Institute, *Gatchina, Russia*
V. Baublis, A. Chevel, V. Ivanov, A. Khanzadeev, L. Kochenda, B. Komkov, P. Kravtsov, V. Riabov, Y. Riabov, E. Roschin, V. Samsonov*, V. Trofimov, E. Vznuzdaev

RIKEN (The Institute of Physical and Chemical Research), *Wako, Saitama 351-0198, JAPAN*
Y. Akiba, T. Chujo, H. Enyo, Y. Goto, K. Hasuko, J.M. Heuser, T. Ichihara, A. Kiyomichi, K. Kurita, J. Murata H. Ohnishi, V.L. Rykov, A. Taketani, K. Tanida, J. Tojo, H. Torii, Y. Watanabe*, S. Yokkaichi

RIKEN BNL Research Center, Brookhaven National Laboratory, *Upton, NY 11973-5000, USA*
(G. Bunce*, BNL), A. Deshpande, O. Jinnouchi, M. Kaneta, K. Okada, Tsuguchika T.

St. Petersburg State Technical University, *St. Petersburg, Russia*
A. Berdnikov, Y. Berdnikov*, Evgeni E., Mikhail M.

Universidade de São Paulo, Instituto de Física, *Caixa Postal 66318, São Paulo CEP05315-970, Brazil*
O. Dietzsch*, M. Kuryiama, M.A.L. Leite, R. Menegasso, C.L. Silva, E.M. Takagui

System Electronics Laboratory, Seoul National University, *Seoul, South Korea*
E. Kim, H. Lim, J. Park*

Chemistry Department, Stony Brook University, SUNY, *Stony Brook, NY 11794-3400, USA*
N.N. Ajitanand, J. Alexander, P. Chung, W. Holzmann, M. Issah, R. Lacey*, A. Taranenko

Department of Physics and Astronomy, Stony Brook University, SUNY, *Stony Brook, NY 11794, USA*
R. Averbeck, S. Butsyk, T. Dahms, A. Devismes, A. Drees, J. Egdemir, T.K. Hemmick, K.H. Ho, R. Hutter, B.V. Jacak*, J. Jia, S. Leckey, F. Matathias, A. Milov, M. Nguyen, V. Pantuev, A.K. Purwar, M. Reuter, A. Sickles, D. Walker

SUBATECH (Ecole des Mines de Nantes, CNRS-IN2P3, Université de Nantes), *BP 20722 - 44307, Nantes, France*
L. Aphecetche, X. Camard, J.P. Cussonneau, H. Delagrange*, C. Finck, F. Gastineau, M. Germain, A. Hadj Henni, G. Martinez, Y. Schutz

University of Tennessee, *Knoxville, TN 37996, USA*
V. Dzhordzhadze, I. Garishvili, A. Glenn, D. Hornback, S. Sorensen*

Department of Physics, Tokyo Institute of Technology, *Tokyo, 152-8551, Japan*
T. Horaguchi, N. Kamihara, K. Nakano, T.-A. Shibata*

Institute of Physics, University of Tsukuba, *Tsukuba, Ibaraki 305, Japan*
S. Esumi, S. Kaminaga, S. Kato, T. Kawagishi, M. Konno, H. Masui, Y. Miake*, Y. Nagata, M. Narisawa, S. Sakai, M. Shimomura, T. Shoujou, S. Takagi

Vanderbilt University, *Nashville, TN 37235, USA*
T. Chujo, S.V. Greene, C.F. Maguire*, T.E. Miller, D. Mukhopadhyay, I.D. Ojha, D. Pal, J. Velkovska, M. Velkovsky

Waseda University, Advanced Research Institute for Science and Engineering, *17 Kikui-cho, Shinjuku-ku, Tokyo 162-0044, Japan*
J. Kikuchi*

Weizmann Institute, *Rehovot 76100, Israel*
A.K. Dubey, Z. Fraenkel, B. Khachaturov, A. Kozlov, M. Naglis, E. Ramasamy, I. Ravinovich, D. Sharma, I. Tserruya*

Yonsei University, IPAP, *Seoul 120-749, Korea*
I.J. Choi, J.H. Kang*, D.J. Kim, H.J. Kim, Y. Kwon, M.K. Lee, S.S. Ryu

*Institutional Board Member for each institution.

Spokesperson: W. A. Zajc
Deputy Spokesperson: G. R. Young
Operations Manager: E. O'Brien
Upgrades Manager: A. Drees
Scientific Secretary: B. M. Johnson

Chapter 1

Overview of the PHENIX Experiment at RHIC

1.1 Conceptual Design of the PHENIX Experiment

The PHENIX Conceptual Design Report [1], submitted to BNL/RHIC management on January 29th, 1993, outlined a comprehensive physics program focused on the search for and characterization of new states of nuclear matter. The measurement of electromagnetic probes and high transverse momentum phenomena formed a major thrust of the proposed program. It was also realized that the measurement of global variables and soft, flavor-identified, hadronic spectra in the same apparatus was essential to the goal of understanding the evolution of the produced matter over all relevant time-scales. These diverse criteria required combining an unprecedented number of sub-systems together with a high bandwidth trigger and data acquisition system into an integrated detector design. Particular attention was given to minimizing the conflicting design criteria of the central arm spectrometers, with their requirement for minimal mass in the aperture, and those of the muon spectrometers which require maximal absorption of the incident hadron flux. The data acquisition and trigger system was designed to accommodate the great variety of interaction rates and event sizes provided by RHIC. Every effort was made to provide for future upgrades, both in the geometry of the experiment and in the architecture and design parameters of the read-out system.

Subsequent developments have greatly increased the scope of the PHENIX physics program, and the corresponding capabilities of the detector. In particular, the commissioning and operation of RHIC as a polarized proton collider creates extraordinary prospects for measurement of the gluon and sea quark spin structure functions. The high rate capabilities and outstanding segmentation of the original PHENIX design, coupled with additional luminosity and polarization monitoring and a second muon spectrometer provide exceptional performance in the channels of interest to the PHENIX Spin program. The addition of the second muon spectrometer also extends the physics reach of the experiment in heavy ion collisions, and is of obvious benefit in asymmetric collisions, such as the recently completed d+Au studies. In the next section we document the time evolution of the PHENIX detector,

both as background to our future plans and to provide some measure of the collaboration's ability to implement a complex detector system while producing outstanding physics. The physics measured to date and the plans for future measurements are summarized in Chapter 2. The upgrades required to implement those plans are described in Chapter 3.

1.2 Detector Evolution

The PHENIX detector has evolved from a partial implementation of the central arms in Run-1 to a completed installation of the baseline + AEE (Additional Experimental Equipment) systems for Run-3. Each of the configurations used for Runs 1-3 was capable of using the delivered luminosity from RHIC to explore heavy ions (Runs 1 and 2), polarized proton collisions (Runs 2 and 3) and deuteron + Au collisions (Run 3).

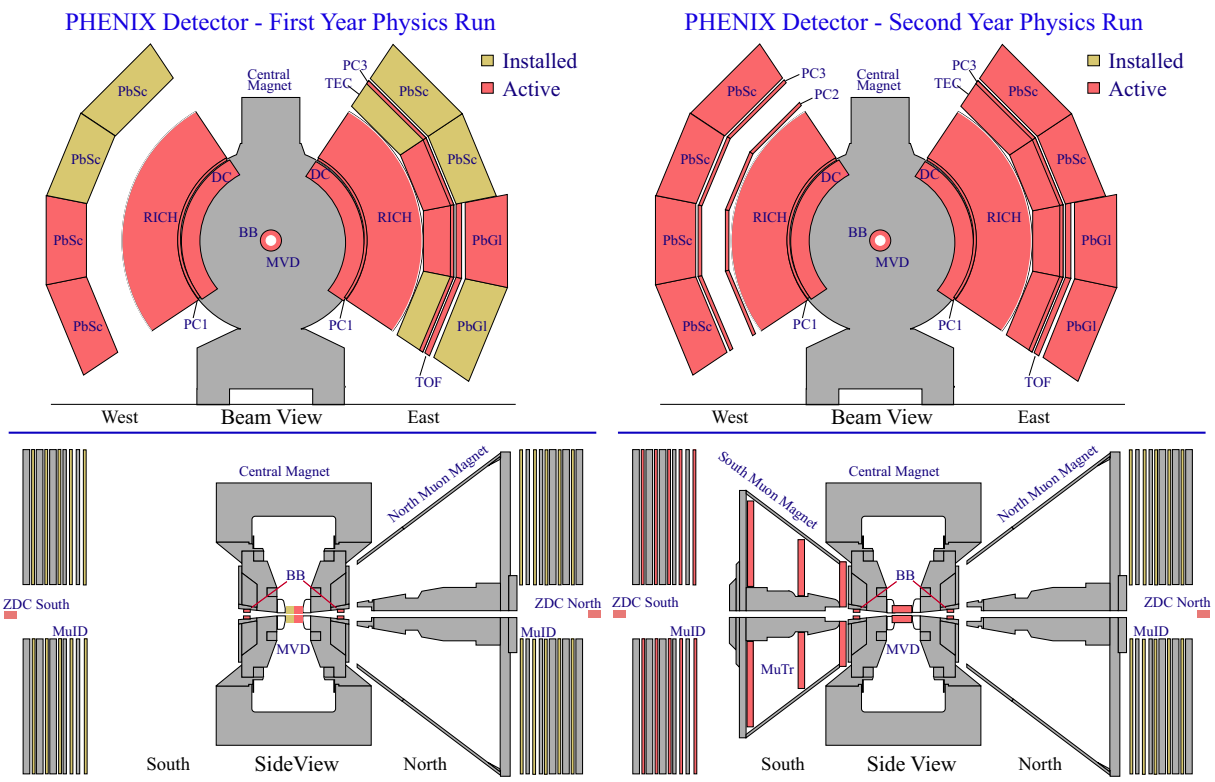

Figure 1.1: Installed and active detectors for the RHIC Run-1 (left) and Run-2 (right) configurations of the PHENIX experiment.

The Run-1 data set of $\sim 1\ \mu\text{b}^{-1}$ Au+Au collisions at $\sqrt{s_{NN}} = 130$ GeV was obtained with a partially instrumented subset of the PHENIX Central Arms, as shown in the left panel of Fig. 1.1. In Run-2 $\sim 24\ \mu\text{b}^{-1}$ of Au+Au collisions at $\sqrt{s_{NN}} = 200$ GeV and ~ 130 nb^{-1} of polarized proton data at 200 GeV were recorded. The right panel of Fig. 1.1 shows that the detector configuration, data acquisition and triggers were significantly upgraded in Run-2. All central arm detectors were read out, and the South Muon Arm was installed.

Figure 1.2 shows the complete PHENIX experiment, which was available for Run-3 and was used to measure 2.7 nb^{-1} of d+Au collisions and 0.35 pb^{-1} of polarized p+p collisions. In fact, three additional "beyond the baseline" components were also installed for Run-3:

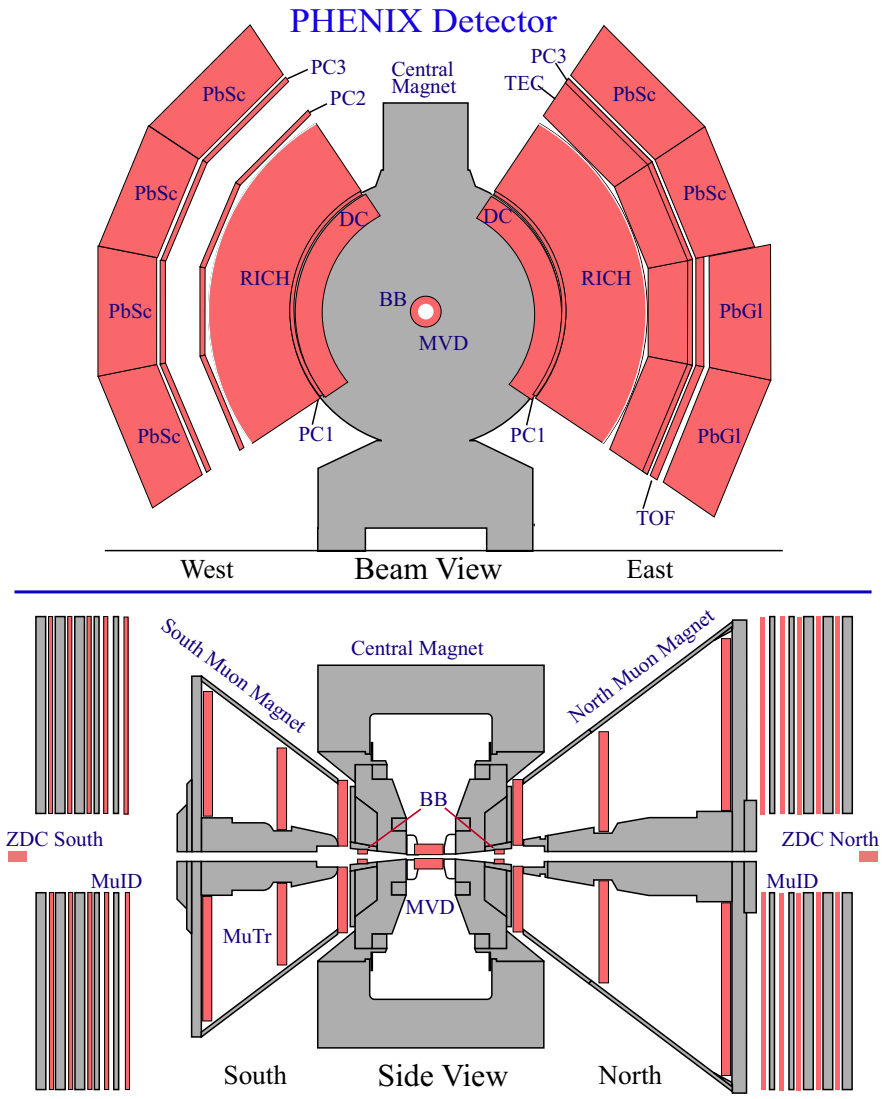

Figure 1.2: RHIC Run-3 configuration of the PHENIX experiment.

1. The Zero-Degree Calorimeters were augmented by a Shower-Max Detector (SMD), which was of crucial importance in providing local polarimetry capabilities during the commissioning of the spin rotators at IP8.

2. Two Forward Calorimeters (FCAL's) were installed to provide event characterization for d+Au collisions.

3. A New Trigger Counter (NTC) was used during p+p running to extend the fraction of minimum bias cross section accessible to the PHENIX Level-1 trigger system.

For Run-4, the capabilities of the PHENIX central spectrometer will be significantly extended through the addition of an Aerogel Cerenkov Counter (ACC). This detector, consisting of 160 elements of hydrophobic aerogel installed in the West arm of PHENIX(Figure 1.4), will provide the additional particle identification capabilities illustrated in Figure 1.3, which will permit a crucial test of quark recombination models[2, 3, 4] for $p_T > 5$ GeV/c.

		Pion-Kaon separation	Kaon-Proton separation
TOF	σ~100 ps	0 - 2.5	- 5
RICH	n=1.00044 γth~34	5 - 17	17 -
Aerogel	n=1.01 γth~8.5	1 - 5	5 - 9

Figure 1.3: Hadron identification in the PHENIX Central Arms with the Aerogel Cerenkov Counter system.

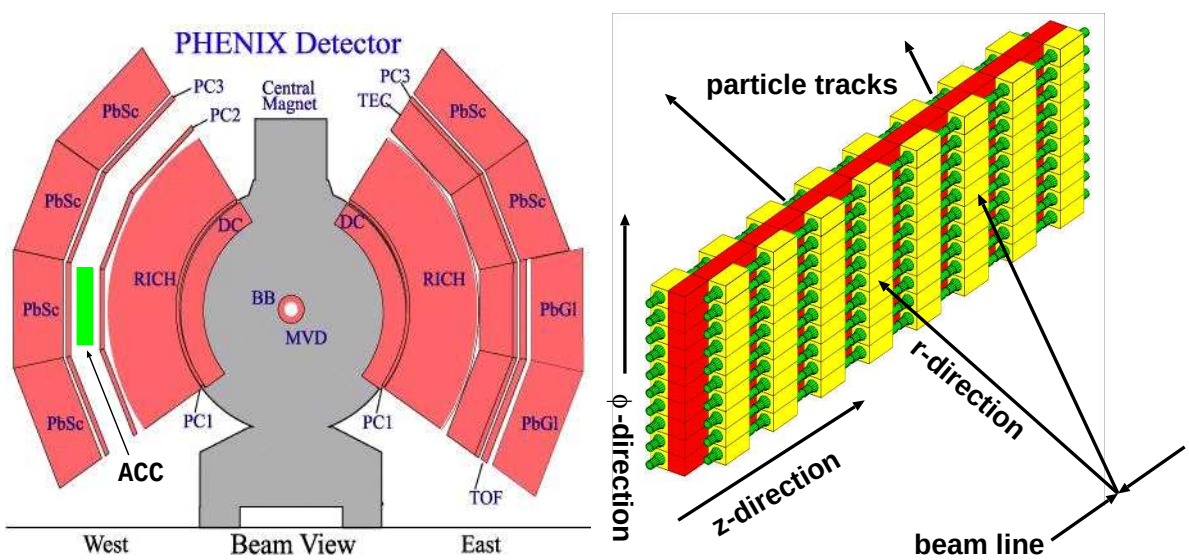

Figure 1.4: The aerogel detector in the west arm between pad chamber 2 (PC2) and 3 (PC3) in the W1 sector (left) and the aerogel detector structure and orientation with respect to the beam line (right) are shown.

1.3 Collaboration Status

PHENIX is a collaboration of over 440 scientists and engineers from 56 institutions located in 12 countries. The collaboration is responsible for operating and maintaining the PHENIX experiment, and carrying out its physics research program. In addition, the PHENIX collaboration initiates, designs, builds and operates all upgrades to the detector. The collaboration is assisted in these tasks by a dedicated, technical support group located at Brookhaven National Laboratory. PHENIX institutions contribute additional technical and engineering support to the experiment, especially in areas directly related to an institution's subsystem responsibilities.

At the time of release of the PHENIX Conceptual Design Report in 1993, the collaboration was composed of approximately 300 scientists and engineers associated with 43 institutions. With rare exception, all of the original signatories of the Conceptual Design Report made contributions to major hardware items. The design and construction of PHENIX was administered by PHENIX governing boards, particularly Project Management, the Executive Council, Detector Council and Institutional Board. The roles and responsibilities of these units were specified in the PHENIX Bylaws[5]. In addition, institutional responsibilities were specified through Memoranda of Understanding (MoU) between PHENIX, BNL and the individual collaborating institutions. PHENIX is currently managed in a similar mode with a set of governing councils (Figure 1.5), and MoU's committing collaborating institutions to particular operations and service responsibilities.

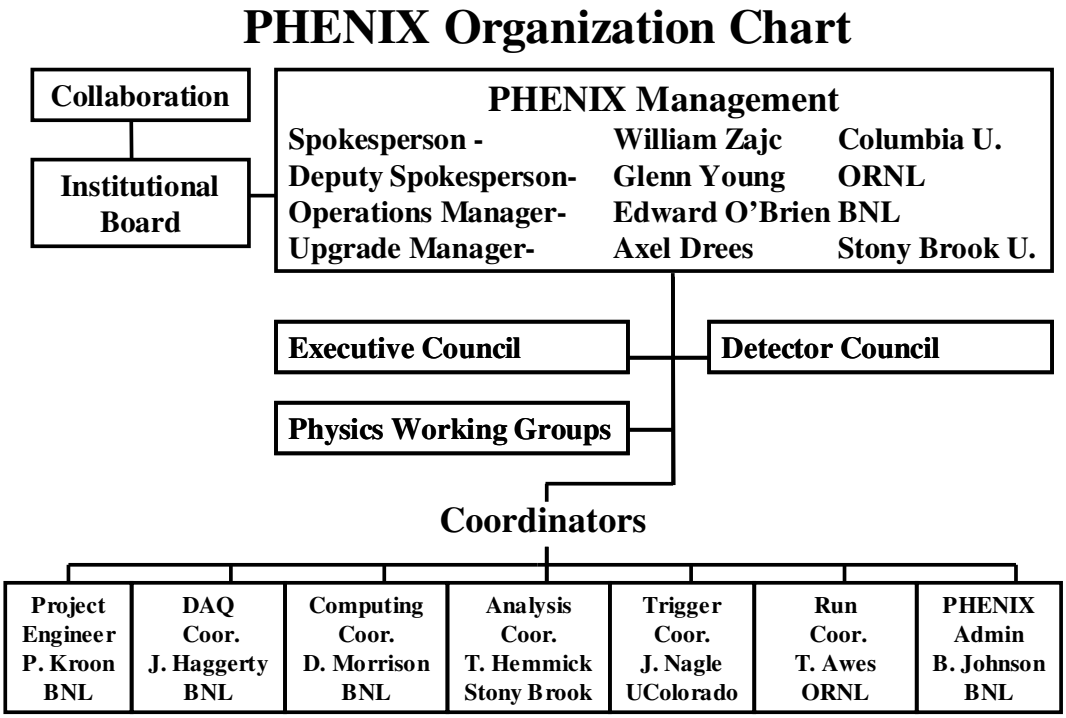

Figure 1.5: PHENIX Management Structure, November, 2003

The four positions in PHENIX Management (PM), the Spokesperson, Deputy Spokesperson, Operations Manager and Upgrade Manager are responsible for planning and executing the research, operations and upgrade program of PHENIX, and managing the collaboration. PM is assisted by six Coordinators and the Project Engineer who manage broad aspects of the PHENIX program. The Coodinators report directly to PM. The Executive Council sets scientific priorities for PHENIX and advises PM on all the scientific issues of the experiment. The Detector Council advises PM on all PHENIX technical, operational and upgrades issues. The Institutional Board decides issues concerning collaboration governance, elects the Spokesperson and members of the Executive Council. The Conveners of the Physics Working Groups manage all physics analysis on PHENIX.

The PHENIX baseline detector was built with funds from the US Department of Energy and with major contributions from non-DOE sources. Japanese collaborators funded by Japanese science agencies STA and Monbu-sho, made major contributions to the fabrication of PHENIX detector subsystems such as the Ring Imaging Cerenkov counters, the Time-of-Flight Array, the Beam-Beam Counters and one fully instrumented Muon Spectrometer Arm. Russian institutions made major contributions to the construction of PHENIX Electromagnetic Calorimeter, Drift Chambers and spectrometer magnets. Institutions from Brazil, France, Germany, India, Israel, Korea and Sweden took important responsibilities in hardware construction projects for the PHENIX baseline detector. There were many in-kind contributions of manpower and equipment from numerous PHENIX institutions. The contribution of funds and equipment to PHENIX construction from non-US sources is estimated to be in excess of $41 M. An important recent example of international contributions was the production of electronics for the North Muon Tracker by French and Korean institutions which joined the collaboration in 2001.

Institutions that built a PHENIX detector subsystem are responsible for operating and maintaining it. New groups that join PHENIX are strongly encouraged to join service groups that are responsible for subdetectors, DAQ and trigger components or software functions. The outside institutions fill a large pool of experts who are necessary to operate PHENIX during both data-taking and data production at the RHIC Computing Facility. The experiment requires 110 people to operate at BNL in any one week while taking data. Approximately 30% of those people are the local PHENIX-BNL staff with the rest being visiting scientists. In 2002 there were 230 visiting scientists at BNL of which 80 were long term visitors with stays of 3 months or more.

The number of PHENIX participants and institutions has grown ∼30% in the last 10 years and we anticipate a similar growth rate in the future. We have had expressions of interest by new groups wanting to participate in both the current PHENIX program and future upgrades. The BNL Chemistry group, for example, has recently signed the upgrade proposal to DOE for a PHENIX Silicon Vertex Detector (VTX). The group will bring a broad experience with silicon detector technology from PHOBOS. In addition to management and physics experience, each group member has specific technical skills that will be important for the successful construction, installation, commissioning, and operation of a silicon detector in the RHIC environment. The group plans to focus on hardware for the PHENIX VTX upgrade in the next few years and foresees joining PHENIX sometime after FY06.

Table 1.1: PHENIX Institutions and Construction or Operational Responsibilities

Detector Subsystem	Institutions Responsible
Beam Beam Counter	Columbia, Hiroshima
Mult. Vertex Detector	LANL, ORNL, UCR, Yonsei
Drift Chamber	PNPI, Stony Brook
Pad Chamber	BNL, Lund, ORNL, Stony Brook, Vanderbilt, Weizmann Inst
Time Expansion Chamber	Acad. Sinica, BNL, ISU, UCR, USP
Ring Imaging Cerenkov	CNS-Tokyo, FSU, KEK, NIAS, Stony Brook, Waseda
Time of Flight	Columbia, Tsukuba
EM Calorimeter	BNL, Debrecen, IHEP, Kurchatov, Münster, ORNL
Muon Tracker	ACU, BARC, CAL, Ecole Polytechnique, IPN-Orsay, Kangnung, KEK, Kyoto, LANL, LPC-Pascal, Myongji, NMSU, ORNL, RBRC, RIKEN, Saclay, Seoul, Subatech-Nantes, UKorea, UNM, Yonsei
Muon ID	CIAE, Kyoto, ORNL, RIKEN, Tokyo Tech, U. Tenn
Norm Trigger Counter	BNL, UIUC
Aerogel Counter	BNL, CNS-Tokyo, JINR-Dubna, Tsukuba
Forward Calorimeter	LLNL
Data Acquisition	BNL, Columbia, GSU, NIAS, ORNL, U Colorado
LVL1 Trigger	BNL, ISU, Kyoto, ORNL, RBRC, RIKEN, UCR, UIUC
LVL2 Trigger	Columbia, FSU, GSU
Online Computing	BNL
Offline Computing	Almost all institutions
Simulations	Vanderbilt
Magnets	BNL, KEK, LLNL, PNPI, RIKEN

Chapter 2

PHENIX Physics Program for the next Decade

2.1 Introduction

Any evaluation of plans for a critical decade of physics exploration at RHIC must begin with an assessment of progress towards previously stated goals. It is instructive to examine the achievements of the PHENIX Collaboration to date in this light. Table 2.1, which is taken directly from the "Physics Goals" section of the PHENIX Conceptual Design Report [1], outlines the full range of physics observables anticipated in 1993. The broad program of measurements foreseen in that document has held up remarkably well during the initial phase of RHIC operations. To date, PHENIX has produced (or is preparing) publications on all of the channels found under "Global" and "Charged Hadrons" categories, on roughly half of those in the "Photon" section, and on a smaller subset of those in the e^+e^-, $\mu^+\mu^-$ and $e\mu$ categories. In some cases (e.g., continuum di-leptons), the principle obstacle has been backgrounds, which is one of the issues being aggressively addressed via our proposed upgrades.

More typically, the issue has been one of integrated luminosity. This is true for both the heavy ion program and particularly so for spin physics, where improvements are required of 10^3 to 10^4 in the figure of merit for double spin asymmetries $\mathcal{P}^4 \int \mathcal{L} \cdot dt$.[1] The recent exercise of developing the PHENIX 5-year Beam Use Proposal for RHIC Runs 4-8, taking as input the detailed guidance from the Collider Accelerator Department, provides a quantitative basis of estimate for anticipated luminosity growth and the physics that will result from those improvements. Whenever possible, we have used that information in producing this Decadal Plan.

In this chapter, we present the PHENIX plans for progress over the next decade in heavy-ion physics, spin physics, and proton-nucleus physics. We have found it useful to present much of that information by identifying a few characteristic channels, for example, the "onium" states, hadron production at high transverse momentum, and direct photon yields, to serve as indicators of sensitivity to the rare processes so essential to continued progress

[1] $\mathcal{P}$ is the longitudinal polarization and $\int \mathcal{L} \cdot dt$ is the integrated luminosity.

in RHIC physics. It must be emphasized that the concentration on these channels does not preclude the program of extensive measurements of low-p_T and global observables that form much of the PHENIX program; rather it is anticipated that continued progress in these areas will be maintained by using the demonstrated ability of the PHENIX data acquisition system to acquire the corresponding minimum bias data sets (see also the discussion of Section 2.2.1.2).

2.2 Heavy-Ion Collision Physics

The published results at $\sqrt{s_{NN}} = 130$ GeV from Run-1 Au-Au collisions [6, 7, 8, 9, 10, 11, 12, 13, 14, 15, 16, 17] and $\sqrt{s_{NN}} = 200$ GeV from Run-2 Au-Au collisions [18, 19, 20, 21, 22, 23, 24], Run-2 proton-proton collisions [25, 26], and Run-3 d+Au collisions [27] clearly demonstrate that PHENIX has the capability to make high quality measurements in both hadronic and leptonic channels for collisions ranging from p+p to Au+Au. Together these 22 publications (and many more in preparation) encompass physics from the barn to the picobarn level; their very breadth precludes a detailed presentation here. Instead we provide a summary of the discoveries and achievements made by PHENIX in this initial segment of RHIC operations:

- Systematic measurement of the dependence of the charged particle pseudo-rapidity density [6] and the transverse energy [7] on the number of participants in Au+Au collisions at $\sqrt{s_{NN}}$=130 GeV.
- Discovery of high p_T suppression of π^0 and charged particle production in Au+Au collisions at $\sqrt{s_{NN}}$=130 GeV [8] and a systematic study of the scaling properties of the suppression [16]; extension of these results to much higher transverse momenta in Au+Au collisions at $\sqrt{s_{NN}}$=200 GeV [18, 22]
- Discovery of absence of high p_T suppression in d+Au collisions at $\sqrt{s_{NN}}$=200 GeV [27].
- Discovery of the anomalously large proton and anti-proton yields at high transverse momentum in Au+Au collisions at $\sqrt{s_{NN}}$=130 GeV through the systematic study of $\pi^{\pm}$, K$^{\pm}$, p and $\bar{p}$ spectra [9]; measurement of Λ's and $\bar{\Lambda}$'s in Au+Au collisions at $\sqrt{s_{NN}}$=130 GeV [12]; study of the scaling properties of the proton and anti-proton yields at in Au+Au collisions at $\sqrt{s_{NN}}$=200 GeV [21].
- Measurement of HBT correlations in $\pi^+\pi^+$ and $\pi^-\pi^-$ pairs in Au+Au collisions at $\sqrt{s_{NN}}$=130 GeV, establishing that the "HBT puzzle" of $R_{OUT} \approx R_{SIDE}$ extends to high pair momentum [10].
- First measurement of single electron spectra in Au+Au collisions at $\sqrt{s_{NN}}$=130 GeV, suggesting that charm production scales with the number of binary collisions [11].
- Sensitive measures of charge fluctuations [13] and fluctuations in mean p_T and transverse energy per particle [14, 24] in Au+Au collisions at $\sqrt{s_{NN}}$=130 GeV.

- Measurements of elliptic flow for charged particles from Au+Au collisions at $\sqrt{s_{NN}}$=130 GeV [15] and identified charged hadrons from Au+Au collisions at $\sqrt{s_{NN}}$=200 GeV [19].
- Extensive study of hydrodynamic flow, particle yields, ratios and spectra from Au+Au collisions at $\sqrt{s_{NN}}$=130 GeV [17] and 200 GeV [23].
- First observation of J/ψ production in Au+Au collisions at $\sqrt{s_{NN}}$=200 GeV [20].
- Measurement of crucial baseline data on π^0 spectra [25] and J/ψ production [26] in p+p collisions at $\sqrt{s}$=200 GeV.

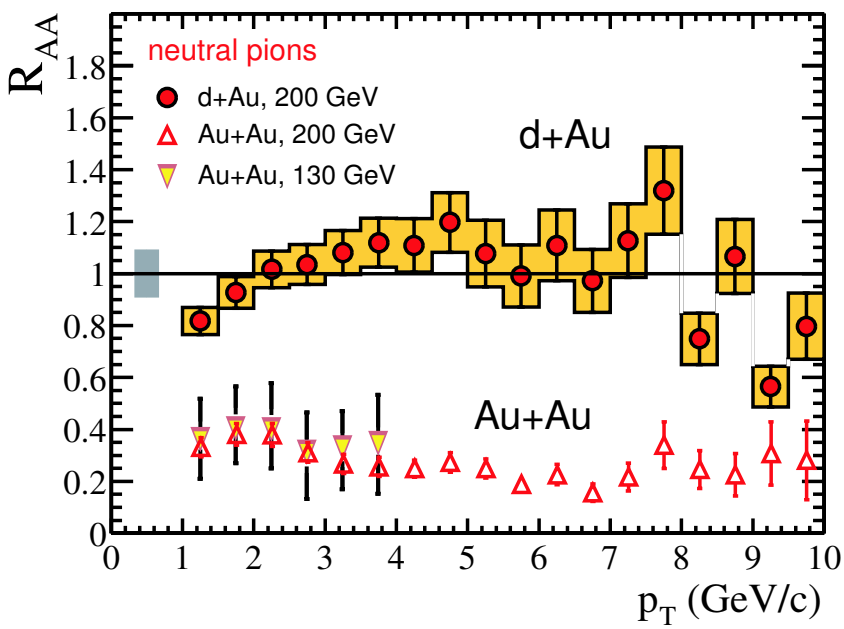

Figure 2.1: The suppression factor R_{AA} measured for π^0 production by PHENIX in Run-1 Au+Au collisions at 130 GeV [8], Run-2 Au+Au collisions at 200 GeV [18], and Run-3 d+Au collisions at 200 GeV [27].

These observations clearly establish that the matter produced in RHIC collisions is extraordinarily dense, sufficiently so as to lead to strong suppression of mesons out to the highest measured transverse momenta. The broad features of final state hadron yields are consistent with a thermally equilibrated system exhibiting strong hydrodynamic flow. The data on elliptic flow strongly suggests that the hydrodynamic flow pattern is established in the initial stages of the collision. The absence of suppression at high p_T in d+Au collisions (illustrated in Figure 2.1) argues against large modifications of the initial-state nuclear wave-function, i.e., the suppression appears to be a result of the transport property of the medium created in nucleus-nucleus collisions. Since this combination of features is not seen in lower-energy heavy ion collisions, it is plausible to conclude that Au+Au collisions have created conditions best described as a new state of matter.

The PHENIX physics program in nucleus-nucleus collisions for the next decade at RHIC is dedicated to performing the crucial measurements to consolidate the accumulating evidence for a new state of matter, so that the current plausible arguments become unequivocable facts. It is anticipated that this program smoothly evolves from the current phase of exploration to one of characterization over the first portion of this period, with the latter years being devoted to detailed measurements providing quantitative information on the properties of the new matter.

To achieve these goals, we have identified the following physics measurements as especially compelling:

- Hard Processes and Jets
- Heavy Quarks
- Light Vector Mesons and the Low-mass Continuum
- Direct Photons

To a very large extent, these signals represent those items in Table 2.1 that still await definitive measurement. The initial round of discovery and exploration at RHIC has confirmed the wisdom of those goals, and in fact reinforced the ability of these channels to provide decisive insights on the nature of the hot dense matter created in nucleus-nucleus collisions. It is also gratifying to note that the long-standing commitment of PHENIX to such a program is closely aligned with the recently formulated long-term performance measures for RHIC from NSAC [28], which we quote verbatim:

> **Proposed Long Term Measures**
>
> - Recreate brief, tiny samples of hot, dense nuclear matter to search for the quark-gluon plasma and characterize its properties.
> - Timeframe - By 2015
> - Expert Review every five years rates progress as "Excellent"
> - Minimally effective - Existence of hot, high-density matter established; some of its properties (e.g., its initial temperature via the photon spectrum) measured; confinement properties, and energy transport (via jets) explored.
> - Successful - Existence of a deconfined, thermalized medium determined; its properties such as temperature history, equation of state, energy and color transport (via jets), and screening (via heavy quark production) characterized.

Both the goals and the proposed time frame of the NSAC report overlap maximally with those of the PHENIX Decadal Plan for heavy ion physics. In the following subsections we explore in detail each of the topics listed above.

Table 2.1: PHENIX Physics Goals from Conceptual Design Report (1993) [1]

Quantity to be Measured	Category*	Physics Objective
e^+e^-, $\mu^+\mu^-$		
• $\rho \to \mu^+\mu^-/\rho \to \pi\pi$, $d\sigma/dp_\perp$	BCD	Basic dynamics (T, τ, etc.,) for a hot gas,
$\omega \to e^+e^-/\omega \to \pi\pi$, $d\sigma/dp_\perp$		transverse flow, etc.
• ϕ-meson's width and $m_{\phi\to e^+e^-}$	QGP	Mass shift due to chiral transition (C.T.)
$\phi \to e^+e^-/\phi \to K^+K^-$	QGP	Branching ratio change due to C.T.
ϕ-meson yield (e^+e^-)	ES	Strangeness production ($gg \to s\bar{s}$)
• $J/\psi \to e^+e^-, \mu^+\mu^-$	QGP, QCD	Yield suppression and the distortion
$\psi' \to \mu^+\mu^-$		of p_T spectra due to Debye screening
$\Upsilon, \to \mu^+\mu^-$		in deconfinement transition (D.T.)
• $1 < m_T(l^+l^-) < 3$ GeV	ES, QGP	Thermal radiation of hot gas, and
(rate and shape)		effects of QGP
• $m_{l^+l^-} > 3$ GeV $\to \mu^+\mu^-$	QCD	A-dependence of Drell-Yan, and
	QGP	thermal $\mu^+\mu^-$
• $\sigma \to \pi\pi, e^+e^-, \gamma\gamma$	QGP	Mass shift, narrow width due to C.T.
$e\mu$ coincidence		
• $e\mu$, $e(p_T > 1$ GeV/c)	QCD, QGP	$c\bar{c}$ background, charm cross section
Photons		
• $0.5 < p_T < 3$ GeV/c γ	ES, QGP	Thermal radiation of hot gas, and
(rate and shape)		effect of QGP
• $p_T > 3$ GeV/c γ	QCD	A-dependence of QCD γ
• π^0, η spectroscopy	BCD	Basic dynamics of hot gas, strangeness in η
• $N(\pi^0)/N(\pi^+ + \pi^-)$ fluctuations	QGP	Isospin correlations and fluctuations
• High p_T π^0, η from jet	QGP	Reduced dE/dx of quarks in QGP
Charged Hadrons		
• p_T spectra for $\pi^\pm$, $K^\pm$, p, $\bar{p}$	BCD	Basic dynamics, flow, T, baryon density,
		stopping power, etc.
	QGP	Possible second rise of $< p_T >$
• $\phi \to K^+K^-$	ES, QGP	Branching ratio, mass width
• K/π ratios	ES	Strangeness production
• $\pi\pi$ + KK HBT	BCD	Evolution of the collision, $R_\perp$
	QGP	Long hadronization time ($R_{\rm out} \gg R_{\rm side}$)
• Antinuclei	QGP	High baryon susceptibility due to C.T.?
• high p_T hadrons from jet	QGP	Reduced dE/dx of quarks in QGP
Global		
• $N_{\rm tot}$ (total multiplicity)	BCD	Centrality of the collision
• $dN/d\eta, d^2N/d\eta d\phi, dE_T/d\eta$	BCD	Local energy density, entropy
	QGP	Fluctuations, droplet sizes

* BCD = Basic collisions dynamics. ES = Thermodynamics at early stages.
QGP = Effect of QGP phase transition. QCD = Study of basic QCD processes.

2.2.1 Hard processes

2.2.1.1 Introduction

In this section we discuss the physics of hard processes in heavy ion collisions at RHIC. A particular focus is on the production and modification of jets, which have been shown to provide a sensitive probe of the produced medium. This information, together with measurements of heavy quark production (discussed in Section 2.2.5) and high p_T direct photons (Section 2.2.2), provide PHENIX with extensive opportunities to make contact with perturbative QCD in heavy ion and proton-proton collisions.

The creation of very high temperature and density matter, with densities much larger than that inside hadrons, has been established at RHIC. While it is plausible that this matter consists of deconfined quarks and gluons, not enough is known about the properties of the medium to demonstrate this unambiguously. Hard probes have been shown to be useful to quantify the medium properties (in particular, the density and/or opacity). However, the data so far suffer from insufficient statistical precision to perform detailed correlation studies, and inadequate reach in transverse momentum to investigate the full range of predicted phenomena. Furthermore, we have observed considerable ambiguity in the very definition of hard processes in heavy ion collisions. At moderate transverse momenta, where the onset of perturbative physics is already apparent in p+p collisions, RHIC data indicate still-significant contributions from collective phenomena typically considered "soft". Understanding this transition is an important goal for the next years.

The initial three runs of PHENIX have shown that jets are strongly modified in central heavy ion collisions, and have demonstrated that the modification is a final state effect of the dense medium, not an initial state effect of the gold nuclei. Elliptic flow indicates that large pressure gradients are established very early in the collision, preserving the spatial asymmetries of the interaction region. The magnitude of the elliptic flow appears to saturate at $p_T \approx$ 2-3 GeV/c, but the reason for the saturation is not well understood. Furthermore, the effect of jets, which produce particles above this momentum, upon elliptic flow analyses is also not understood.

The flavor yields of hadrons in central Au+Au collisions has been shown by PHENIX to be quite surprising. In peripheral collisions, baryon and kaon yields relative to pions correspond very nearly to those in p+p collisions. However, as more central collisions are selected, the yield of baryons increases dramatically. In the most central collisions, as many baryons as pions are observed above 2 GeV/c p_T; the excess observed for antibaryons is similar. There have been multiple explanations offered for this observation, but the current data are unable to resolve them.

PHENIX measures hard processes leading to single high p_T hadrons, and also measures correlations among jets of hadrons, in several channels. Table 2.2 contains a summary of the PHENIX physics signals and topics that fall under this section. In addition to the study of these signals in heavy ion collisions, PHENIX will make complementary measurements in p+p collisions (for baseline cross sections and distributions) and d+A collisions (for studying entrance channel effects and cold nuclear matter effects). The remainder of this section contains short descriptions of the major physics topics.

Table 2.2: Summary of PHENIX signals of hard processes. Many signals can already be studied with the baseline detector, but require considerable increase in integrated luminosity. Some measurements require upgrade hadron identification capability, using the aerogel upgrade. Integrated luminosity values shown in the table are PHENIX recorded luminosities. The required RHIC delivered luminosities are approximately three times higher, largely due to the width of the delivered vertex distribution.

Topic	Signals	p_T (GeV/c)	$\sim$ Lum (μb^{-1})
hadron suppression	single π^0 (energy loss, flow, pQCD recovered)	17	300
modification of known E_{jet} (energy loss)	γ - charged/neutral correlations	7 GeV γ 7 GeV γ 10 GeV γ	300 300 1000
jet modification (back-to-back jets)	charged-charged and neutral-charged 2 hadron correlations	$>$ 5 GeV leading hadron $>$ 7 GeV leading hadron	300 3000
in-medium fragmentation function	identified hadron correlations	3-4 GeV leading hadron + 2-3 GeV partner	300
	$\geq$ 2 particles detected	$>$ 4 GeV leading hadron (requires aerogel)	$>$ 300

2.2.1.2 PHENIX Insights into Soft Processes

PHENIX has successfully carried out the proposed program to study soft processes (at the momentum scale $\leq$ 2 GeV/c p_T). This program has taken advantage of the excellent particle identification, superb momentum resolution, and high rate capability yielding large numbers of minimum bias events.

PHENIX provided the first study of the centrality dependence of charged particle multiplicity [6]. We uniquely measure the transverse energy produced, allowing observation of the surprisingly small evolution of energy per particle with $\sqrt{s}$ and system size [7]. PHENIX has also quantified event-by-event fluctuations in particle number, p_T and E_T distributions [13, 14, 24].

PHENIX has reported the transverse momentum spectra for pions, kaons and protons in Au+Au collisions at 130 and 200 GeV [17, 23], in d+Au collisions at $\sqrt{s_{NN}}$ = 200 GeV and in 200 GeV p+p collisions. The spectra show the presence of radial flow in Au+Au collisions, growing to average transverse velocities $\langle\beta_T\rangle$ of nearly 0.5 in the most central collisions. Kinetic freezeout takes place at a temperature near 120 MeV, considerably lower than the chemical freezeout temperature of 170 MeV, deduced from particle production ratios from all the experiments, including PHENIX [29]. Comparison with the PHENIX single particle spectra covering a wide momentum range was a major factor in proving the

success of hydrodynamical descriptions of the physics at RHIC [30, 31].

PHENIX has made crucial measurements of elliptic flow at RHIC, and is unique in the ability to determine the reaction plane at a rapidity far removed from identified particles whose correlation with the reaction plane is to be tested [15, 19]. We have demonstrated the mass dependence of elliptic flow expected from hydrodynamical models, and have observed deviation from this at $p_T = 2$ GeV/c. The evolution of the elliptic flow strength, v_2, with p_T is being combined with jet analyses to study the transition from soft to hard processes at RHIC.

Identified particle spectra in d+Au show the onset of the Cronin effect, and its increase with p_T as well as hadron mass. Comparison of production rates of particles and antiparticles as well as kaons to protons yields information on the hadrochemistry of the final state of collisions at RHIC. We have measured the evolution as a function of $\sqrt{s}$, colliding system size, and centrality of Au+Au collisions.

PHENIX has provided seminal measurements of two particle correlations, measuring π-π and K-K HBT to larger transverse momentum than previously accessible [10]. The data show the same decrease with p_T of the hadron source size parameters as seen at lower energy, indicating again the presence of radial expansion of the hadron-emitting source. In fact, the values of the apparent source radius parameters are also the same as at lower energy - indicating a nearly total lack of $\sqrt{s}$ dependence of the source size. This observation was in total disagreement with expectations from the otherwise-successful hydrodynamic models, although recent work on more sophisticated Coulomb corrections that omit the correction of pions arising from resonance decays at large distances has reduced some of this discrepancy.

Most channels in the soft processes at RHIC have been thoroughly studied at this time. However, there are several notable exceptions, requiring either higher statistics, detector upgrades, or both. PHENIX certainly aims to measure the thermal photon spectrum, both real and virtual, as discussed below. We have made an initial measurement of ϕ meson production and decay to both K^+K^- and e^+e^-, however more statistics are required for a definitive comparison of yields and p_T spectra in the two decay channels. Although the evolution of most of the soft physics with $\sqrt{s}$ is slow and rather well- understood, it would be prudent to explore an energy regime intermediate between the lowest RHIC energy to date, and that of heavy ion collisions at the CERN SPS.

2.2.1.3 Transition From Soft to Hard Processes

Because of the large hydrodynamic flows developed in heavy ion collisions, soft physics at RHIC extends to higher p_T than in elementary p+p collisions. At transverse momenta around 2-3 GeV/c, where the onset of perturbative physics is already apparent in p+p collisions, RHIC data indicate still-significant contributions from collective phenomena typically considered "soft". It is this p_T region where the elliptic flow strength, v_2, saturates and hadron correlations show a mixture of combinatorial, collectively boosted and jet-like sources of particles. Single particle spectra in this region also appear to be produced by a mixture of thermal (collective) and hard QCD-like processes [17, 32, 4].

Understanding this transition, and the relative contributions of boosted thermal physics and jets emitted dominantly from the surface of the interacting region, are crucial to de-

termining how the hot, dense medium modifies hard processes. Does the energy lost by fast partons to the medium become immediately thermalized, further heating the medium? Does this "turbo-charged" medium, in turn, exert strong influence on the remaining fast partons and change how they fragment into hadrons? Answering these questions will require quantifying the dependence of the soft and hard contributions on system size as well as $\sqrt{s}$. Because the cross sections for hard processes are small, and fall with decreasing $\sqrt{s}$, a significant amount of data must be collected when the energy or beams are changed. A "quick" scan cannot shed light on this very important question. Consequently we await long Au+Au running plus one substantial run with smaller beam nuclei to map out the system size dependence of the soft-hard transition. Running at $\sqrt{s} = 62.4$ GeV will provide data at a lower energy, yet sufficient energy for the hard scattering cross sections to be measureable in a single RHIC run.

2.2.1.4 Medium Modification of Jets

Colored high p_T partons are predicted to lose energy primarily due to gluon Bremsstrahlung as they propagate through the medium [33, 34, 35]. A denser medium is expected to induce higher energy loss. Indeed, the yield of high p_T particles in Au+Au is suppressed by a factor of 4-5, compared to expectations from p-p scaled by the number of nucleon-nucleon collisions in central Au+Au, as shown in figures 2.2 and 2.3 [8, 16, 18, 22].

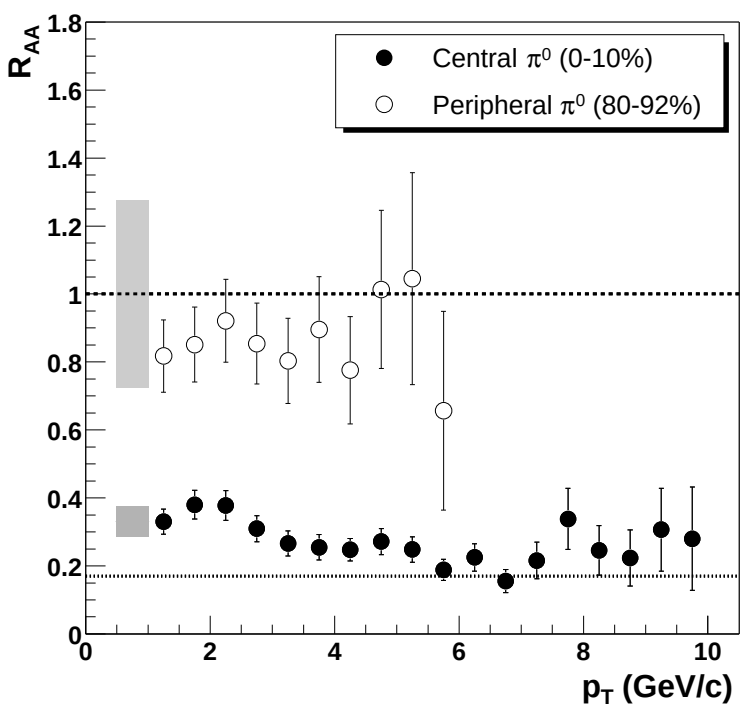

Figure 2.2: Nuclear modification factor R_{AA} for π^0 in central (closed circles) and peripheral (open circles) Au+Au at $\sqrt{s_{NN}} = 200$ GeV.

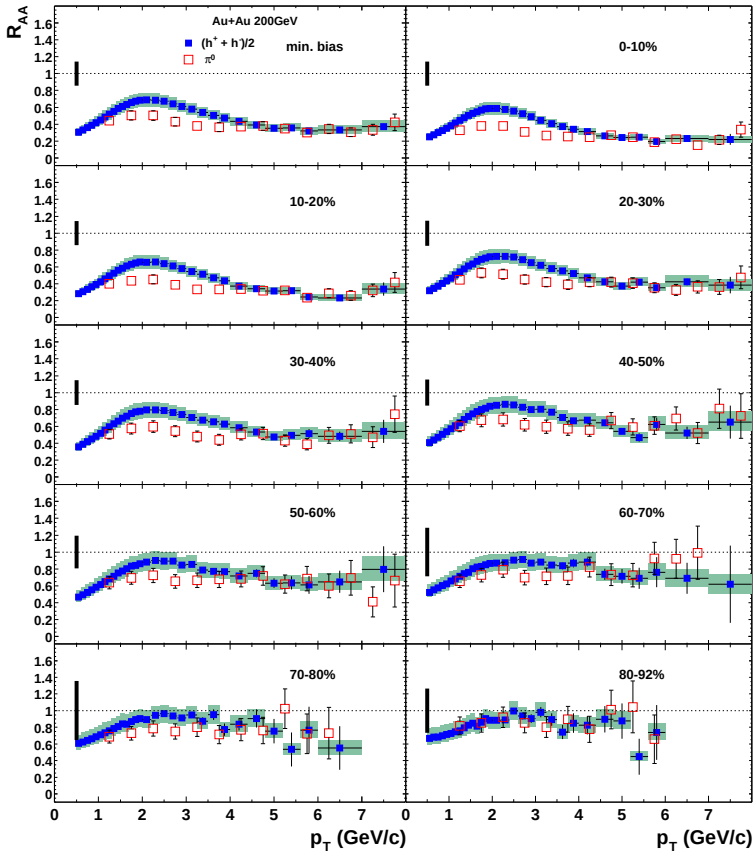

Figure 2.3: R_{AA} for $(h^+ + h^-)/2$ and π^0 in Au+Au collisions as a function of p_T for minimum bias and 9 different centrality classes, ranging from very peripheral to very central.

Energy loss calculations are able to quantitatively reproduce the observed suppression [36], however the energy loss explanation is not unique. Initial state gluon shadowing would deplete the gluon population, reducing the number of hard scatterings leading to jets, and therefore suppress the yield of high momentum hadrons. Furthermore, there are predictions that the ultimate effect of extreme gluon density could be saturation of the gluon distribution functions at low x [37]. Should this be the case, the hard scattering rate in Au+Au collisions would decrease significantly, giving rise to the observed suppression. To determine whether the suppression arises due to an initial state effect, such as gluon saturation, or if it is a final state effect, RHIC collided deuteron and gold beams in Run-3. Figure 2.1 shows the PHENIX measurement of neutral pion yields per nucleon-nucleon collision in d+Au [27], compared to central Au+Au. It is clear that not only is there no suppression in d+Au, but there is even a slight enhancement, similar to that observed in lower energy collisions at Fermilab [38]. Thus PHENIX has unambiguously shown that suppression of high p_T particles is a final, rather than initial state, effect.

The experimental task in the future requires addressing several questions related to the detailed characterization of hot dense nuclear matter. The first is to extend the existing suppression measurements to high p_T and discover the momentum at which normal perturbative

QCD behavior returns. There are various predictions as to where the return to perturbative physics should occur; experimentally, considerably larger reach in p_T than the current ≈ 10 GeV/c will be required to address this. A factor of at least 50 more statistics is needed, and dictates long running time with high luminosity. PHENIX is extremely well-suited to do this measurement as our sophisticated multi-level trigger system provides excellent triggering capability for high momentum π^0.

The next experimental task is to quantify the energy loss and determine what becomes of the energy that is lost. Is it thermalized and thereby simply serves to heat the medium? Or are some additional particles produced, moving collinearly with the remnants of the modified jet? It has already been observed that the yield of intermediate and high momentum particles 180° in azimuth from a jet-like high p_T trigger particle decreases tremendously in central Au+Au collisions [39]. However, it is currently unclear whether these "away-side" jets are simply broadened or whether the energy otherwise carried by jet remnants is fully absorbed by the medium. Such questions are best addressed by study of correlations of two or more high and intermediate momentum particles.

The optimum observable to probe medium effects upon traversing partons is the γ+jet coincidence. Such coincidences result from the QCD Compton process, where the struck quark traverses the dense medium and then fragments into a hadron jet. The Compton scattering rate should be calculable perturbatively, and measurement of the energy of the tagged direct photon provides a good measure of the energy of the opposing jet prior to any modification. PHENIX is optimally designed to trigger on the photon and can collect a significant data sample, given sufficient integrated luminosity. We will then look at charged (and also neutral) particles near 180 degrees in azimuth, to determine how the jets are modified and how the modification depends on the volume of the produced medium. This is a critical measurement, as it is free of the "trigger bias" affecting jet-jet correlations measured to date. This bias arises when we require a high p_T hadron to select events with hard scattering. The rate of such hadrons is known to be suppressed, and those actually observed must - almost by construction - arise from those jets which are not modified by the medium. Consequently, selecting events with a high p_T hadron preferentially selects hard scatterings near the surface of the produced medium. As a direct photon traverses the medium unscathed, this bias does not apply to γ+jet coincidences. The measurement will also determine the broadening of parton k_T in nuclei, although interpretation is complicated by smearing due to energy loss of the jet and by photons from remaining π^0 decays [40]. Such measurements are of course luminosity limited, and a 14 week run at design luminosity yields a delivered integrated luminosity of just over 300 μb^{-1}. At this value of integrated luminosity, jets correlated with photons of 7-8 GeV energy can be measured [41]. With the RHIC luminosity upgrade, 1000 μb^{-1} is possible, providing reach to approximately 10 GeV photons with detected correlated jets.

PHENIX has already performed a number of correlations analyses of Run-2 Au+Au data. Techniques to disentangle azimuthal correlations from elliptic flow and from jet fragmentation are well in hand, as are experimental solutions to issues raised by the limited PHENIX aperture at mid-rapidity. We can quantify the yield of jet-like partners at both near and opposite sides in azimuth from a high p_T trigger partner, as well as study modifications of the

jet widths. In fact, PHENIX is uniquely positioned to study the flavor dependence of leading particles from jet fragmentation because of our excellent particle identification coupled with good data acquisition bandwidth (see in particular the discussion of the particle identification upgrades presented in Section 3.2.1). All such analyses, however, are severely hampered by the limited statistics available in the Run-2 Au+Au sample. Additional statistics corresponding to a factor of 50-100 more events with high p_T particles will allow correlation studies using higher momentum particles, where confusion from residual angular correlations from elliptic flow is much, much smaller.

Both the single high p_T hadron and jet correlations measurements also require further "control" experiments to allow unambiguous interpretation of the results. Baseline measurements in p+p collisions will be greatly improved by use of data collected for spin studies with polarized protons. The existing d+Au data set is currently being utilized to study effects of cold nuclear medium on jet energy loss and fragmentation. However, statistical limitations in d+Au are also significant, and considerably higher integrated luminosity of d+Au will be required. In addition, it will be important to better determine at which $\sqrt{s_{NN}}$ the observed jet modifications begin. The strong suppression observed at RHIC was not seen in $\sqrt{s_{NN}} \approx$ 17 GeV collisions at the CERN SPS [42]. However, suppression is already present at $\sqrt{s_{NN}} =$ 130 GeV at RHIC. Therefore, we need Au+Au collisions at $\sqrt{s_{NN}} = 62$ GeV to provide an energy intermediate between the two. The energy is chosen to coincide with measurements at the CERN ISR of p+p and $\alpha + \alpha$ collisions. The integrated luminosity must be sufficient to measure these rare processes with sufficient statistical accuracy, despite their lower cross section at lower center of mass energy. Although the dependence of jet quenching on system size is studied by varying the impact parameter range in Au+Au collisions, the neutron skin complicates interpretation in the most central and most peripheral collisions. Furthermore, triggering difficulties make it difficult to probe truly small systems. Definitive understanding of dependence on the volume of hot medium requires a substantial run with small nuclei, such as Si+Si.

2.2.1.5 Baryon Puzzle and the Jet Fragmentation Functions

In the very first run of RHIC, at $\sqrt{s_{NN}} = 130$ GeV, PHENIX observed a surprising enhancement of baryon yields at high p_T [9]. This is also the case in $sqrts_{NN} = 200$ GeV Au+Au collisions, as illustrated in Figure 2.4 [21]. In central Au+Au collisions the ratio of baryons and antibaryons to pions at $p_T > 2$ GeV/c greatly exceeds that observed in p+p and peripheral Au+Au collisions, even reaching parity in the most central collisions. This surprising result has generated intense theoretical interest. Current explanations for the baryon excess favor enhanced importance of soft physics at intermediate p_T in central collisions due to hydrodynamic boost of particles arising from large pressure gradients established early in the collision [30, 31]. Indeed the yield enhancement of baryons is particularly sensitive to hydrodynamic flow, if hadrons are formed by recombination, or coalescence, of quarks drawn from a strongly flowing distribution [32, 4, 2].

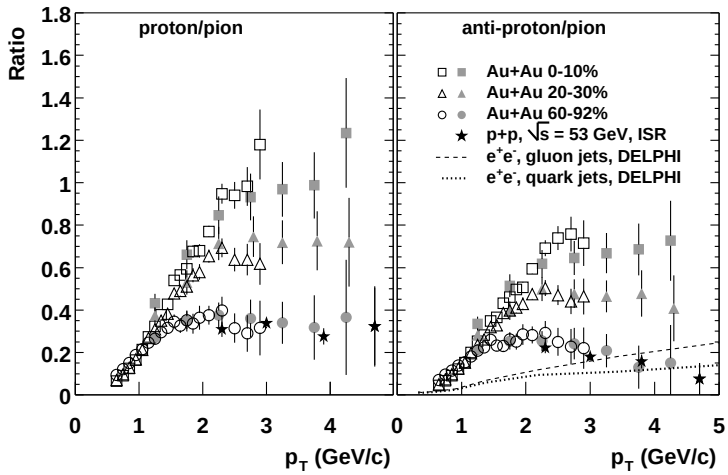

Figure 2.4: p/π (left) and $\overline{p}/\pi$ ratios for central(0-10%), midcentral(20-30%) and peripheral(60-92%) Au+Au collisions at $\sqrt{s_{NN}} = 200$ GeV. Open (filled) points are for $\pi^{\pm}$ (π^0), respectively. Data from $\sqrt{s} = 53$ GeV p+p collisions [43] are shown as stars. The dashed and dotted lines are the $(\overline{p}+p)/(\pi^+ + \pi^-)$ ratio in gluon and quark jets [44].

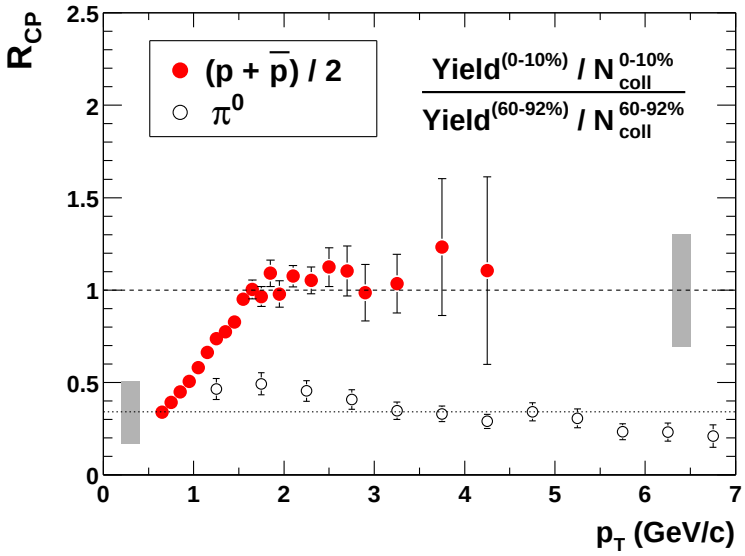

Figure 2.5: Modification factor, R_{CP} for $(\overline{p}+p)/2$ (filled circles) and π^0. R_{CP} is the ratio of yield per binary NN collision in central Au+Au to peripepheral Au+Au. Dashed and dotted lines indicate N_{coll} and N_{part} scaling.

Though such explanations can successfully reproduce the data, they fail to explain why the yield of baryons at p_T = 2-4 GeV/c scales with the number of nucleon-nucleon collisions, while the pion yields are suppressed, as illustrated in Figure 2.5. It would be surprising, indeed, if the parton "knows" ahead of time that it will fragment into a leading baryon and therefore loses less energy. The experimental observation suggests, instead, that the observed proton excess arises due to some sort of medium modification of the jet fragmentation function. Such a modification should cease to be possible for sufficiently high momentum partons, which fragment outside of the medium. Figure 2.6 may in fact provide some first evidence that this is so. However, the return to "normal" hadron ratios for jet fragmentation may also be due to changeover of production mechanism from parton recombination to fragmentation of (suppressed) jets.

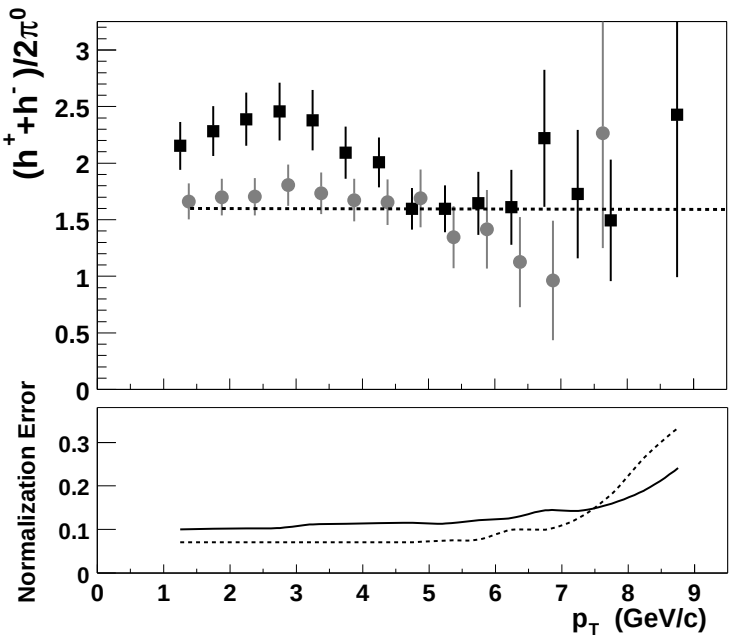

Figure 2.6: Charged hadron to π^0 ratio in central (0-10% - squares) and peripheral(60-92%) Au+Au collisions. The peripheral data points are offset by +130 MeV/c for clarity. The line at 1.6 is the h/π ratio measured in p+p collisions [43]. The lower panel shows the fractional normalization error common to both centrality selections (solid) and the relative error between the two (dashed).

Using the Run-3 d+Au data, PHENIX has measured the difference in the Cronin enhancement of π^0 and inclusive charged hadrons [27]. We observe a difference at intermediate values of p_T, illustrated in Figure 2.7. Furthermore, there is a larger Cronin enhancement for baryons than for mesons, and the baryon Cronin enhancement grows faster with the number of nucleon-nucleon collisions in d+Au than that for the mesons. Figure 2.8 shows the results for identified baryons and mesons in d+Au. These data indicate that already in the cold nuclear medium encountered by partons in d+Au collisions, a difference in the production of $p_T > 2$ GeV/c baryons and mesons is present. Any possible medium modification of jet

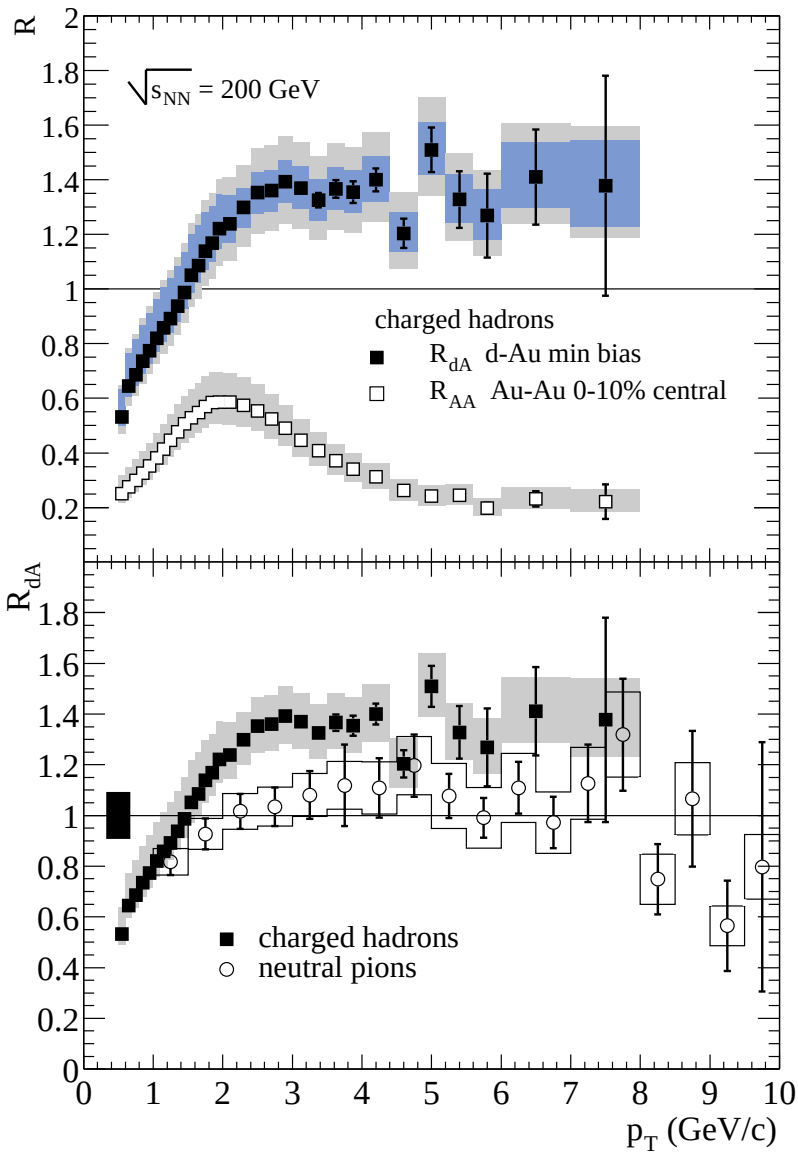

Figure 2.7: Top: Nuclear modification factor, R_{AA} for $(h^+ + h^-)/2$ in minimum bias d+Au compared to R_{AA} in the 10% most central Au+Au collisions. Bottom: Comparison of R_{dA} for $(h^+ + h^-)/2$ and π^0.

fragmentation should have visible consequences in d+Au collisions, and the data may indeed indicate that this is the case.

Differentiating between the two kinds of explanations for the baryon excess will require more data, with extended particle identification capability, and more complex analyses. Correlation analyses searching for jet-like partners accompanying the "extra" high p_T baryons and antibaryons are currently limited by statistics. A factor of at least 50 increase in events is necessary to study the centrality evolution of jets with leading baryons. Identification

of the non-leading jet fragments is also of paramount interest, but suffers similarly from inadequate statistics in the existing data sets.

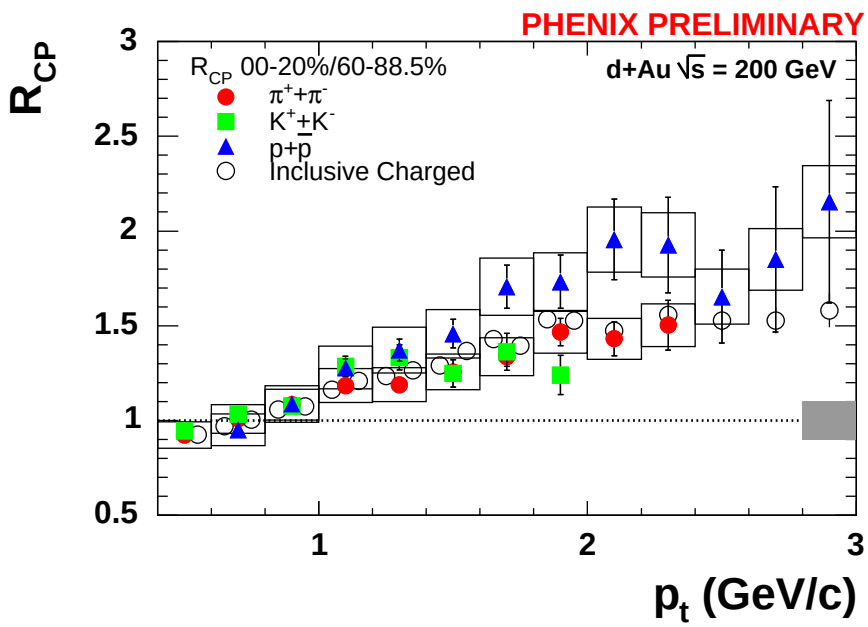

Figure 2.8: The nuclear modification ratio, R_{CP} as a function of p_T for identified charged pions (closed circles), kaons (squares), protons and antiprotons (triangles), and inclusive $(h^+ + h^-)/2$ (open circles).

Quantifying a change in the fragmentation function in nucleus-nucleus collisions requires a good understanding of the baseline fragmentation function in p+p and d+Au collisions. The jets studied at RHIC to date are rather low energy by perturbative QCD standards, and it is known that such jets fragment into fewer particles than in the e^+e^- collisions currently used to tune jet fragmentation algorithms. While fragmentation function analyses of p+p and d+Au are underway using standard particle physics jet algorithms, there is currently not enough data to form a definitive baseline. The job becomes even harder in Au+Au collisions, where large subtractions of combinatorial background underneath two-particle and multi-particle correlations must be performed. Significantly larger data sets of each system will be required, as well as for an intermediate sized system to carefully control the volume of the hot, dense medium.

It is also imperative to increase the particle identification capability of PHENIX to better separate baryons and mesons to higher p_T. The aerogel upgrade discussed in Sections 3.2.1 serves exactly this purpose. Sufficient statistics must be collected with Au+Au, p+p, and d+Au collisions once the aerogel upgrade has been installed and commissioned.

We have discussed comparisons with predictions of perturbative QCD and the need for larger p_T reach to make contact with pQCD possible. It will also be crucial for PHENIX to measure direct photons at high momentum, as presented in the following section.

2.2.2 Direct Photons

High-momentum direct photon production is the gold-plated testing ground for QCD in p+p (unpolarized as well as polarized), p+A and A+A collisions. The dominant subprocess is

$$g + q \rightarrow \gamma + q \qquad . \tag{2.1}$$

The photon is a direct participant which emerges unscathed from the constituent scattering in p+p, p+A and A+A collisions and which can be detected and measured to high precision. At low p_T, detection of direct photons is limited primarily by the background from $\pi^0 \rightarrow \gamma+\gamma$ while at higher p_T where γ/π^0 increases ($\propto x_T$) the limitation is due the merging of the two photons from π^0 decay to mimic a single photon. In PHENIX, the high segmentation of both the PbGl and PbSc calorimeters allows the two photons from π^0 decay to be resolved and separated from a single photon up to $p_T(\pi^0) \leq 25$ GeV/c, which we take for the present discussion as the nominal upper limit for direct photon measurements without using an isolation cut.

The principal physics issues in direct photon production are:

- Measurement of the gluon structure function in p+p collisions
- Measurement of the gluon spin structure function
- Test of jet suppression in A+A collisions since the photon should not be suppressed as it does not strongly interact with the medium
- Second test of jet suppression in A+A collisions, which if due to gluon condensation in the initial state would also suppress direct photon production
- γ+Jet measurements in p+p and A+A collisions i) to measure k_T of the γ-Jet system, which is controversial in the theoretical community, ii) as a measurement of jet suppression where the jet energy is known (since it must balance the γ p_T).
- Measurement of shadowing of the gluon structure function in p+A collisions, which i) has never been measured, ii) is vital to interpreting the A+A results for jet suppression of hadrons.

2.2.2.1 The gluon structure function in p-p and p+A collisions

The gluon structure function of the proton is best measured by direct photon production in p+p collisions. As noted by Ansari [42] (and others) the gluon structure function determined in DIS by the evolution of $F_2(\nu, Q^2)$ is at too low a Q^2 to be meaningfully extrapolated to p-p collisions.

The present status of the gluon structure function measured by direct photon production in p-p collisions is shown in Fig. 2.9

There are huge systematic discrepancies among the experimental data, most notably as a function of $x_T = 2p_T/\sqrt{s}$, as different experiments measure at different accelerators with different c.m. energies. Clearly, a measurement of the gluon structure function by

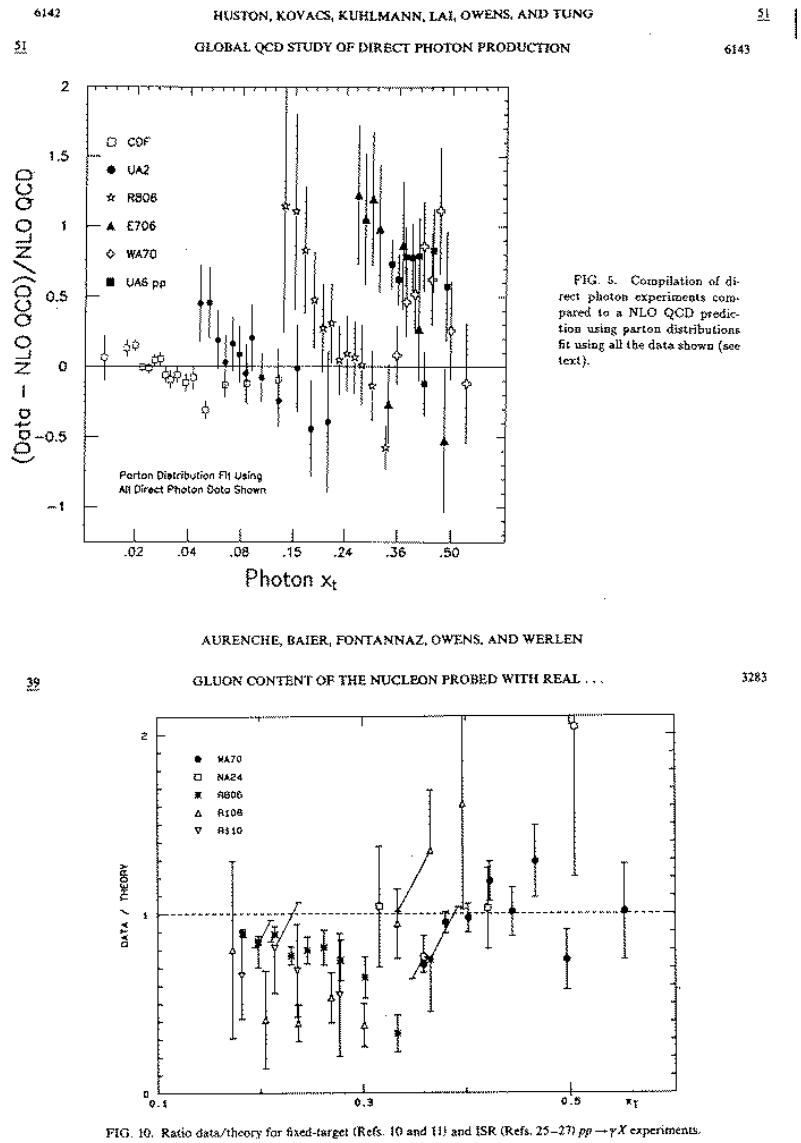

Figure 2.9: Two versions (upper [45] and lower [46]) of direct photon cross section compared to NLO QCD with best gluon structure function.

one experiment over the range $0.02 \leq x_T \leq 0.50$ would remove all of the inter-experiment and inter-accelerator systematic errors and provide the ultimate measurement of the gluon structure function. This is possible using the PHENIX experiment (without further upgrades) which can separate direct photon production from the two-photon background over the range $5 \leq p_T \leq 25$ GeV/c over the whole c.m. energy range that RHIC can provide: $x_{max} = 26/31.2 = 0.80$ (limited to 0.33 by luminosity) to $x_{min} = 5/250 = 0.02$. Measurement of photons emitted at 90° as a function of $\sqrt{s}$ in a fixed detector at a collider guarantees that all systematic errors are common to the whole measurement and cancel when comparing measurements at different $\sqrt{s}$. With an upgrade to an end-cap calorimeter covering the

Table 2.3: Physics yields from the extended PHENIX run plan for 37 cryo weeks per year. The precise timing, duration and sequence of the segments beyond 2010 (labeled as "aa", "bb", etc.) are not known and must be balanced against the priorities of the heavy ion and spin programs. Note: if the region $0.24 \leq x \leq 0.33$ is deemed interesting, a p+Au run may be needed for 15.7/A pb^{-1} at 62.4 GeV. Also run "dd" could be split into half and half p+Au and p+Si since it is for low x. In the calculation of x_T^{max} for photons it is assumed that γ/π^0=0.1.

Run	**Species**	$\sqrt{s_{NN}}$ **(GeV)**	Phys. wks.	$\int \mathcal{L}dt$ **(rec.)**	**J/$_\psi$ N.Arm**	π^0 p_T^{max} **(GeV/c)**	γ p_T^{max}	γ x_T^{max}
4	Au+Au	200	19	203 μb^{-1}	2700	19.0	14.8	0.15
	p+p	200	5	0.5 pb^{-1}	750	13.5	10.5	0.11
5	Si+Si	200	14	4.7 nb^{-1}	3460	17.3	13.4	0.13
	p+p	200	10	3.8 pb^{-1}	6030	17.3	13.4	0.13
6	Au+Au	62.4	19	45 μb^{-1}	120	10.4	8.1	0.26
	p+p	500	2	2.1 pb^{-1}	9,400	22.4	17.4	0.07
7	p+p	200	22	76 pb^{-1}	122,000	24.9	19.4	0.19
		62.4	5	2.7 pb^{-1}	880	11.0	8.6	0.27
8	Au+Au	200	19	1503μb^{-1}	20,000	24.1	18.7	0.18
9	p+p	500	29	377pb^{-1}	1.7M	41.9	32.7	0.13
10	d+Au	62.4	29	2.3nb^{-1}	182	9.6	7.5	0.24
aa	p+p	62.4	29	15.7 pb^{-1}		13.3	10.4	0.33
bb	p+Au	200	29	100/A pb^{-1}		25.7	20.0	0.20
cc	p+Si	200	29	100/A pb^{-1}		25.7	20.0	0.20
dd	p+Au 250 100	316	29					low

aperture of the muon arm, PHENIX can extend the measurements to even lower values of x, which may be of interest for shadowing measurements in p+A collisions.

In Table 2.3, the upper limits of direct photon measurement in both $p_T^{\max}$ and $x_T^{\max}$ are presented for the set of proposed runs found in the most recent PHENIX Beam Use Proposal [47]. The table has been supplemented with several additional runs: a full year p+p run at $\sqrt{s} = 62.4$ GeV to extend the x_T range; p+Au and p+Si runs at $\sqrt{s_{NN}} = 200$ GeV to measure the shadowing in the gluon structure function; a p+Au run at the highest possible $\sqrt{s_{NN}}$, with asymmetric energies, so as to get to the lowest values of x_T while still keeping the photon $p_T > 5$ GeV/c. During the p+A runs, di-muon data probing other

structure functions will also be taken and benefit from the large integrated luminosity. It should also be clear from this exercise that, after taking into account continued heavy ion and spin running in the period 2010+, the range of fundamental physics topics accessible to PHENIX extends even beyond the scope of this decadal planning exercise.

2.2.2.2 Polarized proton collisions

For any of the runs in table 2.3 involving protons, it is assumed that the protons will be polarized. For p-p runs, the gluon spin structure function will be measured, as described in detail in Section 2.3. For p+A runs, the protons can be transversley polarized to study possible single-spin transverse effects in direct photon, π^0 and di-lepton production.

2.2.2.3 A+A collisions

Direct photon production in A+A collisions provides a stringent test of gluon saturation in the initial state. Since the outgoing photon is a participant in the hard scattering which does not strongly interact with the medium, the gluon structure function measured in p+A collisions must give the correct prediction for direct photon production in A+A collisions unless the quark structure functions are saturating or other unexpected phenomena are at work in A+A collisions.

The photon also allows a precision measurement of the medium effect on the outgoing quark jet opposite to the direct photon, since the measured p_T of the photon must balance the original p_T of the quark partner produced in the reaction $g + q \rightarrow \gamma + q$. Modulo any k_T effects, measurement of the difference in energies of the jet or leading π^0 compared to the trigger photon as a function of centrality and A, should give the most precise and clearly understandable measurement of the medium effect. The effect of k_T or transverse momentum imbalance of the jets can also be directly measured from the acoplanarity of the γ-Jet system [42]. It is interesting to note that the importance of k_T effects in NLO calculations of direct photon production is a controversial subject. The experiments either measure k_T [42], or infer k_T from the smearing required to remove the discrepancies with theory shown in Fig. 2.9 [48], while some theorists, notably Aurenche [46] insist that k_T is already included in the NLO calculations. Clearly measurement of both the inclusive γ cross section and k_T in the same experiment will resolve this issue.

2.2.2.4 Direct Photon Appendix—Effect of End Cap EMCalorimeter Upgrade

The proposed End Cap EMcalorimeter for muon triggering discussed in Section 3.2.5 will cover a nominal pseudorapidity range of $1.25 \leq \eta_1 \leq 2.5$. The direction $y_1 = \eta_1$ of the forward quark jet (assumed massless for the purpose of kinematics) is measured by the maximum in the peak of the jet EM energy distribution. The direct photon is detected, as usual, in the central detector, over the range $-0.35 \leq y_2 \leq +0.35$, where e.g. plus points to the north muon arm. The constituent kinematics can then be reconstructed as follows.

$Y = (y_1 + y_2)/2$ is the rapidity of the c.m. system of the constituent-scattering in the overall p-p c.m. system. Clearly for both a photon and jet detected at 90°, $y_1 = y_2 = 0$,

$Y = 0$ so the constituent-scattering c.m. system is the same as that of the p-p collision. The invariant mass squared of the constituent scattering is $\hat{s} = x_1 x_2 s$, where s is the p-p c.m. energy squared and x_1, x_2 are the Bjorken energy fractions of the initial constituents in the proton. Given the measured Y, x_1 and x_2 can be calculated as a function of $\hat{s}/s$:

$$x_1 = \sqrt{\frac{\hat{s}}{s}} e^{Y} \qquad x_2 = \sqrt{\frac{\hat{s}}{s}} e^{-Y} \qquad . \tag{2.2}$$

The scattering angle θ^* of the photon in the constituent-scattering c.m. system is given by

$$\cos\theta^* = \tanh(y_2 - Y) = \tanh(\frac{y_2 - y_1}{2}) \qquad , \tag{2.3}$$

and we can find the p_T of the photon for a given $\hat{s}/s$, y_1, y_2 compared to that of a photon detected at $\theta^* = 90°$ in the constituent-scattering c.m. system, $p_T(\sin\theta^* = 1)$, for the same $\hat{s}/s$:

$$p_T = p_T^* = \frac{\sqrt{\hat{s}}}{2} \sin\theta^* = p_T(\sin\theta^* = 1) \times \sin\theta^* \qquad . \tag{2.4}$$

The detection of the away jet in the range $1.25 \leq \eta_1 \leq 2.25$ coupled with the direct photon in the range $-0.30 \leq y_2 \leq +0.30$ allows x_2 for the γ-jet reaction to be a factor of 0.3 times smaller than the x_T of an inclusive direct photon detected at 90° for the same value of $\hat{s}/s$ as given in Table 2.3. This will be particularly beneficial for the p+A measurement where 'shadowing' or gluon condensation should be more favored at the lowest values of x. For polarized p-p measurements, the γ-Jet coincidence for a given $\hat{s}/s$, gives a lower value of x_2 and a higher value of x_1 than the single inclusive measurement, allowing the low x measurement to profit from the higher proton polarization at larger x_1.

2.2.3 Thermal Radiation

Measuring thermal direct photons, both real and virtual, has been a longstanding goal in the field of relativistic heavy ions, since they offer the promise of being able to view and diagnose directly the initial thermalized state of a nuclear collision. Such a diagnosis is complicated by two sets of problems, however: (1) Experimentally the measurement is very challenging, due to the large background rates - for di-leptons, from Dalitz decays and conversions, and for photons, from hadron decays; and (2) the radiation from the early thermal stage must be disentangled from radiation from other sources, particularly the later thermal stages and initial hard parton scatterings.

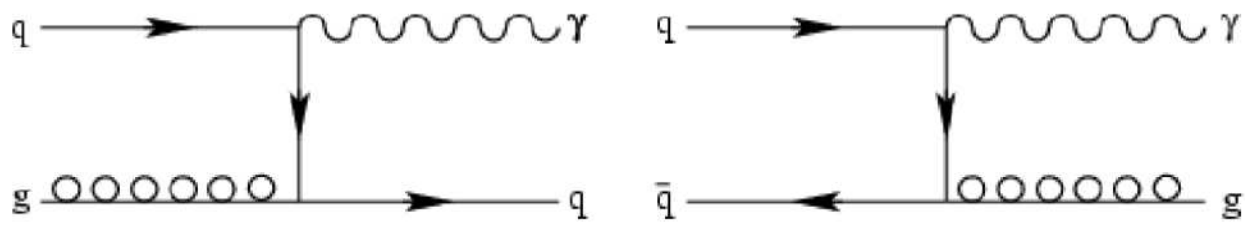

Figure 2.10: Lowest order diagrams for photon production in a plasma. Left: Compton scattering, Right:quark anti-quark annihilation into a photon and a gluon.

Thermal di-leptons are produced from quark anti-quark annihilation. Direct photons are suppressed in this channel since momentum and energy conservation do not allow quark anti-quark annihilation to produce real photons. The primary source of real photons are the diagrams as shown in Fig. 2.10. Photons and di-leptons (both muon and election pairs) give complementary sets of information in that the backgrounds are different depending on the kinematical region.

2.2.3.1 Thermal Di-Leptons: Predictions and Previous Experimental Results

In the case of di-leptons, the spectrum can be studied, not just as a function of the energy or p_T, but also as a function of the mass allowing one to find regions where the thermal spectrum may be the dominant source. In the low mass region, di-leptons from the light vector mesons are expected to dominate the spectrum, while at high mass it is the heavy vector mesons (J/ψ, Υ) and Drell-Yan production which are of interest. It is in the intermediate mass region $1 < M(l^+l^-) < 3$ GeV (that is, between the ϕ and J/ψ masses) where the thermal component of the di-lepton spectrum is expected to be most easily accessible.

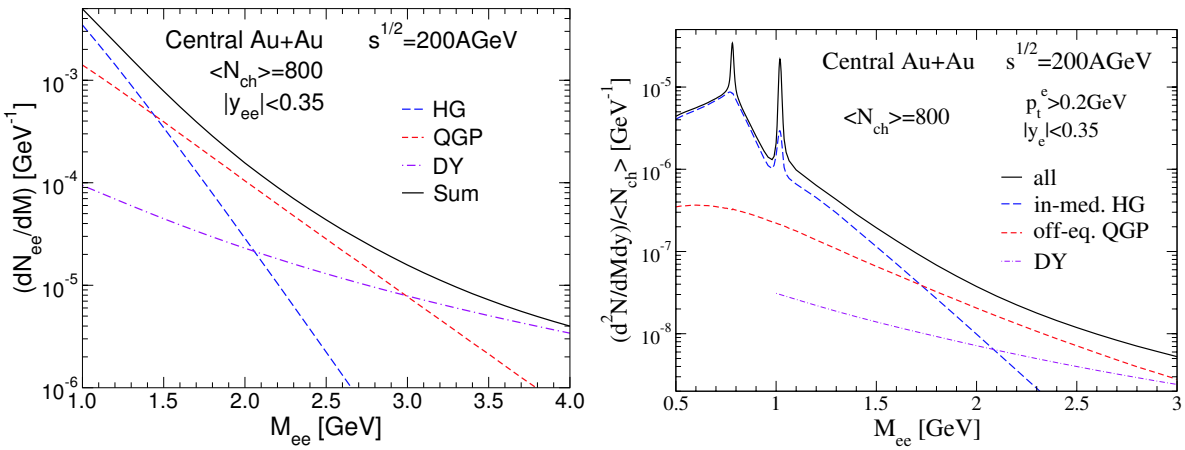

Figure 2.11: Left: Intermediate-mass di-lepton spectra at RHIC energies around midrapidity assuming a chemically equilibrated QGP throughout its lifetime. Shown is the decomposition of the thermal fireball radiation (with $T_0 = 370$ MeV, $t_{fo} = 20$ fm/c) into QGP (short-dashed line) and hadron gas (long-dashed lines) parts (including their respective yields from the mixed phase), compared to Drell-Yan annihilation (dashed-dotted line) and the total sum (note that open charm decays are not accounted for). It is the regions between about 1.5 and 3 GeV where the QGP contribution is expected to dominate over other contributions. Right: Total di-lepton spectrum from b = 1 fm Au+Au collisions at RHIC energies around midrapidity including schematic experimental acceptance cuts appropriate for the PHENIX experiment (ρ, ω, and ϕ cocktail contributions are not separately shown but included in the solid curve). As in the left plot, the semileptonic decays of correlated anti-/charm and anti-/bottom quarks are not included [49].

Figure 2.11 shows the contribution of the hadron gas and the quark-gluon plasma (via quark anti-quark annihilation) to the di-lepton mass spectrum. Details of the calculations shown in Fig. 2.11 are described briefly in the discussion of light-vector mesons (Section 2.2.4) and in detail in Reference [49]. One can see that the thermal contribution dominates the spectrum between about 1.5 and 3 GeV. It is important to note that the yield from correlated leptons pairs from charm pairs is not included in these results. Initial calculations from the extrapolation from p+p collisions indicated that these backgrounds could be quite substantial. Subsequent calculations which included the thermalization of charm showed a softened spectrum thereby reducing the contribution to the background for thermal pairs in the 1-3 GeV region. [50, 51] However, recent measurements from PHENIX suggest that charm may not be suppressed. [11] In any case, it is critical that a good measurement be made on charm production in the relevant kinematic regions, as discussed in Section 2.2.5.

Measurements in this mass region have been pioneered by the Helios collaboration and continued by the NA50 collaboration, both in p+p and A+A collisions. These experiments have seen excesses in the IMR (intermediate mass region). Various models, with and without a deconfined plasma phase are able to explain these excesses, as shown in Figures 2.12 and 2.13.

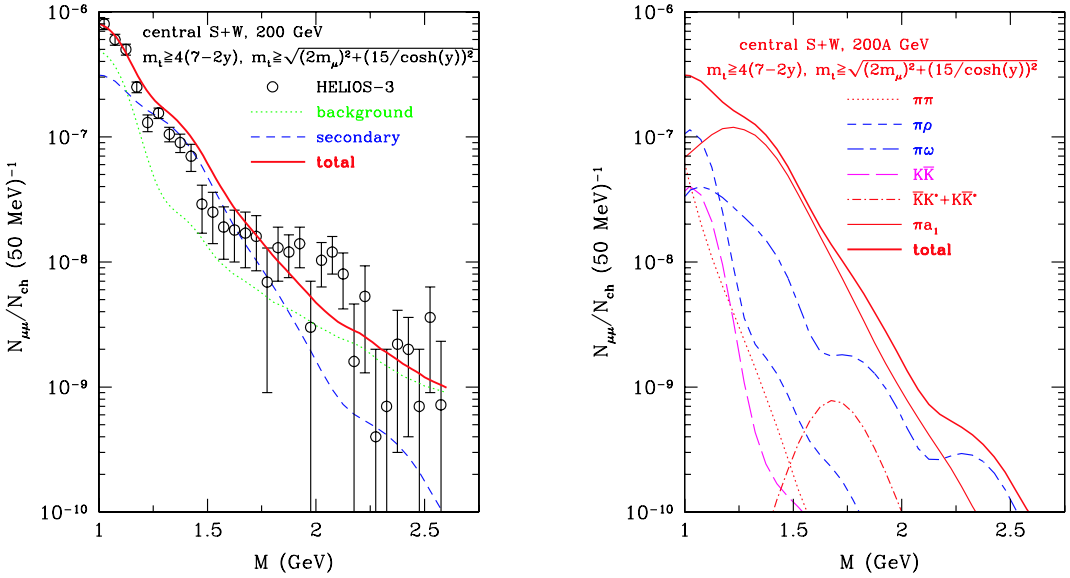

Figure 2.12: Left: HELIOS-3 dimuon data [52] from central S+ compared to the standard background (consisting of Drell-Yan and open charm) and the additional yield from secondary hadronic annihilation processes evaluated within a transport model [53]. Right: decomposition of the secondary reactions [53].

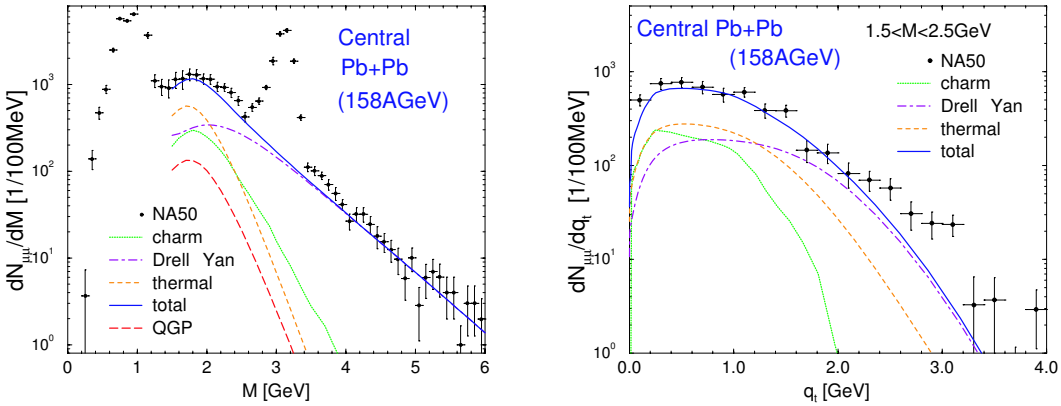

Figure 2.13: Dimuon mass (left) and transverse-momentum (right) spectra from NA50, central Pb(158 AGeV)+Pb collisions [54]. Calculations for the thermal contribution are from [55]. Contributions for open-charm yield from simulations by NA50 have been included.

2.2.3.2 Photons: Previous Experimental Results and Predictions

There have been two significant measurements of the direct photon spectrum from heavy-ion collisions, both in the SPS fixed-target program. The WA80 experiment published [56] upper limits on the direct photon spectrum in the range $p_T < 3$ GeV from S+Pb collisions at 200 AGeV. Similar results have been published by CERES. [57] These have been interpreted [58] as setting upper limits on the possible temperatures of an initial thermalized system; but theoretical opinion to date remains divided as to whether the WA80 upper limits can or cannot definitively rule out a a non-QGP scenario in the S+Pb system at SPS energies (see, for example, the recent review by Gale and Haglin [59]).

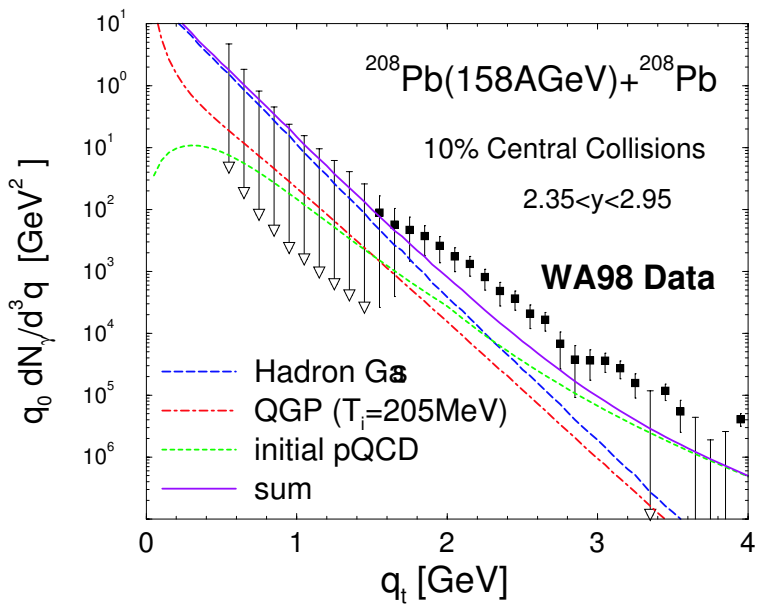

Figure 2.14: A calculation of the spectra from different sources of direct photons for central Pb+Pb collisions at CERN-SPS. [60]

The WA98 experiment published [62] the first measurement (ie upper *and* lower limits) on the spectrum of direct photons from heavy-ion collisions, in the range $1.5 < p_T < 4$ GeV from Pb+Pb collisions at 158 AGeV. These have inspired a new wave of theoretical interpretation of increasing sophistication. This work continues to evolve; the most recent view ([59, 60]) can be summarized in a few points: (i) For nominal assumed initial temperatures of a QGP phase, about 200 MeV, thermal radiation is dominated by the later hadron gas stage despite its lower intrinsic temperature, due to its longer lifetime and substantial boost to the effective observed temperature from radial flow. This is illustrated in Figure 2.14 from the recent work of Turbide, Rapp and Gale [60]. (ii) The data below 2 GeV can be explained by hadron phase radiation, but this source will underestimate the rate in the rage 2-4 GeV. (iii) The rate at higher photon energy can be explained either by an initial QGP state at much higher temperature, approaching 300 MeV, or by hard parton scatterings with substantial intrinsic momentum (k_T). See, for example, Figure 2.15 [61].

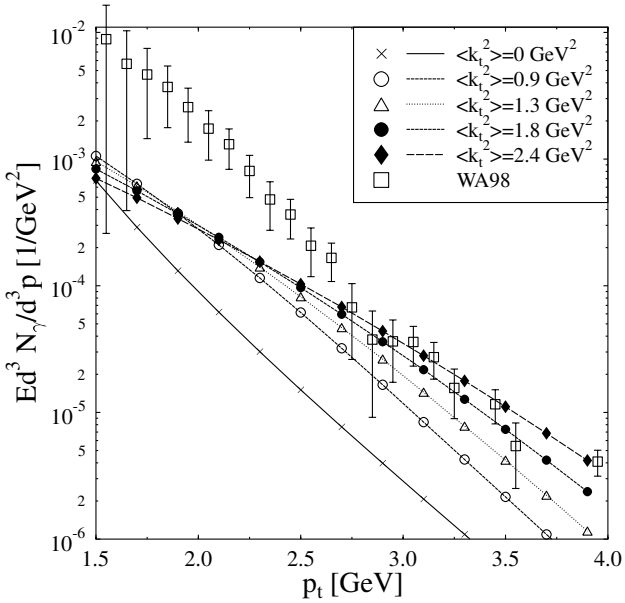

Figure 2.15: Rates for pQCD direct photons under different assumptions of intrinsic parton k_T, compared to the WA98 data, for Pb+Pb collisions at CERN-SPS. Figure is taken from [59] for calculations by Dmitru, et.al.[61]

The ambiguity between a hot initial QGP and substantial parton intrinsic k_T is difficult to disentangle without more detailed understanding of the pQCD source (see the discussion in Section 2.2.2). Theoretical work remains ongoing, but there is not expected to be any new data at SPS energies in the near future.

2.2.3.3 Di-leptons: PHENIX rates and expectations.

PHENIX has as one of its primary strengths the ability to identify and measure electrons and muons to high precision using the RICH and the tracking detectors. However, the measurement of di-leptons faces some rather difficult challenges. Di-electrons have a significant combinatoric background coming from pion Dalitz decays and conversion electrons. A major thrust of the PHENIX upgrades program is the design, construction and installation of a Hadron Blind Detector (HBD), which together with a specially configured magnetic field will be capable of identifying such pairs so they can be essentially eliminated from the combinatoric background. The significant remaining background will come from the leptonic decay of charm.

The basic design of the HBD uses a near field-free region at the center of the tracking devices. Di-electrons from conversions and Dalitz decays will remain at very small angles to each other, and low momentum electrons will not be curled up in a magnetic field. The HBD, which is located in the field-free region, is a Cerenkov detector insensitive to hadrons (low-velocity particles) and is designed to do rudimentary tracking. This will allow close (small angle) pairs to be identified and eliminated from the tracks used to create invariant

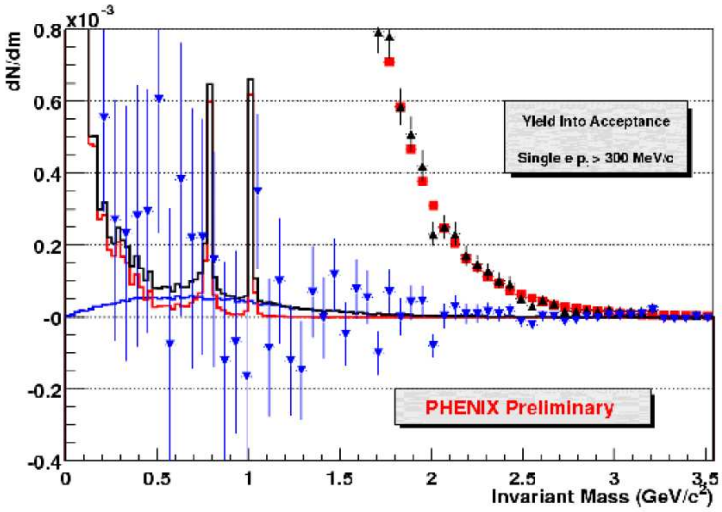

Figure 2.16: The PHENIX minimum bias continuum data are superimposed with Pythia scaled by the number of binary collisions for minimum bias charm production. Pythia is shown as the solid blue curve. Exodus, a PHENIX simulation for the low mass electron contribution form π^0's, η's, the vector mesons, and a variety of other "soft" contributions is shown as the solid red curve. The total of these sources is the solid black curve.

mass pairs and reduces the electrons from conversions and Dalitz decays of π^0's by 90%, thereby reducing the combinatoric background by nearly two orders of magnitude. At this point, electrons from charm begin to dominate the background. (Full details on the HBD are presented in Section 3.2.3.)

As noted, open charm production presents an intrinsic background to the measurement of thermal di-leptons. Initial charm measurements have already been made in PHENIX via single electrons [11]. More detailed charm measurements will come from the study of μ-e pairs, and with the addition of the proposed silicon vertex detector discussed in Section 3.2.2 a good understanding of both the yields and distributions of open charm will be obtained. The detailed understanding of the charm contribution to the di-lepton spectrum from the measurements made by the silicon vertex detector, as well as the rejection of Dalitz and conversion pairs by the HBD are critical upgrades necessary for making this measurement.

Figure 2.16 shows a first measurement of the electron pair mass in Au+Au collisions. Two regions were defined to quantify the excess of continuum electron pairs. The first is the low mass region (LMR) between .3 and 1 GeV, which includes also the ρ and ω. The second is the intermediate mass region (IMR) between 1.1 GeV and 2.5 GeV. These measurements yielded limits on the yield of excess di-electrons of in the LMR of $dN/dm = 10.6 \pm 5.2(stat)^{+9.4}_{-6.5}(sys) \times 10^{-5}$ per GeV/m^2 per event. and in the IMR $dN/dm = 0.27 \pm 1.84(stat)^{+1.0}_{-0.53}(sys) \times 10^{-5}$ per GeV/m^2 per event. This is to be compared to the prediction from using free vacuum masses for the vector mesons and an assumption of scaling by the number of participants and charm scaled by the number of binary collisions which gives 11.4×10^{-5} per GeV/m^2

per event for the LMR and 1.5×10^{-5} per GeV/m^2 per event for the IMR.

					HBD??		HBD in
Run		4a	5a	5b	6	7	8
Species		Au+Au	Si+Si	p+p	Au+Au	p+p	Au+Au
sqrt(s)		200	200	200	62.4	200	200
LMR	N	11060	7480	2267	4095	65059	75495
thermal	Nsigma	5	5	2	3	13	14
	Nsigma(HBD)	36	30	16	22	88	95
IMR	N	4512	3052	925	1671	26544	30802
thermal	Nsigma	3	3	1	2	8	9
	Nsigma(HBD)	22	18	10	13	53	57

Figure 2.17: Table showing the expected yield and significance of the thermal contribution to the di-electron continuum with and without the HBD. This assumes T_0= 380 MeV and T_C=180 MeV. More details are in [49]. The LMR is defined as between 0.3 and 1. GeV, and the IMR as between 1.1 and 2.5 GeV. This assumes that the charm contribution can be measured and subtracted exactly. The measurements for which the HBD will be available are in red.

Table 2.17 shows the yield and significance (Signal/σ) of the signal for the upcoming runs with and without the HBD. This assumes a thermal yield as calculated for the T_0 = 380 MeV case in Figure 2.11. These expectations are extrapolated from the measurement just mentioned which includes a p_T cut of 300 MeV to reduce the background. The HBD together with a field-free regions will allow us to reject much of the background without this cut, making us more sensitive to the low mass regions. As before, charm is not included in this calculation. Assuming binary scaling, charm contributes a similar amount as the thermal signal. With the upgrades, and assuming a yield similar to the model, PHENIX will be able to make a measurement of the thermal di-lepton spectrum.

2.2.3.4 Photons: PHENIX rates and expectations.

In the case of direct photons, we would expect prospects for observing initial-state radiation to be improved at RHIC compared to the SPS, on the general grounds that (i) the initial QGP phase should be hotter, and (ii) the hard parton scattering source can be investigated in great detail with the availability of p+p, p/d+A and a spectrum of light ion collisions. This situation is illustrated by Figure 2.18 for predicted rates of single direct photons in central Au+Au collisions at RHIC energies.

We can see that in this scenario the rate from an initial thermalized QGP phase now dominates that from any later hadron phase for all but the lowest p_T's. At very high transverse momenta the rate will be dominated by prompt pQCD sources, but in this calculation there is a window in the range 1-3 GeV in which the total rate is primarily due to the QGP phase, providing the possibility that its radiation can be observed directly. However, we cannot be

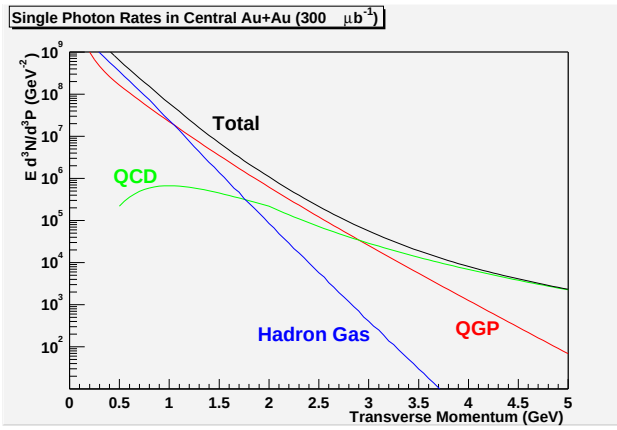

Figure 2.18: Rates published by Turbide, Rapp and Gale [60] scaled up to 300 inverse microbarns of Au+Au, or about 2×10^8 central collisions (0-10% Centrality).

sure we are seeing the QGP source unless we have confidence in our understanding of the prompt pQCD source – that we can constrain, among other things, the intrinsic parton k_T – and this can come only through a detailed, simultaneous examination of a range of data from p+p, p/d+A and A+A collisions. As the figure shows, raw rate is not a problem for observing the direct photon signal at RHIC. The limitations will instead be from systematics: first, the lower bound in p_T down to which the direct photon measurement can be made depends on how well the π^0 extraction, and other hadronic decay sources, are understood.

In the case of both the thermal direct photon, and di-leptons measurements the extraction of the initial thermal state radiation will depend on how well the other sources can be understood. In addition to production from hard initial scatterings, which was present in the direct photon signal at the SPS, RHIC will have additional possible sources of direct photons and di-leptons. First is a "pre-equilibrium" stage , which has been discussed theoretically but not addressed in workable detail (see [60]) and may involve as-yet undescribed physics. Another recently discussed possible source [63] is medium-induced photon bremsstrahlung from high-energy quark jets; it is hoped these can be investigated from measurements of correlations between high-energy photons and high-energy hadrons as a part of the program of investigating hard scattering phenomena in RHIC collisions.

The original promise of thermal direct photons and di-leptons as a direct diagnosis of the initial thermalized state remains compelling at RHIC. Equally compelling is the detailed stages of investigation in p+p and p+A collisions that will be required to remove long-standing ambiguities in the precision description of direct photon production in hadron collisions. Again, it is clear that extended periods of running are necessary to achieve the ultimate levels of quantitative rigor made available by RHIC's high center-of-mass energy.

2.2.4 Light Vector Mesons

2.2.4.1 Introduction

The QCD phase transition exhibits itself in two different ways. The first, and most well known is the deconfinement transition which accounts for the binding of quarks into hadrons. The second, but equally important phase phenomenon, is the chiral phase transition in which the right-left chiral symmetry of massless quarks gets broken as the quarks acquire their dressed quark masses from the QCD vacuum condensate. While it remains possible that these are two entirely different phase transitions, it is more plausible that they are two different manifestations of the same transition, since present indications are that the transition temperatures are the same.

It is this second phenomenon of chiral symmetry restoration which accounts for the masses of the hadrons; this is accompanied by the rather startling assumption that the vacuum is filled with a condensate of quarks and gluons. In a very similar manner, the leptons and bare quarks acquire their masses via the Higgs condensate which also fills the vacuum. It is also very likely that the formation of a condensate powered the early inflation of the universe. [64]

As such, it is important to understand the phenomenon of chiral symmetry breaking, and the manner in which the quark masses evolve from their current-quark values at very high temperature to their constituent masses which appear in "dressed" hadrons. Di-leptons in heavy ion collisions provide a unique opportunity to study directly the changes in mass at high temperature. In a heavy ion collision, chiral symmetry is presumably restored and the masses of the quarks drop to their bare quark values- which on the energy scale of interest 140 MeV, is essentially zero for the light quarks. Because the light vector mesons, such as the ω, the ϕ and particularly the ρ, have such short lifetimes, they will decay inside the fireball (especially since lifetimes are shortened if the widths increase, as expected in most models). Since leptons do not interact via the strong interactions, leptonic decays can yield information about the masses of the vector mesons in the hottest portion of the fireball, leading to predictions of shifts and masses or the broadening and "melting" of these resonances.

The direct calculation of chiral symmetry restoration has been studied extensively in lattice QCD. Such investigations assume a static system in thermal equilibrium, and examine the formation of the chiral condensate as the temperature falls below the critical temperature. The best estimates place the critical temperature at a similar temperature to that expected for the deconfinement transition, at about 170 MeV. One of the outstanding questions in the study of QCD is the precise relationship between the chiral and the deconfinement transition.

Calculations of the mass spectrum of the light vector mesons in actual heavy ion collisions are much more difficult since the system may not be in perfect thermal equilibrium, and because the time evolution may be very rapid. Theoretical calculations have taken basically two approaches. The first starts from the quark degrees of freedom and invokes the assumption that masses of the vector mesons scale like the chiral condensate [65]. The second approach starts with the hadronic degrees of freedom [66]. Both use an effective Lagrangian. Recent work has taken the point of view that these pictures are essentially equivalent descriptions of the same phenomenon, while their regions of validity are different - similar to the usage

of the orbital angular momentum-spin eigenstates vs total angular momentum eigenstates used for studying L·S coupling in elementary quantum mechanics. [67]

Heavy ion experiments provide the exciting opportunity to perform experimental investigations that can shed light on all of these questions- the relationship of the chiral and deconfinement transitions, the relationship between the quark picture versus the hadronic picture of the chiral phase transition and hadronic masses, and the structure of the QCD vacuum.

2.2.4.2 Predictions

Recently Rapp and Wambach have made predictions of the properties of the vector mesons, and the di-lepton mass spectrum at RHIC energies, beginning from assumptions on the time evolution and initial energy density [49]. They looked at the properties of in-medium vector mesons using hadronic chiral Lagrangians (the hadronic approach mentioned above). It is interesting that the spectral functions change primarily in response to the density of baryons. At RHIC, the *net* baryon density (baryons - antibaryons) is low, however the *total* density (baryons+antibaryons) is rather high and in fact similar to that at the SPS. This leads to a change in the spectral function of the vector mesons as shown in Fig. 2.19. The approach assumes a quark-gluon plasma at $T > T_C$, a mixed phase at $T = T_C$, and a hadron gas at $T < T_C$ with a time dependence as shown in left panel of Fig. 2.20.

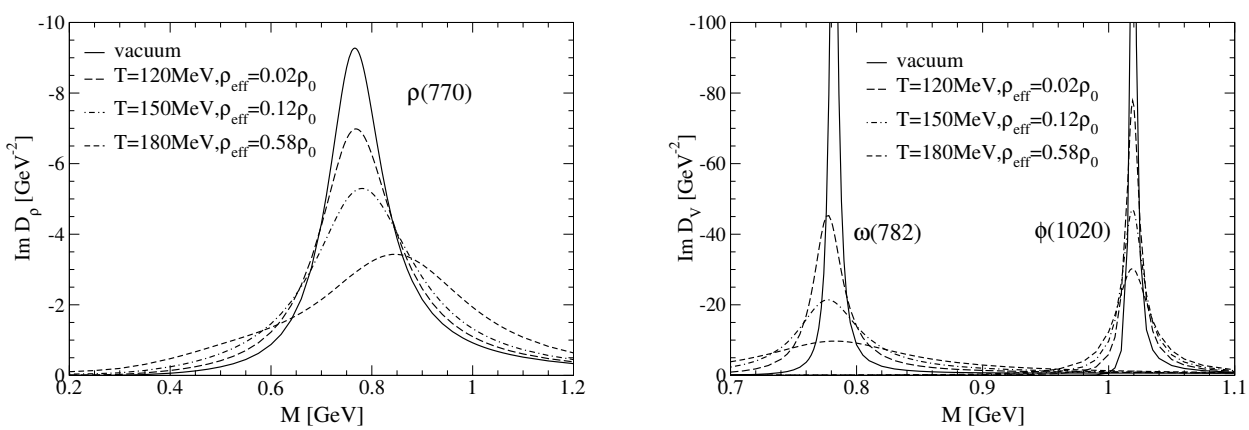

Figure 2.19: Spectral functions of the light vector mesons ρ (left panel) and ω and ϕ (right panel) in vacuum (solid lines) as well as in hot *net* baryon-poor hadronic matter as expected under RHIC conditions: (T;μ_N) = (120; 91) MeV (long-dashed lines), (T; μ_N) = (150; 40) MeV (dashed-dotted lines) and (T; μ_N) = (180; 27) MeV (short-dashed lines). For the definition of ρ_{eff} see [49].

Integration of the spectral function over the time evolution of the collision leads to the final result shown in the right panel of Fig. 2.20. Note that there are considerably more ρ's present then expected in p+p collisions where the ratio of ρ to ω mesons is 1. This is because of a regeneration effect in the pion-rich mixed phase, in which ρ mesons that are

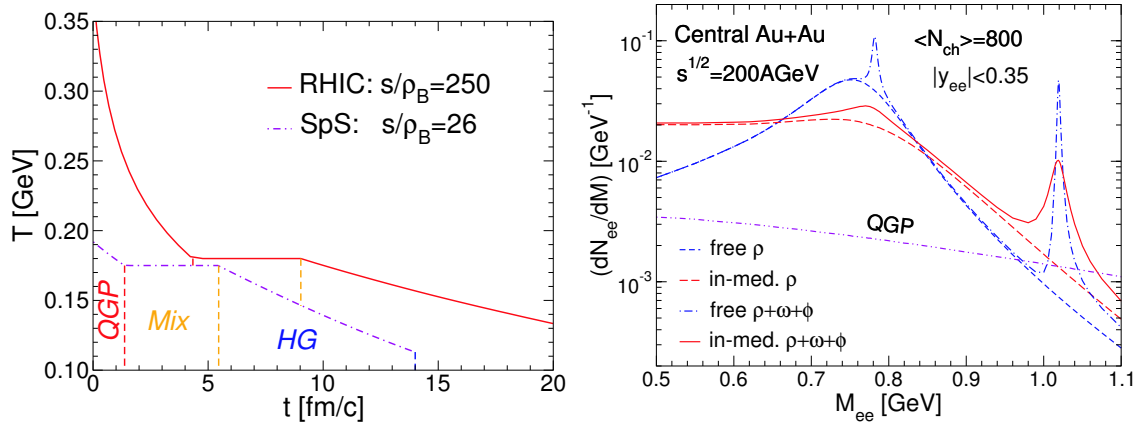

Figure 2.20: Left Panel: the time evolution assumed for the system. Right panel: the contributions to the final spectrum after integrating over the evolution of the system of various components with and without in-medium effects. Also shown is the contribution of perturbative $q\overline{q}$ annihilation (i.e. the QGP).

regenerated from pion interactions continuously decay into electrons. The ω does not have a strong two pion decay channel, and the density of kaons is too low for a similar effect to enhance the ϕ to such a strong degree. This enhancement of the ρ can be used as a clock to indicate the lifetime and/or the pion density of the mixed phase.

One can study the dependence of the invariant mass spectrum as a function of the centrality and transverse momentum of the pair. Changing the centrality changes the volume and energy density; more central events should exhibit stronger effects. Changing the transverse momentum changes the probability that the decay actually takes place outside the fireball since the lifetime of these vector mesons is of the order of several fermi, comparable to to the size of the system. These systematic trends provide a key experimental tools for investigating the phenomena. In peripheral collisions, or for pairs with high transverse momentum, ω's and ϕ's with a longer lifetime should decay primarily outside the fireball and thereby exhibit their vacuum masses and widths. This allows for an all-important baseline to be established in which the effects are not seen.

2.2.4.3 Previous experimental results

Two main experiments have seen evidence for such behavior. The first is the CERES experiment at CERN [68]. Fig. 2.21 shows the results from Pb+Pb collisions at $\sqrt{s}$=17.2 GeV. Shown in solid lines is the expected contribution from a variety of "ordinary" sources with their expected mass resolution. There is a strong enhancement between 200 and 600 MeV which has been attributed to the shifting and broadening of an enhanced ρ meson. As can be seen from the shape of the ω and ϕ expected yields, the mass resolution is not sufficient to see the vacuum ϕ and ω peaks above the background. The enhancement varies with transverse momentum and centrality as expected based on the arguments presented above. The second indication of mass effects in the di-electron spectrum comes from E325 at KEK in which

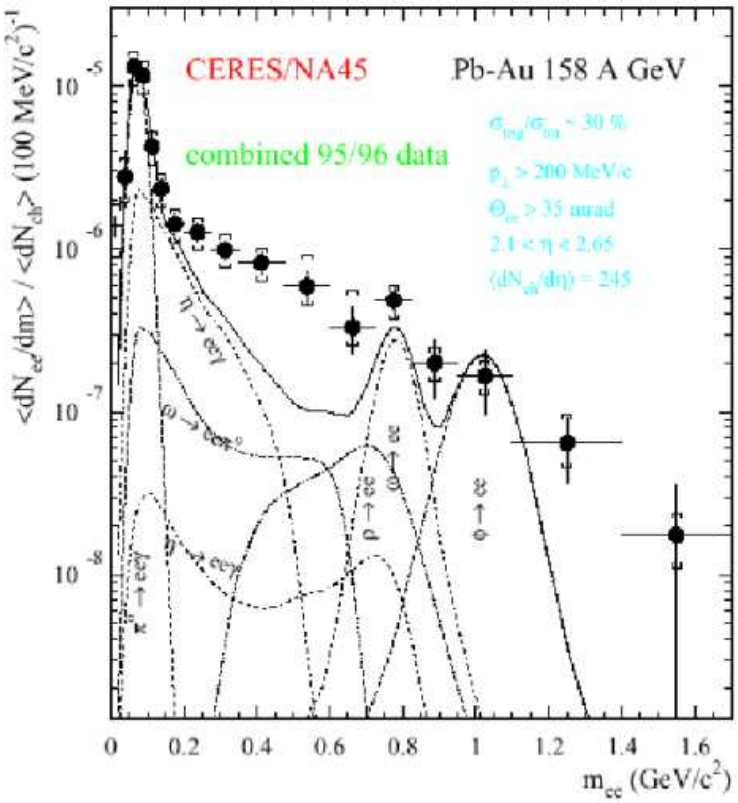

Figure 2.21: Di-electron spectra from the CERES experiment at CERN, showing a large excess at between 200 and 800 MeV in comparison to the expectation (solid line) from a variety of "normal" contributions.

p+A collisions were studied at $\sqrt{s}$=6.7GeV [69]. What is observed in proton collisions on a heavy target (Cu) is an enhancement below the ω (Fig. 2.22) which has been attributed to a modification of the ρ/ω invariant mass. Note that this effect is seen in p+A collisions, i.e. an indication that these effects may be present even in a cold nucleus.

2.2.4.4 PHENIX rates and expectations.

Measurements of the di-lepton spectrum for light vector mesons faces challenges similar to those for the thermal di-leptons discussed in Section 2.2.3.4. While it could be argued that the problems are somewhat less severe, since the rates are higher and at least some fraction the signal is expected to have a mass-peak structure, nonetheless the combinatoric backgrounds, triggering rates, and charm background are all obstacles to isolating the physics signal. The PHENIX program of upgrades, including the Hadron-Blind Detector for the rejection of Dalitz and conversion pairs (Section 3.2.3), the silicon vertex detector for the measurement of charm (Section 3.2.2), and the DAQ upgrades for data-taking speed (Section 3.3) are all crucial elements in the PHENIX strategy for performing these measurements. An important feature of the experimental approach will be careful control of the centrality measurements,

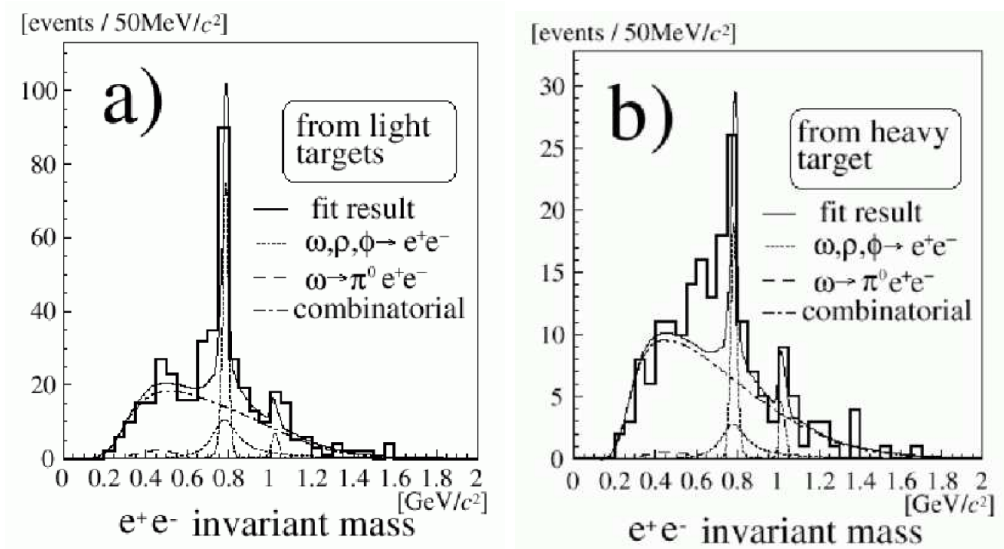

Figure 2.22: Di-electron invariant mass from E325 at KEK. Left panel: Invariant mass from light targets showing a normal vacuum behavior of the peaks. Right panel: Spectra from heavy (Cu) targets showing the excess below the vacuum ω.

since, as mentioned above, one of the predicted characteristic features is that the vacuum spectral shapes of the vector mesons should be clearly seen in peripheral collisions where medium modifications are expected to be small and much of the decay occurs outside the fireball. In addition, the first measurements of the ω and ϕ di-electron decays should be available from run-3 data for deuteron-gold collisions(already in hand) and from run-4 for gold-gold collisions. Most of the measurements will be performed using di-electrons, as the acceptance for di-muon masses below the ϕ mass is very small in the muon arms. We fully expect to measure the di-muon decay of the ϕ via di-muons, however, the mass resolution will be significantly worse than the roughly 2 MeV for the di-electron channel in the central arms.

The first measurements of the low mass vector mesons have been made looking at the di-kaon decay of the ϕ because of the relatively large branching ratio (Fig. 2.23). Because the kaon suffers from hadronic re-interactions, and because only about 10% of detected ϕ's are expected to decay inside the fireball (the lifetime is 40 fm/c), it is very unlikely that change in the spectral shape of the ϕ meson would be visible. However, this remains an important measurement. Since the Q value of the di-kaon decay is so small, any changes in the relative masses of the ϕ or kaons will change the branching ratio dramatically, while the branching ratio to electrons should stay relatively constant [70]. Once PHENIX has been able to measure the yield of ϕ mesons in the di-electron channel- a much easier task than measuring the spectral shape- comparison with the measured di-kaon yield could give a first indication of chiral symmetry restoration. Fig. 2.23 also shows the first suggestion of the di-electron decay of the ω in deuteron-gold collisions.

Yields of the ρ ω and ϕ as expected in the PHENIX detector are shown in table 2.24.

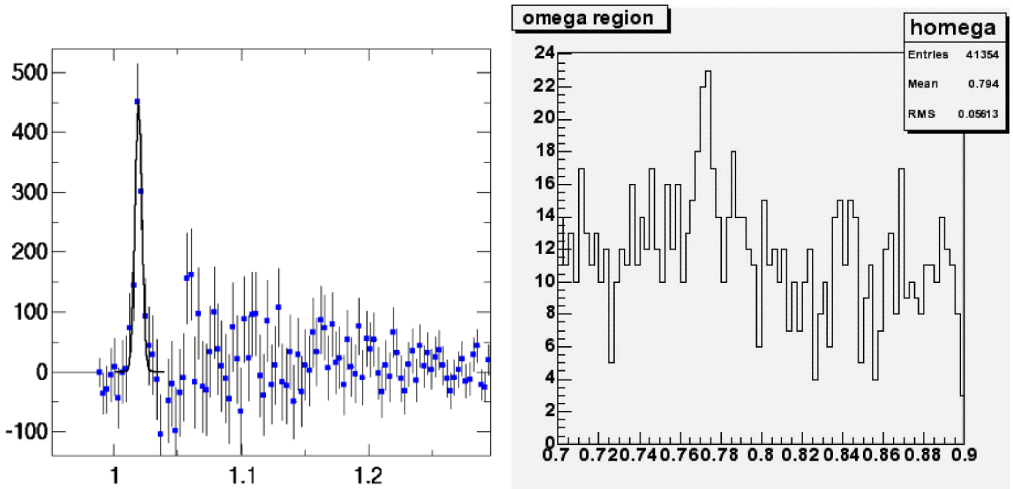

Figure 2.23: Left Panel: KK invariant mass from Au+Au collisions as measured by PHENIX. Kaons are identified in the TOF wall and the EMCAL. Right Panel: Di-electron invariant mass from a small subsample of deuteron-gold collisions from Run 3.

					HBD??		HBD in		HBD in
Run		4a	5a	5b	6	7	8	9	10
Species		Au+Au	Si+Si	p+p	Au+Au	p+p	Au+Au	p+p	d+Au
sqrt(s)		200	200	200	62.4	200	200	500	62.4
Omega	N	1137	799	239	333	12400	7774	50500	234
	Nsigma	10	17	14	5	102	27	206	11
	Nsigma(HBD)	31	28	15	17	111	80	224	15
phi	N	853	300	90	250	4700	5830	19000	88
	Nsigma	9	10	9	5	63	23	126	7
	Nsigma(HBD)	27	17	9	14	68	70	138	9
rho	N	1173	824	247	343	12800	8017	52000	241
	Nsigma	3	7	9	2	66	9	133	5
	Nsigma(HBD)	20	25	15	11	111	52	224	14

Figure 2.24: Expected yields of vector mesons as measured in the di-electron channel for upcoming runs. Also shown in the significance of the signal with and without the HBD. Highlighted in red are the measurements in which the HBD will be crucial.

Also shown are the statistical significances of the signal. These all assume the vacuum masses and shapes. Also included is the Signal/Background for each of these particles with and without the HBD. First measurements of the spectral shapes of the ω and ϕ should become available from Run-4. If the ρ is strongly enhanced, then it too should be visible. However accurate measurements of the ρ will need the HBD which should be available for Run-8 and possibly for the 62 GeV Au+Au run proposed for Run-6. (See Section 2.5 for a summary of the proposed run plan.) As in the case of thermal di-leptons, these expectations are extrapolated from measurements which includes a p_T cut of 300 MeV to reduce the background. The HBD together with a field-free regions will allow us to reject much of the background without this cut.

2.2.5 Heavy Quarks

2.2.5.1 Introduction

In this section we discuss a set of inter-related physics topics that involve charm and beauty production in heavy ion collisions. These heavy quarks are expected to be produced primarily in hard collisions between partons in the colliding ions. Most of the $c\bar{c}$ and $b\bar{b}$ pairs produced will end up separated in D or B mesons (referred to as open charm and beauty). A small fraction of c quarks and b quarks will form $c\bar{c}$ bound mesons (charmonium), and $b\bar{b}$ bound mesons (bottomonium), collectively known as quarkonia. PHENIX detects open charm and beauty primarily using semi-leptonic decays into electrons and muons, and detects quarkonia primarily using their decays to e^+e^- and $\mu^+\mu^-$ pairs. The study of the centrality, rapidity and p_T dependence of open charm, open beauty and quarkonia is expected to be a major key to understanding the early stages of a collision at RHIC, by observing the effects of the hottest and densest phase of the nuclear matter on the heavy quarks before they hadronize. Due to larger mass scales provided by the charm and bottom masses, these same channels are of great utility in both the polarized proton program and in proton-nucleus collisions, as described in Sections 2.3 and 2.4, respectively.

Table 2.4: Summary of PHENIX signals associated with heavy quark physics topics. Some signals can be studied with the baseline detector, but many require the displaced vertex measuring capability of the PHENIX VTX detector, and all of the measurements benefit greatly from the VTX detector. The minimum PHENIX recorded luminosity required to study the signal in 200 GeV Au+Au collisions is indicated. The required RHIC delivered luminosities are approximately three times larger, due to vertex and trigger cuts. Similar numbers of binary collisions will be needed for p+p, d+Au and lighter ion collisions.

Topic	Signals	p_T (GeV/c)	$\sim$ Lum (μb^{-1})	Requires
open charm	$D \to \mu, e\ +\ X$	$0.5 - 2.5$	300	
(energy loss, $\sigma(c\bar{c}), flow$)	$D \to \mu, e\ +\ X$	$0.3 - 6$	1000	VTX
	$D \to K\ +\ \pi$	> 2	1000	VTX
open beauty	$B \to \mu, e\ +\ X$	$1 - 6$	1000	VTX
(energy loss, $\sigma(b\bar{b})$)	$B \to J/\psi \to e^+e^-, \mu^+\mu^- + X$	all	1000	VTX
Prompt charmonium	$J/\psi \to e^+e^-, \mu^+\mu^-$	all	300	
(suppression, coalescence)	$\psi' \to e^+e^-, \mu^+\mu^-$	all	1000	(VTX)
	$\chi_{cJ} \to \gamma\ J/\psi \to \gamma\ e^+e^-$	all	1000	
Charmonium background	$B \to J/\psi \to e^+e^-, \mu^+\mu^- + X$	all	1000	VTX
Bottomonium	$\Upsilon, \Upsilon', \Upsilon'' \to e^+e^-, \mu^+\mu^-$	all	3300	VTX μ trigger

PHENIX detects electrons in the central arms ($|\ \eta\ | < 0.35$) and muons in two muon arms ($1.2 < |\ \eta\ | < 2.2$). This broad rapidity coverage allows us to measure total cross sections for

open charm and beauty, and for quarkonium production. The p_T acceptance of the central arms and muon arms is very broad for single leptons and di-leptons, extending all the way to zero p_T in both cases. The baseline PHENIX detector is expected to be augmented in the next 5 years by a silicon vertex tracker (VTX) that includes a central-arm barrel and endcaps in front of the two muon arms. By allowing the identification of events with displaced decay vertices, the VTX upgrade will have a profound effect on the PHENIX heavy quark program, as detailed in Section 3.2.2 and in the remainder of this section.

Table 2.4 contains a summary of the PHENIX physics signals and topics related to heavy quark production in nuclear collisions. The minimum integrated luminosity required to study these topics in $\sqrt{s} = 200$ GeV Au+Au collisions is listed for each case. In addition to the study of these signals using Au+Au collisions, a similar integrated luminosity (in terms of number of binary collisions) should be collected in a systematic study of p+p, d+Au, and A+A (i.e. lighter heavy ion) collisions at full energy, and at least at one lower energy. This is discussed in the next subsection. The remainder of the section then contains short descriptions of the various physics topics, including a discussion of how we expect their study to evolve over the next decade, followed by a tentative timeline for achieving the major milestones discussed here.

2.2.5.2 Systematic Studies

In addition to studying the signals in Table 2.4 in Au+Au collisions, PHENIX will make a full set of complementary measurements in p+p, d+Au and A+A (i.e. lighter heavy ion) collisions.

Measurements in p+p collisions are used to establish the cross section per binary collision for each physics process, and the baseline p_T and rapidity distributions. These measurements require integrated parton luminosities equivalent to those obtained in heavy ion collisions, because the signatures of nuclear effects in heavy ion collisions will appear as variations in the p_T distributions, for example, with collision centrality. Measurements in d+Au collisions are used to establish how the cross sections and distributions for the various signals are affected by entrance channel effects (such as shadowing) and cold nuclear matter effects.

The precision for measuring the dependence of the signals on the number of binary collisions (which sets the heavy flavor production rate) and number of participants (which determines the nuclear energy density) is poor for peripheral Au+Au collisions. As an example, Fig. 2.25 shows the J/ψ yields plotted versus the logarithm of the number of binary collisions for several symmetric heavy ion systems. It is clear that the study of the heavy flavor signals for smaller numbers of binary collisions requires running with lighter heavy ions, such as Fe+Fe or Si+Si.

One can also lower the energy density without changing the collision geometry by lowering the collision energy. PHENIX will pursue these measurements in lower energy Au+Au collisions, with complementary lower energy measurements in p+p and d+Au for baseline cross sections and distributions.

To the extent possible, the integrated luminosities used for complementary and baseline measurements should yield about the same number of binary nucleon-nucleon collisions as the Au+Au runs that they are to be compared with, since heavy flavor production scales with

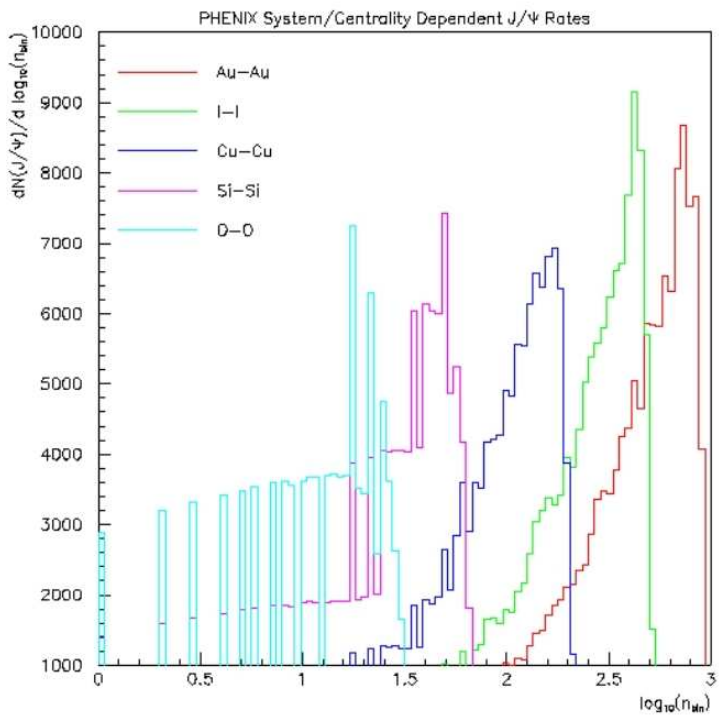

Figure 2.25: Relative J/ψ yields versus the logarithm of the number of binary collisions for several symmetric combinations of heavy ions. The running periods are similar in all cases. This plot illustrates the need to study lighter heavy ion systems to obtain information about lower energy densities.

binary collision rates. Comparable signal yields will be difficult for lower energy measurements, however, where we would require larger integrated parton luminosity to compensate for reduced cross sections, and long runs to compensate for reduced maximum luminosity.

2.2.5.3 Energy Loss of Heavy Quarks

The energy loss of a colored high p_T parton in a hot QCD plasma is expected to be much larger than in cold nuclear matter. Colored high p_T partons are predicted to lose energy primarily due to gluon Bremsstrahlung radiation produced when they scatter from the light partons forming the quark-gluon plasma [33, 34, 35]. The energy loss is found to be very sensitive to interference effects caused by the gluon formation time being comparable to the time between successive collisions.

Heavy quarks in a hot QCD plasma have been predicted [71] to lose less energy than lighter partons. This is due to the suppression of small angle gluon radiation in a "dead-cone" of width $\theta < M/E$ around the quark trajectory, which reduces heavy quark energy loss by a factor of two or so relative to that for light partons. More recently, the magnitude

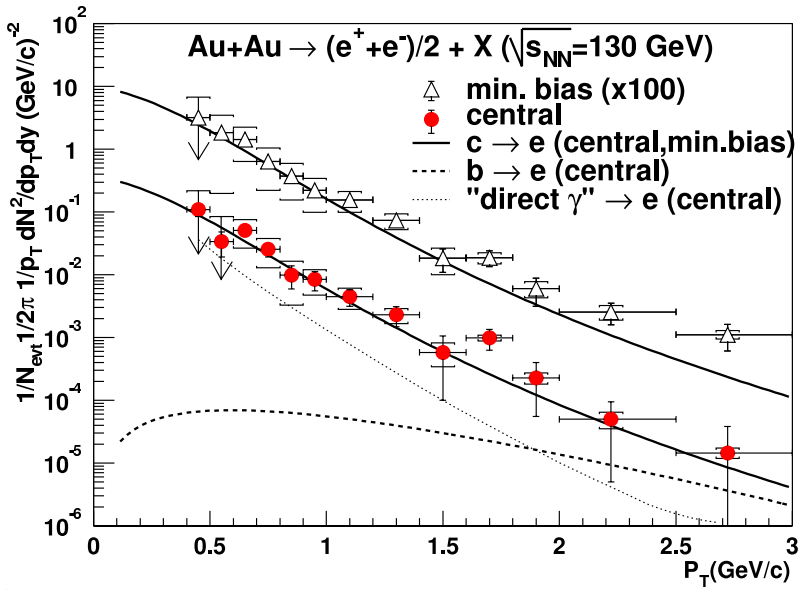

Figure 2.26: The single electron p_T spectrum after subtraction of all known non heavy-quark sources. The remaining signal is thought to be predominantly due to semi-leptonic open-charm decays. The data were extracted from a minimum bias data sample corresponding to 1 μb^{-1} of Au+Au collisions at $\sqrt{s_{NN}} = 130$ GeV.

of the dead cone has been calculated [72, 73, 74] to be smaller than first predicted, but it has been proposed [72, 73] that the energy loss of heavy quarks is further reduced due to a plasmon cutoff in the medium. To shed light on these issues we will need to measure the open charm yields to high values of the transverse momentum.

The PHENIX baseline detector can measure the combined open charm and beauty yields by detecting high p_T single leptons from decays of the D and B mesons containing the primordial c and b quarks. This requires the subtraction of the single lepton yields due to all other sources. Currently, semi-leptonic charm and beauty decays can be distinguished only by their differing p_T dependence, with charm dominant at medium p_T and beauty dominant at high p_T (see the simulation curves in Fig. 2.26). PHENIX has extracted [11] the open charm cross section for $p_T < 2.5$ GeV/c from $\sqrt{s} = 130$ GeV Au+Au collisions, shown in Fig. 2.26. The contribution from open beauty is thought to be negligible relative to the semi-leptonic charm decay yield, because of the relatively small p_T reach accessible with this low integrated luminosity. Unlike the p_T distributions of pions, the open charm p_T distributions are consistent with binary scaling, showing no evidence of energy loss by the c quark. However the statistical accuracy is low and the systematic errors are fairly large due to the subtraction of a large background. A somewhat larger data set was obtained for Au+Au at 200 GeV in Run-2, and the results of a preliminary analysis are shown in Fig. 2.27. The 200 GeV open charm data are also consistent, within errors, with zero c

quark energy loss at all centralities.

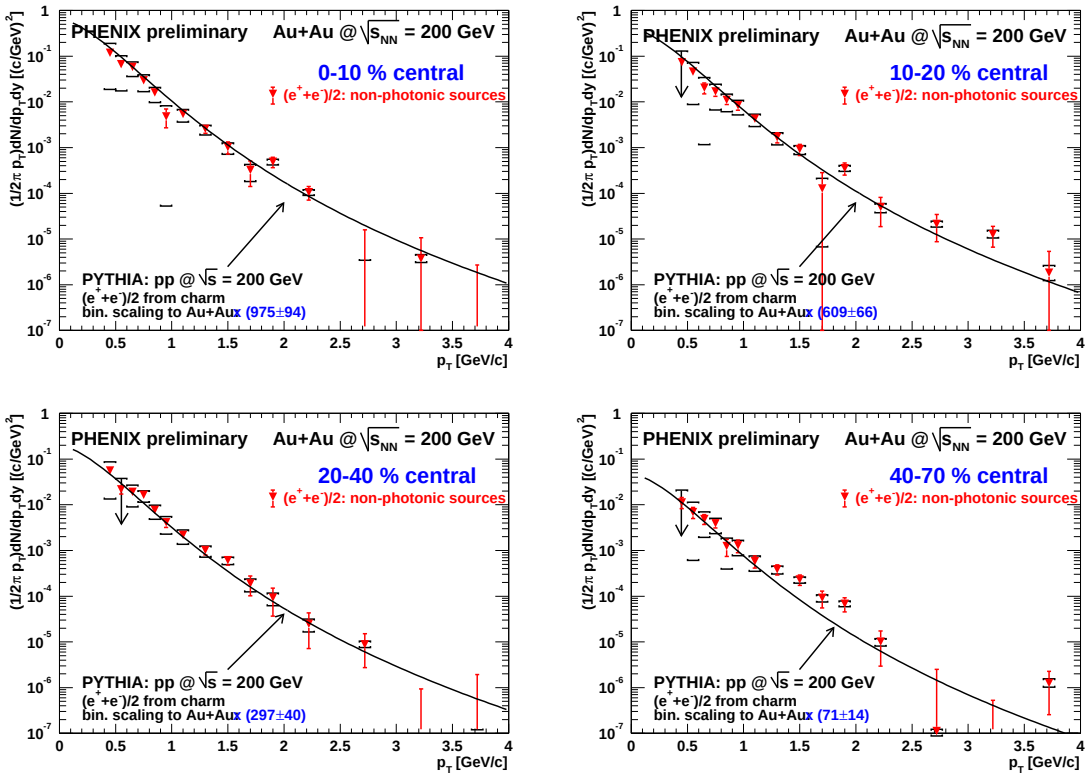

Figure 2.27: Preliminary PHENIX open charm and beauty yields for 200 GeV Au+Au, compared with binary-collision scaled PYTHIA estimates of the electron yield in the central arms due to semi-leptonic decays of D mesons.

Higher integrated luminosity will improve the accuracy of the measurement of the open charm p_T distribution at moderate values of transverse momentum. However, for values of $p_T >\sim 2.5$ GeV/c the charm signal will be overwhelmed by the B decay contribution. The availability of the PHENIX VTX detector described in Section 3.2.2 will greatly improve our ability to study the energy loss of heavy quarks using open charm. By allowing the identification of displaced secondary vertices, the VTX barrel will permit the measurement of the high p_T charm distribution using $D \rightarrow K\ \pi$ decays into the central arms. Charm identification at moderate p_T is also improved by using both VTX endcap and VTX barrel to identify displaced vertices for semi-leptonic decays - by making a distance of closest approach (DCA) vertex cut of 200 μm, the background due to prompt processes can be suppressed considerably with an acceptable loss of heavy quark signal. Figure 2.28 shows DCA distributions from simulations for electrons from open charm, open beauty, and Dalitz decays. These plots show the evolution of the DCA distributions as the minimum p_T is increased.

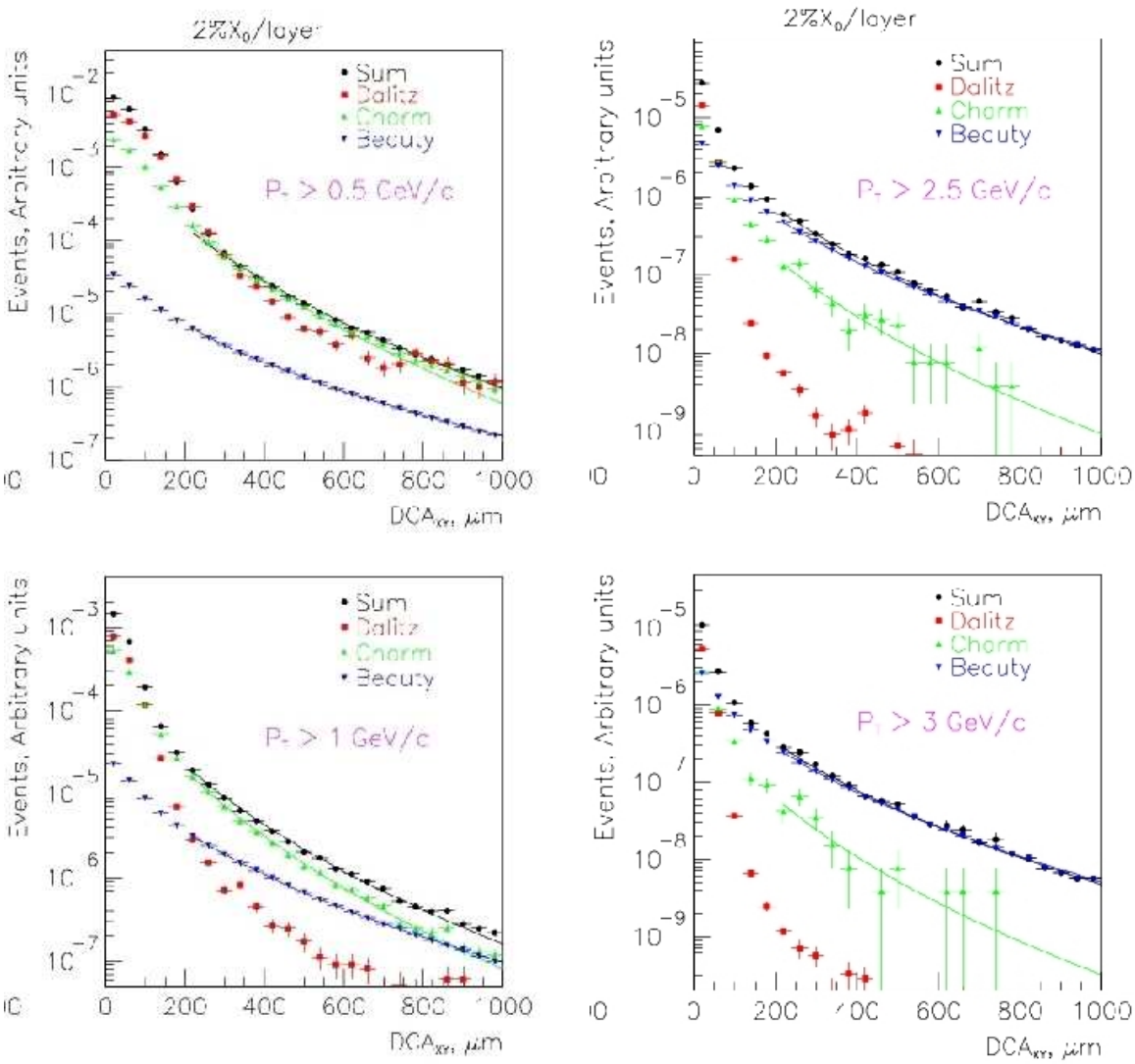

Figure 2.28: Simulated distance of closest approach (DCA) distributions from PYTHIA for electrons from open charm, open beauty, and Dalitz decays. The DCA distributions are integrated over all p_T from 0.5 GeV/c, 1.0 GeV/c, 2.5 GeV/c and 3.0 GeV/c. Note the evolution of the Dalitz, charm and beauty DCA distributions with increasing p_T cut.

As the semi-leptonic charm signal at high p_T is obscured by the B decays, the semi-leptonic beauty signal at lower p_T is obscured by the D decays. The VTX barrel and the VTX endcaps provides a superb opportunity to measure B decays at low p_T by measuring J/ψ's originating from a displaced vertex. Since all other processes producing J/ψ's are prompt, the displaced vertex condition uniquely samples those from B decays. There is also a possibility that the VTX detector will allow direct separation of the semi-leptonic decay signals from charm and beauty - the proper time distributions for the two types of decay are different, and could allow (statistical) separation given sufficient integrated luminosity.

2.2.5.4 Charm Flow?

It has recently been observed [75] that the D meson transverse momentum distribution predicted by PYTHIA, using binary collision scaled perturbative QCD with no final state interactions, is almost identical to that predicted by a thermal hydrodynamic model for $p_T < 3$ GeV/c. Figure 2.29 (left plot) has a comparison of PHENIX 130 GeV Au+Au π^0 data compared with predictions of a hydrodynamic model and PYTHIA. This shows the now well known result that PYTHIA over-predicts the cross section at all p_T for light quark mesons. The hydrodynamic calculation does well for the π^0 out to several GeV/c. The right plot contains a similar comparison for 130 GeV Au+Au single electron data with simulated semi-leptonic decay electron yields from D and B decay given by PYTHIA and a hydrodynamic model. Because the PHENIX open charm p_T distributions do not extend beyond 3 GeV/c, they are consistent with both of these diametrically opposed scenarios. Determining which of these interpretations is correct is clearly an important open issue that can be resolved by the planned PHENIX program in heavy quark physics.

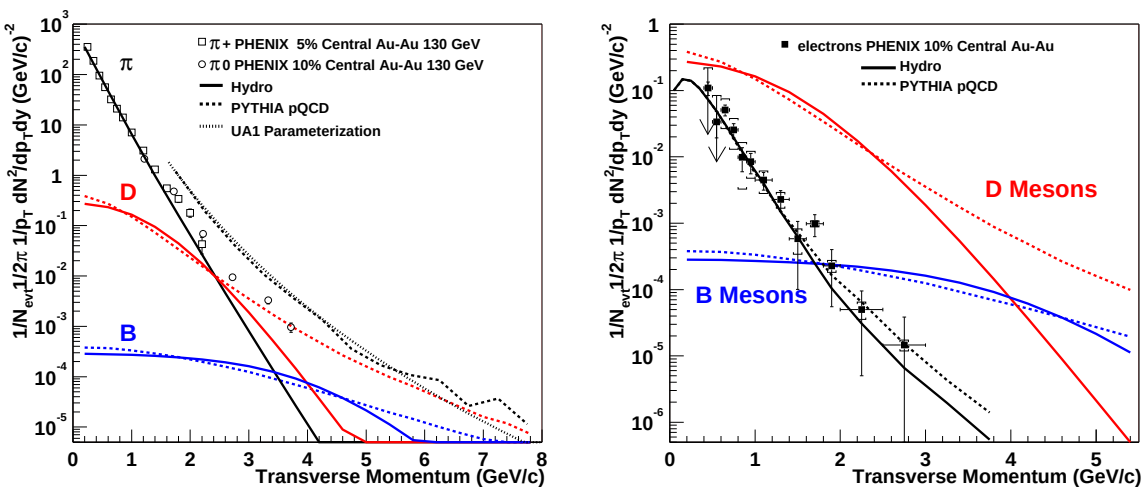

Figure 2.29: Comparison of 130 GeV Au+Au PHENIX π^0 data (left plot) and PHENIX single electron data (right plot) with predictions from PYTHIA and from a hydrodynamic model. Each plot shows the D and B meson p_T distributions. The right plot shows the distributions of their decay products compared with electron data.

If the medium is transparent to c quarks, as is assumed in the binary-scaled PYTHIA calculation, the D meson correlation with the reaction plane would all come from the anisotropic flow of its light quark at hadronization. Hydrodynamic models assume that the opacity of the produced plasma is so high that local equilibrium is established early in the collision and maintained through hadronization. If this applied to the c quark as well as the light quark that make up the D, the anisotropy in the D meson transverse momentum distribution would increase. A recent quark coalescence paper [76] presents estimates of how much the observed D meson flow would be changed as the c quark flow varied from zero up to the light quark value.

There is now an effort within PHENIX to measure the anisotropy parameter, v_2, for electrons from open charm semi-leptonic decays to determine if the parent D meson momentum anisotropy is consistent with the hydrodynamic picture. This is a very difficult analysis because of the large background from Dalitz decay and conversion electrons that has to be subtracted to get the open charm signal. There is also an effort to study electron-hadron correlations as a means of gauging the opacity of the medium.

It seems likely that the two very different descriptions of open charm dynamics can be distinguished by a combination of a) open charm v_2 measurements and correlations with hadrons and b) extending the measurements of leptons from open charm to transverse momenta above 3 GeV/c. Much better statistics are expected for Au+Au collisions in Run-4, and this should improve the v_2 measurement. But extending the p_T reach for charm will require displaced vertex measurements with the VTX detector, such as $D \rightarrow K\ \pi$ decays, that will permit open charm measurements to high p_T without interference from B decays.

2.2.5.5 Open Charm and Beauty Cross Sections

Because the vast majority of heavy quarks appear as open charm and beauty, the total cross sections for charm and beauty production are essentially equal to the open charm and beauty total cross sections. The rapidity, p_T and centrality dependence of open charm and beauty cross sections are crucial baseline data for understanding charmonium and bottomonium production in heavy ion collisions.

Various models have predicted an enhancement in open charm yields due to gluon fusion in the pre-equilibrium phase of heavy ion collisions[77, 78, 79]. The size of the effect is very sensitive to the initial energy density. If the initial temperature is very high (> 500 MeV) there may also be significant thermal charm production. Any enhancement is expected to be negligible for beauty at RHIC energies, and so the beauty production cross section is expected to reflect the initial parton density in the colliding nuclei. For this reason, a program of simultaneous measurement of charm and beauty yields is an extremely powerful tool for characterizing both the initial conditions and the approach from above towards thermal equilibrium. There are predictions that gluon shadowing will be significant in the x range covered by the muon arms, and this will have to disentangled from final state effects using d+Au measurement results.

The existing PHENIX p_T distributions and integrated cross sections for non-photonic single electrons at mid-rapidity (see Figure 2.26) are consistent, within the large uncertainties ($\sim 40\%$), with there being no enhancement or suppression of open charm in Au+Au collisions. Further measurements of open charm using semi-leptonic decays are being pursued in the central and muon arms using data from Run-2, and a large jump in integrated luminosity is expected in Run-4 that will greatly benefit these measurements. As emphasized above, there is no model independent way with the PHENIX baseline detector to measure the open beauty cross section, since most of the yield from semi-leptonic beauty decays is buried under the much larger yield from charm decays at lower p_T. The implementation of the VTX barrel and endcap in 2008, combined with much higher integrated luminosities, will permit the improvement of the open charm and beauty measurements by:

- Allowing the reduction of single lepton background at low p_T from prompt meson decays by using a DCA cut, lowering the measurement threshold to 0.5 GeV/c.
- Permitting the identification of high p_T charm at mid-rapidity using offset vertex $D \rightarrow K\ \pi$ decays.
- Permitting the identification of low p_T beauty at all rapidities using offset vertex $B \rightarrow J/\psi$ decays.
- Permitting the statistical separation of semi-leptonic charm and beauty decays by using their different vertex offset distributions, given large enough integrated luminosity.

Because no enhancement of beauty is expected at RHIC, the ratio of charm and beauty production as a function of collision centrality may be very valuable as a sensitive indicator of charm enhancement in central collisions. In taking this ratio, most of the systematic uncertainties in the two measurements cancel.

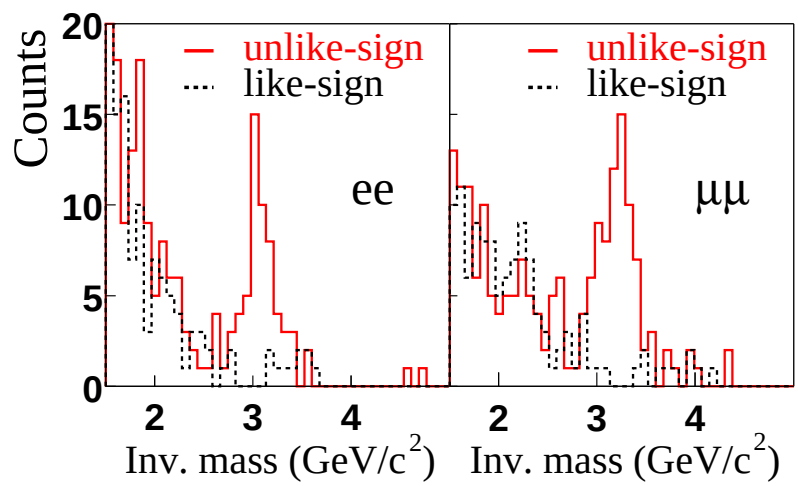

Figure 2.30: The J/ψ invariant mass spectra in the di-electron and the di-muon channels from Run-2 p+p collisions. A total of 150 nb^{-1} was recorded by PHENIX in Run-2.

2.2.5.6 Charmonium Yields

The $c\bar{c}$ bound states η_c, J/ψ, χ_{cJ} (where J=0,1,2), η_c', h_c and ψ' are collectively known as charmonium. Of these, the J/ψ and ψ' are vector mesons with 6% and 1% branches, respectively, to di-leptons. There are significant branching fractions for radiative decays of the ψ' and χ_{cJ} to the J/ψ.

All of the charmonia are expected to be unbound in a QGP. The J/ψ provides the strongest di-leptons signal, and so most of the experimental and theoretical focus has been on the J/ψ so far. Recent models of J/ψ production in heavy ion collisions at RHIC include

loss terms for J/ψ yields due to their passage through a plasma and/or screening, and gain terms from random coalescence of $c\bar{c}$ pairs during hadronization of the plasma. The model predictions vary from strong J/ψ suppression [80, 81] to strong J/ψ enhancement [82, 83] for central collisions. It is likely that J/ψ's produced by coalescence will have a different p_T distribution from primordial J/ψ's. Understanding the balance between primordial J/ψ production and suppression on one hand, and J/ψ production by coalescence at hadronization on the other, will therefore require good measurements of the J/ψ yield vs centrality, p_T and rapidity. Coalescence models also predict a rather distinctive behavior with $\sqrt{s}$ of the ratio of J/ψ yield to open charm yield for central collisions (see for example[81]). Because the J/ψ yield due to recombination increases as the square of the charm multiplicity, the ratio has a minimum value followed by an increase at high $\sqrt{s}$.

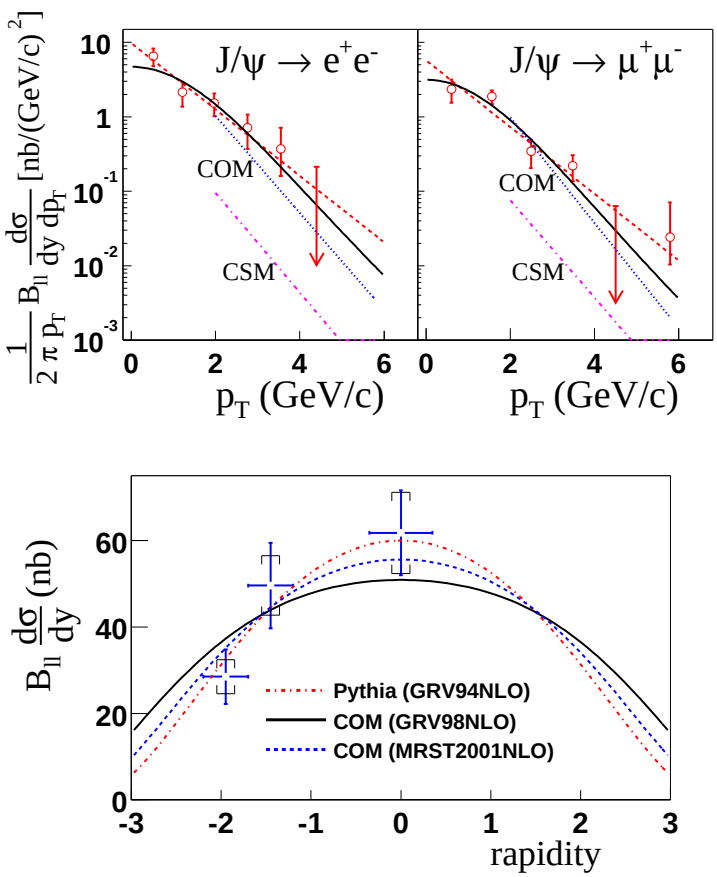

Figure 2.31: Top: The J/ψ p_T distributions for di-muons and di-electrons from Run 2 p+p collisions. Bottom: The J/ψ rapidity distribution from Run-2 p+p collisions. The mid-rapidity point is from the electron measurement in the central arms, the other two points are from the measurement in the south muon arm. The north muon arm was not yet operational in Run-2. A total of 150 nb^{-1} was recorded by PHENIX in Run-2 for p+p collisions.

PHENIX has measured J/ψ yields in the central and muon arms for p+p, d+Au and Au+Au collisions at $\sqrt{s}$=200 GeV. The invariant mass spectra, p_T distributions and rapidity distributions from the Run-2 p+p data [26] are shown in Figure 2.30 and 2.31. It should be noted that this is the first J/ψ total cross section measurement at a hadron collider. The PHENIX p+p J/ψ measurements provide crucial baseline data for PHENIX. Their availability substantially reduces the uncertainties that would result from reliance on perturbative calculations in the color octet model using matrix elements determined from available lepto- and hadro-production J/ψ data. The combined uncertainties from the parton distribution functions, QCD parameters and matrix elements lead to uncertainties of order a factor of two in the rates[26].

The J/ψ yield from Au+Au collisions was measured by PHENIX in Run-2 [20]. The centrality dependence is shown in Figure 2.32, where it is compared with various model calculations [82, 83, 80, 81, 84]. The signal is small due to the relatively low integrated luminosity, with no statistically significant signal for the most central bin. The data are inconsistent with strong J/ψ enhancement, but we cannot yet discriminate between models that produce suppression relative to binary scaling. We expect over one order of magnitude increase in integrated Au+Au luminosity from Run-4, which should allow us to test those models. PHENIX is presently analyzing J/ψ data from Run-3 d+Au (2.7 nb^{-1}) and Run-3 p+p (270 nb^{-1}) which have substantially larger J/ψ yields than the Run-2 data set.

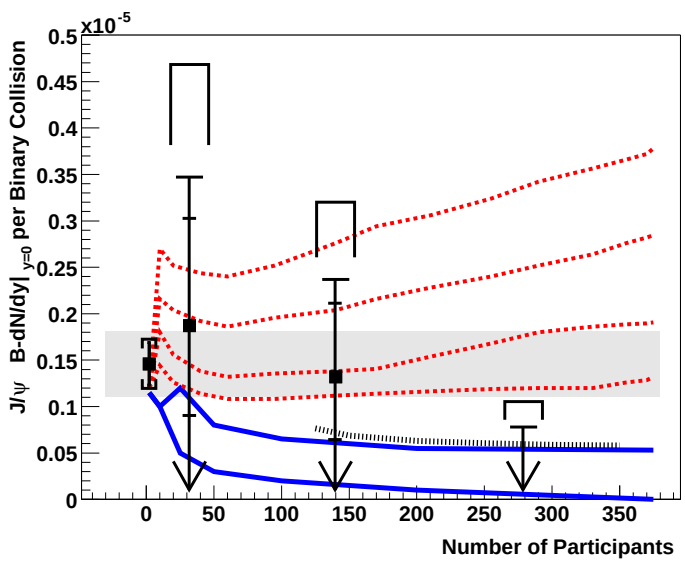

Figure 2.32: The binary-scaled J/ψ yield per collision at mid-rapidity from Run-2 Au+Au collisions. A total of 24 μb^{-1} for Au+Au collisions was recorded by PHENIX in Run-2. The theory curves are discussed in the text.

The background J/ψ yield from $B \rightarrow J/\psi$ decays is likely to be problematic at large p_T, especially if there is strong J/ψ suppression in central collisions. As noted above, the VTX barrel and endcap will allow us to measure the offset-vertex $B \rightarrow J/\psi$ yields, and subtract

this contaminant from the measured J/ψ yield to get the prompt J/ψ signal.

Because an estimated 30% of the observed prompt (i.e. not from B meson decay) J/ψ result from χ_{cJ} decays and another 12% from ψ' decays, all model calculations that are intended for comparison with prompt J/ψ data include those feed-down contributions. But the ψ' will be studied directly by PHENIX, using its di-leptons decays. This will act as a check on the feed-down estimates that go into the J/ψ model calculations, and will provide a second look at charmonium suppression using the heaviest bound charmonium state, which has no feed-down from higher energy states. Studying the ψ' requires much larger integrated luminosity than is needed to study the J/ψ. The improved momentum resolution provided by the VTX barrel and endcap will also be very useful in cleanly separating the J/ψ and ψ' invariant mass peaks.

The (unresolved) χ_{c1} and χ_{c2} can also be studied directly, given sufficient luminosity, by reconstructing their γ J/ψ decays after triggering on the J/ψ. The $\chi_{c1} \rightarrow \gamma$ J/ψ branch is 27% and the $\chi_{c2} \rightarrow \gamma$ J/ψ branch is 14%. The χ_c signal is expected to be larger than the ψ' signal in the PHENIX di-electron measurement, but much weaker in the di-muon measurement because of detector geometry. However, the addition of the proposed nosecone electromagnetic calorimeter (see Subsection 3.2.5) in front of the muon arms would make the χ_c measurement feasible in the muon arms also, allowing the study of χ_c production at all of the rapidities covered by PHENIX for the other quarkonia.

It has been predicted recently [85] that QGP formation will lead to increased J/ψ polarization at low p_T in heavy ion collisions relative to p+p collisions. In any event, it seems likely that measurements of the J/ψ polarization in p+p and Au+Au collisions will be interesting, and may shed light on the mechanisms of J/ψ production in heavy ion collisions. J/ψ polarization measurements will require large integrated luminosity, even at low p_T.

Fully understanding the charmonia data will require that we have accurate measurements of the open charm cross sections as baseline data for all systems studied.

2.2.5.7 Bottomonium Yields

The established $b\bar{b}$ bound states Υ, $\chi_{bJ}(1P)$, Υ', $\chi_{bJ}(2P)$, and Υ'' (where J=0,1,2) are collectively known as bottomonium. Of these, the Υ family are vector mesons with the lowest three states having 1-2% branches to di-leptons. There are generally significant branching fractions for radiative decays of the χ_{bJ} to the lower mass Υ states, and for hadronic decays of the higher to lower Υ states.

Unlike the J/ψ, the bottomonium ground state Υ is not predicted to be suppressed by color screening in central Au+Au collisions [86, 87, 88, 89]. Rather, the Υ is predicted to be (weakly) bound in a QGP to significantly above the deconfinement transition temperature. If the formation time of the plasma is shorter than the formation time of the Υ, and the initial temperature is not extremely high, the plasma will have cooled sufficiently for the Υ to survive, even at low p_T (see for example [88]). Most models predict the survival of the Υ at RHIC, although the estimates of the maximum temperature at which the Υ can survive may be undergoing a downwards revision.

In contrast, the Υ' and Υ'' are expected to be suppressed, as are the χ_{bJ}. Because about 32% of the observed Υ yield is due to χ_{bJ} decay, and 14% due to Υ' decay, the *observed*

Υ yield will be reduced in the case of QGP formation. Additionally, there may be some reduction of the Υ yield due to dissociation caused by gluons, a process that will be very sensitive to the initial temperature and details of the equation of state [86]. To complicate matters, should the equilibration time of the QGP be slower than expected and/or if the initial temperature is very high, the Υ could still be suppressed by color screening [87].

Although the cross sections for production of the Υ family are much smaller than those for the J/ψ, the study of Υ yields is very attractive for obtaining a very different look at medium effects on quarkonia yields. In addition to the differences mentioned above, coalescence is much less of an issue at RHIC than in the J/ψ case, because of the small number of $b\bar{b}$ pairs produced in a central collision, and there is essentially no background in the invariant mass spectrum near the Υ.

Again, understanding the Υ distributions will require accurate open beauty cross section measurements as baseline data, which in turn will require the VTX detector to separate the charm and beauty semi-leptonic decays, or identify displaced vertex J/ψ from B decays. Also, the separation of the Υ(9.46 GeV), Υ'(10.02 GeV) and Υ''(10.36 GeV) states will be marginal until the VTX detector is in place. The VTX detector will improve the mass resolution at the Υ from $\sim$ 170 MeV to $\sim$ 60 MeV in the electron measurement. The very significant improvement in upsilon spectroscopy provided by the VTX detector is shown in Figure 2.33, where a simulated invariant mass spectrum in the region of the Υ mass for a high integrated luminosity di-electron measurement is shown with and without the VTX detector.

The integrated luminosities needed for studying Υ distributions are estimated to be very large ($\sim$ 3.3 nb^{-1} recorded by PHENIX, or $\sim$ 10 nb^{-1} delivered by RHIC, for Au+Au). It is likely that definitive Υ measurements will require RHIC II luminosities. At the very high luminosities required, the proposed muon trigger upgrade described in Section 3.2.5 will be particularly important for studying Υ yields in the muon arms in $A + A$ collisions, and even to some extent in Au+Au collisions. The existing EMCal-RICH level 1 trigger will be effective in the central arms because of the very high energy deposit in the EMCal produced by Υ decay electrons.

2.2.5.8 Correlated Charm

Measurements of correlated semi-leptonic charm decays are of interest for two reasons. The first is that they provide an alternative look at c quark energy loss in nuclear collisions [90]. The second is that, as discussed in Section 2.2.3.4, correlated semi-leptonic charm decays are expected to be the major background at RHIC for a thermal di-leptons signal in the intermediate mass region (i.e. between the ϕ and the J/ψ masses), where they are significantly stronger than the Drell-Yan contribution and perhaps larger than the thermal di-leptons signal [90, 91]. While the first single electron data from PHENIX [11] are consistent with no c quark energy loss, the experimental uncertainties are still substantial. The correlated charm di-leptons mass distributions are relatively sensitive to any c quark energy loss, so that even a small suppression (or enhancement) of open charm could produce a significant change in the intermediate-mass di-leptons yield, and hence in the background for thermal di-leptons. An additional consideration is that the mass distribution from open charm depends critically

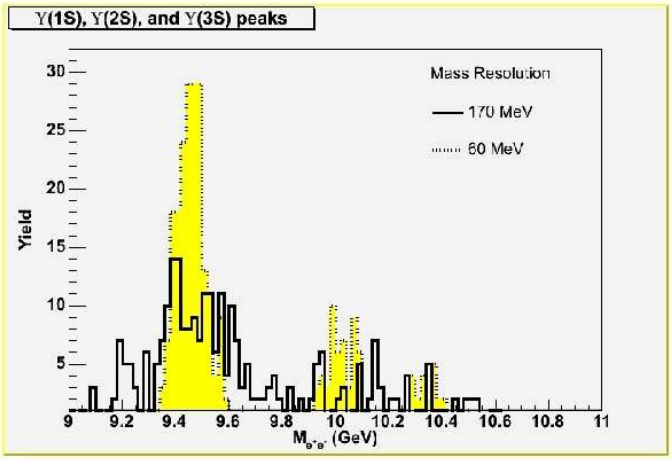

Figure 2.33: The simulated $\Upsilon \rightarrow e^+e^-$ invariant mass spectrum with and without the vertex detector. The simulated yields correspond to a 200 GeV Au+Au PHENIX recorded luminosity of about 3.3 nb^{-1}, or roughly 10 nb^{-1} delivered by RHIC.

on the correlation between the D and $\bar{D}$ mesons.

The importance of understanding the open charm contribution in the intermediate mass region is illustrated by the effort that has gone into trying to understand the origin of the di-leptons excess at intermediate mass observed in Pb+Pb collisions at the SPS (see [92] and references therein). The factor of three or so di-leptons excess has been variously attributed to hadronic rescattering, an overall charm production enhancement, and a thermal di-leptons signal (both hadron gas and plasma). The thermal production scenarios are now considered most probable [91].

The integrated luminosity in Run-4 should be sufficient for a useful measurement of correlated charm (plus beauty) by detecting e-μ coincidences in PHENIX from correlated $D\bar{D}$ (plus $B\bar{B}$) decays. This measurement requires large integrated luminosity, but it is attractive because there can be no contributions from thermal di-leptons or Drell-Yan, since they can produce only e^+e^- or $\mu^+\mu^-$ pairs. Therefore this measurement does not require the ability to identify displaced vertex semi-leptonic decays.

The implementation of the VTX barrel and endcap will make it possible to directly identify displaced vertex semi-leptonic charm and beauty decays in PHENIX. Since open charm is the only large source of di-leptons that is not prompt, it should be possible to characterize the largest background component in the di-leptons spectra independently of any thermal signal. Then Drell-Yan becomes the only significant source of background for intermediate mass di-leptons that has to be estimated theoretically. The calculation for Drell-Yan is on firmer ground, since there are thought to be no final state effects on the Drell-Yan yield.

2.2.5.9 Heavy quark physics timeline

Table 2.5 contains an approximate timeline for the major heavy quark physics milestones discussed in this section.

Table 2.5: Possible timeline for the PHENIX heavy quark physics program available in the 27 week per year scenario for RHIC running.

Year	Species	Energy	Milestone
2001	Au+Au	130	open charm (0.5-2.5 GeV/c)
2002	Au+Au	200	open charm (0.5-2.5 GeV/c)
			low statistics $J/\psi \to ee$ measurement
	p+p	200	low statistics $J/\psi \to ee, \mu\mu$ measurement
2003	d+Au	200	several thousand $J/\psi \to ee, \mu\mu$
	p+p	200	several hundred $J/\psi \to ee, \mu\mu$
2004	Au+Au	200	large $J/\psi \to ee, \mu\mu$ sample
			large increase in open charm statistics (0.5-2.5 GeV/c)
			charm v_2 ?
2005	Fe+Fe	200	lighter ion sample (J/ψ, open charm)
2006	Au+Au	62.4	lower energy Au+Au sample (J/ψ, open charm)
2007	p+p	200	large baseline p+p sample (J/ψ, open charm)
2008			VTX installed, level 1 μ trigger upgrade done
	Au+Au	200	$D \to e, \mu$ (0.3-6 GeV/c)
			$B \to e, \mu$ (1-6 GeV/c)
			$B \to J/\psi$ (open beauty, J/ψ background)
			$\psi' \to ee, \mu\mu$
			$\chi_{cJ} \to \gamma\ J/\psi \to ee$
			$\Upsilon \to ee, \mu\mu$ bottomonium yields
	p+p	62.4	baseline lower energy p+p
	d+Au	62.4	baseline lower energy d+Au
- 2014			

2.3 Spin Physics

Executive Summary

The milestones of the PHENIX spin program through Run-9 are summarized in Table 2.6. Completion of the baseline program by Run-9 is contingent on RHIC performance as a polarized proton collider. The proposed program of PHENIX upgrades (see Chapter 3) will enhance the scope of the spin physics program.

Run	# of weeks	P_B	$\sqrt{s}$ (GeV)	$\int \mathcal{L}dt$ (pb^{-1})	physics	remarks
Run-1	(3)	-	-	-	One ring commissioned	
Run-2	(5)+3	0.15	200	0.15	$\sigma(\pi^0, J/\psi)$; $\mathcal{A}_N(\pi)$	
Run-3	(3)+5	0.27	200	0.35	First $\mathcal{A}_{LL}(\pi^0)$	
Run-4	(5)+0	0.50	200	-	Machine/PHENIX development towards high $\mathcal{L}$ and P_B	new AGS warm snake
Run-5	5-10	0.50	200	3-10	$\Delta g/g$ with $\mathcal{A}_{LL}(\pi^0)$	new AGS cold snake
Run-6/7	19	0.70	200	158	$\Delta g/g$ with $\mathcal{A}_{LL}(\gamma, \gamma + jet, c/b, J/\psi)$	Si-VTX detector
Run-8/9	19-29	0.70	500	540-966	$\Delta g/g$ with $\mathcal{A}_{LL}(\gamma)$ and $\Delta\bar{q}/\bar{q}$ with $\mathcal{A}_L(W^{\pm})$	W-trigger

Table 2.6: Summary of the PHENIX Spin goals for the upcoming several years. For the "# of weeks", the number in parenthesis shows the beam weeks required for commissioning. All future physics topics presented in the table involve longitudinal polarization; there is ongoing discussion regarding transverse polarization.

2.3.1 Introduction

Spin, along with electric charge, mass, and intrinsic symmetries, is one of the most fundamental properties of an elementary particle. Therefore, it is important to understand the spin of hadrons in terms of the underlying fundamental degrees of freedom, i.e., the spin of the quarks and gluons and their orbital motion. In addition, the *axial vector* nature of spin has been useful in testing symmetries in fundamental processes such as parity and time-reversal invariance. Therefore, the importance of physics with polarized proton program at

PHENIX can be understood in two ways. One is elucidation of *the spin structure of the nucleon*, and the other is utilizing the known spin structure to *test symmetries in reactions*.

The spin structure of the nucleon has been studied for over two decades using deep-inelastic scattering of longitudinally polarized leptons off longitudinally polarized-nucleon targets (polarized-DIS) [93, 94, 95, 96, 97, 98, 99, 100, 101, 102, 103, 104]. The goal is to obtain a complete picture of the nucleon spin in terms of quark and gluon degrees of freedom, which are summarized in Table 2.7. The first moments of the spin structure functions, g_1^p and g_1^n, whose parton model interpretation at leading order are

$$g_1^p(x,Q^2) = \frac{1}{2}\left[\frac{4}{9}\Delta\mathcal{U}(x,Q^2) + \frac{1}{9}\Delta\mathcal{D}(x,Q^2) + \frac{1}{9}\Delta\mathcal{S}(x,Q^2)\right], \qquad (\text{for } g_1^n \;\; \mathcal{U} \leftrightarrow \mathcal{D}) \tag{2.5}$$

where $\Delta\mathcal{U} \equiv \Delta u + \Delta\bar{u}$ etc., have been measured to a precision of $\sim 20\%$. The error is largely dominated by uncertainties in extrapolation to the unmeasured x-region[2]. The fraction of the proton spin carried by quark spin, or the first moment of flavor-singlet quark distribution, $\Delta\Sigma(x) \equiv \Delta\mathcal{U}(x) + \Delta\mathcal{D}(x) + \Delta\mathcal{S}(x)$ has been determined in various global analyses assuming flavor SU(3) invariance, with typical values of its first moment at Q^2=1.0 GeV^2 ranging from 0.1 to 0.3[3]. This quantity $\Delta\Sigma$ is the only measured piece of the proton-spin sum rule;

$$\frac{1}{2}^{\text{proton}} = \int_0^1 dx \left[\frac{1}{2}\Delta\Sigma(x) + \Delta g(x)\right] + L_z \quad . \tag{2.6}$$

Here $\Delta g(x)$ and L_z represents contribution from the gluon spin and orbital angular momenta of quarks and gluons, respectively. The experimental information on these unmeasured pieces Δg and L_z is indispensable to completing the picture of the spin structure of the nucleon. Especially direct measurements of **gluon** and **anti-quark** polarization are both essential and missing, since polarized-DIS is primarily sensitive only to the electric charge squared. In addition, the **transversity** distributions of quarks (anti-quarks), δq ($\delta\bar{q}$) have never been measured, and their measurement at RHIC is very important to complete the picture of the nucleon spin structure.

Table 2.7: *Unpolarized* and *polarized* quark and gluon distributions. Gluon *transversity* does not exist for the nucleon which has spin $\frac{1}{2}$. The Q^2 dependence is dropped for simplicity.

	quark	gluon
spin averaged distrib.	$q(x) \equiv q^+(x) + q^-(x) = q^\uparrow(x) + q^\downarrow(x)$	$g(x) \equiv g^+(x) + g^-(x)$
helicity distribution	$\Delta q(x) \equiv q^+(x) - q^-(x)$	$\Delta g(x) \equiv g^+(x) - g^-(x)$
transversity distrib.	$\delta q(x) \equiv q^\uparrow(x) - q^\downarrow(x)$	———

Once these spin structure functions are measured to a reasonable precision, the polarized proton beams can be regarded as *polarized quark and gluon beams* with known luminosities

[2]For the measured region, the precision for the proton (neutron) is 5% (18%) [98].

[3]Here we refer to next-to-leading order fit in $\overline{\text{MS}}$ scheme.

and energies, which can be used to explore searches of new physics. In particular, parity violating effects can be extracted by using longitudinally polarized quark beams, which can potentially reveal the substructure of a quark [105, 106, 107, 108]. Furthermore, the chiral structure of the electro-weak sector of the Standard Model can be tested using the transversely polarized protons as will be described later.

Table 2.8: Initial state spin asymmetries in p+p collisions. (+) and (−) refers to the helicity states of the beams and ↑ and ↓ represent vertically *Up* and *Down* polarization.

Asymmetries	definition	remarks
$\mathcal{A}_{LL}$	$\frac{\sigma(++)+\sigma(--)-\sigma(+-)-\sigma(-+)}{\sigma(++)+\sigma(--)+\sigma(+-)+\sigma(-+)}$	often used to extract Δf
$\mathcal{A}_{TT}$	$\frac{\sigma(\uparrow\uparrow)+\sigma(\downarrow\downarrow)-\sigma(\uparrow\downarrow)-\sigma(\downarrow\uparrow)}{\sigma(\uparrow\uparrow)+\sigma(\downarrow\downarrow)+\sigma(\uparrow\downarrow)+\sigma(\downarrow\uparrow)}$	often used to extract δq
$\mathcal{A}_L$	$\frac{\sigma(+)-\sigma(-)}{\sigma(+)+\sigma(-)}$	sensitive to parity violation
$\mathcal{A}_N$	$\frac{\sigma(\uparrow)-\sigma(\downarrow)}{\sigma(\uparrow)+\sigma(\downarrow)}$	sensitive δq or higher twist effects

Spin asymmetries using initial state polarizations are summarized with their typical usages in Table 2.8. These asymmetries for various reactions in polarized p+p collisions are listed with the primary goals of their measurement in Table 2.9.

In the following subsections, we describe the sensitivity of PHENIX measurements for the questions mentioned above.

Table 2.9: Spin asymmetries for various p+p reactions along with the major goals of their measurement. References shown do not necessarily represent the initial work. "CI" and "2HDM" stand for Contact Interaction and Two Higgs Doublet Model, respectively. $\mathcal{A}_{LT}$ is not listed here but the asymmetry for $pp \to \gamma^* X$ can be found in Ref. [109].

process	$\mathcal{A}_{LL}$	$\mathcal{A}_L$	$\mathcal{A}_{TT}$	$\mathcal{A}_N$
$pp \to \gamma\ (+jet)\ X$	$\Delta g \otimes \mathcal{A}_1^p$ [110, 111]	–	~ 0 [112]	twist-3 [113]
$pp \to jet\ X$	$\Delta g \otimes (\Delta g + \Delta\Sigma)$ [114]	W/Z/CI [115]	~ 0 [112]	–
$pp \to Q\bar{Q}X$	$\Delta g \otimes \Delta g$ [116]	Z/2HDM [117]	–	–
$pp \to J/\psi X$	$\Delta g \otimes \Delta g$ [118]	–	–	–
$pp \to \chi_2 X$	$\Delta g \otimes \Delta g$ [119]	–	–	–
$pp \to W^+ X$	$\Delta u \otimes \Delta\bar{d}$ [120]	$\Delta u, \Delta\bar{d}$ [120]	~ 0 [121]	–
$pp \to W^- X$	$\Delta d \otimes \Delta\bar{u}$ [120]	$\Delta d, \Delta\bar{u}$ [120]	~ 0 [121]	–
$pp \to \gamma^* X$	$\Delta q \otimes \Delta\bar{q}$ [122, 109]	γ^*/Z mixing [123]	$\delta q \otimes \delta\bar{q}$ [124]	twist-3 [125]

2.3.2 Gluon Polarization

The measurements of the polarized gluon distribution at RHIC will be made with two different $\sqrt{s}$ values of 200 and 500 GeV in center of mass energy. While the polarized collider development for the 200 GeV has already started, the 500 GeV development is expected in the next three years depending on the Running Schedule being discussed in various forums. The higher energy running will allow measurements to be extended to lower values of x allowing measurements of the gluon distribution to very low values of $x \approx$ few $\times 10^{-3}$. The PHENIX detector's state of the art electromagnetic calorimetry coupled with the tracking in the central arms and novel muon end-cap tracking and identification scheme will allow measurements of the polarized gluon distribution using many different channels. Given the very different backgrounds and observables in these various channels, the cross-comparisons between them will provide a very strong set of systematic checks that will bring a high degree of confidence to the measurement of gluon polarization.

The PHENIX measurement of the gluon polarization will be performed using the following hadronic interaction channels:

- $\pi^{\pm}$ and π^0 production
- open heavy quark production
- inclusive prompt photon production
- photon + jet production

While the PHENIX baseline detector is able to perform the first three measurements listed above, the photon+jet channel becomes possible only with the PHENIX detector upgrade ideas already under consideration and discussed in Chapter 3. Furthermore, the same upgrades will also improve significantly the quality of the heavy quark and direct photon measurements listed above.

2.3.3 π^0 and $\pi^{\pm}$ Production in polarized pp collisions at PHENIX

PHENIX has recently released a preliminary result on the double spin asymmetry in π^0 production from longitudinal $\vec{p}+\vec{p}$ collisions based on the 200 nb^{-1} of data collected from the very short period of polarized proton running in Run-3. While the statistical significance of this result is limited, we have demonstrated for the first time that double spin asymmetries can be reliably measured with a polarized collider. We will make a decisive measurement of the gluon polarization with π^0 production in the next polarized proton run provided we are able to record a relatively modest ~ 7 pb^{-1} in integrated luminosity for collisions with 0.5 polarization of each beam. Figure 2.34 shows the present preliminary result, along with what could be expected in the next run with the above values of integrated luminosity and polarization.

Analysis of the charged $\pi^{\pm}$ for exploring the gluon polarization is underway and we expect to have preliminary results from Run-3 on this in the next few months. The expected

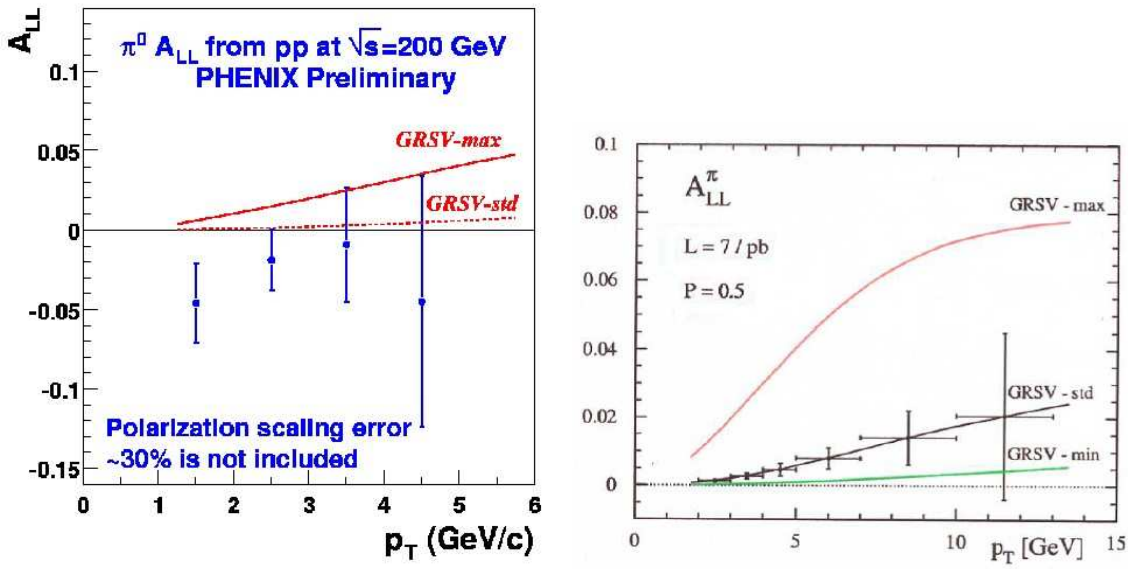

Figure 2.34: Left: The recent preliminary result on A_{LL} released by PHENIX with 0.2 pb^{-1} luminosity and ~ 0.26 average polarization of the beams. Right: What could be achievable in the polarized proton physics run given 7 pb^{-1} of integrated luminosity and 0.5 polarization in each beam.

accuracy is again limited by the low values of integrated luminosity and polarization obtained in Run-3, but the intention of this analysis presently is to show the proof of principle that such measurements can be made with the existing PHENIX detector, and to quantify the improvements anticipated with projected increases in integrated luminosity and beam polarization.

2.3.4 Open Charm and Bottom Production

The open charm and beauty production in p+p scattering is dominated by gluon-gluon fusion ($gg \to Q\overline{Q}$) rather than the quark annihilation process $q\overline{q} \to Q\overline{Q}$). Therefore, heavy flavor production is an excellent probe of the gluon distribution in the nucleon. The analyzing powers for these processes are known to Next-to-Leading-Order, and the double spin asymmetries for such reactions are estimated to be $\sim$ few $\times 10^{-3}$ [126]. While these asymmetries are small, we have recently shown based on our Run 2002/3 that the false asymmetries, which in a collider environment arise principally from lack of knowledge/control over bunch-to-bunch variations of the polarized bunches, can be (and have been) limited to below 2.5×10^{-4}. An effort to reduce this further by factors of 5 to 10 are underway, using an additional independent luminosity monitor and frequent spin reversals. With this perspective we are confident that the physics potential of open-charm and open-beauty production as a probe of gluon polarization is within the reach of the PHENIX detector if the detector systematics related to the detection of complete events in the heavy quark decay chain can be measured reliably in PHENIX.

PHENIX will select heavy flavor tagged events via channels $pp \to \mu^{\pm}X$, $pp \to e^{\pm}X, pp \to \mu^{+}\mu^{-}X, pp \to e^{+}e^{-}X, pp \to \mu^{\pm}e^{\mp}X$. Like-sign leptons are also possible from bottom with one direct b-decay to a lepton and one sequential decay through charm. Charm and bottom events will explore the gluon distribution (polarized and unpolarized) in the nucleon at different momentum fractions and scales. They also enter the analysis with different weights, so that taken together they will give a large range of coverage for the PHENIX polarized gluon distribution measurement.

In the latter portion of the decadal evolution of PHENIX, it is our plan to have the Silicon Vertex Detector (VTX) which will be able to resolve the secondary vertices which will provide another constraint as well as a way to select and analyze events with heavy quarks in them. This is discussed further in Section 3.2.2 of this document. With the VTX, not only does determination of the gluon distribution by each of the methods become robust, but each of the measurements gets an independent confirmation within PHENIX due to the extra systematic checks allowed by such a detector. In addition, the silicon vertex detector provides a significant extension in x to both lower and higher values by increasing the pseudo-rapidity coverage of the PHENIX detector for charged particles.

2.3.5 Prompt Photon Production

Prompt photon production, $pp, p\overline{p}, pN \to \gamma X$ has always been considered as the golden interaction to probe the gluon distributions at intermediate and high x in a nucleon. At leading order the final state photon is dominantly produced at RHIC by the $qg \to \gamma q$ reaction. (The $q\overline{q}$ initial state is suppressed by the low abundance of anti-quarks in the x regime accessible to RHIC). The analyzing power for prompt/direct photon production are large [127]. The experimental signature of a prompt photon is also rather distinct: an isolated single photon without surrounding hadronic activity. It is hence expected that this mechanism will play a significant and unique role in determining the polarized gluon distribution in PHENIX, as well as probing the unpolarized gluon distributions in p+A and A+A physics, as discussed in Section 2.2.2.

Although theoretically apparently clean, experimentally identifying a direct photon event is not without some subtleties. The high p_T photons detected in PHENIX could also be produced via a fragmentation process. Theoretical issues related to the possible origin of the fragmentation photons are summarized in [127]. Experimentally, one then needs to make an isolation criteria for the prompt photon of interest: the fake (fragmentation) high p_T photons are surrounded by hadronic activity and a real prompt photon is not. How to separate them in reality in PHENIX is a topic of intense interest and ongoing discussion in the various PHENIX physics analysis groups. Techniques being developed in the next two years using the actual data recorded by PHENIX will allow us to be reach the ultimate limits for prompt photon physics when the polarization and the luminosities of the collider approach the values necessary to pursue the polarized gluon distribution via this channel. Assuming that we will be able to isolate the prompt photons in the polarized proton collisions at high luminosities and polarization in future, a study was performed to see what statistical sensitivities would be achieved and what selectivity the method would have in PHENIX to identity the correct

polarized gluon distribution from a range of distributions which are presently allowed based on the pQCD fits at NLO of the DIS data. Figure 2.35 shows the statistical accuracy that could be achieved with the PHENIX detector given the design luminosities of RHIC at two different center-of-mass energies.

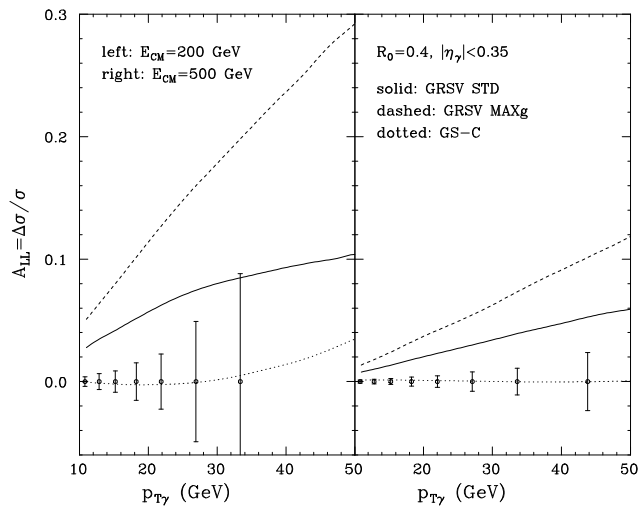

Figure 2.35: PHENIX sensitivity for $\Delta g/g$ with prompt photon production estimated for the integrated luminosity of 320 pb^{-1} ($\sqrt{s}$=200 GeV) and 800 pb^{-1} ($\sqrt{s}$=500 GeV).

Once these data are at hand, and the method to analyze them is perfected, it is natural to envision a global analysis combining these results with the rest of the world's available data on polarized gluon distribution obtained using various different methods. Presumably the best knowledge of the polarized gluon distribution will be extracted over a broad range of momentum fraction x when all these data are analyzed together in a consistent way. Efforts towards this goal are already underway among the various theoretical collaborations dedicated to the analysis of structure functions in QCD. We of course anticipate a strong participation in these combined analyses from the Experimental groups internal to PHENIX.

2.3.6 Flavor Decomposition of Quark and Anti-Quark Polarization

The present dominant source of information on polarized parton distributions, polarized DIS, is only sensitive to the electric charge squared. As a result, it is difficult to separate the contributions of quark and anti-quark to the polarized parton distribution. PHENIX offers the exciting possibility of using the parity violating asymmetry for W production to directly measure the polarization of u, $\bar{d}$, d, and $\bar{u}$ quarks in the polarized proton:

$$\mathcal{A}_L^{W^+} = \frac{\Delta u(x_1)\bar{d}(x_2) - \Delta\bar{d}(x_1)u(x_2)}{u(x_1)\bar{d}(x_2) + \bar{d}(x_1)u(x_2)}. \tag{2.7}$$

(To obtain the W^- asymmetry, u and d should be interchanged.) These measurements will be done in PHENIX by measuring the electrons and muons from the W decays $W \to e\nu$ and $W \to \mu\nu$ in polarized p+p collisions at $\sqrt{s}$=500 GeV.

An alternative approach available at lepton-hadron facilities is to utilize semi-inclusive DIS (SIDIS) of a polarized lepton off the polarized nucleon as was done in the HERMES experiment at DESY and SMC experiment at CERN. The detection of the final state hadron enhances the contribution of a specific flavor, which is, in principle, useful in the flavor decomposition of the quark polarization. The enhancement of specific flavors is determined from the fragmentation functions, which describes the hadronization of quarks/anti-quarks into hadrons. However currently there are no experimental data in the HERMES kinematic region, which results in the major ambiguity in the flavor-separated quark distributions using this method.

In contrast, the W has no fragmentation contribution. The large mass of the W-boson, which determines the Q^2 of the reaction, ensures the reliable application of perturbative QCD. The sensitivity of W measurements with PHENIX Muon Arms and HERMES SIDIS measurements are compared to the models of polarization of quarks [128, 129] as functions of x in Figure 2.36(a). Error bars associated with closed circles represent the projected statistical precision from W measurements at PHENIX ($W \to \mu\nu$ only). Projected errors from all HERMES data (as of November 2000) are represented by the error bars with squares [4]. The HERMES precision is limited especially in the anti-quark measurements due to the relatively smaller contribution of anti-quarks from the target nucleon in the production of hadrons.

In addition to W measurements at full energy of polarized protons at RHIC, Drell-Yan production of lepton pairs contains useful information on the anti-quark polarization. It should be noted that the annihilation process underlying Drell-Yan production posseses the maximally negative asymmetry of -1 at the partonic level.

Based on the measured polarized quark distributions, we can also perform a search for new physics beyond the standard model. The sensitivities with jet production is illustrated in Figure 2.36(c). The measurements will provide significant constraints on the size and/or the chiral structure of possible new physics signals. Further studies on possible searches for new physics are underway [130].

2.3.7 Transversity

High energy, deeply inelastic lepton-nucleon and hadron-hadron scattering cross sections can be described with the help of three independent nucleon helicity amplitudes. Measurements of the nucleon structure functions $F_1(x, Q^2)$ -the helicity average- and $g_1(x, Q^2)$ -the helicity difference-, have explored the helicity conserving part of the cross sections with great experimental accuracy.

In contrast, no information is presently available on the helicity flip amplitude. The absence of experimental measurements is a consequence of the chiral-odd nature of the helicity flip amplitude and the related "transversity quark distributions", $\delta q(x, Q^2)$, which prevents the appearance of helicity flip contributions at leading twist in inclusive DIS experiments.

[4] Private communication with V.Manuella from the HERMES experiment.

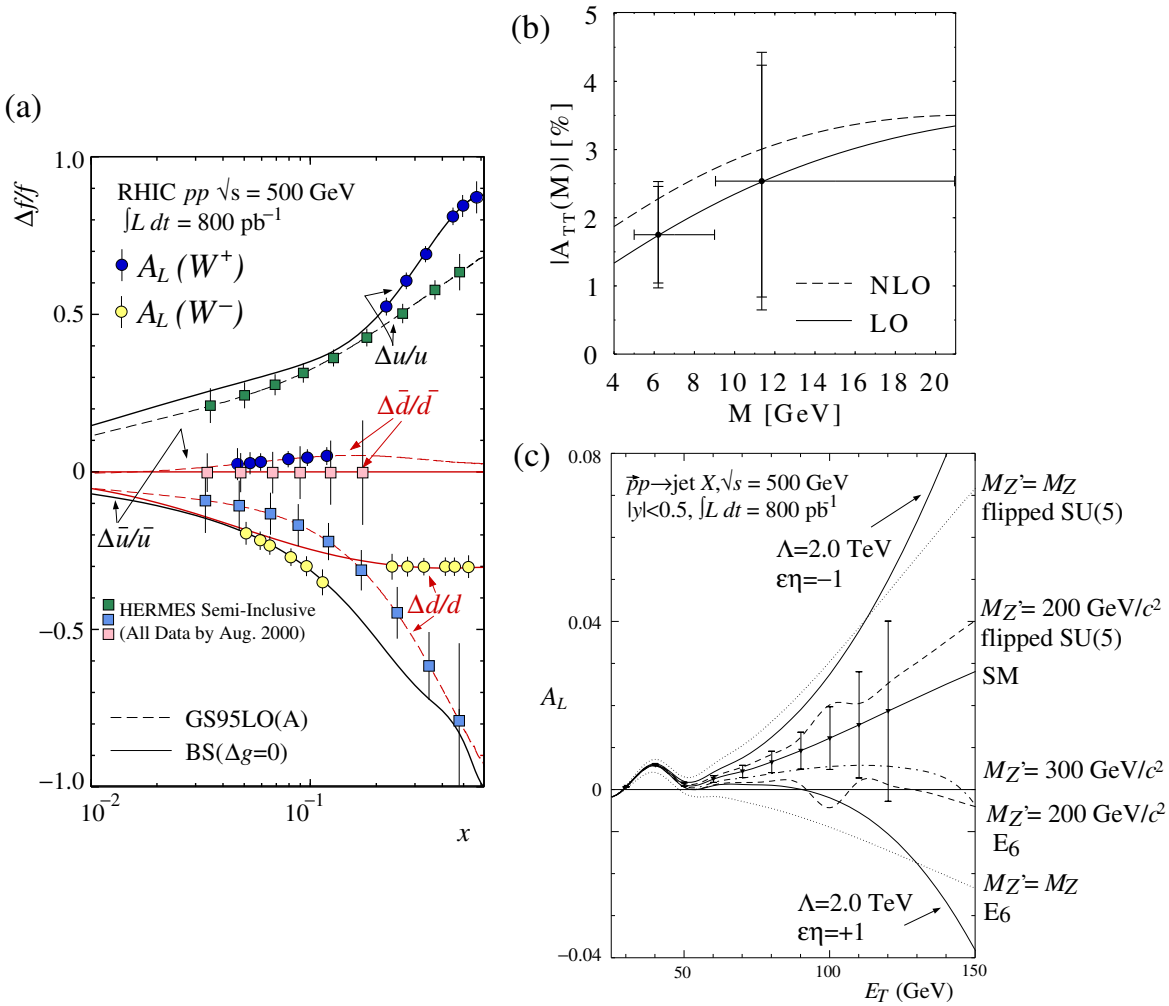

Figure 2.36: Left: Polarization of u, d, $\bar{u}$, $\bar{d}$ as functions of x modeled by Bourreley-Soffer, and Gehrmann-Stirling. Sensitivities of HERMES SIDIS measurements and PHENIX W measurements are shown. Right: Double transverse-spin asymmetry for Drell-Yan dimuon production at $\sqrt{s} = 200$ GeV. (c) Parity violating asymmetry $\mathcal{A}_L$ for jet production compared with the SM, contact interaction, and leptophobic Z' [108].

The current interest in transversity distributions results from recent HERMES [131] and SMC results [132] in semi inclusive deep inelastic scattering. In particular, recent results from HERMES experiment with the transversely polarized target suggest that Collins's function $H_1^{\perp}$ *and* the transversity distribution function δq are different from zero and measurable. Although precise statements on the shape and magnitude of the functions cannot be made from this data, clearly the prospects are exciting to have a tool at hand which, for the first time, provides access to the complete helicity structure of nucleons in hard scattering processes [133].

In a partonic picture of the nucleon transversity distributions are interpreted as distributions that describe the probability of probing a quark with spin parallel vs anti-parallel in a transversely polarized nucleon target. Among the interesting characteristics of transversity distributions are:

- The relation between chiral symmetry breaking and transversity in the nucleon [134].
- The helicity flip gluon distribution is zero at leading order and thus there is no mixing between quark and gluon degrees of freedom in the Q^2 evolution.

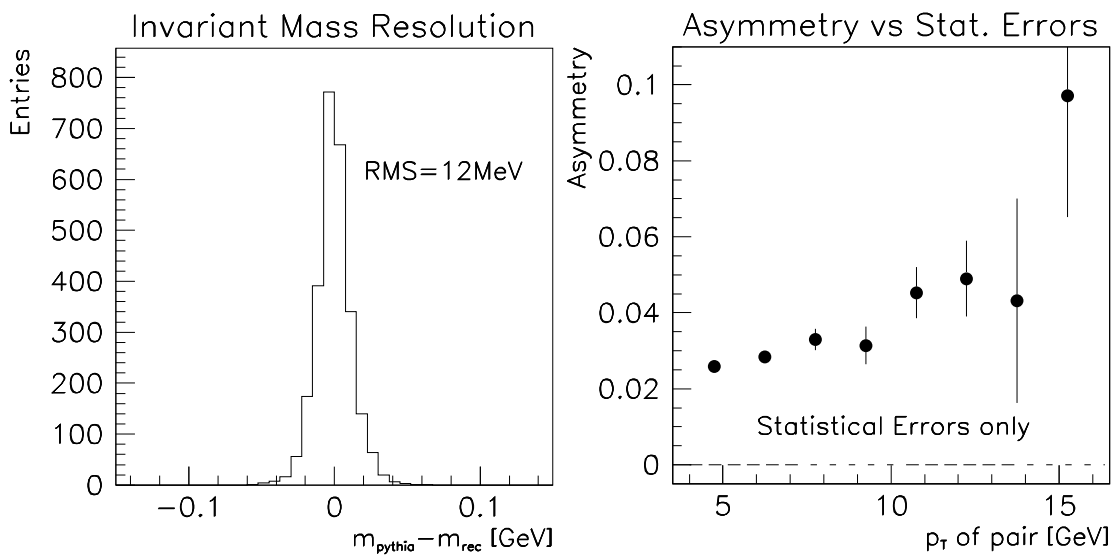

Figure 2.37: **Left**: The invariant mass resolution for pion pairs in the ρ-mass region. **Right**: Projected transverse single spin asymmetries compared to statistical errors, $\int Ldt = 32\,\mathrm{pb}^{-1}$.

At RHIC the proposal of Collins et al. [135] and Jaffe *et al.* [136] to utilize two-meson interference fragmentation appears to be a very promising channel for transversity measurements. Studies of the projected asymmetry measurements at RHIC show favorable results [137]. The relevant process is pion pair production in p+p scattering with one proton transversely polarized. It is essential to experimentally identify pairs of oppositely charged mesons coming from the invariant mass region of S/P-wave interference (e.g. the ρ/σ region). Experimental studies have shown that rates are high at RHIC and that the invariant mass resolution of the PHENIX detectors is more than sufficient for this purpose, see left plot in Figure 2.37. Projected sensitivities, based on Tang's and Jaffe's model calculations [136], are shown in the right plot of Figure 2.37.

2.3.8 New Physics Searches

Jet production in p+p collision is dominated by quark-quark scattering in the high E_T region. Thus the single longitudinal-spin asymmetry $\mathcal{A}_L$ can be expressed as

$$\mathcal{A}_L \approx \sum_{i,j} \frac{\Delta q_i(x_1)}{q_i(x_1)} \cdot \frac{q_j(x_2)}{q_j(x_2)} \cdot \frac{\Delta\sigma}{\sigma}(q_i q_j \to q_i q_j) + (i \leftrightarrow j). \tag{2.8}$$

The quark flavor here is dominated by u and d due to their abundance in the large x region. These distributions will be precisely measured in W production, as described in Section 2.3.6. The ratio of spin-dependent cross section to spin-averaged cross section will be the only unknown in the expression, so that it will be determined from the measurement to compare with the Standard Model (SM) expectation. Any deviation from the Standard Model will immediately indicate the presence of new physics.

The baseline configuration of PHENIX does not have a jet reconstruction capability. However, hadron production, especially neutral pion production with large transverse momentum, which is dominated by hard scattering of quarks, can be used to determine if there is any deviation from the SM prediction. In addition, as described in Section 3.2.2, the proposed upgrade with the Silicon Tracker will add jet reconstruction capability to PHENIX.

In addition to the parity violation studies, an important test of the SM in the electroweak part can be done by using the transversely polarized protons. As described in the previous section, the double transverse-spin asymmetry A_{TT} is sensitive to the transversity distribution of quarks, which probes the interference between right-handed quarks and left-handed quarks. W production in p+p collisions is a pure $V - A$ process and thus selects only the left-handed current. Therefore A_{TT} for W production should be completely zero at the leading order. Further studies have shown that this prediction is unchanged by higher order corrections [121]. This implies that observation of nonzero A_{TT} would immediately suggest the existence of physics beyond the standard model, such as a right-handed W.

The current limit of right-handed W mass, $M_{W_R} > 715$ GeV/c^2 comes from the global electro-weak analyses. At RHIC only virtual effects should be seen. As a consequence, this study represents one of the most important and independent checks of the chirality structure of the electro-weak sector of the SM.

2.4 Proton-Nucleus Collision Physics

It has long been recognized that p+A collisions[5] serve an important role in the search for quark-gluon plasma (QGP) in relativistic heavy-ion collisions. While the QGP is in general not expected to be produced in p+A collisions, a comparison of the A+A with p+A data at identical kinematic conditions is nonetheless crucial for understanding potential modifications to those signatures for QGP formation that are already present in the proton-nucleus environment. This was demonstrated in the AGS and SPS heavy-ion programs, which benefited greatly from the p+A measurements for interpreting the A+A results. This important role of p+A collisions was again demonstrated by the recent (2003) results from the d+Au run at RHIC. In this case the results for high-p_T hadrons and π^0's [27] showed that the suppression effects previously measured [8, 16, 18] at RHIC were truly new phenomena. The Run-3 d+Au data set also establishes a solid baseline for many channels such as J/Ψ's and direct photons that will be studied with the much higher integrated luminosity Au+Au data set that will be measured in Run-4.

In addition to their connection to A+A physics, p+A measurements are important in their own right. Many outstanding questions in hadron physics can be addressed at RHIC, which provides unprecedented opportunities for exploring proton-nucleus collisions. The center-of-mass energy reached at RHIC in p+A collisions is roughly an order of magnitude higher than that for any existing fixed-target proton-nucleus experiments. Moreover, large-acceptance collider detectors such as PHENIX are capable of measuring many particles produced in the p+A collisions simultaneously, which could provide qualitatively new information not accessible in previous fixed-target experiments.

Thus, the data from d+Au collisions will both play an essential role for interpreting the Au+Au data and also will provide unique information on the partonic structure in nuclei and the propagation of partons in a cold nuclear medium. Some specific physics results which could be obtained by PHENIX in p+A or d+A runs include:

- The study of parton energy-loss and jet quenching in cold nuclear matter via the measurement of high-p_T single hadrons up to large p_T values.

- The study of cold nuclear matter effects on particle production in hard and semi-hard processes to higher momentum. This includes measurement of fragmentation functions of moderate energy jets in p+A collisions as well as the Cronin effect for identified hadrons.

- A measurement of J/Ψ (and eventually Υ) production in the nucleus covering a wide kinematic regime including small Bjorken-x and negative x_F. As a result, nuclear shadowing of gluons at small x can be studied.

- A measurement of open-charm and -beauty production and heavy-quark propagation in a cold nucleus via the detection of high-p_T single leptons.

[5] In this discussion the generic term 'p+A' is sometimes used in place of 'd+A'.

- A study of the correlation of various observables with the centrality of the collisions including with the number of "grey tracks" detected with the forward-angle calorimeter.

In addition, an extensive list of physics topics at relatively low p_T such as $dN/d\eta$, $dE_T/d\eta$, elliptic flow, HBT, particle/antiparticle ratios, medium effects on Φ production, event-by-event fluctuation, etc., can also be studied with p+A collisions.

The 2003 d+Au run has demonstrated the capability of colliding asymmetric species at RHIC. The results from that run form an important basis for future planning to realize the full potential of the p+A program at RHIC. In the remainder of this section we briefly summarize some of the physics justifications for d+Au running. The expected event rates for some measurements are also presented. These rates are calculated based on the C-A D model for luminosity development [138]. Vertex cuts, PHENIX up-time, trigger efficiency and realistic acceptances and detector efficiencies are taken into account, so that the predicted yields can be taken as conservative estimates.

2.4.1 Effects on jets of cold nuclear medium

Recent results from PHENIX indicate a strong suppression of high p_T hadrons in central Au+Au collisions [8, 18, 22] that does not occur in d+Au collisions [27]. Figure 2.38 shows a compilation of these striking results. Taken together, these results lead to the conclusion that the observed suppression of both charged and neutral hadrons cannot be an initial state effect of the nuclear medium but must instead be a final state effect of the produced dense medium.

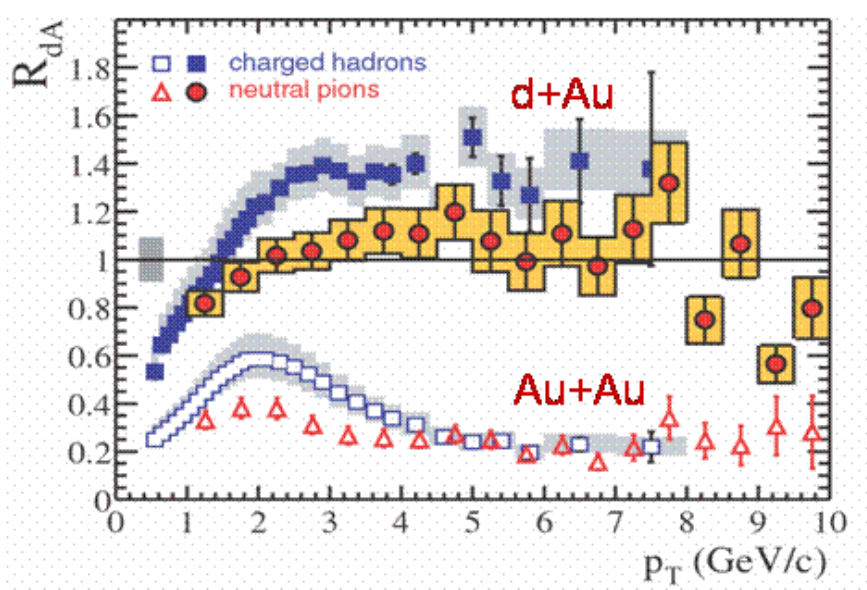

Figure 2.38: Nuclear modification factor of charged hadron and π° p_T spectra for central d+Au and Au+Au collisions at $\sqrt{s} = 200$ GeV. [22, 27]

In d+Au collisions, the yield of high p_T hadrons per nucleon-nucleon collision is actually somewhat enhanced somewhat when compared to p+p collisions. This enhancement, generally referred to as the "Cronin effect", has been shown by PHENIX to increase with the number of nucleons participating in the collision. Theoretical expectations, and observations at lower $\sqrt{s}$ at Fermilab [38], indicate that at sufficiently large p_T the Cronin effect should disappear. The current data have insufficient statistical precision to reliably determine the p_T value at which the yield returns to that expected from p+p collisions at RHIC. An increase of an order-of-magnitude or more in integrated luminosity will be required to address this question.

Furthermore, data from Fermilab indicate that the enhancement is larger for baryons than for mesons [139]. This is observed by PHENIX to also be the case at RHIC at moderate p_T values, as illustrated in Figure 2.39. The physics underlying the Cronin effect is generally ascribed to semi-hard initial state scattering, but the reason for the larger enhancement of baryons is completely unknown. Unraveling the physics of the Cronin effect will require a long d+Au run, and a fully operational aerogel upgrade (described in Section 3.2.1) to extend the hadron identification to higher p_T values.

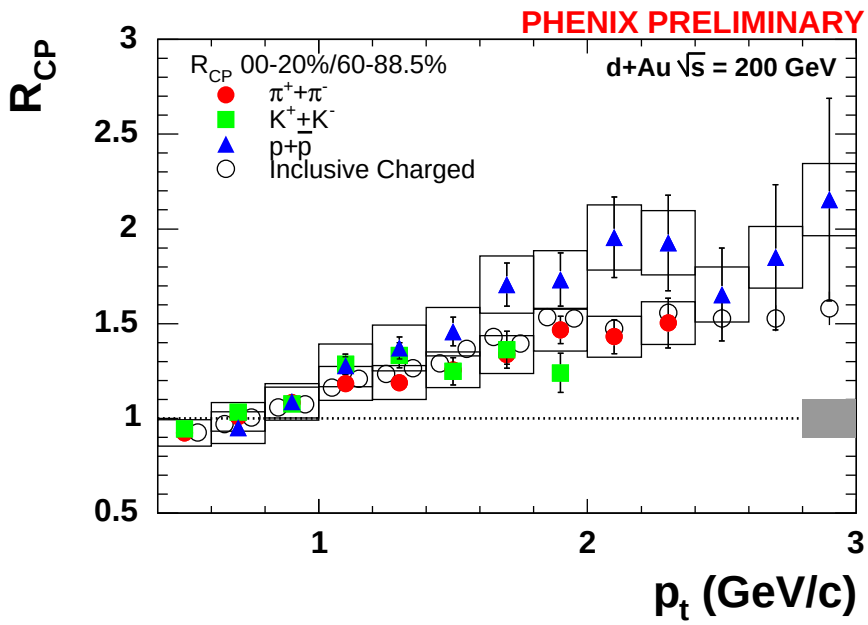

Figure 2.39: Ratio of yields per NN collision of pions, kaons, and protons in central d+Au collisions to yields per collision in peripheral collisions. The data were taken at $\sqrt{s} = 200$ GeV per nucleon pair.

Further d+Au comparison running is also motivated by the need to quantitatively understand the production and fragmentation of moderate energy jets at RHIC (5-15 GeV). A high statistics d+Au data set will allow the study of γ-jet and jet-jet coincidences to determine the broadening of the parton k_T distribution in nuclear matter. This directly influences the

opening angles of dijets used to probe the medium in Au+Au collisions. Single hadron yields at high p_T in Au+Au indicate a surprising enhancement of baryon production. There are numerous papers seeking to explain this, but quantitative understanding is hampered by lack of knowledge of the fragmentation function of jets in the energy range prevalent at RHIC. A long d+Au run will provide sufficient statistics for PHENIX to use its superb existing - and upgraded for higher p_T - particle identification capabilities to measure the fragmentation function in d+Au. We will also compare to measurements planned for p+p collisions. Again, the existing d+Au data set has insufficient p_T reach for a definitive measurement.

2.4.2 Nuclear Shadowing

Proton-nucleus collisions not only provide important baseline information for the study of QCD at high temperatures, they also address the fundamental issues of the parton structure of nuclei. Since the discovery of the EMC effect in the 1980's, it is clear that the parton-level processes and structure of a nucleon are modified when embedded in nuclear matter [140, 141]. These modifications reflect fundamental issues in the QCD description of the parton distributions, their modifications by the crowded nuclear environment of nucleons, gluons and quarks, and the effect of these constituents of the nucleus on the propagation and reactions of energetic partons that pass through them. Of particular interest is the depletion of low momentum partons (gluons or quarks), called shadowing, which results from the large density of very low momentum partons. For gluons at very low momentum fraction, $x < 10^{-2}$, one can associate with them, following the uncertainty principle, a large distance scale. These high-density gluons then will interact strongly with many of their neighbors and by gluon recombination or fusion are thought to promote themselves to larger momentum fraction, thereby depleting small values of x. In recent years a specific model for these processes, called gluon saturation, which affects both the asymptotic behavior of the nucleon gluon distributions as x approaches zero and the modification of this behavior in nuclei, i.e. shadowing, has been discussed extensively by McLerran and collaborators [142, 143, 144].

At RHIC energies many of the observables accessible to PHENIX sample regions of very small x where nuclear shadowing is thought to be quite strong. However, theoretical predictions of the amount of shadowing differ by factors as large as three. For example, in the production of J/Ψ in the large rapidity region covered by the PHENIX muon arms, as shown in Figure 2.40, models from Eskola et al. [145] predict only a 30% reduction due to gluon shadowing, while those of Frankfurt & Strikman [146] or Kopeliovich [147] predict up to a factor of three reduction. Results from the measurements of the just-completed d+Au run should help to clarify how much shadowing is present, but increased statistics from higher luminosity runs and more definitive measurements with enhanced detectors capable of making more exclusive measurements in several channels will be necessary to test the theory with sufficient power to constrain the underlying QCD processes.

During the p+A runs, the large integrated luminosity will allow extensive measurements of the gluon structure function with direct photons to allow direct and unambiguous measurements of shadowing as a function of A. (This is discussed in more detail in Section 2.2.2.1). Should the End Cap EMCalorimeter be installed during these runs, the low end of the x

range will be extended downwards by a factor of 3 using gamma-Jet coincidences compared to the case when measurements are made with inclusive gammas in the central detector. See Section 2.2.2.4 for more details.

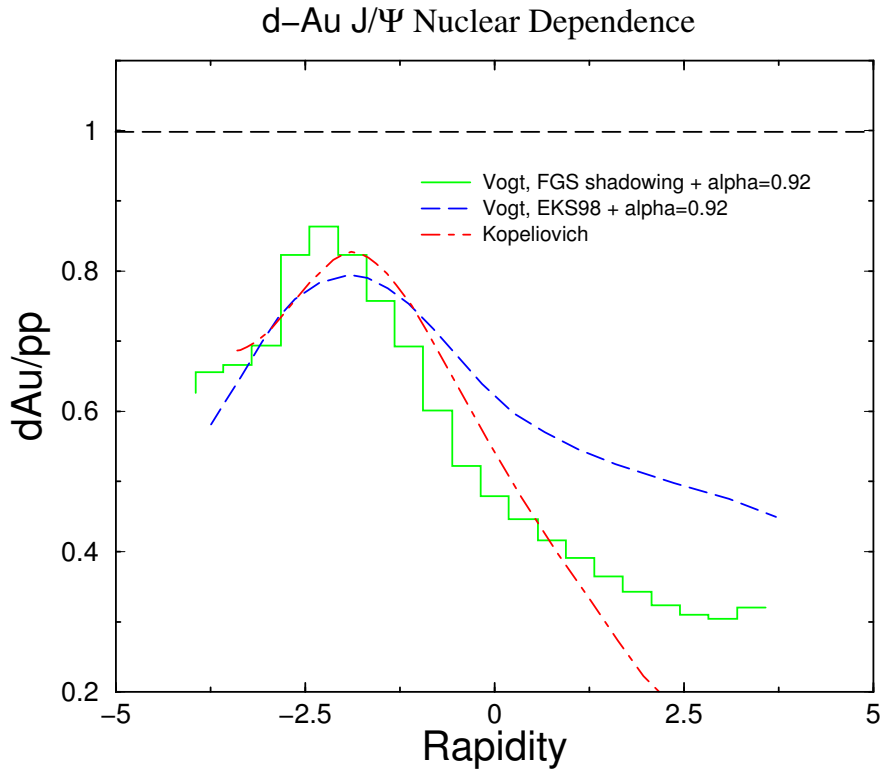

Figure 2.40: Rapidity dependence of shadowing in the nuclear dependence of J/Ψ production for three different shadowing models [145, 146, 147]. The first two curves, green dot-dashed and blue dashed, are calculations from Vogt using the shadowing prescriptions from Frankfurt & Strikman [146] and Eskola [145]. Since Vogt did not include nuclear absorption in these calculations we have added a rapidity-independent absorption factor corresponding to $\alpha = 0.92$. The last model is that of Kopeliovich [147]

2.4.3 J/Ψ Production

The production and suppression of J/Ψ and other heavy vector mesons is a cornerstone of the RHIC physics program. The apparently anomalous suppression of the J/Ψ at CERN was presented as a crucial piece of evidence for the possible creation of a QGP. However, as shown in measurements at Fermilab(Figure 2.41) and CERN the pattern of nuclear suppression in p+A collisions is somewhat complicated. A thorough understanding of the effects of absorption, shadowing, and initial-state gluon energy loss, which are thought to be the most important effects in cold nuclear matter, is critical before definitive conclusions can be drawn from what we might observe in heavy-ion collisions. (It is also clear from Figure 2.41 that

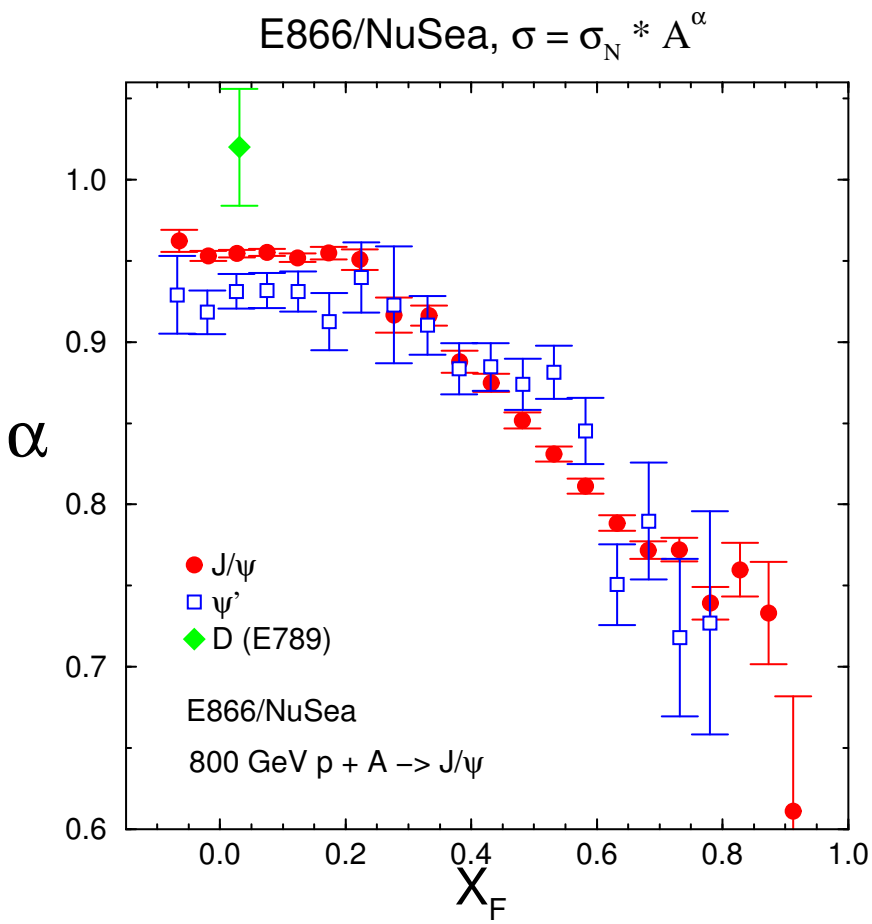

Figure 2.41: Nuclear dependence in 800 GeV p+A collisions from E866/NuSea and E789 [148, 149] showing a comparison of open (D meson) and closed charm (J/Ψ). The lack of suppression for open charm at mid-rapidity where the J/Ψ has substantial suppression is due to absorption, which affects only the J/Ψ.

open charm measurements with better accuracy over a broad range in x_F would be very valuable.) As already discussed in the previous section, gluon shadowing and energy loss in nuclei are also of intrinsic interest, and the careful measurement of their effects can lead to an understanding of some fundamental aspects of QCD in nuclei.

It is clear that a precise knowledge of the shadowed gluon structure functions in nuclei obtained from the study of p+A collisions is essential in understanding several of the important signatures for QGP in heavy-ion collisions at RHIC including open and closed heavy-quark production. Recombination models for J/Ψ production, which might cause an enhancement of that production in heavy-ion collisions due to the large density of charm quarks created in a nucleus-nucleus collision, must be constrained by an accurate measurement of the amount of charm produced given the shadowing of the gluon densities in the colliding nuclei. In the J/Ψ studies done at CERN by NA38/50 [150] the J/Ψ yields were usually divided by the Drell-Yan dimuon yields, since the latter should have little nuclear dependence. But this is actually an unnatural procedure since the Drell-Yan process involves quarks ($q\bar{q}$ annihila-

tion) while J/Ψ production involves gluons (gluon fusion). The nuclear effects on the initial parton distributions for quarks and gluons are likely different and their energy loss in the initial state before the hard interaction are also likely different. Additionally the yields of Drell-Yan dimuon pairs were quite small at CERN and dominated the statistical uncertainties in this ratio. The rates for Drell-Yan at PHENIX are even smaller and making such a ratio even more problematic at RHIC. It is much more natural to compare J/Ψ production to open-charm production, where the initial-state effects are presumably the same. Therefore a robust measurement of open-charm is quite important for the physics of the J/Ψ. Of course, it has also been suggested by some theoretical analyses [151, 152] that the effective gluon distributions are process dependent, and different for e.g. open- and closed-charm production. These models suggest that such a difference, if seen by comparisons of open and closed charm, would indicate that higher-twist contributions to closed charm production were substantial.

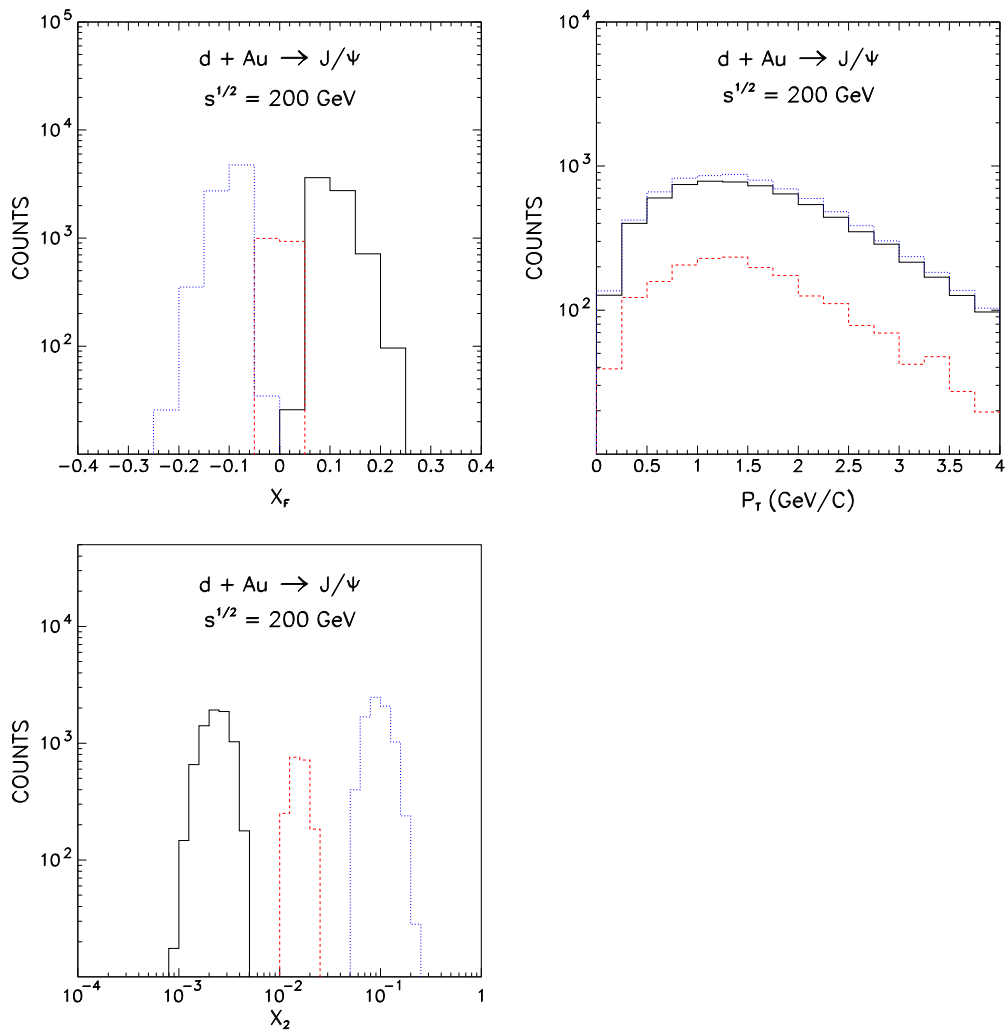

Figure 2.42: Expected event distributions for the J/Ψ in a $20nb^{-1}$ d+Au run at $\sqrt{s} = 200$ GeV. The solid, dashed, and dotted histograms correspond to the North muon arm, central arm, and South muon arm detection, respectively [153].

The event distributions as a function of x_F, p_T and x_2 for approximately 15,000 $J/\Psi \rightarrow \mu^+\mu^-$ reconstructed events for the South and North Muon Arms and about 2,000 $J/\Psi \rightarrow e^+e^-$ events reconstructed in the central arm are shown in Figure 2.42. This corresponds roughly to an integrated d+Au luminosity of approximately 20 nb^{-1}. The coverage in p_T and x_2 is quite broad, allowing a detailed study of the J/Ψ production as a function of these variables. Of course the level of statistical precision needed in a p+A run for J/Ψ observables should match or exceed the levels that will be achieved in the corresponding Au+Au or p+p runs.

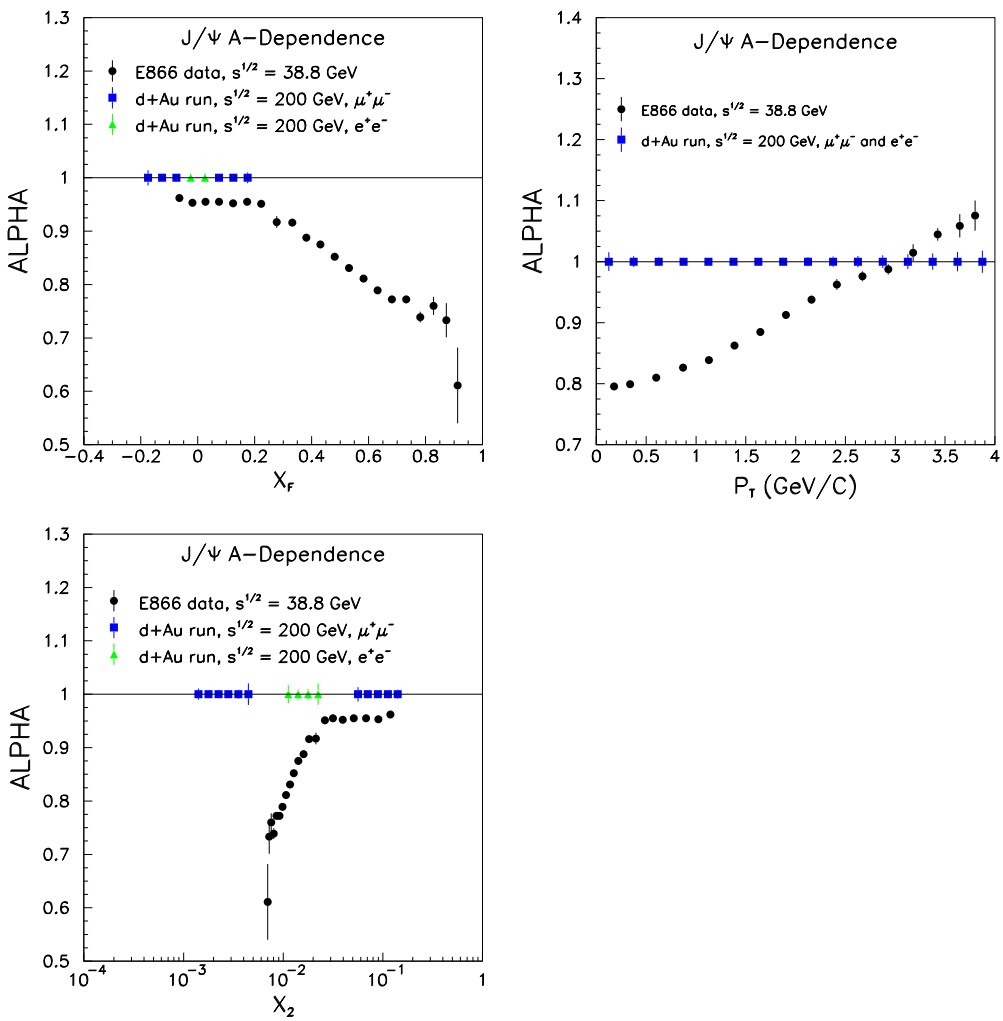

Figure 2.43: Expected statistical precision for measuring the nuclear dependence parameter α from a 20 nb^{-1} d+Au run at PHENIX. Data from a fixed-target experiment [148] at $\sqrt{s}$ = 38.8 GeV are also shown [153].

By comparing the J/Ψ production cross sections of d+Au versus p-p, one can determine the nuclear-dependence parameter α as a function of x_F, p_T, and x_2. The nuclear dependence is parameterized as A^α. Figure 2.43 shows the expected statistical accuracy for α for a d+Au

run with 15,000 J/Ψ's as discussed above. We assume the corresponding p+p run has an integrated luminosity comparable to that of d+Au. Also shown for comparison in Figure 2.43 are the data obtained at the Fermilab fixed-target experiment E866 [148].

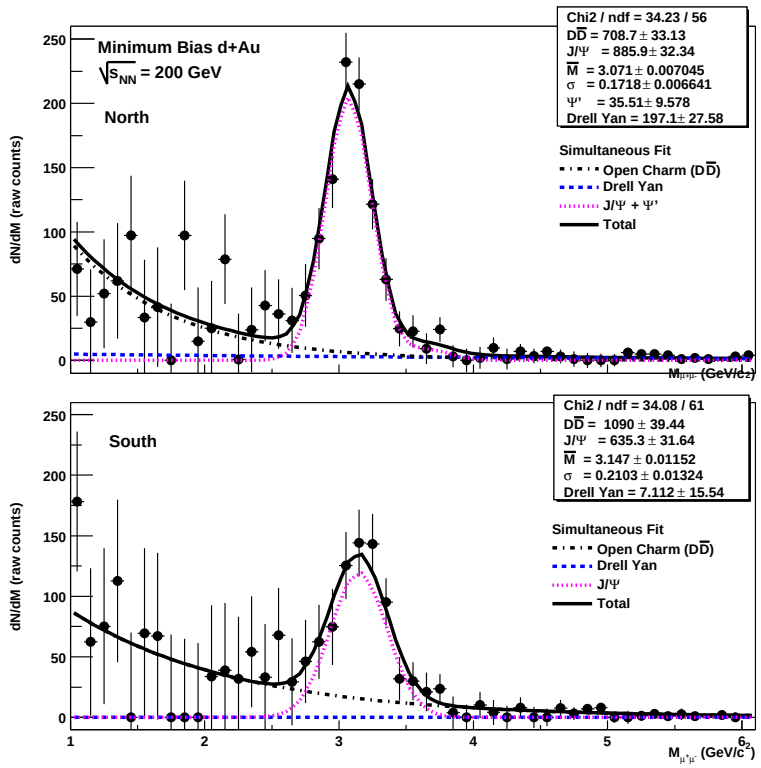

Figure 2.44: $J/\Psi \rightarrow \mu^+\mu^-$ mass peaks from PHENIX for the 2003 d+Au run. These yields are not corrected for efficiencies and relative luminosity for the samples shown for the two muon arms.

In Figure 2.44 shows the recently observed J/Ψ mass peaks from the 2003 PHENIX d+Au run. These data, when fully analyzed, will give us a first look at the physics discussed above, but because of the limited statistics will in all likelihood need to be followed up in the future with a much higher luminosity run.

2.4.4 Open-charm Production

The study of open-charm via high-p_T leptons (electrons and muons) is important

- to complement the J/Ψ studies where some, but not all, of the nuclear modification physics may be the same as for open-charm, and to isolate different nuclear effects from each other,
- to investigate how much energy charm quarks lose in cold nuclear matter and contrast that with the energy loss of light quarks,

- and to establish a cold-nuclear matter baseline for similar measurements in Au+Au collisions, e.g. the possible enhancement of charm production in the presence of a QGP.

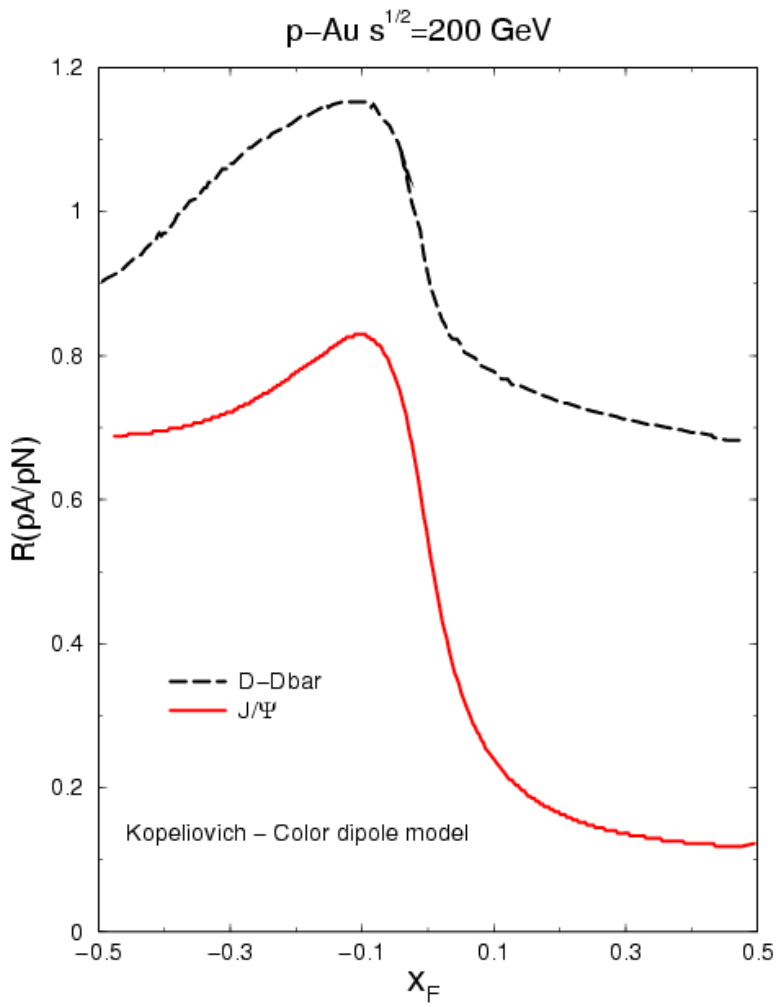

Figure 2.45: The difference in the effect of shadowing on open and closed charm for the color-dipole model [151, 152]. The shadowing difference is exhibited by the larger drop between mid-rapidity and large rapidity for the lower solid curve (J/Ψ) as compared to that for the upper dashed curve (open charm).

Normally, nuclear shadowing of the gluon distributions is a property of the parton distributions in nuclei and is common between open and closed-charm production. Other initial state effects such as the Cronin effect (initial-state multiple scattering of the partons) are

also common. But final-state effects may be quite different for open- and closed-charm, e.g. the absorption of $c\bar{c}$ bound states which would be absent for open-charm. Measurements of open-charm when contrasted to those for closed-charm will serve to separate these two kinds of effects. Furthermore, in some models, the effect of shadowing is dramatically different for closed and open-charm, e.g. in the Kopeliovich model the suppression in p+A collisions at large x_F is more than twice as strong for the J/Ψ as it is for open-charm production, as shown in Figure 2.45 A comparison of J/Ψ and open-charm production should be able to confirm or deny this process dependence [151, 152].

In the results for high-p_T hadrons in Au+Au collisions, light quarks appear to experience substantial energy loss in traversing the hot-dense collision region. On the other hand, the high-p_T charm measurements, within their presently limited accuracy, show no similar effect [11]. If confirmed, this could be the first indication of the so called "dead-cone" effect [71] which predicts that heavy quarks would lose much less energy than light quarks even in hot-dense matter. Therefore it will be quite interesting to contrast these measurements in p+A collisions as well and to look for such differences between light and heavy quark propagation even in cold nuclear matter. A clear strength of the PHENIX detector in addressing these issues is the wide coverage in kinematic variables (e.g. x_{target} or x_F) between the two muon arms and the central arm, all of which can contribute open-charm measurements in different regions of kinematics and can contrast the physics effects which have dramatic dependencies on the kinematic variables.

2.4.5 Centrality Tagging

The centrality dependence of many of the hard processes discussed here is of considerable interest. For instance, the nuclear shadowing of the gluon should have a centrality dependence caused by the larger densities and path-lengths sampled in a central collision versus a peripheral collision [71].

The centrality and the number of nucleon-nucleon collisions in p+A can be characterized using the Beam-Beam counters to count secondary particles, whose yield is proportional to the number of participating target nucleons. In addition, PHENIX has a forward angle calorimeter, installed in 2003. The forward calorimeter can also be used to determine the number of "gray" tracks emitted in a given event and provides an independent measure of the collision centrality in a similar way as was done in lower energy experiments [154].

Of particular interest in d+Au collisions is the ability to tag whether the neutron or the proton in the deuteron interacted with the Au nucleus, using information from the zero-degree and forward calorimeters on the deuteron-going side of PHENIX. Requiring the energy deposit of a beam-energy neutron to be detected in the zero-degree calorimeter, and counting the secondary particle production in the Beam-Beam counter isolates the proton interactions, while requiring a large energy deposit in the forward calorimeter allows identification of n+A collisions by selecting unreacted beam energy protons. Figure 2.46 shows the correlation of energy deposits in the zero degree and forward angle calorimeters.

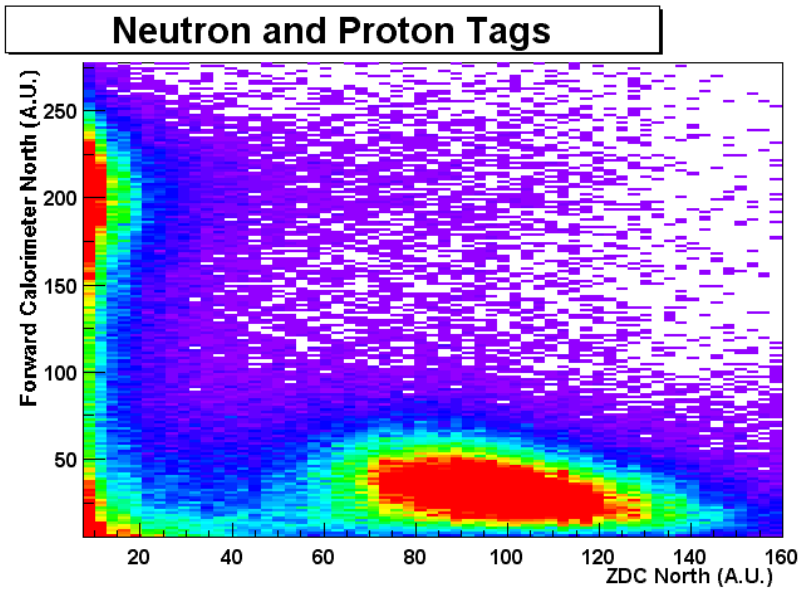

Figure 2.46: The correlation of energy deposits in the zero degree and forward angle calorimeters. The forward calorimeter can also be used to determine the number of "gray" tracks emitted in a given event to provide an independent measure of the collision centrality.

2.4.6 Other physics opportunities at high luminosity

A number of other important physics signals become accessible with substantially higher integrated luminosities than presently available. These are summarized in Table 2.10 and then briefly discussed below.

Table 2.10: Estimated physics yields for d+Au collisions for several processes with various integrated luminosities. For the lower rate process such as the Υ this illustrates the much larger luminosities needed in order to reach this physics.

$\int \mathcal{L}dt$	Process	North Muons	South Muons	Electrons
20 nb^{-1}	J/Ψ	8.3k	6.4k	3.3k
200 nb^{-1}	Ψ'	1650	1280	660
200 nb^{-1}	Υ	47	40	56
200 nb^{-1}	Drell-Yan ($M > 4\ GeV$)	4.9k	3.8k	1k ($M > 3\ GeV$)
200 nb^{-1}	DD ($M > 1.6\ GeV$)	25k	20k	
200 nb^{-1}	$D \rightarrow \mu X$	2B	2B	
200 nb^{-1}	$B \rightarrow \mu X$	5M	5M	

- In a physics sense the Ψ' is a cleaner probe than the J/Ψ because, unlike the Ψ' a large fraction of the J/Ψs (40%) come from feed-down decays of higher mass resonances

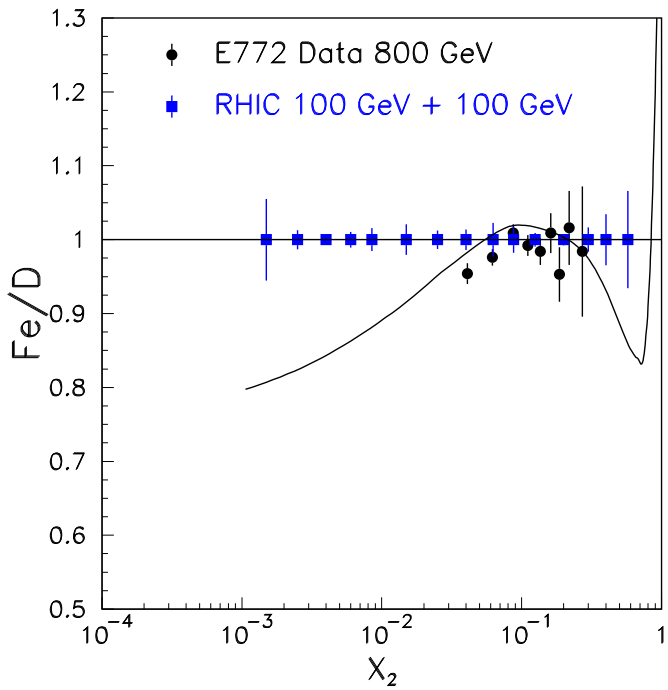

Figure 2.47: The increased reach to low x for Drell-Yan production measured in the PHENIX muon arms compared to 800 GeV p+A fixed target measurements from E772 [155]. Statistical uncertainties are shown for PHENIX (blue squares) for an approximate integrated p-p luminosity of 250nb^{-1}. The curve corresponds to Eskola's parameterization of shadowing which includes anti-shadowing and Fermi motion.

(e.g. the χ_c). In the 2003 d+Au run the Ψ' yield is small (< 50 counts) and is largely buried in the tail of the J/Ψ, making determination of an accurate yield very difficult. With higher luminosity and some anticipated improvements in mass resolution (better tracking and eventually with help from a silicon vertex detector) high precision measurements using the Ψ' will become a useful tool, with cleaner physics than the J/Ψ.

- An important complement to the studies of $c\bar{c}$ bound states are the Υ states which are $b\bar{b}$ bound states. In heavy-ion collisions these heavier, smaller states are expected to have much weaker suppression by color screening in a QGP than the J/Ψ is. But to establish this, just as in the case of the J/Ψ, a thorough knowledge of the effect of cold nuclear matter on the Υ from p+A collisions is essential. In addition the Υ offers another window in x on the modification of the gluon structure functions in nuclei.

- At higher luminosities the higher p_T region for single leptons (above 6 GeV) where the semi-leptonic decay of B mesons begins to dominate becomes available. As in the charm case, these are important as a control for the observations of the Υ. In addition it is important to know the B cross section so that their contributions to the J/Ψ signal can be determined. These contributions would be particularly important in a scenario where color-screening in a QGP created in heavy-ion collisions destroys most

of the direct J/Ψ's and, particularly at higher p_T, the remaining J/Ψ's might become dominated by those from the B decays. An estimate of this from Lourenco [156] several years ago indicated that for central collisions the fraction of J/Ψ's from B decays might be as large as 20% overall.

- In RHIC runs so far, the yield of Drell-Yan pairs at masses above the J/Ψ has been prohibitively small. The Drell-Yan process is quite important in that it gives a clean measure of the structure functions of the anti-quarks and their modification in nuclei. Values of x as low as 2×10^{-3} can be accessed using Drell-Yan masses above the J/Ψ while, with the addition of a silicon vertex detector, even lower values of 10^{-3} might be reachable. The increased reach to small x in PHENIX is shown in Figure 2.47. With the comparison of d+p and p+p collisions one can also measure the flavor asymmetry of the nucleon anti-quark sea as was done in Fermilab E866/NuSea. [157, 158]

- A number of other important physics signals become available with the advent of a silicon vertex detector in PHENIX as described in Section 3.2.2. These include $B \rightarrow J/\Psi + X$, better mass resolution and separation of the Ψ' and Υ states, and access to low-mass Drell-Yan after removal of the semi-leptonic charm decay background. The latter would allow anti-quark shadowing in d+Au collisions to be measured down to substantially smaller values of x.

2.5 The PHENIX Run Plan

PHENIX recently submitted a multi-year run plan for RHIC Runs 4 through 8 for review by the Brookhaven Program Advisory Committee. Based on detailed guidance supplied by the Collider-Accelerator Department for the time development of RHIC luminosity, a detailed run plan was developed by PHENIX that parameterized the physics reach for each proposed run in terms of a few key rare probes. Two scenarios were considered, a "constant effort" scenario defined as 27 weeks of cryogenic operations per year, and an "optimal" scenario consisting of 37 weeks of operation per year. We reproduce here only the summary tables from this exercise as Tables 2.11 and 2.12; for complete details and supporting information the Beam Use Proposal should be consulted [47].

Table 2.11: Physics yields from the PHENIX run plan for 27 cryo weeks per year

Run	**Species**	$\sqrt{s_{NN}}$ **(GeV)**	**Physics Weeks**	$\int \mathcal{L}dt$ **(record.)**	J/ψ **'s N. Arm**	π^0 p_T^{max}	$A_{LL}(\pi^0)$ p_T^{max}
	(GeV/c)	**(GeV/c)**				**(GeV/c)**	
4	Au+Au	200	14	123 μb^{-1}	1640	17.8	
	p+p	200	0				
5	Si+Si	200	9	2.2 nb^{-1}	1570	15.8	
	p+p	200	5	1.2 pb^{-1}	1860	15.1	6.2
6	Au+Au	62.4	19	45 μb^{-1}	120	10.4	
7	p+p	200	19	62 pb^{-1}	98,600	24.3	11.0
8	Au+Au	200	19	841μb^{-1}	11,200	22.5	
9	p+p	500	19	211pb^{-1}	944,000	39.1	19.0
10	d+Au	62.4	19	1.3nb^{-1}	102	9.0	

While the PHENIX Beam Use Proposal encompasses (as per the charge) only the initial portion of this decadal planning document, the scope of the proposal is sufficient to identify several general principles that should guide any long-term planning exercise:

- The demonstrated ability of PHENIX to implement many parallel and highly selective physics triggers forms the basis for a broad program that explores rare phenomena in A+A, p+A and polarized p+p collisions. The program provides a clear connection between the initial exploration phases of Runs 1-3 to the systematic characterization of A+A and d+A collisions in the near future, thereby providing the scientific basis for quark-gluon plasma discovery and measurement of its properties. The same high-rate capabilities of the experiment will permit world-class measurements of the spin structure of the proton as the luminosity and polarization for p+p collisions are developed.

Table 2.12: Physics yields from the PHENIX run plan for 37 cryo weeks per year

Run	**Species**	$\sqrt{s_{NN}}$ **(GeV)**	**Physics Weeks**	$\int \mathcal{L}dt$ **(record.)**	J/ψ **'s N. Arm**	π^0 p_T^{max}	$A_{LL}(\pi^0)$ p_T^{max} **(GeV/c)**
4	Au+Au	200	19	203 μb^{-1}	2700	19.0	
	p+p	200	5	0.5 pb^{-1}	750	13.5	5.0
5	Si+Si	200	14	4.7 nb^{-1}	3460	17.3	
	p+p	200	5	3.8 pb^{-1}	6030	17.3	7.2
6	Au+Au	62.4	19	45 μb^{-1}	120	10.4	
	p+p	500	2	2.1 pb^{-1}	9,400	22.4	9.3
7	p+p	200	22	76 pb^{-1}	122,000	24.9	11.2
		62.4	5	2.7 pb^{-1}	880	11.0	4.8
8	Au+Au	200	19	1503μb^{-1}	20,000	24.1	
9	p+p	500	29	377pb^{-1}	1,700,000	41.9	20.4
10	d+Au	62.4	29	2.3nb^{-1}	182	9.6	

- The compelling physics offered by rare probes and high-p_T phenomena, when coupled with the CAD model for RHIC luminosity growth, places a very high premium on periods of extended running dedicated to developing the highest possible integrated luminosity for a given species. Conversely, frequent alterations of the running conditions do not provide an efficient usage of the valuable cryo weeks.

- There is a qualitative improvement in the physics yields from the "optimal" program, in that the reduction of end effects provides much longer periods to develop integrated luminosity. Because the end effects are a significant fraction of 27 weeks, these advantages accrue rapidly for even modest increases beyond 27 weeks.

- Even in the "optimal" scenario of 37 weeks per year of running, development of the requisite integrated luminosities remain challenging. This is particularly true for the spin program, where higher values of polarization are also required. Every effort must be made to increase these key parameters as rapidly and as efficiently as possible.

- There are many outstanding physics opportunities not addressed in the proposed five year plan, for example, extended measurements of proton-nucleus collisions. It is also clear that many of the baseline measurements in both the heavy ion and spin program will be re-addressed with far higher sensitivity provided by the various upgrades described in the following chapter. Together, these factors suggest that the program of unique and world-leading physics at RHIC extends beyond the scope of even this decadal plan.

Chapter 3

Upgrades Program

3.1 Introduction

A significant fraction of the planned physics measurements presented in the preceding chapter relies upon the timely development of the PHENIX upgrades program. The compelling nature of these physics opportunities will not only enable PHENIX to remain competitive well beyond the turn-on of LHC expected for 2008 but will also advance our understanding of QCD by fully exploiting the unique spin physics capabilities of RHIC. The plan covers a broad range of measurements in A+A, p+A, and p+p physics, with the goal of providing key information which currently can either not be obtained at RHIC or which can be measured with only limited accuracy. The central issues addressed by the PHENIX upgrades program are

1. for the study of QCD matter at high temperatures with heavy ion, p-nucleus, and p+p collisions:
   - High p_T phenomena including identified hadrons in the p_T range from 3-10 GeV/c and γ-jet correlations
   - Thermal radiation and effects of chiral symmetry restoration in the electron-pair continuum, in particular at low masses (<1 GeV/c^2)
   - Production of mesons with open charm and beauty
   - Quarkonia spectroscopy including excited states, J/ψ, ψ', Υ(1s), Υ(2s), and Υ(3s)
2. for an extended exploration of the spin structure of the nucleon
   - Gluon spin structure (ΔG/G) with heavy flavor and γ-jet correlations
   - Quark spin structure (Δq/q) with W-production
   - Transversity
3. for exploration of the nucleon structure in nuclei
   - A-, p_T -, x-dependence of the parton structure of nuclei

The formal development of the PHENIX upgrades program began in response to the recent NSAC long-range plan, which was presented in 2001. The strategy was consolidated at a workshop in Montauk, NY March 2001 and at BNL in August of 2002. Since then individual detector upgrades, specifically for high momentum particle identification, accurate vertex tracking, rejection of electrons from Dalitz decays and γ conversions, and improved muon trigger capabilities, have been developed within four PHENIX study groups.

In this chapter we will summarize the physics goals of our upgrades program, thereby highlighting the main arguments developed in the previous chapter. This will be followed by a discussion of the the overall strategy and presentations in more detail of the planned new detector components.

3.1.1 Physics Goals and Upgrades Strategy

PHENIX was designed to detect rare events in heavy ion and p+p collisions. It combines a large bandwidth DAQ and trigger system with a highly granular detector optimized to measure photons, electrons/positrons, muons and high p_T hadrons. The goal of the proposed upgrades physics program is to provide key measurements that reach beyond the capabilities of the present PHENIX detector. The measurements will complement and enhance the present physics program and will fully exploit the strengths of the existing PHENIX apparatus. PHENIX anticipates the proposed upgrades will be implemented over the next four to six years in a staged approach which allows a smooth integration into the experiment with no major disruptions and which will result in a gradual yet very significant extension of our physics reach.

3.1.2 Study of QCD at high temperatures

Data from the first two Au+Au runs at RHIC have unveiled several interesting high p_T phenomena; perhaps the most exciting discovery is the significant suppression of charged hadrons and identified π^0 with high p_T. This has been discussed as an indication of jet quenching due to QCD energy loss in dense colored matter. (See Section 2.2.1 for a detailed discussion.) The suppression is significantly larger for π^0's than for charged hadrons, and, since the proton and antiproton yields exceed the pion yield above 2 GeV/c, this difference may be due to a large proton and antiproton contribution at high p_T. This result is surprising and cannot be explained in terms of conventional jet fragmentation. New mechanisms such as quark recombination of a hadronizing quark gluon plasma or baryon production mechanisms based on gluon junctions rather than diquarks in dense gluonic matter have been proposed. Also large azimuthal asymmetries in the emission of charged particles have been observed at high p_T. Again differences between pions and protons are observed. A detailed exploration of high p_T phenomena at RHIC has just begun and one can expect many interesting results in the next years. However, to shed light on the apparent puzzles related to the particle composition will require more extensive particle identification above 5 GeV/c that is not provided by the current detectors. This is a primary motivation for the ongoing upgrade described in Section 3.2.1 designed to extend PHENIX's range in transverse momentum for identifying charged hadrons.

Electron pairs are the most promising observable in the quest for the restoration of chiral symmetry expected to take place in the early stages of heavy ion collisions. CERN experiments have confirmed the unique physics potential of the electron pair continuum. The continuum in the mass range from 200 - 600 MeV/c^2 has been systematically studied by the CERES experiment. The most prominent result is the observation of a strong enhancement of low-mass electron pairs in all observed heavy ion collisions. This enhancement has triggered a wealth of theoretical activity, which indicate that agreement with the CERES data is achieved only by invoking in-medium modification of the intermediate ρ meson, as a precursor of chiral symmetry restoration, in the $\pi\pi$-annihilation channel ($\pi\pi \rightarrow \rho \rightarrow \gamma^* \rightarrow e^+e^-$). As discussed in Section 2.2.4, recent theoretical predictions that incorporate the knowledge acquired from the first years of RHIC running show that the enhancement of low-mass e^+e^- pairs should persist at RHIC. The extension of the pair continuum studies under the much better conditions offered at RHIC– higher initial temperature, larger energy density, larger volume and longer lifetime of the system– promises to be very interesting. This challenging measurement will requiring adding the "hadron-blind detector" described in Section 3.2.3 to reject electrons from Dalitz decays and photon conversion.

In recent years, more and more interest has focused on open heavy flavor production in heavy ion physics since it provides a wide range of information not available from hadrons containing only light quarks. PHENIX has measured charm production through single electrons in the p_T range from 1 to 3.5 GeV/c and will complement these by measurements based on single muons and electron-muon pairs in the future. These measurements will give initial results on heavy flavor production, but as noted in Section 2.2.5, a clear separation of charm from bottom will be problematic, as will determining the contribution from thermal lepton pair production (Section 2.2.3.4). To provide a more robust and accurate measurement that can separate charm and bottom, precision tracking close to the interaction point that is capable of identifying displaced decay vertices from the decays of hadrons containing charm and bottom quarks will be essential. The proposed Si-vertex detector outlined in Section 3.2.2 is designed to add this capability to the existing PHENIX central arm tracking systems. A large acceptance particle identification system would provide many additional capabilities, among them tagging heavy flavor with kaons. This would be accomplished via the central TPC discussed in Section 3.2.4.

A precise measurement of open charm and beauty will help determine if heavy flavored quarks are produced only in the initial parton-parton collisions or also during the later stages of the collision. In principle, heavy flavor can be produced both in a dense medium before equilibration and, for sufficiently high temperatures, during the subsequent evolution of the system as well. Although significant effects are only predicted at LHC energies, first hints of enhanced c-quark production might be visible at RHIC. Investigating charm production differentially in p_T is ideally suited to study the possible flavor dependence of QCD energy loss. Charm quarks might thermalize during the collision and show collective phenomena like transverse and elliptic flow. In addition, open charm is the best reference for charmonium production, and it is also an important contribution to the di-lepton continuum, and so must be accurately measured as which must be measured accurately in the di-lepton channel to establish thermal di-lepton radiation.

Color screening effects associated with QGP production give the prime motivation to study J/ψ production in heavy ion collisions. Studying a full suite of heavy quarkonium states, the J/ψ, ψ ' and Υ(1S), Υ(2S) and Υ(3S) will provide detailed information about the QCD potential in colored matter. Since all states have different size and binding energies their simultaneous observation will permit mapping the QCD potential in colored matter. The lowest-lying Υ states are smaller and more tightly bound than the J/ψ and thus probe the QCD potential at shorter distances than the J/ψ. The 1S state should not disintegrate at energy densities reached at RHIC, while the larger and less bound Υ(2S) and Υ(3S) states should be affected by the screening. Separating the Υ(1S) from the Υ(2S), Υ(3S) requires improving the invariant mass resolution to better than 100 MeV (about 1%). Long runs at high luminosity and the proposed Si-vertex tracker will be required for this measurement.

3.1.3 Extended exploration of the spin structure of the nucleon

Understanding the structure of the nucleon in terms of quarks and gluons is one of the outstanding problems of both high energy and nuclear physics. Spin-dependent deep inelastic scattering experiments have revealed that only 30% of the proton spin is carried by quarks. A centerpiece of the PHENIX spin physics program will be the first precise measurement of the gluon polarization. At present we can exploit the measurement of double spin asymmetries in inclusive hadron production. This method seems promising, since first data from PHENIX on inclusive π^0 production in p+p collisions is consistent with next-to-leading order QCD predictions over the entire measured range in transverse momentum [25]. PHENIX will measure prompt photon production in kinematic region 0.01<x<0.3 from quark-gluon Compton scattering and provide the most direct access to the gluon polarization. Because of the fundamental importance of the measurement of the gluon polarization, a measurement with different experimental and theoretical systematics will be critical. Measuring the double-spin asymmetry of charm and bottom flavored quarks will not only provide the necessary verification but also extend the kinematic coverage substantially to 0.001<x<0.3. This would be achieved using the same Si-vertex tracker mentioned above and described in Section 3.2.2.

Recent measurements of the quark flavor dependent polarized parton distribution Δq(x) by the HERMES experiment indicate that the light-quark sea polarization are small. The HERMES measurement is carried out at low Q^2 and the interpretation of the result depends on the validity of the factorization ansatz between quark distributions and fragmentation functions at low scales. A second independent measurement at hard scales is urgently required. PHENIX can provide such a measurement by extracting the longitudinal single spin asymmetry in W^- and W^+ production. Recent work by Yuan and Nadolsky using modern re-summation techniques will permit a clean interpretation of the W-asymmetries in NLO pQCD from first principles. At $\sqrt{s}$ = 500 GeV RHIC will copiously produce W bosons. However, the collision rates at luminosities of $2\text{x}10^{32}\text{cm}^{-2}\text{s}^{-1}$ will be as high as 12 MHz. At this rate, it poses a significant experimental challenge to select muons from W-decays over the very large background of low momentum muons from hadron decays in jets. Before successful measurements can be carried out a substantial upgrade of the existing first level

muon trigger is required, as described in Section 3.2.5.

In addition to the quark structure functions q(x) and Δq(x) a third class of distributions, transversity δq(x) , is needed for a complete description of nucleon structure at leading twist. Transversity distributions are experimentally unknown and offer a new window on nucleon spin structure with distinct advantages: Transversity involves a helicity spin flip amplitude and therefore is free of admixtures from gluons. The first moment of transversity distributions is a tensor charge and thus strictly a measure of valence quarks. The measurement of transversity distributions through spin-dependent fragmentation of hadrons requires the knowledge of the jet-axis. For example, in Collins-Heppelman fragmentation the sensitivity to the transverse quark spin results from the azimuthal distribution of hadrons around the jet-axis. The present geometric acceptance ($\Delta\eta < 0.7$) of the PHENIX central arms is to small to permit a sufficient reconstruction of the jets-axis, since jets typically extend over about one unit in pseudo rapidity. However, the new tracking systems proposed in Sections 3.2.2 and 3.2.4 significantly extend the geometric acceptance to ($\Delta\eta < 2.0$) and provide the necessary jet reconstruction.

3.1.4 Exploration of the nucleon structure in nuclei

Proton-nucleus collisions not only provide important key baseline information for the study of QCD at high temperatures, they also address the fundamental issues of the parton structure of nuclei. Since the discovery of the EMC effect in the 1980's, it is clear that the parton structure of a nucleon changes if it is bound in a nucleus. It is still unclear why the rather weak nuclear binding force can have such pronounced effects on the parton distributions. With the advent of RHIC, high-energy p-nucleus collisions will give access to structure functions in nuclei in a completely new region. The prime objectives for us are to measure the gluon and antiquark distributions in nuclei. In general all processes suitable to measure the gluon structure in nucleons are also ideal for probing gluon and antiquark distributions in nuclei. Therefore, this part of our physics program will also profit greatly from the anticipated upgrades to PHENIX, in particular from the ability to measure all processes to lower values of x.

3.1.5 Upgrade Strategy

All of the proposed measurements have low cross sections and/or high backgrounds, and as a result require taking data at high luminosity over extended periods of time. We anticipate that a luminosity of $8\text{x}10^{26}$ cm^{-2}s^{-1} for Au+Au and $2\text{x}10^{32}$ cm^{-2}s^{-1}for polarized proton beams will be reached over the next several years. These luminosities will be sufficient for most of the measurements listed above, but note that some of them (specifically upsilon spectroscopy and γ-jet coincidences) would benefit greatly from a further increase of the Au+Au luminosity by a factor of 10 through electron cooling. While each of the detector upgrades will make important physics measurements without this ultimate luminosity increase, the PHENIX upgrade plan also emphasizes increasing our data rate capabilities to fully utilize such an increase in luminosity when it becomes available.

PHENIX has prepared a detailed plan of detector upgrades necessary for the proposed physics program. The plan is based on the recognition that the three broad research areas suggested above require similar detector upgrades. All proposed measurements exploit the robust features of the existing PHENIX detector central and muon arms. We plan to augment these detector systems by a new vertex spectrometer with a flexible magnetic field configuration, high precision vertex tracking with silicon detectors, and with a compact TPC combined with hadron blind electron detection. An Aerogel Cerenkov detector system is being installed in one of the central arms, which, when combined with the existing RICH and TOF, will provide continuous π-K-p separation out to 10 GeV/c. The capabilities of the muon arms will be extended via the proposed upgrade to the muon trigger system. All of these upgrades rely on the large bandwidth DAQ of PHENIX, which is capable of utilizing ~12kHz event rates by higher level triggers. Improved first level trigger capabilities (specifically to detect single muons) will enable PHENIX to make full use of the anticipated luminosity.

The plans for the new multi-detector particle identification system for the PHENIX west central arm spectrometer are already in a mature stage. Supported through US-Japan and DOE funds the first detector, an Aerogel Cerenkov counter, has been implemented in 2004. A new TOF detector will follow most likely in 2005. Silicon vertex tracking for the central arm acceptance can be implemented as barrel based on existing technologies. Thanks to institutional contributions the R&D for this project is mostly completed and a corresponding proposal to fund the construction starting in FY05 through FY07 has been submitted to DOE in Fall 2003. Roughly 40% of the costs will be covered by the RIKEN Institute. Technology studies for a corresponding forward vertex tracker are underway so that a proposal to DOE can be prepared within a year. Detector options to upgrade the muon system are under discussion. The current planning calls for funding these detectors through the NSF and foreign funding agencies.

3.2 Specific Detectors for Planned Upgrades

The main new detector system is a vertex spectrometer, which combines a flexible magnetic field configuration, high precision vertex tracking in the central and forward region, and electron identification and tracking. The layout of this new system is shown in Figure 3.8.

The addition of a second inner coil to the PHENIX central magnet, which was installed in the summer shutdown of 2002 provides the flexible magnetic field. The second coil, which was already foreseen in the original design of the magnet yoke, may be operated in two modes: a (+ +) mode in which the inner field is in the same direction as the field of the outer coil, and a (+ -) mode where the inner field is in the opposite direction to the field of the outer coil. In the (+ +) configuration the field integral is increased by a factor of ~1.7 to 1.2 T-m. Combined with the tracking near the beam axis, the mass resolution for reconstructing the Υ via the $\Upsilon \rightarrow e^+e^-$ decay is reduced to ~60 MeV/c, which will enable PHENIX to separate the 1S, 2S, and 3S exited states of the Υ, (given sufficient integrated luminosity). In the (+ -) mode, a region with zero field integral can be created around the beam axis, which when combined with electron identification and tracking, will open the

avenue towards a low-mass di-lepton measurement.

The vertex tracking is based on highly segmented silicon strip or pixel detectors at mid rapidity and silicon pixel detectors in the forward direction. The central detectors (silicon barrel) cover $-1.2 < \eta < 1.2$ and almost 2π in azimuth and provide a single-track resolution of ~ 50 μm at the vertex. The forward silicon detectors are designed to provide coverage in the angular acceptance of the forward muon arms. The forward silicon cover $1.2 < |\Delta\eta| < 2.7$ and the almost full azimuth angle with a resolution of $\sim$150 μm. Both systems provide sufficient resolution to measure electrons and muons from semi-leptonic decays of D or B mesons, which carry open charm or bottom respectively. A robust measurement of open charm and bottom will provide two new channels for the ΔG/G measurement with a substantial kinematic coverage from $0.002 < x < 0.3$. Data from this subsystem on heavy flavor production in nuclear collisions will provide one of the missing keys to a full picture of QCD at high temperatures. Besides tagging inclusive electrons from charm and bottom decays, many other measurements become available with this device. For example, the forward detectors will also provide tagging of J/ψ's from B decays, and due to the large rapidity acceptance of the silicon tracker, it will be possible to reconstruct D-mesons via the D$\rightarrow$ πK decay mode in A+A and p+p collisions. In addition, jet tagging in p+p will be possible, which is essential for a transversity measurement.

A compact hadron blind detector (HBD) combined with a micro-TPC completes the vertex spectrometer. The device is based on micro-pattern detectors (GEM's) for both the TPC and HBD. It covers $-1 < \eta < 1$ and essentially 2π in azimuth and has as its primary function to detect and track electrons. Electron identification and tracking in a low field region, provided by the (+ -) field mode, is the key for the measurement of the low mass di-lepton continuum. The central problem of this challenging measurement is the large combinatorial pair background stemming from electron and positrons of different physics origin. The most important source of such background electrons are photon conversions and Dalitz decays. In both processes, electron-positron pairs of small opening angle are produced for which typically only one of the two particles is reconstructed in the central arm acceptance. In the absence of a strong magnetic field, and with electron identification and tracking, the background can be reduced by more than an order of magnitude and the low mass hi-lepton continuum becomes accessible. It is important to note that RHIC might provide the highest beam energies where such a measurement is feasible, since at higher beam energies, the irreducible background from uncorrelated semi-leptonic charm decays will dominate.

An Aerogel Cerenkov detector in the west arm provides another important enhancement to PHENIX's capabilities. Together with the already existing RICH detector and the time-of-flight measurement provided by either the electromagnetic calorimeter or a new TOF system, full π-K-p separation will be available up to transverse momenta of 10 GeV/c. This particle identification, along with charm and bottom measurements and γ-jet coincidences, will allow a detailed and comprehensive study of jet production at RHIC.

For the W-measurements in p+p and for Υ spectroscopy in A+A at the anticipated luminosities the selectivity of the existing first level single muon and muon pair triggers need to be increased by a factor of $\sim$50. Making a rough momentum measurement available at

the trigger level can provide this increase of selectivity. This requires new dedicated muon level-1 trigger detectors, which will be integrated into the two PHENIX muon spectrometers.

Finally, all new detector systems will require upgrades of the data acquisition (DAQ) and computing systems to cope with the additional data volume and the anticipated higher luminosities. Important research and development funds are needed in the early years to be in a position to take advantage of new digital technology for the next generation data collection modules, Level-1 trigger system, and optical technology.

3.2.1 Aerogel

3.2.1.1 Introduction

A prominent feature of the PHENIX experiment is a strong particle identification capability. The baseline PHENIX detector has four major subsystems contributing to particle ID in the central spectrometer arms. The PHENIX detector subsystems consisting of the Time of Flight (TOF), the Ring Imaging Cerenkov Counter (RICH), the EM Calorimeter (EMCal) and the Time Expansion Chamber/Transition Radiation Detector (TEC/TRD) together allow PHENIX to do single particle identification of γ, e, π, K, p over a large range in momentum. The first three years of RHIC running have produced physics results which were greatly enhanced by the experiment's ability to identify particles. The heavy ion physics results described in the previous chapter include measurements of partonic energy loss, elliptic flow, correlations, energy density, temperature, and particle production mechanisms.

A greatly improved insight into a number of intriguing results from the initial PHENIX data could be gained by extending the PHENIX particle identification capability for π/K/p particle to significantly higher p_T. Currently the PHENIX TOF can separate K/$\pi \leq 2.5$ GeV/c, and p/K ≤ 4.2 GeV/c. The time-of-flight ability of the EMCal allows π/K/p separation at somewhat lower momenta. The RICH begins to trigger on charged π's at $p_T \geq$ 5.5-6.0 GeV/c. As shown in Figure 3.1, the addition of an Aerogel detector with a properly chosen index of refraction can combine with the TOF, RICH and EMCal to expand PHENIX π/K/p identification to beyond 8 GeV/c in p_T

3.2.1.2 Physics with High p_T Particle ID

To illustrate the questions to be addressed by this subsystem, we present characteristic examples of the intriguing topics made accessible by the ability to identify π/K/p to higher transverse momenta. The first of these focuses on one of the most exciting discoveries in the first years of RHIC: the suppression effect of high p_T particles. This effect has been described in terms of a 'jet-quenching' mechanism which may be revealing important information about the early stage of the heavy ion collision where very hot, dense partonic matter could exist. The PHENIX results show a difference in suppression between π°'s and inclusive charged hadrons. This difference leads to proton production being roughly comparable to pion production above 2 GeV/c which in turn may be evidence for a large initial-state gluon density. It is necessary to be able to identify protons and charged pions beyond 5 GeV/c to get a better understanding of this topic.

		Pion-Kaon separation	Kaon-Proton separation
TOF	σ~100 ps	0 - 2.5	- 5
RICH	n=1.00044 γth~34	5 - 17	17 -
Aerogel	n=1.01 γth~8.5	1 - 5	5 - 9

Figure 3.1: Hadron PID of PHENIX with an Aerogel Cerenkov Counter containing Aerogel with index n = 1.010.

The large azimuthal anisotropies, v_2, observed in heavy ion collisions are another exciting discovery at RHIC. The large values of v_2 seen at RHIC suggest that thermalization is taking place much faster than expected from normal hadronic rescattering. At p_T's below 2.0 GeV/c the curves of π/K/p's in v_2 vs p_T plots are consistent with the hydrodynamic flow picture. However, it is believed that the v_2 values for particles above 2.0 GeV depend on an interplay between jet quenching and quark recombination. Extending particle identification capabilities to p_T's $\geq$ 8 GeV/c allows us to study anisotropies in a range very sensitive to jet physics and fragmentation.

A very fundamental question for the jet-quenching mechanism is whether there is a difference in jet quenching between gluon jets and quark jets. Different quenching strengths between gluon and quark jets would result in modified particle ratios, $p/\bar{p}$ for instance, and could be observed by identifying π/K/p's at high p_T. Likewise, the ability to identify K^-'s at high p_T could be used to tag gluon jets and further study differences in quark and gluon jet characteristics in what seems to be a very hot and dense partonic medium.

3.2.1.3 The Aerogel Counter

Aerogel is a very low density SiO_2-based, semi-transparent solid which has an index of refraction between that of liquids and gases. The Aerogel is used as a radiator material in Cerenkov counter modules readout by phototubes (PMT's). The refractive index of the Aerogel used by PHENIX (n=1.0114) allows charged particle identification over momentum ranges inaccessible to other detector technologies. The PHENIX Aerogel counter is installed in one sector of the West Carriage and is located radially between PC2 and PC3. It has an active area which covers $\Delta\eta = \pm 0.35$ and $\Delta\phi = 14°$. The Aerogel counter is composed of 160 separate modules. Each module contains an 11 cm x 11 cm x 22 cm stack of Aerogel, a light mixing box, GORETEX reflector and a pair of 3" PMT's with bases. The outer shell of the module is 0.5 mm aluminum sheet metal.The modules are stacked into an array 10

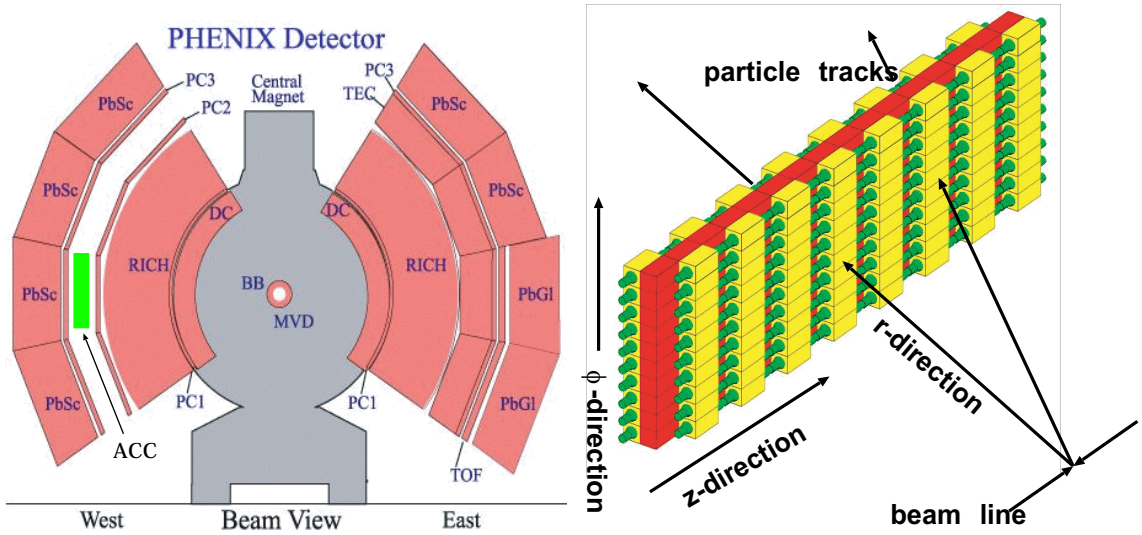

Figure 3.2: The aerogel detector in the west arm between pad chamber 2 (PC2) and 3 (PC3) in the W1 sector (left) and the aerogel detector structure and orientation with respect to the beam line (right) are shown.

modules high by 16 modules wide (Figure 3.2).

To best fill the PHENIX π/K/p PID gap one would like an aerogel index of 1.010 or perhaps slightly lower. As can be seen in the figures, the PHENIX TOF handles π/K separation to 2.5 GeV/c and K/p until 4.2 GeV/c. Aerogel (n=1.010) starts to trigger on K's at 3.7 GeV, though pulse height analysis may make π/K separation with aerogel possible to 5.5 GeV/c. The RICH starts to identify pions around 5.5-6.0 GeV/c and does not trigger in K's until $\geq$ 20 GeV/c. The aerogel starts to see protons around 7.5 GeV/c, but as with the kaons, pulse height analysis may make the proton separable up to 10 GeV/c.

The choice of the specific aerogel material is a compromise between desired physics performance and practical issues. PHENIX has decided to use Matsushita SP-12M for its aerogel material after consideration of product yield, optimum index of refraction, fragility and cost. This material is a hydrophobic formulation of aerogel with an index of refraction n=1.0114. The measured transmission for a 10mm thick piece is 64% (400 nm) and 88% (550 nm). Test beam results predict that the average light yield/module is $\geq$ 14 photoelectrons/charged particle over threshold. The hadronic identification capability of aerogel with this index of refraction is shown in Figure 3.3.

A single module of the aerogel counter is shown in Figure 3.4. Each module has three parts, the aerogel Cerenkov radiator, the integration air gap and PMT/base area. Beam studies have shown that the integration air gap, which is a goretex wrapped light mixing box, is essential for producing a uniform position dependence in the aerogel light-yield. To minimize dead space, modules have been stacked reversing the module orientation in alternate rows. All sensitive aerogel volumes are kept in one plane in this configuration, which contributes to the uniform detector response. In this design, half the modules have

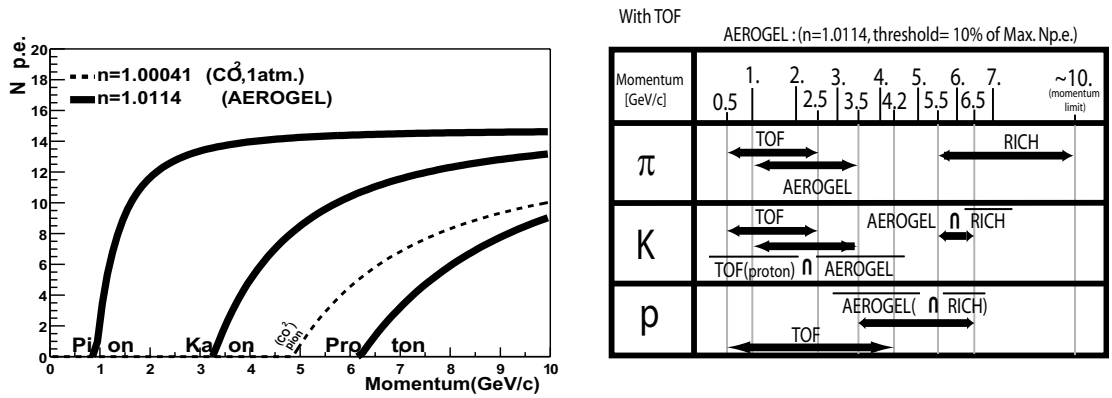

Figure 3.3: Detected number of photo-electrons for [solid line] n= 1.0114, and [dashed line] RICH (CO_2, n=1.00041, 1 atm.) as a function of momentum. $N_{p.e.}$ is for the 12 cm thick of aerogel.[Left] PID capabilities with AEROGEL, RICH and additional TOF. Aerogel is based on n = 1.0114 with a threshold at 10 % of maximum number of photoelectrons.[Right]

particles entering in a reverse direction. Beam tests have determined that the photoelectron response only differs by 10-20% due to this alternate orientation. The difference in response is not considered significant.

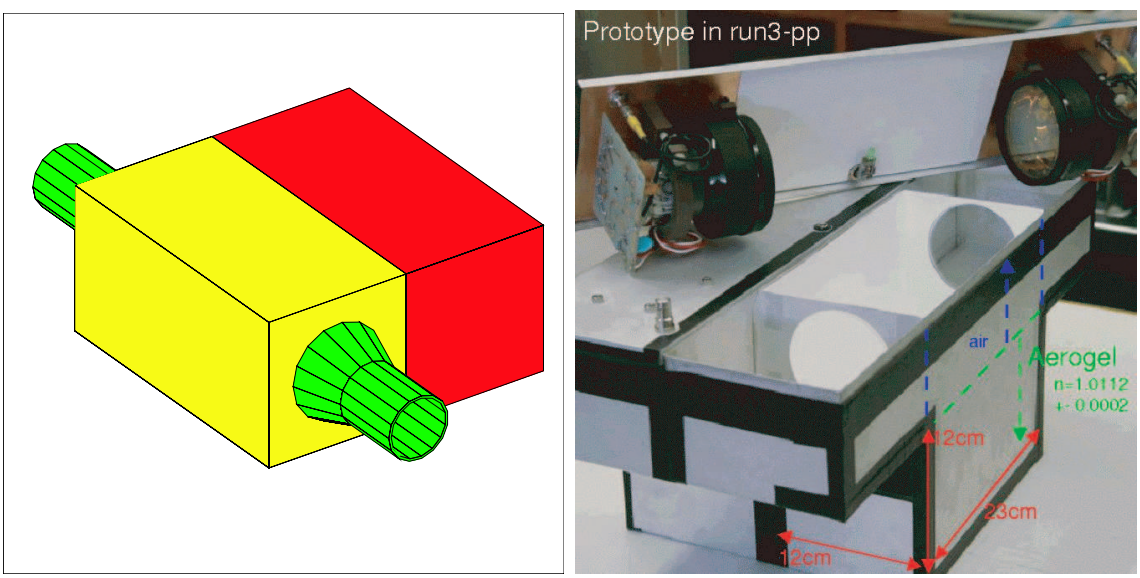

Figure 3.4: Drawing of aerogel module with 2 PMT's and light mixing box [Left] and prototype module tested in RHIC Run 3 [Right].

The electronics chain of the of the aerogel counter is very similar to that of the PHENIX RICH. Signals output from the bases on the aerogel PMT's are routed to preamps located at the edge of the array. The preamplified signals are directed to West carriage racks containing

crates of Front-End Electronics (FEE's). The FEE crates contain 1 controller-timing board, five 32-channel AMU/ADC digitizing boards and a data formatter/readout card. The three types of boards located in the aerogel FEE crate are essentially identical to the FEE for the PHENIX RICH. The AMU/ADC boards provide both digital pulse height and timing information. The AMU/ADC chip has 32 channels of 64-cell analog memory and a Wilkinson 12-bit Analog to Digital Converter. The digital timing signals on the AMU/ADC board come through integrating amplifiers and a Time-to-Amplitude converter. A branch exists in the aerogel electronics chain which will enable a future implementation of the Aerogel counter in the PHENIX Level1 trigger.

3.2.1.4 Future Expansion

One half-sector of the aerogel counter will be installed and commissioned prior to RHIC Run 4. The second half sector of the counter will be prepared for operation in PHENIX in RHIC Run 5. Future plans call for the installation of a high resolution time-of-flight wall in the space immediately behind the aerogel sector. Together, the aerogel and time-of-flight west is called the PHENIX High p_T detector.

In the baseline PHENIX detector, all time-of-flight measurements in the West Carriage are provided by the EMCal which has a timing resolution roughly 3.5 times worse than the high resolution TOF wall located on the East Carriage. A TOF wall in the West carriage will be designed to have a timing resolution of 100 psec, similar to the TOF array on the East carriage. Once the TOF and aerogel array are completely installed on the West carriage, it will be possible to individually identify pions, kaons and protons to greater than 8 GeV/c in p_T. Until the West TOF is complete, most identified particle physics studies will be limited to statistical studies that use the identified spectra from the east TOF wall to do subtractions of various identified hadron contributions in order to derive the spectrum of interest. The West TOF is also a necessary compliment to the Aerogel if we want to form a LVL1 or LVL2 trigger for identified particles in certain ranges of p_T.

1. Identify track-by-track π/K/p to $p_T \geq 8$ GeV/c
2. Fill in tagged pID gap from $2.5 \leq p_T \leq 5.5$ GeV/c
3. Reduce systematic errors on all π//K/p pID measurements in the range 1.2 GeV/c $\leq p_T \leq$ 2.5 GeV/c (π/K) and 2.5 GeV/c $\leq p_T \leq$ 4.2 GeV/c for protons.
4. Enhance triggering capability on high p_T identified particles

The West Time-of-Flight is currently envisioned as approximately 200-400 slats of Bicron BC404 scintillator read out on both ends with PMT's. The scintillator wall would cover the fiducial volume of the Aerogel counter: $\Delta\eta = \pm 0.35$, $\Delta\phi = 14°$ with an active area of 118 cm x 400 cm. The readout electronics would be identical to the FEE's on the PHENIX TOF in the East Carriage.

Consideration is also being given to extend the High-p_T detector into other sectors of the West Carriage. A determining factor in this possible future upgrade will be the effectiveness of the new detector in RHIC Run 4 and Run 5.

3.2.2 Silicon Vertex Detector

Heavy-flavor production provides a wide-ranging spectrum of key information in three broad areas of physics addressed by RHIC. While PHENIX has begun a program of heavy flavor measurements via single-inclusive leptons, many of the necessary measurements are either not possible or can be performed only with very limited accuracy with the baseline apparatus. Precise vertex tracking is imperative for a robust measurement of heavy-flavor production. The proposed VTX detector adds such tracking capabilities to the central arms of the PHENIX experiment. With this detector charged particles detected in the central arms can be identified as decay products from charm- or beauty-carrying particles by the displacement of their trajectories to the collision vertex. A broad p_T range for charm and beauty measurements is achieved by using different decay channels to reach different parts of phase space.

PHENIX has prepared a detailed proposal[159] describing the physics potential, R&D status and plans for the construction of a Silicon Vertex Tracker (VTX). The VTX detector provides a major enhancement in the physics capabilities of the PHENIX central arm spectrometers. The prime motivation for this subsystem is precision measurements of heavy-quark production (charm and beauty) in $A + A$, $p(d) + A$, and polarized $p + p$ collisions. These are key observables for the future RHIC program, both for the heavy ion program as it moves from the discovery phase towards detailed investigation of the properties of the dense nuclear medium created in heavy ion collisions, and for spin program's investigation of the proton's spin-structure functions. In addition, the VTX will also considerably improve other measurements in PHENIX, as can be seen from the list of physics topics addressed by the VTX:

- Hot and dense strongly interacting matter
  - Potential enhancement of charm production
  - Open beauty production
  - Flavor dependence of jet quenching and QCD energy loss
  - Accurate charm reference for quarkonium
  - Thermal di-lepton radiation
  - High p_T phenomena with light flavors above 10-15 GeV/c in p_T
  - Upsilon spectroscopy in the e^+e^- decay channel
- Gluon spin structure of the nucleon
  - ΔG/G with charm
  - ΔG/G with beauty
  - x dependence of ΔG/G with γ-jet correlations
- Nucleon structure in nuclei

– Gluon shadowing over broad x-range

With the present PHENIX detector, heavy-quark production has been measured indirectly through the observation of single electrons. These measurements are inherently limited in accuracy by systematic uncertainties resulting from the large electron background from Dalitz decays and photon conversions. In addition, this approach via measurement of inclusive electron yields without detailed vertex information does not permit separation charm from beauty production. The VTX detector will provide vertex tracking with a resolution of <50 μm over a large coverage both in rapidity ($|\eta| < 2.7$) and in azimuthal angle ($\Delta\phi \sim 2\pi$). With this device, significantly enhanced and qualitatively new data can be obtained. A more robust and accurate measurement of heavy-quark production over a wide kinematics range will be possible.

The main benefits accrue in three areas. Firstly, by selecting electrons with a distance of closest approach (DCA) to the primary vertex larger than ∼100 μm, the background will be suppressed by several orders of magnitude and thereby a clean and robust measurement of heavy flavor production in the single electron channel will become available. Secondly, because the lifetime of mesons with beauty is significantly larger than that of mesons with charm, the VTX information will allow us to disentangle charm from beauty production over a broad p_T range. Thirdly, a DCA cut on hadrons will reduce the combinatorial background of $D \to K\pi$ to an extent that a direct measurement of D mesons through this decay channel will become possible. In addition, the VTX detector will substantially extend our p_T coverage in high p_T charged particles, and it also will enable us to measure γ+jet correlations.

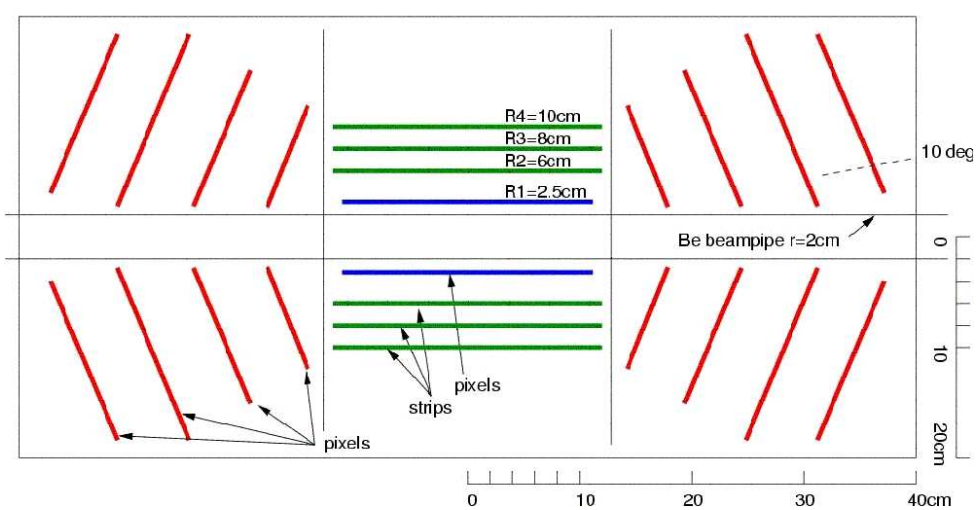

Figure 3.5: Side view of the proposed VTX detector showing the central barrel detector and the forward end-cap detectors.

Figure 3.5 gives a schematic view of the proposed VTX detector with barrel and end-cap detectors covering the central ($|\eta| < 1.2$) and forward ($1.2 < |\eta| < 2.7$) rapidity regions, respectively. The tracks in the central arms are connected to the barrel detector, and their

vertex positions are measured with high precision. The end-cap detector provides corresponding vertex information on the muon tracks measured by the two PHENIX muon arms.

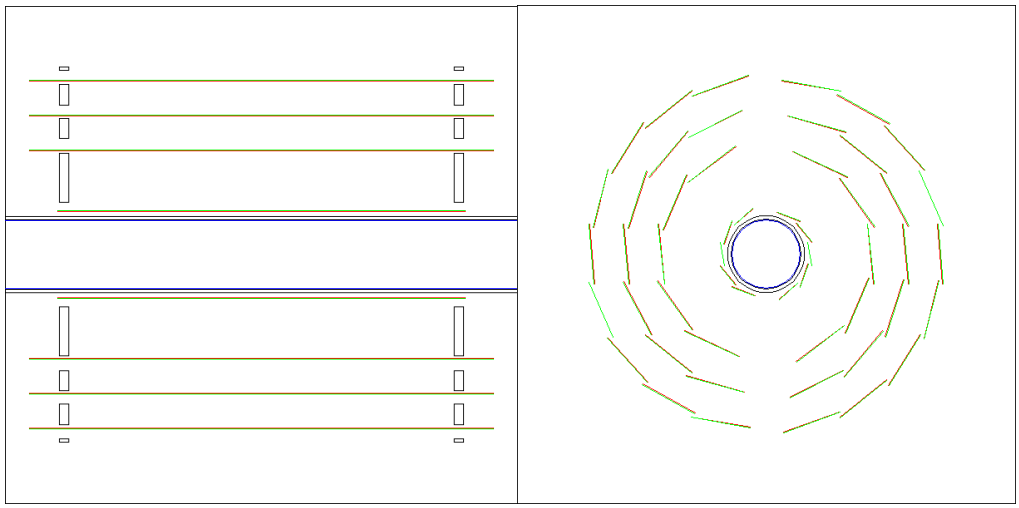

Figure 3.6: Cross sectional views of the proposed barrel VTX detector with four layers of Silicon detector. The inner most layer is a Silicon pixel detector, and the outer three layers are Silicon strip detectors. Each layer of the strip detector has ϕ strips and U strips.

Figure 3.6 shows cross sectional views of the barrel detector, which has four tracking layers. To avoid cost-intensive and time consuming R&D, we have investigated to what extent existing technology can meet our needs. For the inner most layer we propose the use of a silicon pixel device with 50×425 μm channels that was developed for the ALICE experiment at the CERN LHC. Our preferred technology choice for the outer layers is a silicon strip detector developed by the Instrumentation Division at BNL. This device has two projection views read out in single side of silicon. With stereoscopic strips of 80 μm $\times$ 3 cm, these devices achieve an effective pixel size of 80 $\times$ 1000 μm. We plan to use the SVX4 readout chip developed at FNAL to read out the strip detectors.

Figure 3.7 shows the end cap VTX detector. It consists of four layers of Silicon mini-strip detectors. The mini-strips vary in size from 50 μm $\times$ 2000 μm to 50 μm $\times$ 9000 μm as the radius increase. We plan to use a modified version of FPIX2 Silicon read-out chip that FNAL has developed for the planned BTeV experiment. The main change required is to adapt the physical chip geometry to accommodate the larger mini-strips of the end-cap VTX. We are starting R&D with FNAL to develop the modified PHX read-out chip.

Table 3.1 summarizes the physics reach of the barrel VTX detector. The detector will extend the p_T range for measurement of electrons from charm decay to about 6 GeV/c. This is an important extension, since the high p_T region from 2.5 GeV/c to 6 GeV/c is sensitive to charm quark energy loss in the hot dense matter created in heavy ion collision at RHIC. The quark flavor dependence of the energy loss will be a very useful tool to study the property of the dense matter. Another major benefit of the VTX detector is measurement of b quark production. The VTX detector provides separation of b-decay electrons from c-

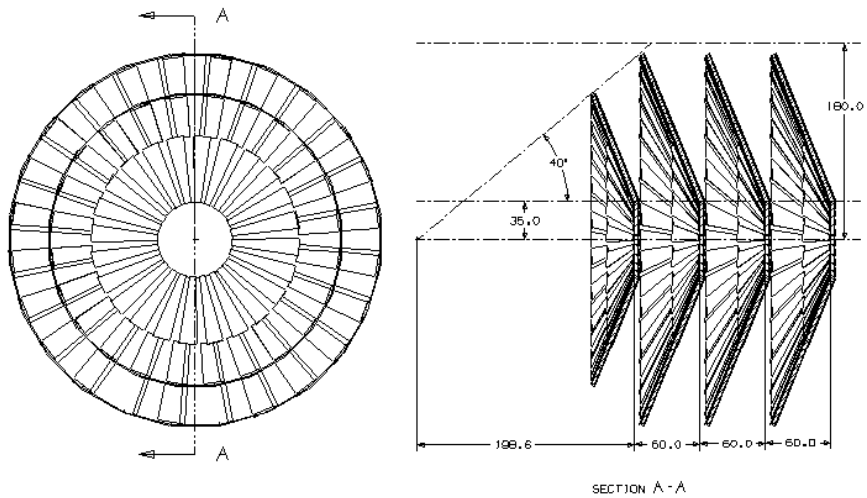

Figure 3.7: Schematic views of the proposed end-cap VTX detector with four layers of Silicon detector. Each station has 96 silicon detectors. The stations are spaced at $\sim$ 20, 26, 32, and 38 cm from the interaction point.

Table 3.1: Summary of physics measurement gained by the barrel VTX detector. The column "without VTX" shows the present capability of PHENIX, while the measurement range with the VTX detector is shown in the column "with VTX". If the process is not measurable, it is marked as "No".

Process	Without VTX	With VTX
$c \to e$	$0.5 < p_T < 2.5$ GeV/c	$0.3 < p_T < 6$ GeV/c
$D \to K\pi(p_T > 2$ GeV/c)	No (2σ significance in central Au+Au)	> 7 σ significance in central Au+Au
Total charm yield	$\sim$ 20 %	$\sim$ 10 %
$(c \to e)/(b \to e)$ ratio	No	$\sim$ 1 %
$b \to e$	$p_T > 3$ GeV/c with model dependence	$1 < p_T < 6$ GeV/c
$B \to J/\psi$	No	$\Delta\sigma/\sigma \sim 10$ - 15 %
Total beauty yield	No	$\sim$ 10 %
High p_T charged	$p_T \leq 10$ GeV/c	$p_T < 15$ -20 GeV/c
ΔG(x) from $c \to e$	$0.03 < x < 0.08$	$0.01 < x < 0.15$
ΔG(x) from $b \to e$	No	$0.02 < x < 0.15$
ΔG(x) from g+jets	No	$0.04 < x < 0.3$
Nuclear shadowing of G(x)	$0.03 < x < 0.3$	$0.01 < x < 0.3$

decay electrons over a very wide momentum range of 1 GeV/c to 6 GeV/c. This will enable PHENIX to determine the total production yield of b quarks in addition to performing a detailed study of their momentum distribution. We can also study the production ratio of c and b very precisely. This is a very sensitive method to look for small enhancements of charm production, predicted as about 10-20% of initial production, due to pre-thermal production. In addition, we can determine the charm contribution to the di-electron continuum in the intermediate mass region, where a signal of thermal di-electrons from the QGP is expected. We can also significantly improve the x coverage in the measurement of gluon distribution function $G(x)$ and its polarization $\Delta G(x)$ in polarized p+p collisions at RHIC.

The end-cap detector that covers the large rapidity region measured by the forward muon arms will significantly increase the physics reach of the VTX detector. The end-cap provides robust b- and c- quark measurement in the forward rapidity region, thereby extending the study of c- and b-quark energy loss and possible charm enhancement to a much wider kinematical range. Since the combination of the muon arm and the end-cap VTX has a much larger acceptance than that of the central arms and the barrel VTX, these measurements will have the added benefit of significantly higher statistical precision than the central arm measurements. The added forward rapidity coverage also significantly expands the x coverage of $G(x)$ and $\Delta G(x)$ measurement in polarized p+p collision, and extends the measurement of the shadowing of $G(x)$ in $p + A$ and $d + A$ collision to to a very small $x \sim 10^{-3}$ that is not accessible by the barrel detector. The small x measurement is very interesting since theoretically a large shadowing effect and gluon density saturation is expected in this low region. The end-cap VTX detector also improves the mass resolution of di-muons measured in the muon arms, which is of particular importance in the spectroscopy of the upsilon states.

With the help of institutional contributions PHENIX has been able to maintain a small but well-focused effort over the past two years to gain experience with the relevant silicon technologies and to launch the necessary R&D to adapt them to the PHENIX requirements. We are confident that the remaining issues can be solved within the next year and that the detector construction could be started by beginning of FY05.

A collaboration of 65 members from 14 institutions has formed to carry out the VTX upgrade project. The collaboration brings in expertise in all phase of the construction of a silicon vertex detector, design and commissioning of modern readout electronics, mechanical and integration issues, detailed knowledge of all aspects of the PHENIX experiment as well as expertise in data analysis and a broad interest in different physics aspects addressed by the VTX. We have recently submitted a proposal to build the barrel VTX detector. In the proposal, we propose building the detector in three years, from FY05 to FY07. A part of the detector will be completed and will be installed in Run-7, with the whole detector becoming available for data taking in Run-8. Work continues on the R&D of the end-cap VTX detector with the goal of submitting a a proposal to build the end-cap VTX detector within a year.

3.2.3 Hadron Blind Detector

The importance of low-mass e^+e^- pairs as a sensitive tool in the study of chiral symmetry restoration was emphasized in detail in Section 2.2.4. However, this is a very challenging measurement. The main difficulty is the overwhelming yield of pairs originating from conversions and π^0 Dalitz decays which leads to a huge combinatorial background. For example, the PHENIX detector in its Run-2 configuration achieved a signal to background ratio in the ω-meson region of S/B$\sim$ 1/250, making impossible a high-quality measurement of the low-mass pair continuum. An appropriate upgrade is needed to identify and reject this background. The main strategy is to identify electrons in a field-free region and reject the γ conversions and π^o Dalitz decay pairs exploiting the small opening angle of these pairs. In anticipation of such an upgrade, provision was made in the original design of the PHENIX detector for the installation of an inner coil which would create an nearly field-free region extending out to 50-60 cm in the radial direction. This inner coil has recently been installed in the PHENIX detector. In addition to this coil, the key element of the upgrade is a Hadron Blind Detector (HBD) located in the field-free region which will fulfill the electron identification and rejection tasks. An interesting possibility that is under consideration is to combine the HBD with a Time Projection Chamber (TPC, see section 3.2.4) which could enhance, and add redundancy to, the identification and rejection of low-mass pairs. Figure 3.8 shows the layout of the inner part of the PHENIX detector together with the location of the inner coil and the proposed location of the HBD/TPC.

3.2.3.1 The HBD concept

In order to quantify the benefit of the HBD and to determine its specifications, extensive Monte Carlo simulations were performed. The results of the study are presented in the PHENIX Technical Note 391.0 [160]. A detector providing electron identification with a very high efficiency of at least 90% is required. This also implies a double (electron) hit recognition at a comparable level. On the other hand, a moderate π rejection factor of a few hundred is totally adequate. With such a detector the combinatorial background originating from gamma conversions and π^0 Dalitz decays is suppressed by two orders of magnitude, making the contribution from open charm the dominant factor in the S/B ratio. Possible choices for the detector are also discussed in [160]. After critical evaluation of various options for the key elements (radiator gas, window, detector gas, photocathode, detector element, readout scheme), the choice that emerged is an HBD with the following configuration: a Cerenkov detector operated with pure CF_4 both as radiator and detector gas, in a special windowless proximity focus geometry, with a reflective CsI photocathode and a triple GEM detector element with pad readout. (The layout of the detector element is shown in Figure 3.9).

Since a mirror-type RICH detector in the center of PHENIX is very difficult or nearly impossible to implement, we were led to a design without mirrors and without a window in which the Cerenkov light from particles passing through the radiator is directly collected on a CsI photosensitive plane which evaporated on the top face of the first GEM. This "proximity focused" geometry creates a circular blob image rather than a ring as in a RICH detector.

The combination of a windowless detector with a CsI photocathode and CF_4 results

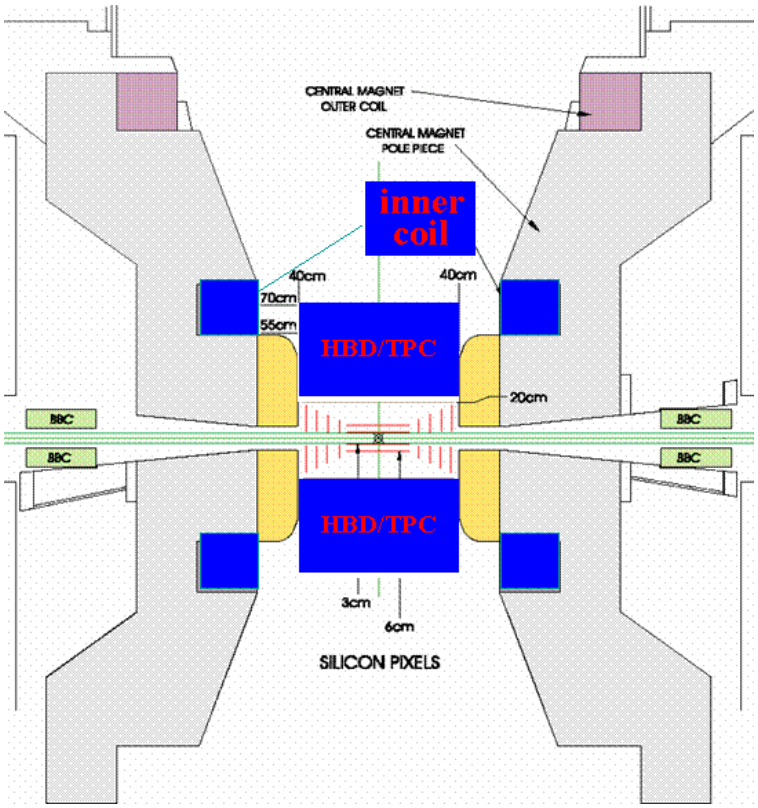

Figure 3.8: Layout of the inner part of the PHENIX detector showing the location of the HBD/TPC and the inner coil.

in a very large bandwidth (from 6 to 11.5 eV) and a very high figure of merit $N_0 = 940$ cm^{-1}. With these unprecedented numbers, one expects approximately 40 detected photoelectrons per incident electron in a 50 cm long radiator, after including losses induced by the optical transparency of the entrance mesh and the photocathode. This large number of photoelectrons ensures the necessary high level of single electron detection efficiency and, more importantly, is crucial to achieving a double hit recognition larger than 90%.

The reflective photocathode scheme totally screens the CsI from photons produced in the avalanche. The scheme foresees the detection of the Cerenkov blob in a pad plane with the pad size approximately equal to the blob size ($\sim$10 cm^2). This has been determined to be more than adequate for the detection criteria established by PHENIX, and results in a low granularity detector, which in turn simplifies the requirements on the GEM read-out. In addition, since the photoelectrons produced by a single electron will be distributed between at most three pads, one can expect a primary charge of at least 10 e per pad allowing operation of the detector at a relatively moderate gain of a few times 10^3.

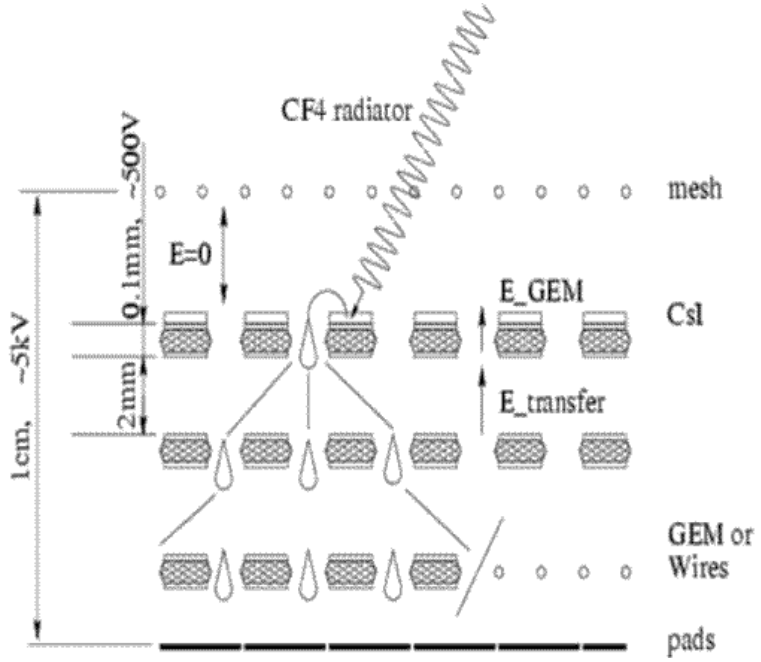

Figure 3.9: Detector configuration with reflective CsI photocathode, triple GEM and pad readout.

3.2.3.2 HBD R&D Results

The proposed concept has several novel properties which raise a number of questions, including generic detector R&D issues (e.g. can GEM detectors operate in pure CF_4?, are there aging effects of the GEM foils or of the CsI photocathode with pure CF_4?, can the detector operate at the desired gain in a stable mode? is the concept hadron blind? what is the rejection factor of hadrons?...). Over the last ten months, PHENIX has been engaged in a comprehensive R&D program addressing these questions and aiming at demonstrating the validity and feasibility of the proposed concept.

Extensive studies using 3×3 and 10×10 cm^2 detectors have been performed using a Hg UV lamp, an Fe^{55} X-ray source, an Am^{241} alpha source and cosmic rays. Many measurements were also performed with the conventional Ar/CO_2 (70/30%) gas mixture for comparison. A detailed account of some of the results obtained so far can be found in [161], only a brief summary is presented here.

The triple GEM detector with or without CsI photocathode operates in a stable mode at gains up to 10^4 in the presence of heavily ionizing particles (see Figures 3.10 and 3.11). The slope of the gain curve is similar to that of the conventional Ar/CO_2 (70/30%) gas mixture, however $\sim$ 140 V higher voltage across the GEM's is needed for a given gain. The gain curve starts deviating from exponential growth when the total charge in the detector exceeds $\sim 4 \times 10^6$ e, and the gain is fully saturated when the total avalanche charge reaches $\sim 2 \times 10^7$ e (see Figure 3.11). This is a very interesting property making the system more robust against discharges as compared to Ar/CO_2.

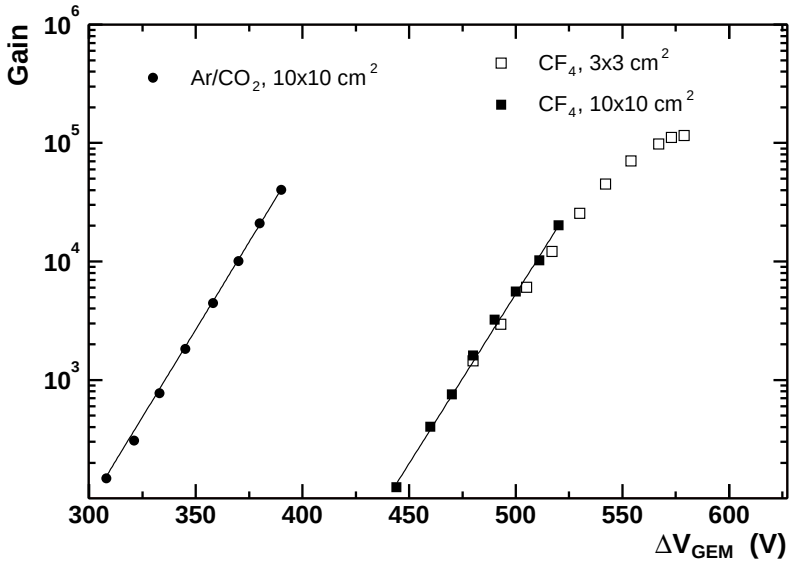

Figure 3.10: Gain as a function of GEM voltage measured with Fe^{55} X-ray source. The 3×3 cm^2 detector had a CsI layer deposited on the top face of GEM1. The lines represent exponential fits to the data with 10×10 cm^2 GEM's.

No deterioration of the GEM foil performance in pure CF_4 atmosphere was observed for a total accumulated charge of $\sim$ 10 mC/cm^2 at the pad readout board. The ion back-flow to the photocathode is close to 100%, independent of the operating gas and of the transfer field E_t between successive GEM's. At a gain of 10^4, the ion back-flow factor can be reduced to $\sim$ 70% by applying a relatively high induction field of $E_i \sim 5$ kV/cm between the last GEM and the pad board. In spite of the high ion back-flow no sizable deterioration of the CsI quantum efficiency was observed when the photocathode was exposed to a total ion charge of $\sim$ 7 mC/cm^2. This value is larger by about two orders of magnitude than the total integrated ion charge density expected during the lifetime of the planned HBD.

The hadron blindness property of the detector is illustrated in Figure 3.12. The figure shows the detector response to alpha particles from an Am^{241} source and to UV photons from a Hg lamp as a function of the drift field E_D, i.e. the field between the entrance mesh and the first GEM (see Figure 3.9). When the drift field is positive, the primary ionization electrons produced in the drift region by the passage of the alpha particles are collected with basically constant efficiency. However, as soon as the drift field is reversed, the primary charges are repelled towards the mesh and the detection efficiency drops abruptly. The behavior for UV photons is very different: as the drift field approaches zero, from the positive side, the photoelectron efficiency slightly increases, reaching its maximum at E_D=0 and then slowly decreases as the drift field becomes more and more negative. At a slightly negative value of E_D, the photoelectron detection efficiency is practically preserved at its maximum value of $\sim$100% whereas the primary ionization charge is largely suppressed.

A sophisticated cosmic ray trigger is used to trigger on high momentum, p$\geq$ 4 GeV/c as well as low-momentum muons, allowing us to simultaneously study and optimize the HBD

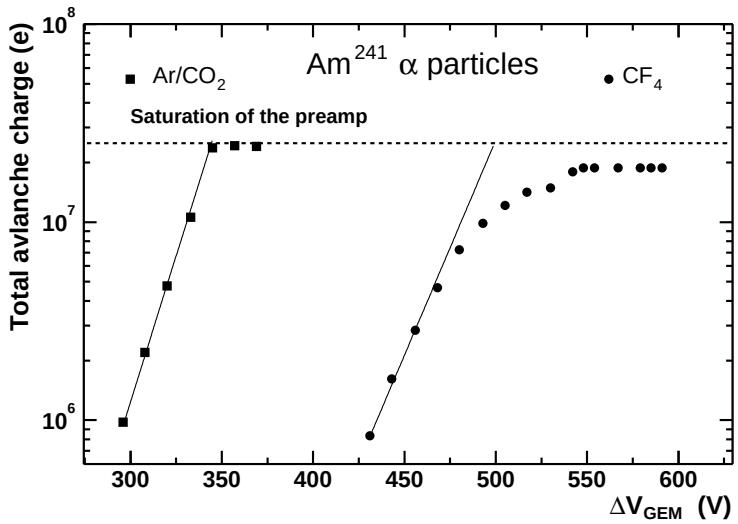

Figure 3.11: Total avalanche charge as a function of GEM voltage measured with Am^{241} α-particles. The lines represent exponential growth of the total charge in the avalanche derived from the low gain points.

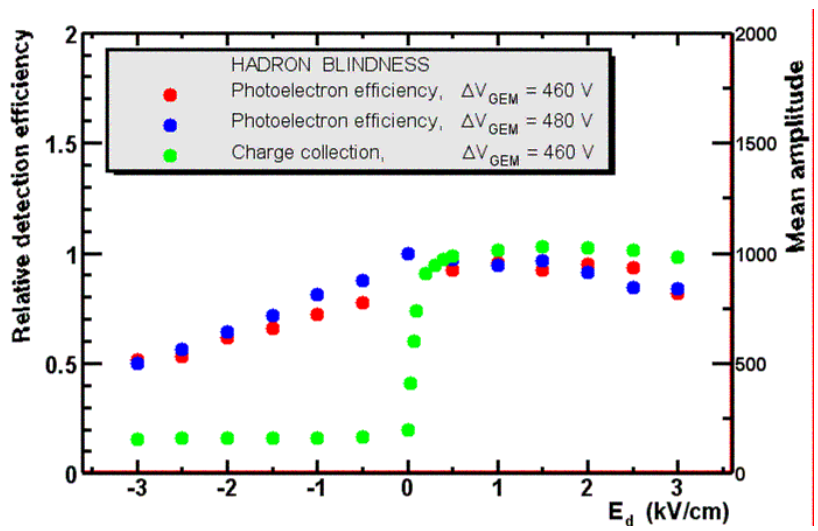

Figure 3.12: Demonstration of the hadron blindness property of the detector. When the drift field is reversed the ionization signal from a charged particle traversing the detector is considerably reduced whereas the photoelectron signal generated by UV photons is almost preserved.

response to "electrons" and minimum ionizing particles. In these studies the detector box is directly coupled to a 50 cm long radiator making it possible to directly measure the UV photon Cerenkov yield. First results for the number of detected photoelectrons as a function of the cosmic particle momentum seem to confirm the expected yield of ~ 40 pe per electron.

3.2.4 A Fast, Compact Time Projection Chamber

The current PHENIX baseline detector does not include a tracking device inside the central magnetic field. To date this has not limited our ability to track particles over a wide range of momenta for data taken during the first three RHIC runs. PHENIX has reported results for charged particles with momenta ranging from $\sim$ 200 MeV/c up to more than 10 GeV/c in the Run-3 data set. However, the inability to track inside the magnetic field does present a number of limitations for future running. In particular, it is not possible to observe the most decay vertices, secondary interactions and conversions in the material before the drift chamber. The inability to detect these phenomena results in a background of false tracks at high p_T that is very difficult to eliminate with the present PHENIX tracking detectors. As future measurements extend our measured charged particle spectra out to higher transverse momenta, this problem will become increasingly more difficult. In addition, with the present standard magnetic field configuration, particles below 200 MeV/c are not tracked at all. However, with the implementation of the new inner coil, it will be possible not only to increase the central field for better momentum resolution at high p_T, but also (alternatively) to create a greatly reduced field inside the region of the inner coil. Running in this reversed-field mode will allow the measurement of very low momentum particles, while at the same time preserving a high magnetic field outside that region for measuring particles with higher momenta.

This added flexibility of the central magnet, combined with a new inner tracking detector inside the magnetic field, offers a wide range of new physics opportunities for PHENIX. Perhaps one of the most interesting of these would be the measurement of low mass electron pairs. As discussed in Section 3.2.3 above, the measurement of low mass pairs in heavy ion collisions at RHIC is extremely difficult due to the overwhelming background of electron pairs resulting from photon conversions and Dalitz decays. The HBD detector will add tremendous capability in rejecting these pairs, but the virtues of multiple methods of attack on signal enhancement suggest that an additional handle on this background would be advantageous. Adding a tracking device inside the magnetic field which is able to track the low momentum electrons from Dalitz pairs and conversions, measure their dE/dx , and make a precise association of these tracks with the Cerenkov hits on the image plane of the HBD, will significantly improve the rejection capability for these backgrounds. In addition, having measured the charge and momentum of all tracks, it will be possible to make an effective mass cut on possible pair candidates, rather than just an opening angle cut, which will further improve our background rejection capabilities for Dalitz pairs and conversions and will help preserve the signal electrons from low mass vector mesons. The combination of having both a tracking device and an enhanced electron identifier will certainly add significant additional rejection power and redundancy for this extremely difficult physics measurement.

In addition to playing an important role in the low mass pair measurement, the new inner tracking detector will also greatly extend the azimuthal and rapidity coverage of the present PHENIX tracking system. By providing coverage over the full geometric aperture of the central magnet, the rapidity coverage is increased from $|\eta| < 0.35$ to $|\eta| < 1$, with nearly full 2π azimuthal acceptance. The detector would be used in conjunction with the proposed new silicon vertex detector (VTX) to track particles over this entire range with good momentum

resolution ($\sim$ 2% δp/p), and would enhance its ability to find displaced secondary vertices. The large rapidity and azimuthal coverage would also allow the detector to be used to find and study jets, such as in tagged γ-jet and two jet events, in both p+p and heavy collisions. Finally, the ability to track low p_T particles while simultaneously measuring particles at high p_T would also add new physics capabilities to PHENIX.

The inner tracker would combine the features of the tracking detector with the HBD into a common device that would be located within the region of the inner coil inside the central magnet, as shown in Fig. 3.8 in Section 3.2.3. The tracking detector would be a small, high resolution TPC that would utilize a very fast drift gas such that it could be operated at the highest rates anticipated for both heavy ion and p+p running at RHIC, including the planned luminosity upgrades. Figure 3.13 shows a conceptual design of the TPC, which would have an overall length of 80 cm, comprised of two 35 cm drift regions in opposite directions. The entire detector would be located between 20 and 70 cm in radius, providing 50 cm of radiator gas for the HBD, while the TPC alone would be situated between 20 and 55 cm in radius.

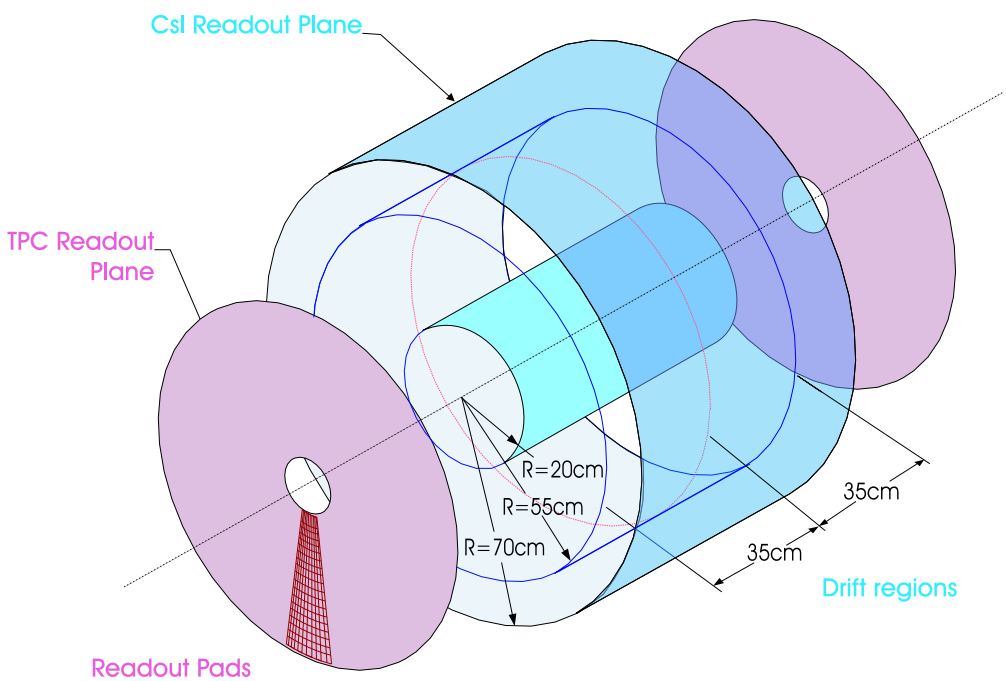

Figure 3.13: Conceptual design of a combined TPC and HBD detector for PHENIX.

The TPC will use the HBD radiator as an ionization gas volume. Charge produced in this region would be drifted over the distance of 35 cm to readout planes on both ends of the detector where it would be amplified and detected on a high-resolution pad plane using multistage GEM detectors, similar to those used in the HBD. The gas must have a high drift velocity and low diffusion in order to provide both the speed and spatial resolution required for operating in both a high rate and high multiplicity environment. A number of fast gases have drift velocities on the order of 10 cm/μsec or higher and would provide an overall drift time of < 4 μsec, which is within the time required for a Level 1 trigger within

PHENIX. Gas mixtures that include CF_4 are an attractive possibility, as CF_4 also has a low diffusion coefficient and would also be compatible with the choice of the radiator gas for the HBD. However, CF_4 is also known to be a difficult and aggressive gas to work with in many detectors. Therefore, finding a single gas or gas mixture that would serve as both the radiator gas for the HBD, the drift gas for the TPC, as well as the working gas for both sets of GEM detectors is a challenging task, and one for which significant R&D will need to be carried out.

The TPC will be required to achieve a spatial resolution of ∼200-300 μm at the readout plane in order to have good two particle separation with the high density of tracks produced in heavy ion collisions. While this is easily achievable with the GEM detectors, it will require a pad size of ∼2 x 10 mm and would result in ∼80K readout channels. In addition, good gain uniformity over the entire area of the detector is required in order to have good dE/dx resolution. Both of these requirements will necessitate a careful design of the readout plane.

A substantial effort must also be devoted to developing the readout electronics for the TPC in order to achieve the high packing density and low heat dissipation required. This will require the development of new monolithic ASIC chips for the analog front end and digital readout. The scheme presently envisioned utilizes a fast flash ADC on each channel with a sampling frequency of 40-50 MHz with at least 8 bits of precision. A complete zero suppression and multi-event buffering scheme will also have to be implemented in order to keep the total data volume from the detector down to a level consistent with the PHENIX readout architecture.

In terms of the long range plan for PHENIX, it is expected that the R&D on developing a new, fast TPC detector in combination with the HBD will take several years. It involves a number of new technologies, including the use of GEM detectors with fast drift gases and CsI photocathodes, the development of new, highly integrated readout electronics, and designing a detector that will operate stably and reliably over an extended period of time under the highest luminosity running conditions at RHIC. The current plan calls for R&D on the TPC extending though FY05, with construction starting in FY06 and finishing in FY07, and the first possible physics run to take place in FY08.

3.2.5 Forward Detector Upgrade

Many of the important long-term physics goals in PHENIX require the collection of large data samples over extended periods of time at the highest available luminosities. We anticipate that a luminosity of $L = 8 \times 10^{26}\,\mathrm{cm}^{-2}\ \mathrm{s}^{-1}$ for Au+Au and $L = 2 \times 10^{32}\,\mathrm{cm}^{-2}\mathrm{s}^{-1}$ for polarized proton beams will be reached over the next several years. In order to fully exploit the physics potential of the PHENIX detector at the highest luminosities achievable at RHIC it is important to further expand the data rate capabilities of the detector. In this section we discuss the upgrade of the first level muon trigger and a closely related proposal for a new forward calorimeter covering the PHENIX muon arm acceptance. The principal physics goals of the upgrade are as follows:

- Flavor separation of quark- and anti-quark polarizations in the proton through the measurement of longitudinal single spin asymmetries for W-production in polarized proton-proton collisions. This measurement will require an upgraded momentum-sensitive first level muon trigger and might require the addition of a nosecone calorimeter for the off-line separation of high momentum muons in W-production from background muons produced through hadron decays in jets by imposing isolation cuts to separate the muon from the jet-axis.
- Measurement of the gluon distribution at small x in photon+jet event samples using the combination of the present PHENIX central arm spectrometers and the planned nosecone calorimeter. This measurement will be carried out in polarized p+p collisions and d+A collisions leading to a rich agenda of physics from nuclear effects on structure functions to the study of the gluon polarization at small x.
- Measurement of π^0 cross sections in the forward rapidity region $1.2 < \eta < 2.4$.
- χ_c spectroscopy through photonic decays.
- Study of heavy quarkonium states at the highest obtainable luminosities utilizing the momentum sensitivity of the upgraded muon trigger.

It should be noted that the last three items specified above will be measured in p+p, A+A and p+A collisions.

3.2.5.1 Performance of the Present Muon Trigger

We have used the proton data sample acquired in 2003 to evaluate the performance of the PHENIX muon trigger both using the present CAMAC-based trigger processors as well as the custom-built PHENIX trigger boards. We find background rejection factors between 100 and 200 for the CAMAC electronics and of about 250 for the custom trigger board. At the present collision rates of typically less than 50 kHz in proton-proton collisions this has led to event rates of about 300 Hz in the single muon channel. This rate is compatible with the maximum expected bandwidth available for the first level trigger into the eventbuilder and second level trigger. We estimate the total usable bandwidth will reach 6-8 kHz and that a

fraction of about 2 kHz can be used for the single muon trigger. The remaining bandwidth will be reserved for competing rare event triggers, e.g. single electrons, di-leptons and high energy photons.

At the full luminosity expected for proton-proton collisions at 500 GeV of $L = 2 \times 10^{32}\,\mathrm{cm}^{-2}\mathrm{s}^{-1}$, which leads to event samples of $\int Ldt = 800\,\mathrm{pb}^{-1}$ for a 10 week physics run, the present first level muon trigger will count at rates of about 50 kHz or about a factor 25 more than the available bandwidth. The high background rate results from the large number of muons from hadron decays in jets (about 20kHz) and beam related backgrounds extrapolated from the situation observed in Run-3. A data taking run of $\int Ldt = 800\,\mathrm{pb}^{-1}$ results in a sample of about 10000 W^+ and W^-. The limited size of this data sample argues against "solving" the trigger bandwidth problem by random selection of a smaller sub-sample (pre-scaling). Instead it will be necessary to increase the selectivity of the muon trigger for W-production. All proposed upgrade ideas exploit the difference in the momentum spectra for muons from hadron decay (background) and W-production (signal). The momenta of the background muons are largely confined to the region below 10 GeV/c while muons from W-decays have energies ranging from 10 to well over 100 GeV/c.

In addition to the collision related background the present muon trigger has been found to be vulnerable to beam related backgrounds during the past proton runs at RHIC. The Collider Accelerator Department at BNL is presently inserting significant shielding in the beam tunnel upstream of the two PHENIX muon identifier walls in order to resolve this issue. However, in studying different upgrade proposals it is important to evaluate the performance of the proposed new muon trigger in the presence of beam related backgrounds.

3.2.5.2 Trigger Upgrade Options

Three possible solutions for the trigger upgrade have been studied. 1) The introduction of momentum information either from the existing muon tracker chambers or new dedicated trigger detectors upstream and downstream of the muon magnet. In the present version of the muon tracker electronics no information is sent to the first level trigger processors. A significant re-design of the front-end electronics would be required in order to introduce muon tracker information into the level 1 trigger. 2) The utilization of threshold information from a segmented Cerenkov-counter to match muon roads from the muon identifier. 3) The insertion of a nosecone calorimeter to exploit topology differences between background jet production and signal events.

A complete GEANT simulation, including the performance of a new trigger processor, has been carried out at UCR and BNL studying a new trigger using tracking information. In the simulation tracking information was provided either by a combination of the current muon tracker Station-1 and a new dedicated detector downstream of the muon tracker magnet or a pair of dedicated trigger detectors up- and downstream of the muon tracker magnet. In both cases a angular resolution of 1 degree and a matching of the muon identifier road to the upstream track to better than 30 cm have resulted in a muon trigger rejection in excess of 20,000.

The simulation studies have led to an R&D program at Kyoto University and the University of New Mexico which focuses on the possibility to read muon tracker information into

the level one trigger processors. At UIUC the possibility of new dedicated trigger detectors is being studied. The R&D is funded through support from Kyoto University and the NSF grant at UIUC.

A Cerenkov detector, introducing a lower momentum cut-off, could be placed in the beam tunnel or between the muon arm magnets and the upstream muon identifier walls. The integration issues in the north muon arm are difficult and are presently being investigated by collaborators at RBRC, BNL and RIKEN. GEANT simulations of soft electron background indicate that a modest segmentation, e.g. 5 by 5 elements, would result in rejection factors of about 30. RIKEN and Kyoto collaborators have carried out an effort to survey the relevant backgrounds in the past RHIC run 2003. The analysis of the Cerenkov test data is in progress.

The integration of the new trigger detectors will require a new set of local level-1 processors. A new regional trigger processor will combine and analyze the information from the local level 1 processors before passing the muon trigger decision to the PHENIX global level-1 system. Possible solutions are presently being discussed at Nevis and Iowa State University.

3.2.5.3 The Nosecone Calorimeter

In addition to aiding in triggering, the nosecone electromagnetic calorimeter will be able to measure photons, electrons, and hadronic jets at high rapidities matching the present muon spectrometer acceptance. The detector must be capable of resolving high energy π^0's which requires a small Moliere radius for good two-photon resolution. One of the present designs calls for a tungsten calorimeter read out by silicon detectors. In this design it will be possible to read out the silicon plane located at the maximum shower development with high segmentation.

3.2.5.4 Schedule and Funding

We plan to complete simulation studies and the analysis of Cerenkov test data in December 2003. We will seek support for the PHENIX muon trigger upgrade through a collaborative NSF-MRI grant proposal to be submitted in January 2004. We have started to formulate the final scope of the upgrade project. Collaborators at the Universities of California at Riverside, Colorado in Boulder, New Mexico at Albuquerque, Illinois in Urbana Champaign and Iowa State University, are working on a proposal to the NSF. At the same time groups at RIKEN and Kyoto University have applied to Japanese funding agencies for support. Limited funds are available for R&D from the NSF grant and internal funding at UIUC. Assuming a successful NSF grant application we aim at a first trigger integration stage based on prototypes in Fall 2006 and a completely installed and commissioned trigger in late 2008.

3.3 Data Acquisition

3.3.1 Summary of Current PHENIX Online System

The PHENIX online system was originally designed to be able to sample the maximum beam crossing rate of 10 MHz (106 ns clock), and sample the physics from up to ten times the nominal design luminosity for Au+Au reactions. The specification for the PHENIX front-end modules (FEM's) enforces a digitization time corresponding to a maximum Level-1 accept rate of 25 kHz. Physics projections indicated that all rare probe physics could be sampled at the Level-1 trigger and fit into the 25 kHz bandwidth even at very high luminosity. The limit of 25 kHz is embedded into all of the existing PHENIX front-end electronics and the data collection modules (DCM) that receive their non-zero suppressed data in the PHENIX control room. The current configuration of the PHENIX Data Acquisition (DAQ) architecture reflects cost-saving measures taken during the construction phase of the PHENIX Project, wherein 2 front-end electronics modules are multiplexed into one DCM channel, leading to a current limit on the Level-1 trigger accept rate of 12.5 kHz.

The Level-1 trigger for PHENIX is formed from a reduced data set from specific detector subsystems (Beam-Beam Counters, Muon Identifier, Electromagnetic Calorimeter, Ring Imaging Cerenkov Counter) every beam crossing (106 ns). This reduced data set provides our Level-1 event selection with a maximum latency of 4.24 μs. These electronics are built with anti-fuse Field Programmable Gate Array (FPGA) technology. The Data Collection Modules (DCM) receives non-zero suppressed data from all subsystems via Gigabit fiber optic connections. The DCM's zero suppress the data at full clock speed in programmable FPGA's and perform the first stage of event building. The data are further collected into Partition Modules, and then sent to the Event Builder. A commercial Gigabit network switch serves as the fabric for constructing events. Banks of PC's after the switch fabric receive all of the data fragments for a given event. These same PC's also serve as the PHENIX Level-2 trigger farm. Event passing the Level-2 event selection are then archiving locally on disk before being sent to the RHIC Computing Facility (RCF). The local archiving to a large disk array is used a staging area to smooth out fluctuations in data taking and RCF archiving rates.

PHENIX uses a global timing system to synchronize all the front-end electronics to the RHIC clock and coordinate event accepts and resets. This Granule Timing System coordinates with the Global Level-1 Trigger for full partition synchronization. ARCNET is the protocol used for slow download of configuration information to all the front-end electronics.

The PHENIX Data Acquisition System has performed to expectations and continues to undergo incremental improvements in speed and reliability. The ability to partition the system into smaller data-taking entities has proven to be an invaluable feature for commissioning many independent sub-systems in parallel, and to introduce new sub-systems. Several additional detectors and Level-1 triggers have been incorporated into the system over the last two years, first as individual "granules", then later merging into the global DAQ readout architecture.

3.3.2 PHENIX Upgrade Program: DAQ Implications

The proposed PHENIX upgrade program described in the previous sections includes the addition of major new detector subsystems. The proposed Time Projection Chamber and Silicon Vertex Detector represent significant increases in front-end electronics channel counts. Most likely these systems will require zero-suppression at the front-end electronics before Level-1 accepted events are sent to the data collection modules. This will be critical in terms of design of the front end systems in terms of power, space and reduced output bandwidth.

Due to the rapid evolution in electronics technology, some of the critical components used in the existing DCM are no longer available. In addition, DCM's for these new subsystems will need to perform higher-level zero suppression and data re-organization. A revised design for the DCM based on new technology is now necessary and will allow us to take advantage of faster processing and data transmission technology. A subset of the new detectors will also require the construction of new Level-1 trigger electronics. In order to take advantage of both the new measurement capabilities and higher RHIC luminosity, fast triggering is essential.

The fundamental function of the PHENIX Timing System remains unchanged and is expected to be suitable for the new detectors. Minor modifications to meet new optical technology will be necessary. The ARCNET slow controls system is a standard that has faded from the market. With support waning, we will probably look for new industrial standards for the new front-end electronic systems.

The event builder is based on commercial Ethernet switching technology as well as commodity-market PC's. With the increasing data bandwidth from the upgrade detectors, we expect we will require incremental upgrades in a continuous process. The upgrade will certainly include faster network switches and higher performance computing. This process has already been ongoing during the initial phase of PHENIX operations.

Depending on the Level-2 processor farm task load, a Level-3 trigger system may need to be constructed. It would be an extension of the Level-2 system, with the key difference being an architecture unconstrained by event building interfaces. This would make it possible for the Level-3 system to take directly implement subsets of the offline reconstruction code.

3.3.3 PHENIX Upgrade Program: The Next Step for DAQ

As the RHIC luminosity grows it will be important to recover the full design Level-1 bandwidth of 25 kHz, thereby doubling PHENIX's sensitivity to rare physics. We will certainly upgrade the Level-1 Trigger System as the interaction rate increases well above design luminosity. New technology and faster clock speeds will allow us to run more complex Level-1 algorithms while staying within the specified 40 μs latency time. A specific proposal for the muon trigger systems is currently being developed (Section 3.2.5) and will be added to the existing suite of parallel Level-1 triggers. We would also propose de-multiplexing the FEM's for all subsystems, thereby doubling the system bandwidth. The transition is expected to be straight forward except for the time needed to modify the existing FEM's. These new systems would be commissioned during the annual RHIC maintenance period.

A hardware trigger system will also be added between the DCM and Event Builder.

While the hardware-based scheme is of course less flexible than higher-level software-drive triggers, their are significant advantages for a well-specified algorithm. In particular, the hardware-based trigger can take advantage of full pipelining and parallelism in a bank of FPGA's. It could greatly reduce the load on the upper level triggers, yielding more time for complete event reconstruction.

Important research and development funds are essential throughout the entire span of planned upgrades to be in a position to take advantage of new digital technology for the next generation data collection modules, Level-1 trigger system, and optical technology.

3.4 Computing

PHENIX places enormous demands on many aspects of computing, from online monitoring and calibration to data handling, primary event reconstruction, simulation and analysis. The decadal plan has implications for all these current computing activities, as well as for other activities which are still on the horizon. The impact on computing will come not only from the increased volume of data expected in coming years, but also from the facts that data will be recorded by additional detectors, that the data will be enriched by sophisticated triggering, and that off-site computing will become more deeply integrated into the overall computing effort.

The computing of PHENIX starts before the data are even archived to tape, with activities that rely heavily on the computing power available in the counting house. We have seen a natural growth in the amount of computing there, and this is a trend that one should expect to continue, if not accelerate, as the experiment matures. The first few years of taking data with a detector as complex as PHENIX have seen a long process of developing both the expertise and the software to monitor the quality of data as they were acquired, to calibrate those data, and then to perform primary event reconstruction. This software has become both more sophisticated and more resource demanding over time, as more computing is done closer in time to when the data were acquired.

The PHENIX triggering hierarchy currently ends with, at most, a Level-2 decision, which is implemented in relatively spare algorithms that run on the Assembly and Trigger Processors (ATP's) of the Event Builder. However, as noted in the previous section, a Level-3 trigger becomes attractive when one considers the possibility of running actual reconstruction code as part of the trigger decision. All proposed implementations of Level-3 triggers rely upon a farm of loosely coupled computing nodes, very much along the lines of the RCF farms.

The RHIC Computing Facility (RCF) provides the main large-scale computing resource for PHENIX. The RCF has an architecture fairly typical of a single High-Energy Energy and Nuclear Physics (HENP) reconstruction and/or analysis site, a large farm of loosely coupled commodity computers. This sort of architecture has been quite stable since at least the mid-1980s and seems unlikely to change radically in the foreseeable future. The main changes one should expect over the next decade are ones of overall scale and of technical detail.

The RCF has demonstrated the ability to archive data to tape at sustained rate of 100 MB/sec, with bursts just over 200 MB/sec having also been accomplished. The limit on the sustained rate is largely determined by the number of STK 9940B tape drives available, each of which has a throughput in excess of 20 MB/sec. The limit on the burst rate is set by the number of Gbit links from the counting house to the RCF. We have two such links now, and the observed maximum burst rate corresponds closely to the line speed of those links. It should be possible to raise the number of such links to accommodate PHENIX plans, though doing so would need close cooperation with the RCF staff.

The average time that is takes to reconstruct the tracks in a sample of minimum bias Au+Au PHENIX events is around 10 seconds on a 2 GHz Pentium processor. At present

it is not certain how the detectors anticipated as part of the PHENIX upgrade plans will affect this number. If new tracking detectors are used only to confirm seed tracks propagated inward from the existing set of central-arm tracking detectors, the overall computing time needed to reconstruct a track should not increase substantially. If, however, an independent reconstruction of track segments is done in a detector near the vertex, and then those tracks are matched to segments in outer detectors, the time needed will have an significant effect on the overall reconstruction speed.

The PHENIX analysis model relies heavily on centralized data storage servers. At present, these are mainly Sun Solaris NFS servers, each serving several terabytes of data to the farm of analysis nodes. This is likely to change, as technology enables the effective use of more and more distributed disk. However, it seems unlikely that we will ever be able to store more than a small fraction of the data of current interest on disk at any one time.

PHENIX is fortunate to have several off-site sources of computing power. The largest of these, the PHENIX Computing Center in Japan (CC-J), is approximately of the same scale as the PHENIX share of the RCF. There are also significant resources available to PHENIX at Vanderbilt University, the University of New Mexico, IN2P3 in Lyon, and on a slightly smaller scale at other institutions affiliated with PHENIX. These facilities generate the bulk of our simulations, some event reconstruction and a wide variety of analyses. The main complication in harnessing these off-site resources is the difficulty in distributing and collecting data from them, the bookkeeping required to track all of the ongoing efforts, and the general coordination of manpower that is needed. As PHENIX data sets increase in size, these complications will have to be solved, since we will rely more and more heavily on them for the production of simulated data and for the support of regional analysis activities.

The inter-facility architecture is the focus of intense activity among the computing community of HENP physics, and will likely see significant improvements over the next decade. PHENIX is a member of the Particle Physics Data Grid, one of the main U.S.-centered efforts to develop and deploy inter-facility an architecture able to serve the needs of experiments in the coming years. To this end, we have demonstrated our ability to use the existing, early, Grid tools to enable remote job submission and file movement.

One function of PHENIX computing that will in all probability be the first to take advantage of Grid technology is simulation. Almost all simulations for PHENIX are performed at sites other than BNL. As an example, the Los Lobos cluster at the University of New Mexico performed about 250,000 CPU hours of computing in support of PHENIX analyses based on data collected in the 2002 run and one should expect these sorts of numbers to continue to grow. The limiting factor in scaling up the PHENIX simulations is the manpower required to organize the overall effort and to collect and move the results to BNL (where they are stored in HPSS). Grid technology for remote job submission and data movement are focused on these very tasks, and there are already efforts underway in PHENIX to develop those technologies where necessary, adapt them where possible, and deploy them to make the most efficient use of the limited manpower available.

The general trend in PHENIX computing over the next decade will be one of increased scale. Except for the inclusion of Grid computing technology, the basic architecture seems suitable for handling significantly larger quantities of data than have been collected to date.

Appendix A: Charge Letter

Director's Office

Building 510F P.O. Box 11973-5000
Phone 631 344-5414
Fax 631 344-5820
tkirk@bnl.gov

February 28, 2003

Prof. William Zajc, Spokesperson
PHENIX Collaboration
Nevis Laboratories
P.O. Box 137
Irvington, NY 10533

Dear Bill:

The RHIC experimental program is now fully underway and the physics discoveries are emerging at a rapid and exciting pace. The relativistic heavy ion community, of which the collaborators of PHENIX are a central and key part, is currently reaping the benefits of a science planning and construction period that started in the 1980s when the RHIC ideas were first seriously pursued. In view of the decadal time scales that now characterize the evolution of 'big science' programs, it is not too early to expand our planning efforts for the next phases of the RHIC scientific program to include persons and communities not already participating. The recent Review of RHIC detector R&D proposals by an international panel of heavy ion and detector experts represents an important step in actualizing the planning that has occupied the RHIC experimental community since the start of the Nuclear Physics Long Range Plan activities in the fall of 2000. We now seek to inform the wider nuclear physics community about the development plans for RHIC and its future physics program.

In this letter, I intend to focus primarily on the strategic time frame beyond the mining of accessible data regimes from our present facilities and detectors and their incremental improvements. Efforts to consider this longer-term planning regime have already been underway for some time in a number of venues as noted above, but this letter comes to solicit your participation in a specific planning exercise that will be of paramount importance for the U.S. Department of Energy and for the wider nuclear physics community. By this, I

mean the clear identification of next generation science goals and the planning of facilities on the scale of the electron cooling luminosity upgrade of RHIC and its detectors, as well as eRHIC and possible large new detectors in the RHIC complex to realize these goals.

How does this objective link PHENIX and the management of BNL? I intend to involve the leadership of the present RHIC experimental collaborations, together with BNL's HENP Program Advisory Committee (PAC), in a joint consideration of the future ideas and options for evolution of the RHIC science program and facilities. Why choose this particular combination? I believe that the present RHIC collaborations have already engaged the best and brightest members of the heavy ion nuclear physics community and therefore represent the most natural starting point for consideration of future research paths for this field of science. I also believe that the BNL PAC represents a wise and experienced group of scientists who will provide insight and astute general criticism of the emerging plans of the RHIC community and how it can best realize these plans in a very competitive scientific marketplace.

To engage these partners in a productive dialog, the method that I plan to employ relies on the ability of the RHIC collaborations to produce concise documents that identify decade-scale science goals and facilities paths to reach these goals, together with the ability of the PAC to critique these goals and development paths from the perspective of the larger nuclear science community. At a later stage of this longer-term planning process, it is likely that workshops will be carried out to consolidate the goals and facility planning and members of the PAC will be encouraged to participate in these. For now, the PAC will act as reviewers and critics of the documents requested here.

So, to put this concept into action, I am asking you to organize within the PHENIX Collaboration, a group to produce a paper on the strategic physics goals of the collaboration as it evolves into the high luminosity phase of the RHIC program, a period that will be reached operationally not before about 2009 and will likely be complete only after 2010. For this exercise, you should address both the heavy ion and the polarized proton aspects of the contemplated program. Your plan should also describe the evolution of the PHENIX detector to meet the stated physics goals. The time period that is appropriate for this paper is the ten-year period from 2004-2013. Accompanying this letter is a short summary of how the luminosity of RHIC is anticipated to evolve that you may use as a time-frame guideline. You should also refer to planned PHENIX detector R&D as this work impacts your plans. At first glance, it may seem like a very early time to begin addressing the physics and detector issues that will dominate RHIC physics after 2009, but a purposeful examination of the strategic R&D and developmental time scales will confirm the need to begin planning now.

Because the Laboratory is also planning to develop a new collider capability, eRHIC, that will enable the field of virtual photon-hadron physics to be pursued at BNL, you are invited to address the physics goals and detector concepts for exploring this field as well. At the present time, we envision eRHIC as producing collisions only at the 12-o'clock interaction point while heavy ion collisions continue running simultaneously in the RHIC yellow and blue rings. We further envision that a new collaboration will form to exploit this new physics opportunity and that the new collaboration may attract some of its members from the existing RHIC experimental collaborations. I intend to provide an opportunity for such

persons to begin discussing their ideas for eRHIC physics in this same time frame. The HENP PAC will consider the eRHIC ideas as well as the future RHIC program plans.

I should also note that the RHIC program from 2008 forward will face vigorous competition from the LHC heavy ion program. In addition to the ALICE detector collaboration, both the ATLAS and CMS detector collaborations are studying their respective capabilities for performing heavy ion experiments and are expected to participate in the LHC heavy ion program. The RHIC program for heavy ion collisions will need to be carefully planned to compete in this arena. There will be, on the other hand, interesting opportunities for productive collaborations on instrumentation with LHC groups that may be of value for PHENIX to explore in a cooperative RHIC-LHC R&D context. The polarized proton and eRHIC programs will face no direct competition but will still need to be generally compelling to continue to compete effectively for resources.

In addition to these strategic questions, there is one near-term issue that requires some careful thought on the part of PHENIX. This concerns the primary scientific goal that was identified for RHIC when it was approved for facility construction. This, of course, is the search for Quark Gluon Plasma. You and I, together with the other RHIC spokespersons, have already engaged in discussions of how to proceed in publicly announcing the QGP discovery (assuming we don't conclude that QGP is not created under RHIC conditions!), but we haven't yet engaged in discussion of what minimal and feasible set of measurements will provide strongly convincing evidence of QGP's existence. Accordingly, I ask you to provide the list of experimental measurements that PHENIX expects to achieve that bear on this question and a best guess as to the time frame for having such measurements in hand.

All this having been considered, let me now be more specific about the document that I am soliciting from PHENIX. The strategy paper should contain the following elements:

1. A list of the physics topics that the PHENIX collaboration expects to address in the period 2004-2013, with a short (paragraph length) statement of the anticipated physics impact of a successful measurements program. It is understood that unanticipated physics directions may emerge as the program evolves but there are prospective physics topics of significant interest that have already been identified and described. Please indicate a time and luminosity frame over which these topics are expected to evolve.

2. A brief outline of how the PHENIX detector is expected to evolve to meet the requirements of the prospective physics program. R&D necessary to meet the detector evolution should be noted and its time frame also incorporated in your plans.

3. A list of measurements that PHENIX expects to provide that bear on the question of the existence of QGP and when you expect that these measurements will become available.

4. A brief statement of how your collaboration is expected to evolve to carry out the projected plans. If you envision large changes in the composition or focus of the collaboration, please describe these and the reasons for them.

I would like the PHENIX paper to be completed and submitted to me no later than June 1, 2003. Upon receipt, I will provide it to the PAC members for their information and comments. By the time of the September 2003 PAC Meeting, the Laboratory will have formulated a plan for maximizing the scientific benefits of the submitted papers from all the contributing parties and will ask for PAC comments and recommendations on this plan. The Nuclear Physics Division of DOE will be kept abreast of these evolving strategic developments and their input incorporated.

A full set of strategic RHIC research direction papers have been solicited from each of the present RHIC collaborations and additional contributions in this area will also be solicited, through separate announcement posted to the RHIC Users website, from other interested parties in the nuclear physics community. The prospective eRHIC program and facility is one obvious example. As these strategic directions evolve, the related supporting arguments and detailed plans will be strengthened by appropriately targeted workshops and other developmental activities. These actions and activities will be announced later.

I have always believed that science is best carried out in a 'bottoms-up' manner and should be driven by practicing researchers. By adopting this approach of strategy papers from working collaborations, I hope to achieve both a comprehensive outreach and a researcher driven outcome. Your collaboration is expected to be a central player in this effort. I hope you will be able to respond effectively to this solicitation.

I am available to discuss the content of this letter as you may wish.

Best regards,

Thomas B.W. Kirk
Associate Laboratory Director
High Energy and Nuclear Physics

Cc: BNL HENP Program Advisory Committee Members
D. Kovar, DOE-NP

List of Figures

1.1 Installed and active detectors for the RHIC Run-1 (left) and Run-2 (right) configurations of the PHENIX experiment. 1–2
1.2 RHIC Run-3 configuration of the PHENIX experiment. 1–3
1.3 Hadron identification in the PHENIX Central Arms with the Aerogel Cerenkov Counter system. 1–4
1.4 The aerogel detector in the west arm between pad chamber 2 (PC2) and 3 (PC3) in the W1 sector (left) and the aerogel detector structure and orientation with respect to the beam line (right) are shown. 1–4
1.5 PHENIX Management Structure, November, 2003 1–5

2.1 The suppression factor R_{AA} measured for π^0 production by PHENIX in Run-1 Au+Au collisions at 130 GeV [8], Run-2 Au+Au collisions at 200 GeV [18], and Run-3 d+Au collisions at 200 GeV [27]. 2–3
2.2 Nuclear modification factor R_{AA} for π^0 in central (closed circles) and peripheral (open circles) Au+Au at $\sqrt{s_{NN}} = 200$ GeV. 2–9
2.3 R_{AA} for $(h^+ + h^-)/2$ and π^0 in Au+Au collisions as a function of p_T for minimum bias and 9 different centrality classes, ranging from very peripheral to very central. 2–10
2.4 p/π (left) and $\overline{p}/\pi$ ratios for central(0-10%), midcentral(20-30%) and peripheral(60-92%) Au+Au collisions at $\sqrt{s_{NN}} = 200$ GeV. Open (filled) points are for $\pi^\pm$ (π^0), respectively. Data from $\sqrt{s} = 53$ GeV p+p collisions [43] are shown as stars. The dashed and dotted lines are the $(\overline{p}+p)/(\pi^+ + \pi^-)$ ratio in gluon and quark jets [44]. 2–13
2.5 Modification factor, R_{CP} for $(\overline{p}+p)/2$ (filled circles) and π^0. R_{CP} is the ratio of yield per binary NN collision in central Au+Au to peripepheral Au+Au. Dashed and dotted lines indicate N_{coll} and N_{part} scaling. 2–13
2.6 Charged hadron to π^0 ratio in central (0-10% - squares) and peripheral(60-92%) Au+Au collisions. The peripheral data points are offset by +130 MeV/c for clarity. The line at 1.6 is the h/π ratio measured in p+p collisions [43]. The lower panel shows the fractional normalization error common to both centrality selections (solid) and the relative error between the two (dashed). 2–14
2.7 Top: Nuclear modification factor, R_{AA} for $(h^+ + h^-)/2$ in minimum bias d+Au compared to R_{AA} in the 10% most central Au+Au collisions. Bottom: Comparison of R_{dA} for $(h^+ + h^-)/2$ and π^0. 2–15

2.8 The nuclear modification ratio, R_{CP} as a function of p_T for identified charged pions (closed circles), kaons (squares), protons and antiprotons (triangles), and inclusive $(h^+ + h^-)/2$ (open circles). 2–16

2.9 Two versions (upper [45] and lower [46]) of direct photon cross section compared to NLO QCD with best gluon structure function. 2–18

2.10 Lowest order diagrams for photon production in a plasma. Left: Compton scattering, Right:quark anti-quark annihilation into a photon and a gluon. 2–22

2.11 Left: Intermediate-mass di-lepton spectra at RHIC energies around midrapidity assuming a chemically equilibrated QGP throughout its lifetime. Shown is the decomposition of the thermal fireball radiation (with $T_0 = 370$ MeV, $t_{fo} = 20$ fm/c) into QGP (short-dashed line) and hadron gas (long-dashed lines) parts (including their respective yields from the mixed phase), compared to Drell-Yan annihilation (dashed-dotted line) and the total sum (note that open charm decays are not accounted for). It is the regions between about 1.5 and 3 GeV where the QGP contribution is expected to dominate over other contributions. Right: Total di-lepton spectrum from b = 1 fm Au+Au collisions at RHIC energies around midrapidity including schematic experimental acceptance cuts appropriate for the PHENIX experiment (ρ, ω, and ϕ cocktail contributions are not separately shown but included in the solid curve). As in the left plot, the semileptonic decays of correlated anti-/charm and anti-/bottom quarks are not included [49]. 2–23

2.12 Left: HELIOS-3 dimuon data [52] from central S+ compared to the standard background (consisting of Drell-Yan and open charm) and the additional yield from secondary hadronic annihilation processes evaluated within a transport model [53]. Right: decomposition of the secondary reactions [53]. 2–24

2.13 Dimuon mass (left) and transverse-momentum (right) spectra from NA50, central Pb(158 AGeV)+Pb collisions [54]. Calculations for the thermal contribution are from [55]. Contributions for open-charm yield from simulations by NA50 have been included. 2–24

2.14 A calculation of the spectra from different sources of direct photons for central Pb+Pb collisions at CERN-SPS. [60] 2–25

2.15 Rates for pQCD direct photons under different assumptions of intrinsic parton k_T, compared to the WA98 data, for Pb+Pb collisions at CERN-SPS. Figure is taken from [59] for calculations by Dmitru, et.al.[61] 2–26

2.16 The PHENIX minimum bias continuum data are superimposed with Pythia scaled by the number of binary collisions for minimum bias charm production. Pythia is shown as the solid blue curve. Exodus, a PHENIX simulation for the low mass electron contribution form π^0's, η's, the vector mesons, and a variety of other "soft" contributions is shown as the solid red curve. The total of these sources is the solid black curve.
2–27

2.17 Table showing the expected yield and significance of the thermal contribution to the di-electron continuum with and without the HBD. This assumes T_0= 380 MeV and T_C=180 MeV. More details are in [49]. The LMR is defined as between 0.3 and 1. GeV, and the IMR as between 1.1 and 2.5 GeV. This assumes that the charm contribution can be measured and subtracted exactly. The measurements for which the HBD will be available are in red.
2–28

2.18 Rates published by Turbide, Rapp and Gale [60] scaled up to 300 inverse microbarns of Au+Au, or about 2×10^8 central collisions (0-10% Centrality).
2–29

2.19 Spectral functions of the light vector mesons ρ (left panel) and ω and ϕ (right panel) in vacuum (solid lines) as well as in hot *net* baryon-poor hadronic matter as expected under RHIC conditions: (T;μ_N) = (120; 91) MeV (long-dashed lines), (T; μ_N) = (150; 40) MeV (dashed-dotted lines) and (T; μ_N) = (180; 27) MeV (short-dashed lines). For the definition of ρ_{eff} see [49]. 2–31

2.20 Left Panel: the time evolution assumed for the system. Right panel: the contributions to the final spectrum after integrating over the evolution of the system of various components with and without in-medium effects. Also shown is the contribution of perturbative $q\overline{q}$ annihilation (i.e. the QGP). . . 2–32

2.21 Di-electron spectra from the CERES experiment at CERN, showing a large excess at between 200 and 800 MeV in comparison to the expectation (solid line) from a variety of "normal" contributions. 2–33

2.22 Di-electron invariant mass from E325 at KEK. Left panel: Invariant mass from light targets showing a normal vacuum behavior of the peaks. Right panel: Spectra from heavy (Cu) targets showing the excess below the vacuum ω. 2–34

2.23 Left Panel: KK invariant mass from Au+Au collisions as measured by PHENIX. Kaons are identified in the TOF wall and the EMCAL. Right Panel: Di-electron invariant mass from a small subsample of deuteron-gold collisions from Run 3. 2–35

2.24 Expected yields of vector mesons as measured in the di-electron channel for upcoming runs. Also shown in the significance of the signal with and without the HBD. Highlighted in red are the measurements in which the HBD will be crucial. 2–35

2.25 Relative J/ψ yields versus the logarithm of the number of binary collisions for several symmetric combinations of heavy ions. The running periods are similar in all cases. This plot illustrates the need to study lighter heavy ion systems to obtain information about lower energy densities. 2–38

2.26 The single electron p_T spectrum after subtraction of all known non heavy-quark sources. The remaining signal is thought to be predominantly due to semi-leptonic open-charm decays. The data were extracted from a minimum bias data sample corresponding to 1 μb^{-1} of Au+Au collisions at $\sqrt{s_{NN}}$ = 130 GeV. 2–39

2.27 Preliminary PHENIX open charm and beauty yields for 200 GeV Au+Au, compared with binary-collision scaled PYTHIA estimates of the electron yield in the central arms due to semi-leptonic decays of D mesons. 2–40

2.28 Simulated distance of closest approach (DCA) distributions from PYTHIA for electrons from open charm, open beauty, and Dalitz decays. The DCA distributions are integrated over all p_T from 0.5 GeV/c, 1.0 GeV/c, 2.5 GeV/c and 3.0 GeV/c. Note the evolution of the Dalitz, charm and beauty DCA distributions with increasing p_T cut. 2–41

2.29 Comparison of 130 GeV Au+Au PHENIX π^0 data (left plot) and PHENIX single electron data (right plot) with predictions from PYTHIA and from a hydrodynamic model. Each plot shows the D and B meson p_T distributions. The right plot shows the distributions of their decay products compared with electron data. 2–42

2.30 The J/ψ invariant mass spectra in the di-electron and the di-muon channels from Run-2 p+p collisions. A total of 150 nb^{-1} was recorded by PHENIX in Run-2. 2–44

2.31 Top: The J/ψ p_T distributions for di-muons and di-electrons from Run 2 p+p collisions. Bottom: The J/ψ rapidity distribution from Run-2 p+p collisions. The mid-rapidity point is from the electron measurement in the central arms, the other two points are from the measurement in the south muon arm. The north muon arm was not yet operational in Run-2. A total of 150 nb^{-1} was recorded by PHENIX in Run-2 for p+p collisions. 2–45

2.32 The binary-scaled J/ψ yield per collision at mid-rapidity from Run-2 Au+Au collisions. A total of 24 μb^{-1} for Au+Au collisions was recorded by PHENIX in Run-2. The theory curves are discussed in the text. 2–46

2.33 The simulated $\Upsilon \to e^+e^-$ invariant mass spectrum with and without the vertex detector. The simulated yields correspond to a 200 GeV Au+Au PHENIX recorded luminosity of about 3.3 nb^{-1}, or roughly 10 nb^{-1} delivered by RHIC. 2–49

2.34 Left: The recent preliminary result on A_{LL} released by PHENIX with 0.2 pb^{-1} luminosity and $\sim$ 0.26 average polarization of the beams. Right: What could be achievable in the polarized proton physics run given 7 pb^{-1} of integrated luminosity and 0.5 polarization in each beam. 2–55

2.35 PHENIX sensitivity for $\Delta g/g$ with prompt photon production estimated for the integrated luminosity of 320 pb^{-1} ($\sqrt{s}$=200 GeV) and 800 pb^{-1} ($\sqrt{s}$=500 GeV). 2–57

2.36 Left: Polarization of u, d, $\bar{u}$, $\bar{d}$ as functions of x modeled by Bourreley-Soffer, and Gehrmann-Stirling. Sensitivities of HERMES SIDIS measurements and PHENIX W measurements are shown. Right: Double transverse-spin asymmetry for Drell-Yan dimuon production at $\sqrt{s} = 200$ GeV. (c) Parity violating asymmetry $\mathcal{A}_L$ for jet production compared with the SM, contact interaction, and leptophobic $Z^{'}$ [108]. 2–59

2.37 **Left**: The invariant mass resolution for pion pairs in the ρ-mass region. **Right**: Projected transverse single spin asymmetries compared to statistical errors, $\int Ldt = 32\,\mathrm{pb}^{-1}$. 2–60

2.38 Nuclear modification factor of charged hadron and π° p_T spectra for central d+Au and Au+Au collisions at $\sqrt{s} = 200$ GeV. [22, 27] 2–63

2.39 Ratio of yields per NN collision of pions, kaons, and protons in central d+Au collisions to yields per collision in peripheral collisions. The data were taken at $\sqrt{s} = 200$ GeV per nucleon pair. 2–64

2.40 Rapidity dependence of shadowing in the nuclear dependence of J/Ψ production for three different shadowing models [145, 146, 147]. The first two curves, green dot-dashed and blue dashed, are calculations from Vogt using the shadowing prescriptions from Frankfurt & Strikman [146] and Eskola [145]. Since Vogt did not include nuclear absorption in these calculations we have added a rapidity-independent absorption factor corresponding to $\alpha = 0.92$. The last model is that of Kopeliovich [147] 2–66

2.41 Nuclear dependence in 800 GeV p+A collisions from E866/NuSea and E789 [148, 149] showing a comparison of open (D meson) and closed charm (J/Ψ). The lack of suppression for open charm at mid-rapidity where the J/Ψ has substantial suppression is due to absorption, which affects only the J/Ψ. 2–67

2.42 Expected event distributions for the J/Ψ in a $20nb^{-1}$ d+Au run at $\sqrt{s} = 200$ GeV. The solid, dashed, and dotted histograms correspond to the North muon arm, central arm, and South muon arm detection, respectively [153]. 2–68

2.43 Expected statistical precision for measuring the nuclear dependence parameter α from a 20 nb^{-1} d+Au run at PHENIX. Data from a fixed-target experiment [148] at $\sqrt{s} = 38.8$ GeV are also shown [153]. 2–69

2.44 $J/\Psi \to \mu^+\mu^-$ mass peaks from PHENIX for the 2003 d+Au run. These yields are not corrected for efficiencies and relative luminosity for the samples shown for the two muon arms. 2–70

2.45 The difference in the effect of shadowing on open and closed charm for the color-dipole model [151, 152]. The shadowing difference is exhibited by the larger drop between mid-rapidity and large rapidity for the lower solid curve (J/Ψ) as compared to that for the upper dashed curve (open charm). 2–71

2.46 The correlation of energy deposits in the zero degree and forward angle calorimeters. The forward calorimeter can also be used to determine the number of "gray" tracks emitted in a given event to provide an independent measure of the collision centrality. 2–73

2.47 The increased reach to low x for Drell-Yan production measured in the PHENIX muon arms compared to 800 GeV p+A fixed target measurements from E772 [155]. Statistical uncertainties are shown for PHENIX (blue squares) for an approximate integrated p-p luminosity of 250nb^{-1}. The curve corresponds to Eskola's parameterization of shadowing which includes anti-shadowing and Fermi motion. 2–74

3.1 Hadron PID of PHENIX with an Aerogel Cerenkov Counter containing Aerogel with index n = 1.010. 3–10

3.2 The aerogel detector in the west arm between pad chamber 2 (PC2) and 3 (PC3) in the W1 sector (left) and the aerogel detector structure and orientation with respect to the beam line (right) are shown. 3–11

3.3 Detected number of photo-electrons for [solid line] n= 1.0114, and [dashed line] RICH (CO_2, n=1.00041, 1 atm.) as a function of momentum. $N_{p.e.}$ is for the 12 cm thick of aerogel.[Left] PID capabilities with AEROGEL, RICH and additional TOF. Aerogel is based on n = 1.0114 with a threshold at 10 % of maximum number of photoelectrons.[Right] 3–12

3.4 Drawing of aerogel module with 2 PMT's and light mixing box [Left] and prototype module tested in RHIC Run 3 [Right]. 3–12

3.5 Side view of the proposed VTX detector showing the central barrel detector and the forward end-cap detectors. 3–15

3.6 Cross sectional views of the proposed barrel VTX detector with four layers of Silicon detector. The inner most layer is a Silicon pixel detector, and the outer three layers are Silicon strip detectors. Each layer of the strip detector has ϕ strips and U strips. 3–16

3.7 Schematic views of the proposed end-cap VTX detector with four layers of Silicon detector. Each station has 96 silicon detectors. The stations are spaced at $\sim$ 20, 26, 32, and 38 cm from the interaction point. 3–17

3.8 Layout of the inner part of the PHENIX detector showing the location of the HBD/TPC and the inner coil. 3–20

3.9 Detector configuration with reflective CsI photocathode, triple GEM and pad readout. 3–21

3.10 Gain as a function of GEM voltage measured with Fe^{55} X-ray source. The 3×3 cm^2 detector had a CsI layer deposited on the top face of GEM1. The lines represent exponential fits to the data with 10×10 cm^2 GEM's. 3–22

3.11 Total avalanche charge as a function of GEM voltage measured with Am^{241} α-particles. The lines represent exponential growth of the total charge in the avalanche derived from the low gain points. 3–23

3.12 Demonstration of the hadron blindness property of the detector. When the drift field is reversed the ionization signal from a charged particle traversing the detector is considerably reduced whereas the photoelectron signal generated by UV photons is almost preserved. 3–23
3.13 Conceptual design of a combined TPC and HBD detector for PHENIX. . . . 3–25

List of Tables

1.1 PHENIX Institutions and Construction or Operational Responsibilities . . . 1–7

2.1 PHENIX Physics Goals from Conceptual Design Report (1993) [1] 2–5

2.2 Summary of PHENIX signals of hard processes. Many signals can already be studied with the baseline detector, but require considerable increase in integrated luminosity. Some measurements require upgrade hadron identification capability, using the aerogel upgrade. Integrated luminosity values shown in the table are PHENIX recorded luminosities. The required RHIC delivered luminosities are approximately three times higher, largely due to the width of the delivered vertex distribution. 2–7

2.3 Physics yields from the extended PHENIX run plan for 37 cryo weeks per year. The precise timing, duration and sequence of the segments beyond 2010 (labeled as "aa", "bb", etc.) are not known and must be balanced against the priorities of the heavy ion and spin programs. Note: if the region $0.24 \leq x \leq 0.33$ is deemed interesting, a p+Au run may be needed for 15.7/A pb^{-1} at 62.4 GeV. Also run "dd" could be split into half and half p+Au and p+Si since it is for low x. In the calculation of x_T^{max} for photons it is assumed that γ/π^0=0.1. 2–19

2.4 Summary of PHENIX signals associated with heavy quark physics topics. Some signals can be studied with the baseline detector, but many require the displaced vertex measuring capability of the PHENIX VTX detector, and all of the measurements benefit greatly from the VTX detector. The minimum PHENIX recorded luminosity required to study the signal in 200 GeV Au+Au collisions is indicated. The required RHIC delivered luminosities are approximately three times larger, due to vertex and trigger cuts. Similar numbers of binary collisions will be needed for p+p, d+Au and lighter ion collisions. . . 2–36

2.5 Possible timeline for the PHENIX heavy quark physics program available in the 27 week per year scenario for RHIC running. 2–50

2.6 Summary of the PHENIX Spin goals for the upcoming several years. For the "# of weeks", the number in parenthesis shows the beam weeks required for commissioning. All future physics topics presented in the table involve longitudinal polarization; there is ongoing discussion regarding transverse polarization. 2–51

2.7 *Unpolarized* and *polarized* quark and gluon distributions. Gluon *transversity* does not exist for the nucleon which has spin $\frac{1}{2}$. The Q^2 dependence is dropped for simplicity. 2–52
2.8 Initial state spin asymmetries in p+p collisions. (+) and (−) refers to the helicity states of the beams and ↑ and ↓ represent vertically *Up* and *Down* polarization. 2–53
2.9 Spin asymmetries for various p+p reactions along with the major goals of their measurement. References shown do not necessarily represent the initial work. "CI" and "2HDM" stand for Contact Interaction and Two Higgs Doublet Model, respectively. $\mathcal{A}_{LT}$ is not listed here but the asymmetry for $pp \to \gamma^* X$ can be found in Ref. [109]. 2–53
2.10 Estimated physics yields for d+Au collisions for several processes with various integrated luminosities. For the lower rate process such as the Υ this illustrates the much larger luminosities needed in order to reach this physics. 2–73
2.11 Physics yields from the PHENIX run plan for 27 cryo weeks per year 2–76
2.12 Physics yields from the PHENIX run plan for 37 cryo weeks per year 2–1

3.1 Summary of physics measurement gained by the barrel VTX detector. The column "without VTX" shows the present capability of PHENIX, while the measurement range with the VTX detector is shown in the column "with VTX". If the process is not measurable, it is marked as "No". 3–17

References

[1] PHENIX Conceptual Design Report 1993 (PX20, BNL48922, internal report).

[2] V. Greco, C. M. Ko and P. Levai *Phys. Rev.* **C68** (2003) 034904 [`nucl-th/0305024`].

[3] V. Greco, C. M. Ko and P. Levai `nucl-th/0301093`.

[4] R. J. Fries, B. Muller, C. Nonaka and S. A. Bass *(to be published)* (2003) [`nucl-th/0306027`].

[5] Available at http://www.phenix.bnl.gov/phenix/WWW/docs/bylaws/current/bylaws.htm.

[6] **PHENIX** Collaboration, K. Adcox *et. al. Phys. Rev. Lett.* **86** (2001) 3500–3505 [`nucl-ex/0012008`].

[7] **PHENIX** Collaboration, K. Adcox *et. al. Phys. Rev. Lett.* **87** (2001) 052301 [`nucl-ex/0104015`].

[8] **PHENIX** Collaboration, K. Adcox *et. al. Phys. Rev. Lett.* **88** (2002) 022301 [`nucl-ex/0109003`].

[9] **PHENIX** Collaboration, K. Adcox *et. al. Phys. Rev. Lett.* **88** (2002) 242301 [`nucl-ex/0112006`].

[10] **PHENIX** Collaboration, K. Adcox *et. al. Phys. Rev. Lett.* **88** (2002) 192302 [`nucl-ex/0201008`].

[11] **PHENIX** Collaboration, K. Adcox *et. al. Phys. Rev. Lett.* **88** (2002) 192303 [`nucl-ex/0202002`].

[12] **PHENIX** Collaboration, K. Adcox *et. al. Phys. Rev. Lett.* **89** (2002) 092302 [`nucl-ex/0204007`].

[13] **PHENIX** Collaboration, K. Adcox *et. al. Phys. Rev. Lett.* **89** (2002) 082301 [`nucl-ex/0203014`].

[14] **PHENIX** Collaboration, K. Adcox *et. al. Phys. Rev. C* **66** (2002) 024901 [`nucl-ex/0203015`].

[15] **PHENIX** Collaboration, K. Adcox *et. al. Phys. Rev. Lett.* **89** (2002) 212301 [nucl-ex/0204005].

[16] **PHENIX** Collaboration, K. Adcox *et. al. Phys. Lett.* **B561** (2003) 82–92 [nucl-ex/0207009].

[17] **PHENIX** Collaboration, K. Adcox *et. al. (to be published)* (2003) [nucl-ex/0307010].

[18] **PHENIX** Collaboration, S. S. Adler *et. al. Phys. Rev. Lett.* **91** (2003) 072301 [nucl-ex/0304022].

[19] **PHENIX** Collaboration, S. S. Adler *et. al. (to be published)* (2003) [nucl-ex/0305013].

[20] **PHENIX** Collaboration, S. S. Adler *et. al. (to be published)* (2003) [nucl-ex/0305030].

[21] **PHENIX** Collaboration, S. S. Adler *et. al. (to be published)* (2003) [nucl-ex/0305036].

[22] **PHENIX** Collaboration, S. S. Adler *et. al. (to be published)* (2003) [nucl-ex/0308006].

[23] **PHENIX** Collaboration, S. S. Adler *et. al. (to be published)* (2003) [nucl-ex/0307022].

[24] **PHENIX** Collaboration, S. S. Adler *et. al. (to be published)* (2003) [nucl-ex/0310005].

[25] **PHENIX** Collaboration, S. S. Adler *et. al. (to be published)* (2003) [hep-ex/0304038].

[26] **PHENIX** Collaboration, S. S. Adler *et. al. (to be published)* (2003) [hep-ex/0307019].

[27] **PHENIX** Collaboration, S. S. Adler *et. al. Phys. Rev. Lett.* **91** (2003) 072303 [nucl-ex/0306021].

[28] Available from http://www.phy.anl.gov/NSACperformancemeasures/ .

[29] D. Magestro *J. Phys.* **G28** (2002) 1745–1752 [hep-ph/0112178].

[30] D. Teaney, J. Lauret and E. V. Shuryak *(to be published)* (2001) [nucl-th/0110037].

[31] P. F. Kolb and U. Heinz *(to be published)* (2003) [nucl-th/0305084].

[32] R. J. Fries, B. Muller, C. Nonaka and S. A. Bass *Phys. Rev. Lett.* **90** (2003) 202303 [nucl-th/0301087].

[33] R. Baier, D. Schiff and B. G. Zakharov *Ann. Rev. Nucl. Part. Sci.* **50** (2000) 37–69 [hep-ph/0002198].

[34] U. A. Wiedemann *Nucl. Phys.* **B588** (2000) 303–344 [hep-ph/0005129].

[35] M. Gyulassy, P. Levai and I. Vitev *Nucl. Phys.* **B594** (2001) 371–419 [nucl-th/0006010].

[36] I. Vitev *Phys. Lett. B* **562** (2003) 36 – 44 [nucl-th/0302002].

[37] D. Kharzeev, E. Levin and L. McLerran *Phys. Lett.* **B561** (2003) 93–101 [hep-ph/0210332].

[38] D. Antreasyn *et. al. Phys. Rev. D* **19** (1979) 764–778.

[39] **STAR** Collaboration, C. Adler *et. al. Phys. Rev. Lett.* **90** (2003) 082302 [nucl-ex/0210033].

[40] X. Wang and Z. Huang *Phys. Rev. C* **55** (1997) 3047 [hep-ph/9701227].

[41] X. Wang *Prog. Theor. Phys. Suppl.* **129** (1997) 45 [hep-ph/9711026].

[42] **UA2** Collaboration, R. Ansari *et. al. Z. Phys.* **C41** (1988) 395.

[43] B. Alper *et. al. Nucl. Phys. B* **100** (1975) 237.

[44] P. Abreu *et. al. Eur. Phys.J. C* **17** (2000) 207 – 222 [hep-ex/0106063].

[45] J. Huston *et. al. Phys. Rev.* **D51** (1995) 6139–6145 [hep-ph/9501230].

[46] P. Aurenche, R. Baier, M. Fontannaz, J. Owens and M. Werlen *Phys. Rev.* **D39** (1989) 3275.

[47] Available as http://www.phenix.bnl.gov/phenix/WWW/publish/zajc/sp/presentations/RBUP03/ProposalText/RBUPforRun4-8.pdf .

[48] L. Apanasevich *et. al. Phys. Rev.* **D59** (1999) 074007 [hep-ph/9808467].

[49] R. Rapp *Phys. Rev.* **C63** (2001) 054907 [hep-ph/0010101].

[50] E. V. Shuryak *Phys. Rev.* **C55** (1997) 961–963 [nucl-th/9605011].

[51] K. Gallmeister, B. Kampfer and O. P. Pavlenko *(to be published)* (1999) [hep-ph/9902265].

[52] **HELIOS** Collaboration, M. Masera *Nucl. Phys.* **A590** (1995) 93c–102c.

[53] G.-Q. Li and C. Gale *Phys. Rev.* **C58** (1998) 2914–2927 [nucl-th/9807005].

[54] **NA38/NA50** Collaboration, M. C. Abreu *et. al. Nucl. Phys.* **A661** (1999) 538–541.

[55] R. Rapp *(to be published)* (2000) [hep-ph/0001291].

[56] **WA80** Collaboration, R. Albrecht *et. al. Phys. Rev. Lett.* **76** (1996) 3506–3509.

[57] **CERES** Collaboration, R. Baur *et. al. Z. Phys.* **C71** (1996) 571–578.

[58] J. Sollfrank *et. al. Phys. Rev.* **C55** (1997) 392–410 [nucl-th/9607029].

[59] C. Gale and K. L. Haglin *(to be published)* (2003) [hep-ph/0306098].

[60] S. Turbide, R. Rapp and C. Gale *(to be published)* (2003) [hep-ph/0308085].

[61] A. Dumitru, L. Frankfurt, L. Gerland, H. Stocker and M. Strikman *Phys. Rev.* **C64** (2001) 054909 [hep-ph/0103203].

[62] **WA98** Collaboration, M. M. Aggarwal *et. al. Phys. Rev. Lett.* **85** (2000) 3595–3599 [nucl-ex/0006008].

[63] R. J. Fries, B. Muller and D. K. Srivastava *Phys. Rev. Lett.* **90** (2003) 132301 [nucl-th/0208001].

[64] N. R. C. Committee on the Physics of the Universe, *Connecting Quarks with the Cosmos: Eleven Science Questions for the New Century.* The National Academies Press, 2003.

[65] G. E. Brown and M. Rho *Phys. Rev. Lett.* **66** (1991) 2720–2723.

[66] R. Rapp and J. Wambach *Adv. Nucl. Phys.* **25** (2000) 1 [hep-ph/9909229].

[67] G. E. Brown, G.-Q. Li, R. Rapp, M. Rho and J. Wambach *Acta Phys. Polon.* **B29** (1998) 2309–2321 [nucl-th/9806026].

[68] **CERES/NA45** Collaboration, G. Agakishiev *et. al. Phys. Lett.* **B422** (1998) 405–412 [nucl-ex/9712008].

[69] **E325** Collaboration, K. Ozawa *et. al. Phys. Rev. Lett.* **86** (2001) 5019–5022 [nucl-ex/0011013].

[70] D. Lissauer and E. V. Shuryak *Phys. Lett.* **B253** (1991) 15–18.

[71] Y. L. Dokshitzer and D. E. Kharzeev *Phys. Lett.* **B519** (2001) 199–206 [hep-ph/0106202].

[72] M. Djordjevic and M. Gyulassy *Phys. Rev. c* **68** (2003) 034914 [nucl-th/0305062].

[73] M. Djordjevic and M. Gyulassy *Phys. Lett.* **B560** (2003) 37–43 [nucl-th/0302069].

[74] B.-W. Zhang, E. Wang and X.-N. Wang, *Heavy quark energy loss in nuclear medium*, 2003.

[75] S. Batsouli, S. Kelly, M. Gyulassy and J. L. Nagle *Phys. Lett.* **B557** (2003) 26–32 [nucl-th/0212068].

[76] Z.-W. Lin and D. Molnar *Phys. Rev.* **C68** (2003) 044901 [nucl-th/0304045].

[77] E. V. Shuryak *Phys. Rept.* **61** (1980) 71–158.

[78] P. Levai, B. Muller and X.-N. Wang *Phys. Rev.* **C51** (1995) 3326–3335 [hep-ph/9412352].

[79] Z.-W. Lin and M. Gyulassy *Phys. Rev. C* **51** (1995) 2177–2187 [nucl-th/9409007].

[80] L. Grandchamp and R. Rapp *Nucl. Phys.* **A709** (2002) 415–439 [hep-ph/0205305].

[81] L. Grandchamp and R. Rapp *Phys. Lett.* **B523** (2001) 60–66 [hep-ph/0103124].

[82] R. L. Thews, M. Schroedter and J. Rafelski *Phys. Rev.* **C63** (2001) 054905 [hep-ph/0007323].

[83] R. L. Thews, *Quarkonium formation from uncorrelated quark antiquark pairs*, 2003. hep-ph/0302050.

[84] A. Andronic, P. Braun-Munzinger, K. Redlich and J. Stachel *Phys. Lett.* **B571** (2003) 36–44 [nucl-th/0303036].

[85] B. L. Ioffe hep-ph/0310343.

[86] S. C. Benzahra *Phys. Rev.* **C61** (2000) 064906 [hep-ph/9904231].

[87] J. F. Gunion and R. Vogt *Nucl. Phys.* **B492** (1997) 301–337 [hep-ph/9610420].

[88] D. Pal, B. K. Patra and D. K. Srivastava *Eur. Phys. J.* **C17** (2000) 179–186 [hep-ph/0002298].

[89] C.-Y. Wong *J. Phys.* **G28** (2002) 2349–2364 [nucl-th/0112064].

[90] K. Gallmeister, B. Kampfer and O. P. Pavlenko *Nucl. Phys.* **A715** (2003) 705–708 [nucl-th/0208006].

[91] R. Rapp, *Thermal lepton production in heavy-ion collisions*, 2002.

[92] I. Kvasnikova, C. Gale and D. K. Srivastava *Phys. Rev. C* **65** (2002) 064903 [hep-ph/0112139].

[93] M. J. Alguard *et. al. Phys. Rev. Lett.* **37** (1976) 1261.

[94] M. J. Alguard *et. al. Phys. Rev. Lett.* **41** (1978) 70.

[95] G. Baum *et. al. Phys. Rev. Lett.* **51** (1983) 1135.

[96] **European Muon** Collaboration, J. Ashman *et. al. Phys. Lett.* **B206** (1988) 364.

[97] **Spin Muon** Collaboration, B. Adeva *et. al. Phys. Rev.* **D58** (1998) 112001.

[98] **Spin Muon** Collaboration, B. Adeva *et. al. Phys. Rev.* **D58** (1998) 112002.

[99] **E142** Collaboration, P. L. Anthony *et. al. Phys. Rev.* **D54** (1996) 6620–6650 [hep-ex/9610007].

[100] **E143** Collaboration, K. Abe *et. al. Phys. Rev.* **D58** (1998) 112003 [hep-ph/9802357].

[101] **E154** Collaboration, K. Abe *et. al. Phys. Rev. Lett.* **79** (1997) 26–30 [hep-ex/9705012].

[102] **E155** Collaboration, P. L. Anthony *et. al. Phys. Lett.* **B463** (1999) 339–345 [hep-ex/9904002].

[103] **HERMES** Collaboration, K. Ackerstaff *et. al. Phys. Lett.* **B404** (1997) 383–389 [hep-ex/9703005].

[104] **HERMES** Collaboration, A. Airapetian *et. al. Phys. Lett.* **B442** (1998) 484–492 [hep-ex/9807015].

[105] P. Taxil and J. M. Virey *Phys. Lett.* **B364** (1995) 181–187 [hep-ph/9507434].

[106] P. Taxil and J. M. Virey *Phys. Rev.* **D55** (1997) 4480–4483 [hep-ph/9607390].

[107] P. Taxil and J. M. Virey *Phys. Lett.* **B383** (1996) 355–361 [hep-ph/9604331].

[108] P. Taxil and J. M. Virey *Phys. Lett.* **B441** (1998) 376–382 [hep-ph/9807487].

[109] R. L. Jaffe and X.-D. Ji *Phys. Rev. Lett.* **67** (1991) 552–555.

[110] C. Papavassiliou, N. Mobed and M. Svec *Phys. Rev.* **D26** (1982) 3284–3286.

[111] E. L. Berger and J.-W. Qiu *Phys. Rev.* **D40** (1989) 778.

[112] R. L. Jaffe and N. Saito *Phys. Lett.* **B382** (1996) 165–172 [hep-ph/9604220].

[113] J.-W. Qiu and G. Sterman *Phys. Rev. Lett.* **67** (1991) 2264–2267.

[114] D. de Florian and S. Frixione *Phys. Lett.* **B457** (1999) 236–244 [hep-ph/9904320].

[115] C. Bourrely, J. Soffer, F. M. Renard and P. Taxil *Phys. Rept.* **177** (1989) 319.

[116] M. Karliner and R. W. Robinett *Phys. Lett.* **B324** (1994) 209–216 [hep-ph/9310346].

[117] C. Kao, D. Atwood and A. Soni *Phys. Lett.* **B395** (1997) 327–333 [hep-ph/9608383].

[118] O. Teryaev and A. Tkabladze *Phys. Rev.* **D56** (1997) 7331–7340 [hep-ph/9612301].

[119] R. L. Jaffe and D. Kharzeev *Phys. Lett.* **B455** (1999) 306–310 [hep-ph/9903280].

[120] C. Bourrely and J. Soffer *Phys. Lett.* **B314** (1993) 132–138.

[121] D. Boer *Phys. Rev.* **D62** (2000) 094029 [hep-ph/0004217].

[122] P. Ratcliffe *Nucl. Phys.* **B223** (1983) 45.

[123] E. Leader and K. Sridhar *Phys. Lett.* **B311** (1993) 324–328.

[124] W. Vogelsang and A. Weber *Phys. Rev.* **D48** (1993) 2073–2082.

[125] N. Hammon, O. Teryaev and A. Schafer *Phys. Lett.* **B390** (1997) 409–412 [hep-ph/9611359].

[126] I. Bojak and M. Stratmann *Phys. Rev.* **D67** (2003) 034010 [hep-ph/0112276].

[127] G. Bunce, N. Saito, J. Soffer and W. Vogelsang *Ann. Rev. Nucl. Part. Sci.* **50** (2000) 525–575 [hep-ph/0007218].

[128] C. Bourrely and J. Soffer *Nucl. Phys.* **B445** (1995) 341–379 [hep-ph/9502261].

[129] T. Gehrmann and W. J. Stirling *Phys. Rev.* **D53** (1996) 6100–6109 [hep-ph/9512406].

[130] A. Ogawa, V. L. Rykov and N. Saito *(to be published)* (2000) [hep-ph/0102220].

[131] **HERMES** Collaboration, A. Airapetian *et. al. Phys. Rev. Lett.* **84** (2000) 4047–4051 [hep-ex/9910062].

[132] **Spin Muon** Collaboration, A. Bravar *Nucl. Phys. Proc. Suppl.* **79** (1999) 520–522.

[133] HERMES coll., The HERMES Physics Program & Plans for 200 1-2006, DESY PRC 00-xxx..

[134] Talks of R. Jaffe and C. Weiss, Proceedings of the RBRC Workshop on Future Transversity Measurements, September 18-20, 2000, BNL.

[135] J. C. Collins, S. F. Heppelmann and G. A. Ladinsky *Nucl. Phys.* **B420** (1994) 565–582 [hep-ph/9305309].

[136] R. L. Jaffe, X.-M. Jin and J. Tang *Phys. Rev. Lett.* **80** (1998) 1166–1169 [hep-ph/9709322].

[137] M. Grosse Perdekamp, Transversity Measurements at RHIC, DIS2000, Proceedings (2000).

[138] T. Roser, *Rhic run 3 (FY2003) running projections*, June, 2002.

[139] P. B. Straub *et. al. Phys. Rev. Lett.* **68** (1992) 452–455.

[140] M. Arnedo *Phys. Rep.* **240** (1994) 301–393.

[141] K. J. Eskola, V. J. Kolhinen, P. V. Ruuskanen and C. A. Salgado *Nucl. Phys.* **A661** (1999) 645–648 [hep-ph/9906484].

[142] L. D. McLerran and R. Venugopalan *Phys. Rev.* **D49** (1994) 2233–2241 [hep-ph/9309289].

[143] A. H. Mueller and J.-W. Qiu *Nucl. Phys.* **B268** (1986) 427.

[144] L. V. Gribov, E. M. Levin and M. G. Ryskin *Phys. Rept.* **100** (1983) 1–150.

[145] K. J. Eskola, V. J. Kolhinen and P. V. Ruuskanen *Nucl. Phys.* **B535** (1998) 351–371 [hep-ph/9802350].

[146] L. Frankfurt and M. Strikman *Eur. Phys. J.* **A5** (1999) 293–306 [hep-ph/9812322].

[147] B. Kopeliovich, A. Tarasov and J. Hufner *Nucl. Phys.* **A696** (2001) 669–714 [hep-ph/0104256].

[148] **FNAL E866/NuSea** Collaboration, M. J. Leitch *et. al. Phys. Rev. Lett.* **84** (2000) 3256–3260 [nucl-ex/9909007].

[149] **E789** Collaboration, M. J. Leitch *et. al. Phys. Rev. Lett.* **72** (1994) 2542–2545.

[150] **NA50** Collaboration, M. C. Abreu *et. al. Phys. Lett.* **B410** (1997) 327–336.

[151] B. Z. Kopeliovich and A. V. Tarasov *Nucl. Phys.* **A710** (2002) 180–217 [hep-ph/0205151].

[152] J. Raufeisen, 2002. private communication.

[153] J.-C. Peng, *J/Ψ production for a d+Au run at PHENIX*, 2002. http://www.phenix.bnl.gov/WWW/publish/jcpeng/da/jpsi_10.ps.

[154] I. Chemakin *et. al. Phys. Rev. Lett.* **85** (2000) 4868–4871 [nucl-ex/0003010].

[155] **FNAL E772** Collaboration, D. M. Alde *et. al. Phys. Rev. Lett.* **64** (1990) 2479–2482.

[156] C. Lourenco, *Workshop on quarkomium production in relativistic nuclear collisions*, 1998. Seattle, 11 May 1998 and private communication.

[157] **FNAL E866/NuSea** Collaboration, E. A. Hawker *et. al. Phys. Rev. Lett.* **80** (1998) 3715–3718 [hep-ex/9803011].

[158] **FNAL E866/NuSea** Collaboration, R. S. Towell *et. al. Phys. Rev.* **D64** (2001) 052002 [hep-ex/0103030].

[159] Available as https://www.phenix.bnl.gov/WWW/publish/akiba/2003/SVTX/PHENIX-VTX-proposal.pdf.

[160] Z. Fraenkel *et. al.*, "Proposal for a hadron blind detector for phenix." PHENIX Technical Note 391, http://www.phenix.bnl.gov/phenix/WWW/forms/info/view.html.

[161] A. Kozlov, I. Ravinovich, L. Schekhtman, Z. Fraenkel, M. Inuzuka and I. Tserruya, "Proposal for a hadron blind detector for phenix." phys/0309013, submitted to Nucl. Instrum. Meth.